DOCTORAL THESIS

Mixed anionic and cationic polyphosphazene complexes for effective gene delivery to glioblastoma in vitro and in vivo

Wei-Hsin Hsu

Doctoral Program in Nanomedicine and Pharmaceutical Innovation

Faculty of Pharmacy

SANTIAGO DE COMPOSTELA

2018

USC
UNIVERSIDADE
DE SANTIAGO
DE COMPOSTELA

TESIS DOCTORAL

Complejos a base de polifosfacenos aniónicos y catiónicos para la administración eficaz de genes al glioblastoma in vitro e in vivo

Wei-Hsin Hsu

Programa de doctorado en Nanomedicina e Innovación Farmacéutica

SANTIAGO DE COMPOSTELA
2018

USC
UNIVERSIDADE
DE SANTIAGO
DE COMPOSTELA

AUTHORIZATION OF THE THESIS SUPERVISORS

Mixed anionic and cationic polyphosphazene complexes for effective gene delivery to glioblastoma in vitro and in vivo

Prof. Marcos García Fuentes, Associate Professor, Department of Pharmacology, Pharmacy and Pharmaceutical Technology, University of Santiago de Compostela, Spain

Prof. Cameron Alexander, Full Professor of Polymer Therapeutics, Head of Division of Molecular Therapeutics and Formulation, School of Pharmacy, University of Nottingham, UK

REPORT:

That the present thesis, corresponds to the work carried out by Mr. Wei-Hsin Hsu, under our supervision, and that we authorize its presentation considering it gathers the necessary requirements of article 34 of the USC Doctoral Studies regulation, and that as supervisors of this thesis, it does not incur in the abstention causes established by the law 40/2015.

At Santiago de Compostela, on _____2018

Prof. Marcos García Fuentes

Prof. Cameron Alexander

USC
UNIVERSIDADE
DE SANTIAGO
DE COMPOSTELA

AUTORIZACIÓN DEL DIRECTOR / TUTOR DE LA TESIS

Complejos a base de polifosfacenos aniónicos y catiónicos para la administración eficaz de genes al glioblastoma in vitro e in vivo

D. Marcos García Fuentes

D. Cameron Alexander

INFORMA/N:

Que la presente tesis, se corresponde con el trabajo realizado por D. Wei-Hsin Hsu, bajo mi dirección, y autorizo su presentación, considerando que reúne los requisitos exigidos en la Regulación de Estudios de Doctorado de la USC, y que como director de ésta no incurre en las causas de abstención establecidas en la Ley 40/2015.

En Santiago de Compostela a _____ *de 2018*

Prof. Marcos García Fuentes

Prof. Cameron Alexander

USC
UNIVERSIDADE
DE SANTIAGO
DE COMPOSTELA

PhD CANDIDATE STATEMENT

Mixed anionic and cationic polyphosphazene complexes for effective gene delivery to glioblastoma in vitro and in vivo

Mr. Wei-Hsin Hsu

I submit my Doctoral thesis, following the procedure according to the Regulation, stating that:

1) This thesis gathers the results corresponding to my work.
2) When necessary, explicit mention is given to the collaborations the work may have had.
3) The present document is the final version submitted for its defence and coincide with the document sent in electronic format.
4) I confirm that this thesis does not incur in any plagiarism of any other authors or documents submitted by me for obtaining other degrees.

At Santiago de Compostela, _____ *2018*

Mr. Wei-Hsin Hsu

USC
UNIVERSIDADE
DE SANTIAGO
DE COMPOSTELA

DECLARACIÓN DEL AUTOR/A DE LA TESIS

Complejos a base de polifosfacenos aniónicos y catiónicos para la administración eficaz de genes al glioblastoma in vitro e in vivo

D. Wei-Hsin Hsu

Presento mi tesis, siguiendo el procedimiento adecuado a la Regulación, y declaro que:

1) La tesis abarca los resultados de la elaboración de mi trabajo.
2) De ser el caso, en la tesis se hace referencia a las colaboraciones que tuvo este trabajo.
3) La tesis es la versión definitiva presentada para su defensa y coincide con la versión enviada en formato electrónico.
4) Confirmo que la tesis no incurre en ningún tipo de plagio de otros autores ni de trabajos presentados por mí para la obtención de otros títulos.

En Santiago de Compostela a _____ *de 2018*

Sr. Wei-Hsin Hsu

USC
UNIVERSIDADE
DE SANTIAGO
DE COMPOSTELA

Reach for it. Push yourself as far as you can.

CHRISTA MCAULIFFE

Whatever the outcomes,
at least I tried and will not regret in the future.

Wei-Hsin Hsu 2018

USC
UNIVERSIDADE
DE SANTIAGO
DE COMPOSTELA

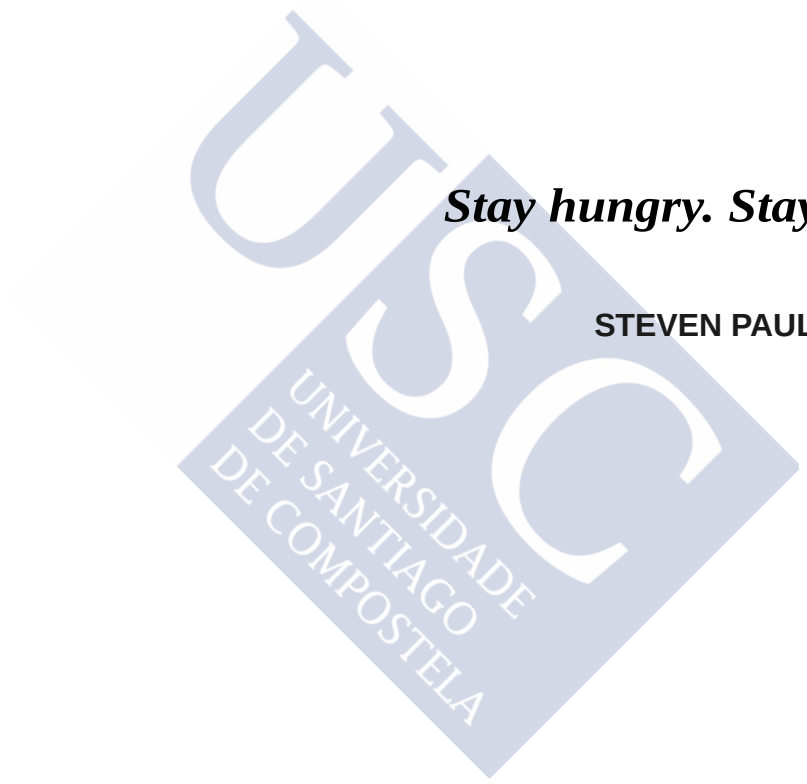

Stay hungry. Stay foolish.

STEVEN PAUL JOBS, 2005

USC
UNIVERSIDADE
DE SANTIAGO
DE COMPOSTELA

Acknowledgements

I cannot thank NanoFar Joint Doctorate Project (Erasmus Mundus grant) though, for supporting my PhD program and 3-year adventures. This fantastic international program gathered students from more than ten countries, providing academic meetings for extending our knowledge, brainstorming activities for thinking outside the box, and strengthening our network and friendships in this small United Nations. Deeply thank you Prof. Frank Boury and related NanoFar members for their dedication to this European doctorate program.

Firstly, I would like to thank deeply my supervisors, Prof Marcos Garcia-Fuentes and Prof. Noemi Csaba in my home university, University of Santiago de Compostela. Marcos is not only a supervisor also a mentor, not only providing me almost everything I need for scientific researches, also guiding me how to efficiently address many issues logically, sharpening my organization ability. In addition, I cordially appreciate his corrections for all of my scientific reports and articles. Corrections of a non-native speaker's writing are not an easy job and need tons of patience. With his great dedication and passion, I took a big stride forward and realized my potential. Here, I am sincerely appreciating advice and guidance from Marcos and Noemi.

In the second year, I went to my host university, the University of Nottingham. Here, I also express sincerely appreciation to my supervisor, Prof. Cameron Alexander, an honourable scientist. He not only guided me in the polymer chemistry world but also introduced me to work with Dr. Delyan P. Ivanov (in the lab of Prof. Anna Grabowska) and to learn how to establish 3D-tumor models for my PhD study. He strongly supported me and almost gave the best resource to me in this scientific

adventure. Although his schedules were quite busy, he still squeezed a time slot for discussion of my experimental work and we usually discussed scientific work overtime. He also made a lot of efforts on revision of my thesis, letting me learn many excellent skills in academic writing. I really appreciate all of his inspiration and contribution.

At the end of the third year, I went to Instituto de Salud Carlos III (ISCIII) through Prof. Marcos G.F.'s introduction, and thank you for Dr. Pilar Sánchez-Gómez for giving me the chance for PhD-expert internship in ISCIII. Here, I would like to express my cordially gratitude to Pilar. She opened my eyes in molecular biology and neuro-oncology world, guiding me how to walk in this road. She never lost patience and motivation in teaching this foreign at entry level; in light of this, I could really enter the gene "therapy" field. Not only that, she is also selfless to provide me their developed animal models and helped me to establish them in my thesis.

Of course, this thesis cannot be finished without our outstanding co-operators. Dr. Esther G. Traba synthesized several precious plasmids that had been used in this thesis. In the first year, we cooperated to screen many conditions of formulations via luciferase expression assays. Dr. Adriana Martinez Ledo is like my sister and provided countless supports, from paper work to scientific experiments, etc, and most importantly las cervezas after work. Adriana and Maruthi Prasanna are the key people to help me in the thesis submission. Carla García Mazás helped me for delivery of samples for biodegradable experiments mucha veces. Specially, the pEGFPLuc plasmid DNA was a kind gift from Prof. A. Vidal and Dr. C. Carneiro (University of Santiago de Compostela). The primary GBM cell-line (GBM1) was a kind donation from the lab of Dr. MD. Bernard Rogister (University of Liege). Much knowledge of glioma margins and regions of infiltration came from Dr. Ruman Rahman (University of Nottingham).

During this journey, technical supports are considerably important to me. In University of Santiago de Compostela, Dr. Manuel Martin-Pastor guided me to analyse NMR spectra (DOSY and HSQC, etc.) and Dr. Jose Manuel Ageitos is an outstanding scientist as well as an artist, helping us how to use vector graphic software. In the Nanobiofar lab, I would like to say thank to some key people in my PhD life, Purificacion Dominguez (Puri), Belen Cuesta, and Rafael Romero for supports of paper work and orders of chemicals. Especially for Puri, I cannot appreciate more for her so many helps, from applications for VISA to USC registration, etc. In the University of Nottingham, I also acknowledge the expert technical supports from Pamela Collier, Christine Grainger-Boultby, Paul Cooling. Also, I would like to show a great gratitude to Colin Rowe and Carol Turrill for helping me a lot of paper work and smoothing the project. Ali Alazzo, Dr. Vincenzo Taresco, and Tchoryk Aleksandra (Alex) supported me in experimental work, including GPC measurements and cryosection. In ISCIII, thank you Dr. Esther Hernández and Paloma Fernández in molecular biological assays and for all of supports in vivo experiments.

My special appreciation goes to Dr. Niu Zhigao, who is like a brother, guiding me how to enjoy the life in the Santiago de Compostela, and I would like to say thank to the “Asian group” in NanoFar, including Maruthi, Paul, Bhanu, Ulong, and Surasa. We had a lot of fun and hold many food-exchange parties for relieving my home sick. Maruthi also held many sport activities for unifying the NanoBioFar lab and better work-life balance for us. Recalling the happy living time in Santiago de Compostela, I would like to thank a gracious lady, María Sampedro Pena, my landlord, who offered una habitación to me and treated me very friendly.

Not only that, I also would like to acknowledge all the members of lovely NanoBioFar family and B15 members in Nottingham, including Belén López Bouzo

(my neighbor), Jose Crecente Campo, Sonia Reimóndez Troitiño, Natalya Storozhylova, Carmen Teijeiro Valiño, Andrea Gonella, Eleni Samaridou, Tamara Gómez Dacoba, Matilde Durán Lobato, Diego Pan Delgado, Ana Olivera, and others and others; even a trivial help, it is meaningful to me. Overall, I deeply believed that Spain is a friendly country full of passion, and England is an elegant and well-organizational kingdom. Regarding this, I acknowledge Marcos and Cameron again for giving me precious opportunities to befriend people from different countries and broadening my horizons not only in science but also in humanities and network. Finally, I would like to say thank you so much for my beloved family in Taiwan. They are always supporting me to chase this dream journey.

Last but not the least, as a scholarship holder, I sincerely thank the European Commission for an Erasmus Mundus grant to me (NanoFar Joint Doctorate Program). This work was also funded by EPSRC (Grants EP/H005625/1, EP/N03371X/1) and the Royal Society (Wolfson Research Merit Award WM150086) to Prof. Cameron Alexander, Ministerio de Economía y Competitividad (MINECO-RETOS, Grant SAF2015-65175-R to Dr. Pilar Sanchez Gomez and SAF2014-58189-R to Prof. Marcos G.F, FEDER Funds), and Fundación BBVA 2014-PO0110 to Marcos G.F.

CONFLICT OF INTEREST

The authors declare no conflicts of interest.

Mr. Wei-Hsin Hsu

USC
UNIVERSIDADE
DE SANTIAGO
DE COMPOSTELA

Content

USC
UNIVERSIDADE
DE SANTIAGO
DE COMPOSTELA

Abstract/Resumen

Abstract/Resumen

Abstract

Gene delivery vectors that are safe, efficient and affordable could significantly enhance the prospects for genetic-based therapies. Here we describe an approach to such vectors, using new variants of polyphosphazene materials and describe the synthesis of a series of degradable polyphosphazenes with both cationic and anionic side-chains, and report their use as mixed polyelectrolyte complexes for DNA and RNA delivery to glioblastoma cells *in vitro* and *in vivo.* Precursor poly(allylamino-phosphazene)s were converted to cationic and anionic derivatives via α, ω-thiolated alkylamines and alkylcarboxylates, respectively. Simultaneous co-incubation of alkylamine- and alkylcarboxylate-poly(phosphazenes) with nucleic acids generated polyelectrolyte complexes which were more compact than poly(alkylamino-phosphazene):DNA analogues but with similar positive surface charges. Screening of a series of these complexes for transfection of U87MG glioblastoma cells, showed that 6-mercaptohexanoic acid substituted poly(phosphazene)s mixed in the polycation/DNA complexes resulted in the highest luciferase expression in the cells. These data were consistent with an increased buffering capability of the 6-mercaptohexanoic acid substituted polymer across the early endosomal pH range in comparison with other anionic side-chain substituted polymers. Transfection assays in 3D spheroid models and in subcutaneous xenograft U87MG tumours confirmed higher transgene expression for these mixed cationic and anionic poly(phosphazene)s compared to the related poly(alkylamino-phosphazene)-DNA complexes, and also to PEI-DNA complexes. Extension of the approach to siRNA delivery showed that the mixed cationic and anionic poly(phosphazene)s were able to silence a gene encoding for a kinase implicated in

tumour progression (DYRK1A), resulting in a reduced renewal ability of U87MG cells *in vitro* and in delay of tumour growth in a xenograft model.

Resumen

Los vectores de administración de genes seguros, eficientes y asequibles podrían mejorar significativamente las perspectivas de las terapias génicas. Aquí describimos un enfoque para el desarrollo de tales vectores, usando nuevas variedades de polifosfacenos. Específicamente, describimos la síntesis de una serie de polifosfacenos degradables con cadenas laterales tanto catiónicas como aniónicas, y mostramos su uso como complejos polielectrolíticos mixtos para la administración de ADN y ARN a células de glioblastoma *in vitro* e *in vivo*. Los poli(alilamino-fosfacenos) precursores se convirtieron en derivados catiónicos y aniónicos a través de αώ-alquilaminas -tioladas y ácidos carboxílicos, respectivamente. La co-incubación simultánea de alquilaminas y alquilcarboxilatos de polifosfaceno con ácidos nucleicos generó complejos de polielectrolíticos más compactos que los poli (alquilamino-fosfacenos) -ADN análogos, pero con cargas superficiales positivas similares. Un cribado de los complejos sintetizados en base a la transfección de células de glioblastoma U87MG, mostró que el polifosfaceno sustituido con ácido 6-mercaptohexanoico mezclado en los complejos de policatión/ADN dio como resultado la expresión de luciferasa más alta en las células. Estos datos fueron en consonancia con una capacidad de tamponamiento incrementada del polímero sustituido con ácido 6-mercaptohexanoico en el rango de pH del endosoma temprano en comparación con otros polímeros sustituidos de cadena lateral aniónica. Los ensayos de transfección en modelos 3D de esferoides y en tumores de xenoinjerto subcutáneo U87MG confirmaron una mayor expresión del transgen para estos polifosfacenos aniónicos y catiónicos mixtos en comparación con los complejos de poli(alquilamino-fosfaceno)-ADN análogos, y también con complejos de PEI-ADN. La

ampliación del enfoque a la administración de ARNi mostró que los polifosfacenos catiónicos y aniónicos mixtos fueron capaces de silenciar un gen que codifica una quinasa implicada en la progresión tumoral (DYRK1A), promoviendo una reducción en la capacidad de renovación de células U87MG *in vitro* y un retraso del crecimiento tumoral en un modelo de xenoinjerto.

Resumen in extenso

Resumen in extenso

I. Antecedentes y Introducción

Administración de genes mediante vehículos poliméricos para el desarrollo de terapias frente al cáncer

El cáncer se ha convertido en la mayor causa de muerte del siglo XXI y varias limitaciones de las terapias convencionales llevan consigo una baja eficacia terapéutica y un bajo índice de supervivencia en los pacientes tratados[1-3]. Este conjunto de enfermedades van frecuentemente ligadas a desórdenes genéticos y han desarrollado mecanismos para su autoprotección, como las mutaciones que confieren multirresistencia a fármacos y previenen la apoptosis, las capacidades de auto-renovación y metástasis, resultando en tratamientos ineficaces y bajos índices terapéuticos[4-6]. Esta elevada mutación genómica pone de relevancia la importancia de la terapia génica[5]. Los éxitos recientes en ensayos clínicos y un gran número de nuevas terapias emergentes basadas en polinucleótidos están suscitando una urgente demanda de vehículos de genes más seguros y eficientes[7-9]. A pesar de que la administración de genes mediante vehículos virales es el método más avanzado en cuanto al número de ensayos clínicos[10], todavía existen preocupación acerca de la seguridad a largo plazo de estos vectores, y muchos de los nuevos polinucleótidos son más fácilmente integrables en vehículos no virales. Entre estos vehículos, los sistemas basados en polímeros presentan varias ventajas frente a los vectores virales, como su potencial seguridad, la facilidad de producción a gran escala, y su fácil preparación y modificación, como evidencian los resultados prometedores en ensayos clínicos[11]. Sin embargo siguen existiendo varias limitaciones para la aplicación práctica de estos vehículos poliméricos[12-15], incluyendo una administración eficiente en los tejidos dianas así como un adecuado balance entre la protección de los ácidos nucleicos y su

posterior liberación una vez en el lugar de acción. La administración de genes mediante policationes toma ventaja de la tendencia de las cargas electrostáticas a pasar a través de las membranas celulares e incluso asociarse a estas, dando lugar a un tráfico intracelular adecuado[16,17]. Sin embargo, esta carga positiva de los policationes también puede provocar la disrupción de las membranas celulares dando lugar a efectos tóxicos indeseados, y una lenta disociación de los ácidos nucleicos que conlleva una baja eficiencia de transferencia génica[18]. En conjunto, los criterios de diseño que aún no han sido conseguidos por la mayoría de los vehículos de genes incluyen: (a) estabilidad, biocompatibilidad y biodegradabilidad, (b) una biodistribución selectiva y una adecuada farmacocinética, (c) la habilidad para traspasar barreras de tejido y extracelulares, (d) transporte a través de barreras intracelulares y liberación específica en orgánulos celulares.

La necesidad de crear complejos de poliiones híbridos para terapia génica

Para el ensamblaje electrostático de complejos para uso en terapia génica, se requiere que polímeros catiónicos y ácidos nucleicos con carga negativa sean mezclados adecuadamente construyendo vehículos similares a nanopartículas. La polietilenimina (PEI) es el polímero más ampliamente utilizado y puede formar complejos con pDNA cuando el ratio N/P $\geq$ 3, pero para conseguir una transfección significativa in vitro, estudios previos en varias líneas celulares tumorales han mostrado que se requieren ratios N/P $\geq$10 PEI/ácidos nucleicos. Este exceso molar de PEI es necesario para facilitar la internalización y la liberación intracelular del material genético, sin importar si esta PEI en exceso estaba libre en solución o fuera añadida previamente con el complejo PEI a N/P=3. En esta transfección "mediada por

polímeros", estos polímeros catiónicos adicionales promueven la transfección pero también pueden causar efectos secundarios no deseados. Además, este exceso de policationes no es eficaz in vivo, dado que los polipéptidos no unidos pueden ser retirados por fluidos intersticiales o atascados en la matriz extracelular[19]. En esta tesis, proponemos una estrategia para evitar los efectos secundarios derivados de un exceso de polímeros catiónicos, mediante la utilización de complejos de polímero/gen bien condensados formados a través de la mezcla de policationes con polianiones, llamados "poliplexos mixtos" como alternativa a los complejos de policatión tradicionales.

Extensión de la flexibilidad de los polifosfacenos biodegradables

Los polifosfacenos son considerados como materiales prometedores para la administración de genes ya que combinan biodegradabilidad con una gran flexibilidad química para alcanzar los criterios mencionados anteriormente. Se ha especulado que dicha flexibilidad sería ideal para generar cribados de química combinatoria para optimizar la estructura de los polímeros. Sin embargo, su aplicación para administración de genes ha sido relativamente escasa dado que la ruta sintética principal para la modificación de estos polímeros, la sustitución nucleofílica del precursor polidiclorofosfaceno, es problemática para la mayoría de los derivados de interés. La causa es que los grupos funcionales con varios centros nucleofílicos (ej. aminas, hidróxidos, ácidos carboxílicos, etc.) usados en terapia génica tienen la capacidad de entrecruzar el polímero precursor. Inspirados por estudios recientes[20] que proponen la potencial introducción de radicales click en polifosfacenos (PPZs), en esta tesis demostramos que la introducción de un grupo vinilo a través de la formación de un polímero precursor secundario, alilamino-polifosfacenos (AAPPZ), permite su

modificación sencilla con grupos funcionales de interés para administración de genes mediante reacciones de adición tiol-eno. Mediante este método, se pueden sintetizar PPZs con aminas primarias sin necesidad de utilizar una reacción de desprotección, y se ha generado una pequeña librería de otros derivados con aminas terciarias o ácidos carboxílicos como radicales, generando varios policationes y polianiones para la formación de "complejos mixtos" como vehículos para aplicación en terapia génica. El proceso de síntesis y evaluación biológica ha dado lugar a relaciones estructura/actividad interesantes (**Esquema I**).

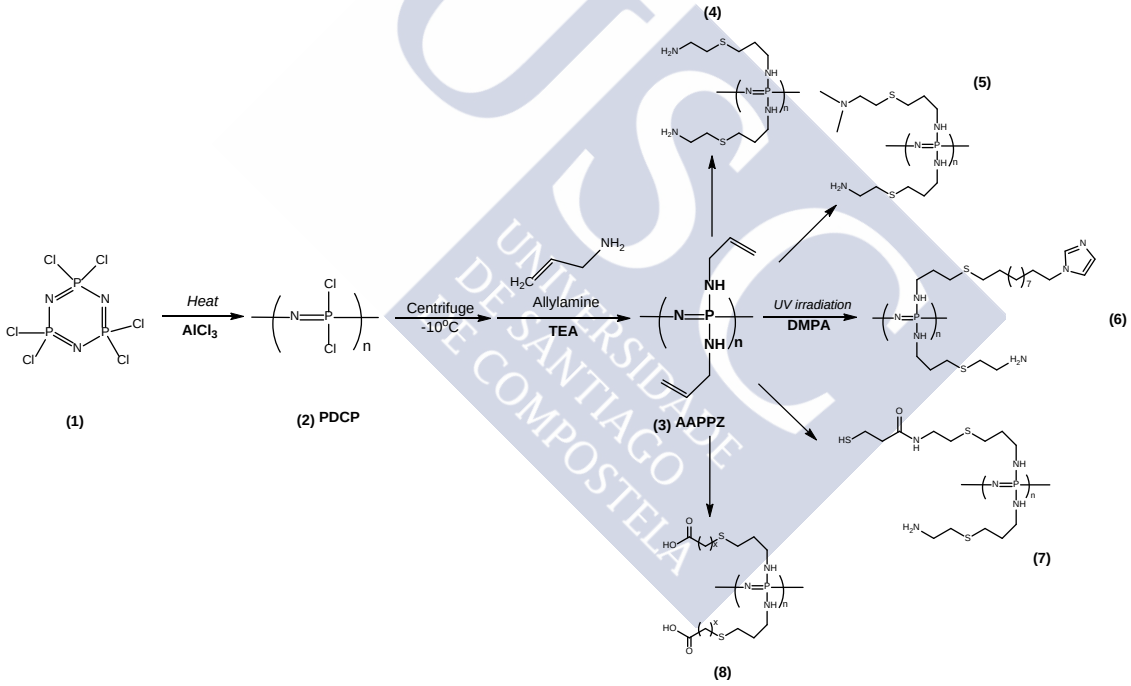

Esquema I. Polimerización de anillo-abierto de polifosfacenos y su funcionalización mediante adición click tiol-eno para aplicación en terapia génica. Adición tiol-eno de alquilamina (**4**-**5**) y mezcla de alquilamina y alquil imidazol (**6**), mezcla de alquilamina

y tiol-eno terminal modificado (**7**), y diferentes longitudes de alquilcarboxilato en el esqueleto de poli(fosfaceno) (**8**).

II. Hipótesis

Sobre la base de los conocimientos explicados, elaboramos las siguientes hipótesis:

1. Administración factible a través de tratamientos locales para GBM

En este estudio, nos centramos en cánceres altamente agresivos y malignos, Glioblastoma Multiformes (GBM) que están clasificados como grado IV por la Organización Mundial de la Salud (OMS) debido a la alta tasa de recurrencia. La cirugía es el tratamiento clínico más común si los tumores pueden extirparse, lo que permite que las administraciones locales de fármacos terapéuticos sean otro medio factible para tratar las células tumorales GBM remanentes o las células tumorales iniciales (TIC) después de la extirpación de los tumores principales.

2. Administración sistémica de genes y superación de las trampas endosómicas

En general, la composición de los vehículos de terapia génica se optimiza en base a su eficacia de transfección en cultivos celulares 2D in vitro. Sin embargo, algunas publicaciones sugieren que la optimización de las formulaciones en cuanto a su eficacia de transfección in vitro puede no ser eficiente. En estos estudios, se usan relaciones N/P más altas para conseguir una transfección génica más eficiente, pero muchas veces la transfección resulta incrementada por policationes no unidos debido a

efectos en la internalización y el escape endosomal[21-23]. En la presente tesis, seleccionamos varios polianiones sensibles al pH como un excipiente para la formación de complejos binarios poliiones/gen con una estabilidad óptima en medios complejos, donde la estabilidad de poliplexos altamente catiónicos se vería comprometida. Además, hipotetizamos que estos polianiones sensibles al pH ayudarían a los nanocomplejos a escapar de los compartimentos endo-lisosómicos mediante el mecanismo de "esponja de protones" y la disrupción de la membrana celular (**Esquema II**).

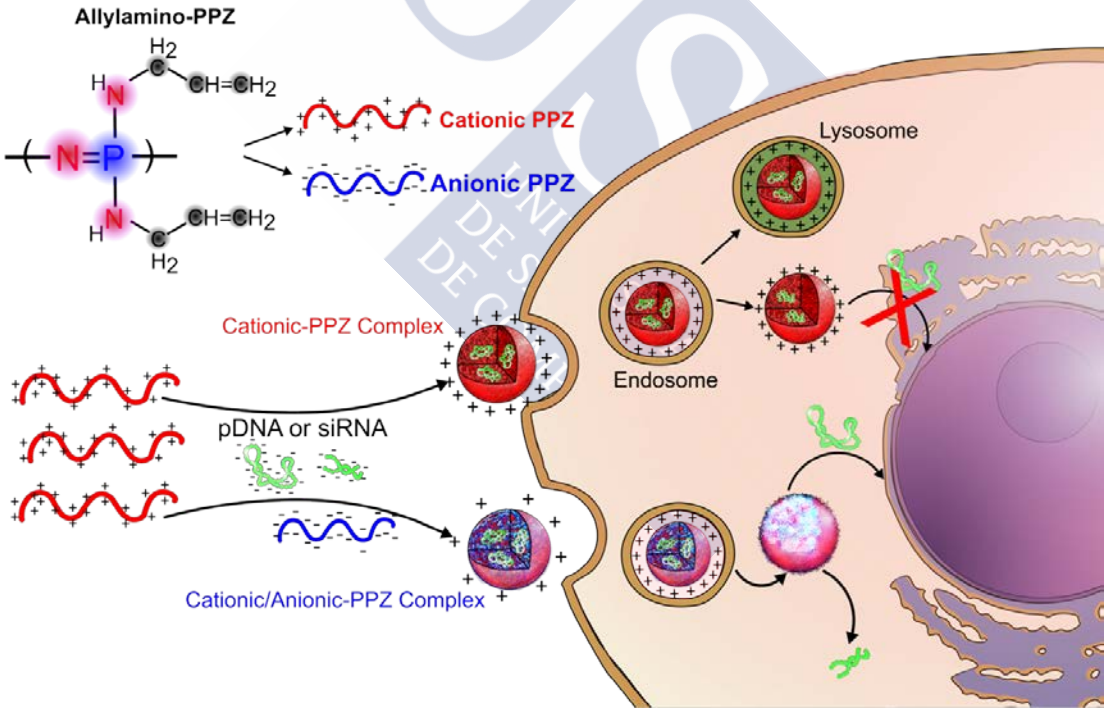

Esquema II. Polianiones sensibles a pH, el polifosfaceno (PPZ) aniónico se mezcla con los complejos de PPZ catiónico para facilitar el escape de los compartimentos endosomales y liberar el ácido nucleico.

3. Minimizar la citotoxicidad y facilitar la liberación de los vehículos

Como se ha descrito anteriormente, dos inconvenientes de los vehículos poliméricos en la administración intracelular son la toxicidad inducida por el policatión y la difícil disociación completa de los policationes y cargas génicas incluso después del escape endosómico. De la co-formulación de policationes con polianiones puede esperarse la neutralización parcial del exceso de cargas positivas de los nanocomplejos antes de la internalización, evitando daños graves a la membrana celular. Además, después de la endocitosis, el ambiente ligeramente ácido en los compartimentos endosomales sería amortiguado por los complejos poliméricos mixtos, reduciendo además la neutralización de los polianiones debido a la protonación, aumentando así las cargas positivas de los nanocomplejos así como aumentando la hidrofobicidad de los polianiones, estableciendo por tanto dos mecanismos para la disrupción de la membrana celular (**Esquema II**). En este trabajo hipotetizamos que esta acción dual de los complejos mixtos resultará en un aumento del escape endosomal así como una mejora en la eficacia de transfección.

Resumen in extenso

III. El objetivo de esta tesis

Los polímeros catiónicos se diseñaron para complejar ácidos nucleicos cargados negativamente con el objetivo de construir vehículos de terapias génicas similares a nanopartículas a través de interacciones electrostáticas hace algunas décadas. Sin embargo, la falta de suficiente estabilidad del complejo polimérico y la liberación controlada de los ácidos nucleicos en los lugares diana son las dos principales razones que limitan su aplicación en clínica. Aquí, proponemos una estrategia para complejos de polímero/gen bien condensados a través de la mezcla de policationes con polianiones en comparación con complejos de policatión tradicionales.

Obj I. Sintetizar polifosfacenos policatiónicos y polianiónicos para su uso en terapia génica

Obj II. Elaborar complejos mixtos policatión-polianión con ácidos nucleicos, analizar su nanoestructura y caracterizar sus propiedades fisicoquímicas.

Obj III. Evaluar potenciales polianiones en base a su capacidad tamponante de protones y discutir las propiedades de los complejos poliméricos para el escape endosomal mediante efectos de esponja de protones y/o disrupción de membrana.

Obj IV. Optimizar estos complejos a base de poli-iones binarios en base a su eficacia de transfección en modelos in vitro.

Obj V. Evaluar el potencial de los vehículos a base de poli-iones binarios como

agentes de transfección en modelos bio-relevantes, incluyendo modelos de esferoides 3D (modelos de GBM para mimetizar tumores recurrentes en estadíos tempranos) y modelos xenograft.

Obj VI. Realizar una prueba de concepto de la eficacia de silenciamiento de los vehículos cargados con siRNA en modelos de glioblastoma multiforme.

IV. Resultados y discusión

La estrategia para la síntesis de varios polifosfacenos sustituídos fue mediante la polimerización de anillo-abierto térmica del monómero cíclico hexaclorofosfaceno (**1**) y la reacción del poli(diclorofosfaceno) resultante con alilamina bajo condiciones básicas para permitir las cadenas laterales vinílicas[20]. Las ventajas de este precursor AAPPZ residen en su fácil derivatización tiol-eno, y aquí utilizamos esta reacción para dar lugar a una serie de policationes (**4-5**) y polianiones (**8**) (**Esquema I**). Para esta reacción, se obtuvieron altos grados de conversion (cadena lateral/grupo alílico) ≧90% y altos rendimientos de reacción (≧71%) mediante reacciones tiol-eno.

Varias cadenas laterales funcionales fueron añadidas exitosamente a los polifosfacenos. Comparados con los complejos basados únicamente en policationes (Policatión/pDNA, diámetro 80 nm, +40 mV), los complejos mixtos (Policatión/polianión/pDNA) presentaron una estructura nanométrica más compacta y una reducción de -10 mV en su carga superficial. En cultivos 2D en monocapa de células U87MG, se hizo un cribado de varias longitudes de cadenas laterales alifáticas en el polímero aniónico, obteniéndose la expresión más alta de luciferasa para el polímero sustituido con ácido 6-mercaptohexanoico en los complejos policatiónicos (**Figura I-a**). Estos resultados son consistentes con la más alta capacidad tampón del ácido 6-mercaptohexanoico dentro del rango de pH del endosoma temprano en comparación con las otras cadenas aniónicas. Además, la toxicidad del complejo mixto en 2D fue reducida en comparación con los otros complejos, probablemente debido a la neutralización de la carga. Por otro lado, la mayor parte de los PPZ polianiónicos no consiguieron aumentar la eficacia de los nanocomplejos para la liberación de genes,

con excepción del 6MHA-PPZ. Esto es probablemente debido a la capacidad específica de la estructura del 6MHA-PPZ para tamponar protones. Al analizar el mecanismo detrás del mejor funcionamiento de estos nanocomplejos, nuestros estudios han mostrado que la presencia de 6MHA-PPZ en el nanocomplejo, resulta en una menor co-localización con los compartimentos endosómicos (**Figura I-b**). Este eficiente escape endosomal está probablemente ligado a la capacidad de 6MHA-PPZ para romper las membranas celulares en el ambiente ácido de los endosomas tal y como hemos confirmado mediante tests de hemólisis (**Figura I-c**). En este trabajo, complejos integrando 6MHA-PPZ fueron los únicos que presentaron un efecto hemolítico despreciable a pH neutro, pero un efecto hemolítico comparable con poli-L-lisina (PLL) a pH ácido. Este efecto de rotura de membrana puede ser mediado por la hidrofobización de 6MHA-PPZ ya que este polímero pierde sus cargas mediante protonación entre los pH fisiológicos y endosomales. Es interesante mencionar que 6MHA-PPZ parece también capaz de mejorar la transfección celular en combinación con policationes estándar con bajas capacidades de escape endosomal como la PLL.

En comparación con los cultivos en monocapa 2D, los cultivos 3D constituyen mejores modelos de la arquitectura tisular (e.g. extracellular matrix, cell interactions)[24] y los patrones de expresión génica[25]. A día de hoy, pocos estudios han investigado la administración de ácidos nucleicos en esferoides tumorales a pesar del hecho de que constituyen adecuados modelos previos a los estudios in vivo. Según se obseva mediante imagen fluorescente tomográfica, los complejos CA-/6MHA-PPZ:pDNA, dieron lugar a una mayor transfección de los esferoides de U87MG en comparación con los compejos CA-PPZ:pDNA y los complejos de referencia PEI:pDNA; esto fue particularmente remarcable a la dosis más baja de 2 µg/mL (**Figura II-a**). Esta

eficacia incrementada fue también acompañada de una toxicidad mínima. Esta observación podría deberse a las propiedades fisicoquímicas de los complejos CA-/6MHA-PPZ:pDNA, cuyas cargas catiónicas parcialmente neutralizadas an pH fisiológico podrían apantallar al sistema de una unión indiscriminada a la matriz extracelular en los esferoides tumorales. Aunque los datos fueron más difíciles de interpretar debido a los niveles de transfección no homogéneos entre el sitio de inyección y los sitios más distales, estos resultados van en consonancia con los del experimento in vivo (**Figura II-a**).

Siguiendo las mismas condiciones del experimento piloto in vivo con GFP-pDNA, utilizamos la misma formulación optimizada para la liberación de una secuencia de siRNA con actividad conocida para suprimir las células iniciantes de glioblastoma (siRNA contra DYRK1A, siDYR)[26]. La formulación CA-/6MHA-PPZ:siDYR fue evaluada en un modelo xenograft U87MG de ratón, en un esquema terapéutico que incluye el co-tratamiento con el quimioterapéutico de primera línea temozolamida. Este experimento encontró un retraso significativo en la progresión del tumor en los ratones que recibieron TMZ y CA-/6MHA-PPZ:siDYR vs los ratones que recibieron TMZ y CA-/6MHA-PPZ complejado a una secuencia siRNA no funcional (**Figura II-b**). Por lo tanto, nuestros resultados sugieren un beneficio terapéutico en combinar la terapia génica CA-/6MHA-PPZ:siDYR con el tratamiento farmacológico estándar de glioblastoma. Futuros ensayos serán necesarios para elucidar el posible impacto clínico de esta terapia combinada en modelos más avanzados y mediante un análisis fenotípico adicional de los tumores.

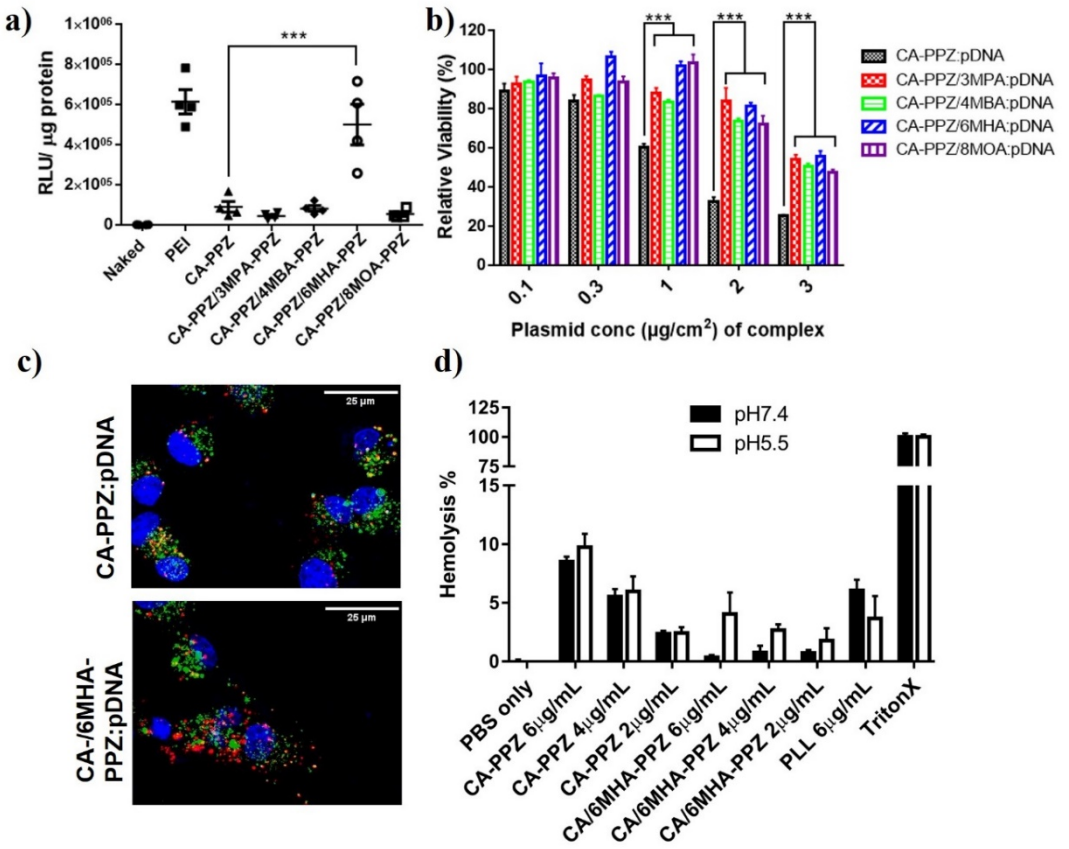

Figura I. Optimización y estudios mecanísticos de los complejos PPZ iónicos en cultivos 2D en monocapa de U87MG. (**a**) Expresión de luciferasa mediante cuantificación de las RLU/µg proteína obtenidas después de la transfección de células U87MG con los complejos CA-PPZ:pDNA (8:1 N/P ratio) y los complejos CA-PPZ/polianiónicos PPZ:pDNA (N/C/P ratio of 8:4:1, dosis de pDNA 1 µg/cm^2). Se muestra la transfección con PEI:pDNA como un control interno. (**b**) Actividad metabólica celular 48h después del tratamiento con diferentes concentraciones de los mismos complejos (**c**) Imágenes de microscopía confocal mostrando la localización intracelular del pDNA (Rojo) administrado en complejos poliméricos, con respecto al endosoma (Verde). (**d**) Estudiode hemólisis de los diferentes complejos poliméricos.

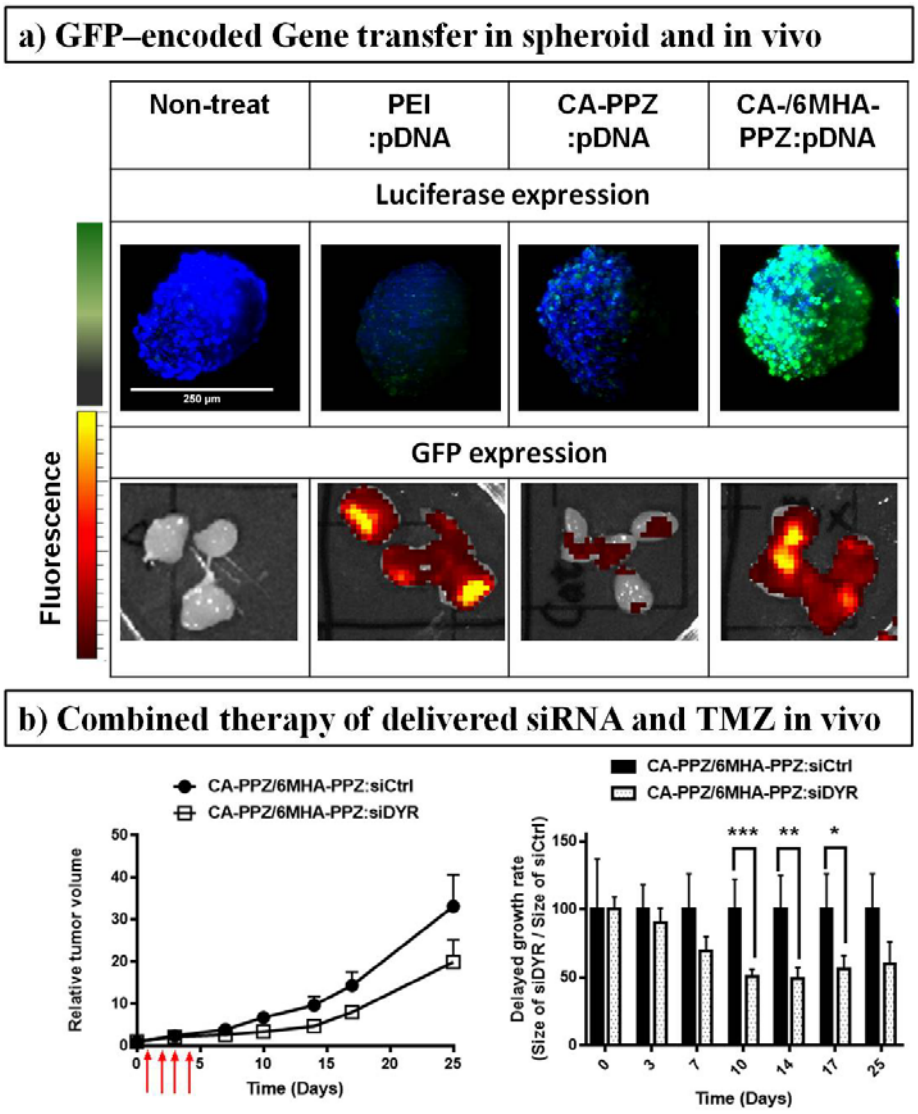

Figura II. Eficacia de los complejos PPZ en modelos de esferoide in vitro y en un modelo xenograft in vivo. **(a)** Imágenes tomográficas 3D de esferoides transfectados con GFP tomadas mediante LSFM y transfección en tumores U87MG subcutáneos mediante IVIS. (**b**) Volumen tumoral relativo en un modelo xenograft de U87MG tratado con CA-PPZ/6MHA-PPZ complejando una secuencia de siRNA terapéutica (siDYR) o scrambled (siCtrl) (16 µg por tumor) y terapia combinada con la inyección intraperitoneal de TMZ 5 mg/kg con 4 tratamientos en total.

Resumen in extenso

V. Conclusiones

Hemos desarrollado una estrategia sintética sencilla para la preparación de una pequeña librería de polifosfacenos de interés para administración de genes, basada en la generación de un polímero precursor con asas click, y su posterior derivatización mediante adiciones tiol-eno. Esta estrategia nos ha permitido testar una variedad de compuestos y llevar a cabo relaciones estructura/función. Basándonos en los cribados, hemos seleccionado un polímero con presencia de aminas primarias (CA-PPZ) y un polifosfaceno aniónico análogo (6MHA-PPZ) para la administración de pDNA. Estos complejos binarios poliión/gen mostraron una eficacia de transfección significativamente mayor que el sistema padre con sólo policatión en cultivos monocapa 2D, esperoides de U87MG 3D y un modelo xenograft subcutáneo, debido a un mejor transporte intratumoral y a unas mejores características de tráfico intracelular. Este sistema optimizado también mostró indicaciones de una mejor eficacia en comparación con complejos PEI "gold-standard", particularmente en modelos tumorales 3D. Cuando se usaron para terapias de RNA interferente, los complejos CA-PPZ/6MHA-PPZ consiguieron liberar el siRNA contra DYRK1A en células U87MG, induciendo una reducción significativa en la capacidad de auto-renovación in vitro y un efecto anti-tumoral significativo en un modelo de glioblastoma in vivo. En conclusión, estos datos describen un nuevo sistema de liberación de genes polimérico, biodegradable y versátil basado en polifosfacenos con una capacidad remarcable para la transfección celular, la penetración de tumores y con un buen perfil de acción in vivo.

VI. Bibliografía

1. Ferlay, J., *et al.* Cancer incidence and mortality patterns in Europe: estimates for 40 countries in 2012. *European Journal of Cancer* **49**, 1374-1403 (2013).
2. Shi, J., Kantoff, P.W., Wooster, R. & Farokhzad, O.C. Cancer nanomedicine: progress, challenges and opportunities. *Nature Reviews Cancer* **17**, 20 (2017).
3. Torre, L.A., *et al.* Global cancer statistics, 2012. *CA: a cancer journal for clinicians* **65**, 87-108 (2015).
4. Pattabiraman, D.R. & Weinberg, R.A. Tackling the cancer stem cells—what challenges do they pose? *Nature Reviews Drug Discovery* **13**, 497-512 (2014).
5. Bar-Zeev, M., Livney, Y.D. & Assaraf, Y.G. Targeted nanomedicine for cancer therapeutics: Towards precision medicine overcoming drug resistance. *Drug Resistance Updates* **31**, 15-30 (2017).
6. Huang, W., *et al.* Nanomedicine-based combination anticancer therapy between nucleic acids and small-molecular drugs. *Advanced drug delivery reviews* **115**, 82-97 (2017).
7. Zelikin, A.N., Ehrhardt, C. & Healy, A.M. Materials and methods for delivery of biological drugs. *Nat Chem* **8**, 997-1007 (2016).
8. Kanasty, R., Dorkin, J.R., Vegas, A. & Anderson, D. Delivery materials for siRNA therapeutics. *Nat Mater* **12**, 967-977 (2013).
9. Yin, H., *et al.* Non-viral vectors for gene-based therapy. *Nature Reviews Genetics* **15**, 541-555 (2014).
10. Titze-de-Almeida, R., David, C. & Titze-de-Almeida, S.S. The Race of 10 Synthetic RNAi-Based Drugs to the Pharmaceutical Market. *Pharmaceutical Research* **34**, 1339-1363 (2017).
11. Chen, J., Guo, Z., Tian, H. & Chen, X. Production and clinical development of nanoparticles for gene delivery. *Molecular therapy. Methods & clinical development* **3**, 16023 (2016).
12. Scholz, C. & Wagner, E. Therapeutic plasmid DNA versus siRNA delivery: Common and different tasks for synthetic carriers. *Journal of Controlled Release* (2012).
13. Krivitsky, A., *et al.* Structure–Function Correlation of Aminated Poly(α)glutamate as siRNA Nanocarriers. *Biomacromolecules* **17**, 2787-2800

(2016).

14. Moghimi, S.M. & Wagner, E. Nanoparticle Technology: Having Impact, but Needing Further Optimization. *Molecular Therapy* **25**, 1461-1463 (2017).
15. Lachelt, U. & Wagner, E. Nucleic Acid Therapeutics Using Polyplexes: A Journey of 50 Years (and Beyond). *Chemical Reviews* **115**, 11043-11078 (2015).
16. Cohen, R.N., van der Aa, M.A., Macaraeg, N., Lee, A.P. & Szoka, F.C. Quantification of plasmid DNA copies in the nucleus after lipoplex and polyplex transfection. *Journal of Controlled Release* **135**, 166-174 (2009).
17. Brunner, S., Fürtbauer, E., Sauer, T., Kursa, M. & Wagner, E. Overcoming the nuclear barrier: cell cycle independent nonviral gene transfer with linear polyethylenimine or electroporation. *Molecular Therapy* **5**, 80-86 (2002).
18. Hirschhaeuser, F., *et al.* Multicellular tumor spheroids: an underestimated tool is catching up again. *Journal of biotechnology* **148**, 3-15 (2010).
19. Chauhan, V.P. & Jain, R.K. Strategies for advancing cancer nanomedicine. *Nat Mater* **12**, 958-962 (2013).
20. Qian, Y.C., *et al.* A versatile approach to the synthesis of polyphosphazene derivatives via the thiol–ene reaction. *Journal of Polymer Science Part A: Polymer Chemistry* **50**, 5170-5176 (2012).
21. Yue, Y., *et al.* Revisit complexation between DNA and polyethylenimine—effect of uncomplexed chains free in the solution mixture on gene transfection. *Journal of Controlled Release* **155**, 67-76 (2011).
22. Dai, Z., Gjetting, T., Mattebjerg, M.A., Wu, C. & Andresen, T.L. Elucidating the interplay between DNA-condensing and free polycations in gene transfection through a mechanistic study of linear and branched PEI. *Biomaterials* **32**, 8626-8634 (2011).
23. Boeckle, S., *et al.* Purification of polyethylenimine polyplexes highlights the role of free polycations in gene transfer. *The journal of gene medicine* **6**, 1102-1111 (2004).
24. Enam, S.A. & Klaus, E. Role of extracellular matrix in tumor invasion: migration of glioma cells along fibronectin-positive mesenchymal cell processes. *Neurosurgery* **42**, 599-608 (1998).
25. Hamer, P.D.W., *et al.* The genomic profile of human malignant glioma is altered early in primary cell culture and preserved in spheroids. *Oncogene* **27**, 2091 (2008).
26. Pozo, N., *et al.* Inhibition of DYRK1A destabilizes EGFR and reduces EGFR-dependent glioblastoma growth. *The Journal of clinical investigation*

123, 2475-2487 (2013).

General introduction

USC
UNIVERSIDADE
DE SANTIAGO
DE COMPOSTELA

I. Background and Introduction

Polymer-gene delivery in need for cancer therapy

Cancer has become a leading death cause in the 21th century and several limitations and issues in conventional therapies, currently causing poor therapeutic efficacy and low survival rate of treated patients[1]. This highly gene-disorder disease developed own self-protection mechanisms, like multi-drug resistance and anti-apoptosis mutation, self-renewal and metastatic capacities, resulting in ineffective anticancer treatments and discounting therapeutic index[2-4]. Herein, their genomic mutation emphases the importance of gene therapy[5]. Current successes in clinical trials and many emerging novel therapies based on polynucleotides are driving an urgent demand for more efficient and safer gene carriers[6-8]. While viral-based gene delivery is the most advanced in terms of number of clinical trials[9], there are still concerns over long-term safety of viral vectors, and many of the new polynucleotides are easier to integrate in non-viral gene delivery systems. Among them, polymer-based gene systems have several advantages over viral vectors, such as their potential safety, large-scale production, and easy preparation and modification, providing a number of promising results in clinical trials[10]. However, there remain several limitations for polymer-based gene vehicles in practical applications[11-14], including efficient delivery to targeting locations and a trade-off between gene protection before and unloading of nucleic acids after arriving at the destinations. Polycation-mediated gene delivery takes advantages on electrostatic charging tendency to pass through cell membranes and even attach on nuclear membranes, benefiting on intracellular delivery[15,16]. However,

the polycation-driven membrane disruption brings unwanted toxic effects and slow dissociation of polycations and nucleic acids with reduced gene-transferring efficiency[17]. Taken together, design criteria that are yet unfulfilled in most synthetic polymer-gene carriers include: (a) stability, biocompatibility and biodegradability, (b) selective biodistribution and adequate pharmacokinetics, (c) ability to surmount tissue and extracellular barriers, (d) transport across intracellular barriers and organelle-specific release.

The needs for hybrid polyions complexes in gene delivery

For electrostatic assembly of complexes in gene delivery applications, cationic polymers and negatively charged nucleic acids are required to be mixed properly to construct nanoparticle-like vehicles. Polyethylenimine (PEI) is the most intensively investigated polycation and can complex with pDNA when N/P ratio ≥ 3, but for significant *in vitro* transfection prior reports have shown that ratios of N/P ≥ 10 for PEI/nucleic acids are needed for efficacy in several tumour cell lines [18,19]. These excess PEI is necessary to facilitate internalisation and intracellular delivery, no matter whether the excess PEI is free in solution or added in advance with the PEI-complex at N/P = 3. In this “polymer-mediated” transfection, the extra cationic polymers promote transfection but can also cause unwanted side effects. More importantly, excess polycation is not such effective in vivo, as unbound polycations may be sequestered by interstitial fluids or be retained in extracellular matrices[20]. In this thesis, we have proposed a strategy for avoiding excess polycation-mediated side effects by utilising well-condensed polymer/gene complexes formed via mixing polycation with synthetic anionic polymers in addition to the polyanionic nucleic acids, and have compared these “mixed polyplexes” with traditional polycation-only complexes in gene delivery.

Extension of biodegradable polyphosphazene flexibility

Polyphosphazenes have been considered promising materials for gene delivery since they combine biodegradability and great chemical flexibility for meeting those above-mentioned criteria. It was envisaged that such flexibility would be ideal for generating combinatorial chemistry screens to optimize polymer structure. Still, their application for gene delivery has remained relatively scarce because the main synthetic route for polymer modification, the nucleophilic substitution of the precursor poly(dichlorophosphazene), is problematic for most derivatives of interest. The reason is that functional groups with several nucleophilic centres (i.e. amines, hydroxides, carboxylic acids, etc.) used in gene therapy will cross-link the precursor polymer. Inspired by recent reports[21] that proposed the potential introduction of click handles in PPZs, this thesis further demonstrates that introduction of a vinyl group through the formation of a secondary polymer precursor, allylamino-poly(phosphazene) (AAPPZ), enables its simple modification with functional groups of interest for gene delivery using a thiol-ene addition reaction. By this method, PPZs with primary amines can be synthesized without any protection/deprotection processes, and a small library of other derivatives with tertiary amines or carboxylic acid pendent groups (**Scheme I**). The streamlined synthetic process has drawn interesting structure/performance relationships. The scheme showed all functional polymers derived from allyl-modified PPZ we synthesized, but only cationic (**4, 5**) and anionic (**8**) side-groups introduced PPZ are deeply discussed in this thesis.

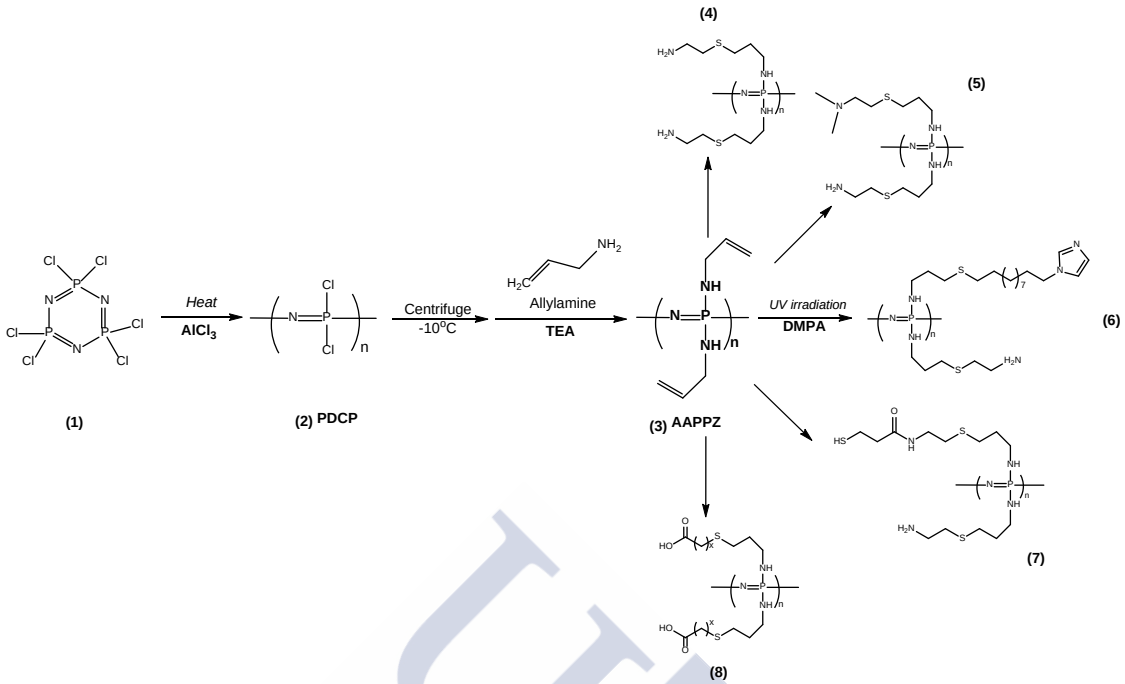

Scheme I. Ring-opening polymerisation of polyphosphazene and functionalisation by thiol-ene click addition for gene delivery applications. Thiol-ene addition of alkylamine (**4**-**5**) and mixing alkylamine and alkyl imidazole (**6**), mixing alkylamine and thiol-ene modified terminals (**7**), and different lengths of alkylcarboxylate on polyphosphazene backbone (**8**).

II. Hypothesis

On the basis of general knowledge in clinical use and pharmaceutical science, we set out the following hypotheses to test:

1. Feasible administration via local treatments for GBM

In this study, we focus on highly aggressive and malignant cancers, Glioblastoma Multiformes (GBM), which are classified as grade IV by the World Health Organization (WHO) due to their high rate of recurrence[3]. Surgery is the most typical clinical treatment if the tumours can be excised, allowing local administrations of therapeutic drug to treat leftover GBM tumour cells or tumour initial cells (TIC) after primary tumour excision. As this accessible administration, we design an intra-tumoural injection of our polymeric gene vehicles for gene therapy application.

2. Systemic gene delivery and overcome endosomal traps

In general, the best formulation composition ratios of polymer gene-carriers are usually defined from the highest transfection efficiencies obtained in 2D in vitro cultures. However, some literature reports have indicated problems for formulation optimization regarding in vitro transfection. Higher N/P ratios are used for higher efficiency of gene transfection until dose-induced toxicity, in which unbound polycations however facilitated the carriers for internalisation and endosomal escape.[18,19,22] Herein, we screen various pH-responsive polyanions as an excipient to mediate the electrostatic driving force for formation of binary polyions/gene

complexes and their stability in complex media where highly positively-charged conventional polymer complexes would be sub-optimal. In addition, we hypothesize that these pH-responsive polyanions would help the nanocomplexes to escape from endolysosomal compartments via a 'proton-sponge' mechanism and membrane disruption (**Scheme II**).

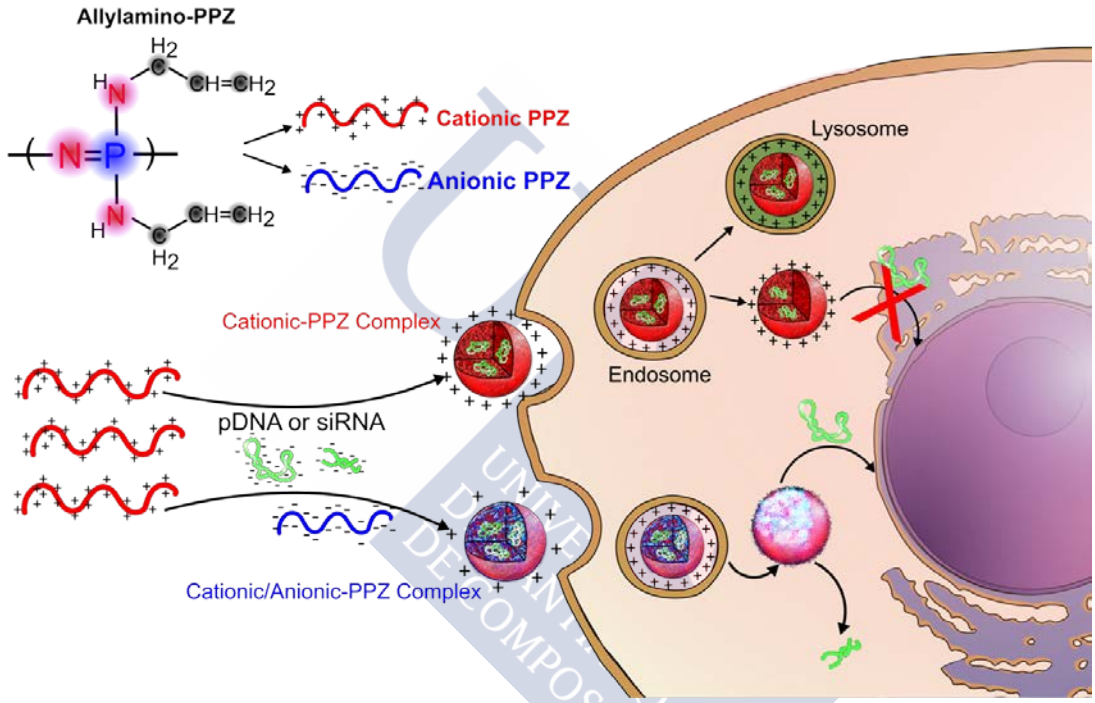

Scheme II. pH-sensitive polyanionic polyphosphazene (PPZ) mixing into polycationic complexes for facilitating escape from endosomal compartments and release of nucleic acids.

3. Minimize cytotoxicity and release efficiency from vehicles

As described above, two drawbacks of current polymers in used for nucleic acid delivery are polycation-induced toxicity and the difficulty in ensuring complete dissociation of polycations and gene cargos even after endosomal escape.

Co-formulation of polycations as well as polyanions can be expected to neutralize partially the excess positive charges on the nanocomplexes before internalisation, avoiding serious damages to cell membrane. Furthermore, after endocytosis, the acidified environments in the intracellular digestive endosomal compartments would be buffered by mixed polyanion/polycation complexes as well as reduce neutralization by the polyanions due to protonation, increasing the positive charges on the polymeric complexes as well as enhancing the hydrophobicity of the polyanions, thus establishing two mechanisms for disrupting intercellular membranes (**Scheme II**). We hypothesize that this dual action of the mixed complexes will result in enhancement of endosomal escape and improved overall transfection.

III. The objective of this thesis

In general, cationic polymers that designed for complexation with negatively charged nucleic acids to construct nanoparticle-like gene vehicles via electrostatic interactions are well-established in the pharmaceutical science literature. However, the lack of systemic stability of conventional polymer-gene complexes and controlled release of the nucleic acid cargo once at the targeting locations are two of the main reasons for delay in clinical applications[18,19]. Herein, we propose a strategy for enhanced efficacy of polymer/gene complexes through the mixing of polycations with additional polyanions during the complexation stage with nucleic acids.

Obj I. To synthesize polycationic and polyanionic polyphosphazenes via click-chemistry addition for use in polymeric gene delivery

Obj II. To establish mixed polycation and polyanion nanocomplexes with nucleic acids and to analyse their nanostructure and particle characterisation.

Obj III. To evaluate potential polyanions as suggested by proton-buffering capacity and to discuss that facilitated polymeric complexes escaping from endosomal compartments through proton-sponge effects and/or membrane disruption.

Obj IV. To optimize these binary-polyions gene complexes by transgene efficiency in vitro models.

Obj V. To evaluate the optimal binary-polyions vehicles as gene transfection agents in

bio-relevant models, including 3D spheroid models (GBM models for mimicking early stage tumour in recurrence) and xenograft models.

Obj VI. To provide a proof-of-concepts for gene silence therapy by using the optimal polymer carriers delivering siRNA in a xenograft GBM tumour model.

References

1. Ferlay, J., *et al.* Cancer incidence and mortality patterns in Europe: estimates for 40 countries in 2012. *European Journal of Cancer* **49**, 1374-1403 (2013).
2. Eramo, A., *et al.* Chemotherapy resistance of glioblastoma stem cells. *Cell death and differentiation* **13**, 1238 (2006).
3. Kelly, P.J. Gliomas: survival, origin and early detection. *Surgical neurology international* **1**(2010).
4. Van Meir, E.G., *et al.* Exciting new advances in neuro-oncology: the avenue to a cure for malignant glioma. *CA Cancer J Clin* **60**, 166-193 (2010).
5. Bar-Zeev, M., Livney, Y.D. & Assaraf, Y.G. Targeted nanomedicine for cancer therapeutics: Towards precision medicine overcoming drug resistance. *Drug Resistance Updates* **31**, 15-30 (2017).
6. Zelikin, A.N., Ehrhardt, C. & Healy, A.M. Materials and methods for delivery of biological drugs. *Nat Chem* **8**, 997-1007 (2016).
7. Kanasty, R., Dorkin, J.R., Vegas, A. & Anderson, D. Delivery materials for siRNA therapeutics. *Nat Mater* **12**, 967-977 (2013).
8. Yin, H., *et al.* Non-viral vectors for gene-based therapy. *Nature Reviews Genetics* **15**, 541-555 (2014).
9. Titze-de-Almeida, R., David, C. & Titze-de-Almeida, S.S. The Race of 10 Synthetic RNAi-Based Drugs to the Pharmaceutical Market. *Pharmaceutical Research* **34**, 1339-1363 (2017).
10. Chen, J., Guo, Z., Tian, H. & Chen, X. Production and clinical development of nanoparticles for gene delivery. *Molecular therapy. Methods & clinical development* **3**, 16023 (2016).
11. Scholz, C. & Wagner, E. Therapeutic plasmid DNA versus siRNA delivery: Common and different tasks for synthetic carriers. *Journal of Controlled Release* (2012).
12. Krivitsky, A., *et al.* Structure–Function Correlation of Aminated Poly(α)glutamate as siRNA Nanocarriers. *Biomacromolecules* **17**, 2787-2800 (2016).
13. Moghimi, S.M. & Wagner, E. Nanoparticle Technology: Having Impact, but Needing Further Optimization. *Molecular Therapy* **25**, 1461-1463 (2017).
14. Lachelt, U. & Wagner, E. Nucleic Acid Therapeutics Using Polyplexes: A Journey of 50 Years (and Beyond). *Chemical Reviews* **115**, 11043-11078 (2015).
15. Cohen, R.N., van der Aa, M.A., Macaraeg, N., Lee, A.P. & Szoka, F.C. Quantification of plasmid DNA copies in the nucleus after lipoplex and polyplex

transfection. *Journal of Controlled Release* **135**, 166-174 (2009).

16. Brunner, S., Fürtbauer, E., Sauer, T., Kursa, M. & Wagner, E. Overcoming the nuclear barrier: cell cycle independent nonviral gene transfer with linear polyethylenimine or electroporation. *Molecular Therapy* **5**, 80-86 (2002).
17. Ong, S.-M., *et al.* Engineering a scaffold-free 3D tumor model for in vitro drug penetration studies. *Biomaterials* **31**, 1180-1190 (2010).
18. Boeckle, S., *et al.* Purification of polyethylenimine polyplexes highlights the role of free polycations in gene transfer. *The journal of gene medicine* **6**, 1102-1111 (2004).
19. Yue, Y., *et al.* Revisit complexation between DNA and polyethylenimine—effect of uncomplexed chains free in the solution mixture on gene transfection. *Journal of Controlled Release* **155**, 67-76 (2011).
20. Chauhan, V.P. & Jain, R.K. Strategies for advancing cancer nanomedicine. *Nat Mater* **12**, 958-962 (2013).
21. Qian, Y.C., *et al.* A versatile approach to the synthesis of polyphosphazene derivatives via the thiol–ene reaction. *Journal of Polymer Science Part A: Polymer Chemistry* **50**, 5170-5176 (2012).
22. Dai, Z., Gjetting, T., Mattebjerg, M.A., Wu, C. & Andresen, T.L. Elucidating the interplay between DNA-condensing and free polycations in gene transfection through a mechanistic study of linear and branched PEI. *Biomaterials* **32**, 8626-8634 (2011).

USC
UNIVERSIDADE
DE SANTIAGO
DE COMPOSTELA

Abbreviation List

Abbreviated name	Full name
^{1}H-DOSY	^{1}H Diffusion-ordered spectroscopy
7-AAD	7-Aminoactinomycin D
AAPPZ	Allylamino-substituted polyphosphazene (**3**)
3MPA-PPZ	3-Mercaptopropanoic acid introduced on AAPPZ (x=2 at structure **8**)
4MBA-PPZ	4-Mercaptobutanoic acid introduced on AAPPZ (x=3 at structure **8**)
6MHA-PPZ	6-Mercaptohexanoic acid introduced on AAPPZ (x=5 at structure **8**)
8MOA-PPZ	8-Mercaptooctanoic acid introduced on AAPPZ (x=7 at structure **8**)
CA-PPZ	Cysteamino-introduced on AAPPZ (**4**)
CA-PPZ complex	Complexes of CA-PPZ with pDNA
CA-/6MHA-PPZ complex	Complexes of CA-PPZ and 6MHA-PPZ with pDNA
Cy3 ; Cy5	Cyanine 3; Cyanine 5
Diglyme	Diethylene glycol dimethyl ether
DLS	Dynamic light scattering
DMAES-PPZ	2-(dimethylamino)ethanethiol side-chain addition on AAPPZ
DYRK1A	Dual specificity tyrosine-phosphorylation-regulated kinase 1A
ECM	Extracellular matrix
EGFP	Enhanced green fluorescent protein
EGFR	Epidermal growth factor receptor
FRET	Förster resonance energy transfer
GBM	Glioblastoma multiforme
GICs	glioblastoma initiating cells
HEPES	4-(2-hydroxyethyl)-1-piperazineethanesulfonic acid
IVIS	In Vivo Imaging Instruments
KCPs	Kilo counts per second, which is an unit of total derived count
LSFM	Light-sheet based fluorescent microscopy
RBC	Red blood cells
N/P ratio	The ratio of polycationic amines (N) to negative DNA phosphates (P)

N/C/P ratio	The ratio of polycationic amines (N), polyanionic carboxylates (C) and negative DNA phosphates (P)
NTA	Nanoparticle Tracking Analysis
PDCP	Poly(dichlorophosphazene)
pDNA	Plasmid DNA
PEI	Polyethylenimine
PLL	Poly-L-lysine
PPZ	Polyphosphazene
RLU	Relative luminometer units
ROIs	The regions of interest
siCtrl	a scramble sequence of siRNA as control
siDYR	siRNA against DYRK1A
TIC	Tumour initial cells
TMZ	Temozolomide

Chapter I / Capítulo I

Literature Reviews of Polymer-based designs on gene delivery

Chapter I / Capítulo I

Abstract

Gene delivery is one of the most ancient processes on earth, as it is central to the lifecycle of all organisms. In addition, viruses and bacteria utilise certain aspects of gene delivery for infection of higher organisms. Synthetic gene delivery is of particular importance for medical applications, and a wide range of different vectors have been used to enhance delivery of therapeutic gene. Viral-based gene carriers have been the most investigated vectors in clinical trials, but the drawbacks of viral vectors still limit the range of medical applications. Non-viral gene vehicles, particularly lipid-based vehicles or polymeric carriers have advantages in gene delivery because of their low-risk of immunogenicity and carcinogenicity compared to viral counterparts. In this chapter, we firstly introduce the general field of gene therapy and its clinical progress, and then we focus on polymeric gene delivery and discuss the related challenges of non-viral gene delivery in practice.

Chapter I / Capítulo I

1.1 Gene delivery

Gene delivery involves the transfer of foreign nucleic acids to host cells, and therapies based on this concept hold promise for gene-associated human diseases, such as cancers, neurodegenerative disorders and cystic fibrosis. However, there are many biological barriers that significantly hinder delivery of exogenous nucleic acids to target locations and the nucleic acids (DNA, RNA) themselves are fragile and rapidly degraded by enzymes (e.g. nucleases). There is a clear motivation for developing materials or carriers that can protect nucleic acids during formulation, administration to the body, and in transit across the many biological barriers before precisely delivering therapeutic genes to their targets. These gene carriers, or vectors can be generally divided to two main classes, i.e. viral vectors and non-viral carriers, and both methods have been applied for systemic delivery in clinical trials [1,2].

Viruses are one of the most ancient biological agents and have evolved over billions of years on earth, developing highly efficient approaches to deliver their genomes to many different host cells. Scientist have employed viruses as vehicles for gene delivery since the 1970s[3] and engineered various viruses as gene carriers including adenoviruses, adeno-associated viruses (AAVs), lentiviruses, and retroviruses. In the last decade, around 70% of clinical trials in gene therapy have utilised viral vehicles[4]. As shown in **Figure 1-1**, adenoviruses are the most commonly used vehicle in the data-base, with an early example being a treatment for the genetic disorder ornithine transcarbamylase deficiency. However, in this particular case, a young patient died due to severe inflammation and multi-organ failures[5]. After that, problems relating to pre-existing immune response, the effectiveness of certain viruses integrating into the

human genome, and long-term safety have increased concerns relating to viral-based gene therapy. In addition, although recent vectors of lentivirus and adeno-associated virus (AAV) have shown improved clinical safety[1], several innate drawbacks of viral gene vectors still remain. These include immunogenicity and carcinogenicity, low genetic payloads, and the high cost of viral vector production at scale. These limitations are driving research into synthetic nucleic acid carriers.

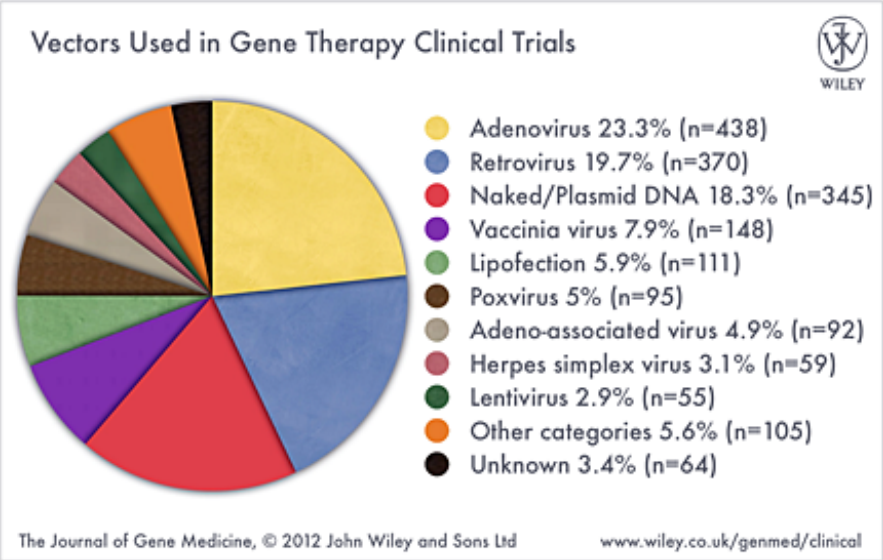

Figure 1-1 Gene vehicles used in clinical trials from 1989 to 2012.[4] [Reproduced from Ginn et al, J Gene Med 2013; 15: 65–77, with a Creative Commons license.].

Non-viral gene delivery approaches generally include two categories based either on physical or chemical methods (**Figure 1-2**)[6]. In terms of the physical methods, jet injection, ultrasound and biolistics have all been used to generate transient holes in cell membranes or on tissue boundaries, allowing gene transfer directly into the cytoplasm of host cells. Fine needle puncture and electric impulses have also been employed for bypassing the known barriers to delivery, and have been very effective for single or multiple cells. However, the low amount of delivered nucleic acids and the high costs of

a delivery method which is difficult to use in large-scale have limited clinical applications to date.

Chemical methods of gene delivery have advantages relative to viral vectors, including safety profile, higher gene loading capacity, and potential for large-scale production. In general, for these vectors, cargos of DNA or RNA are condensed or packaged in complexes / encapsulates via electrostatic interactions and the resulting 'polyplexes' are able to pass through cell membranes via a range of endocytic pathways. Materials used for gene carriers of this type include natural molecules, such as cationic lipids (which form so-called Lipoplexes) and both synthetic and natural polymers which form polyelectrolyte complexes (Polyplexes) with polyanionic nucleic acids. Other complexes can be formed by addition of the nucleic acids to inorganic salts containing di- or multivalent cations such as calcium phosphates.

Polyelectrolyte formulations from these polycation-nucleic acid complexes can be produced as suspensions of virus-sized particles (< 100 nm) but with low-risks of immunogenicity and carcinogenicity. These artificial nanoscale carriers are able to upload larger amount of genetic payloads and various kinds of gene sequences than viral analogues [7,8]. In addition, the risk of those artificial gene carriers in human tests can be evaluated prior to clinical trials, an advantage compared with viral vectors. However, poor efficiency in delivery, attributable to the inability to cross all the biological barriers in routes to target cells and organelles, is still a problem for non-viral vectors, promoting scientists and engineers to endeavour to address those issues[9].

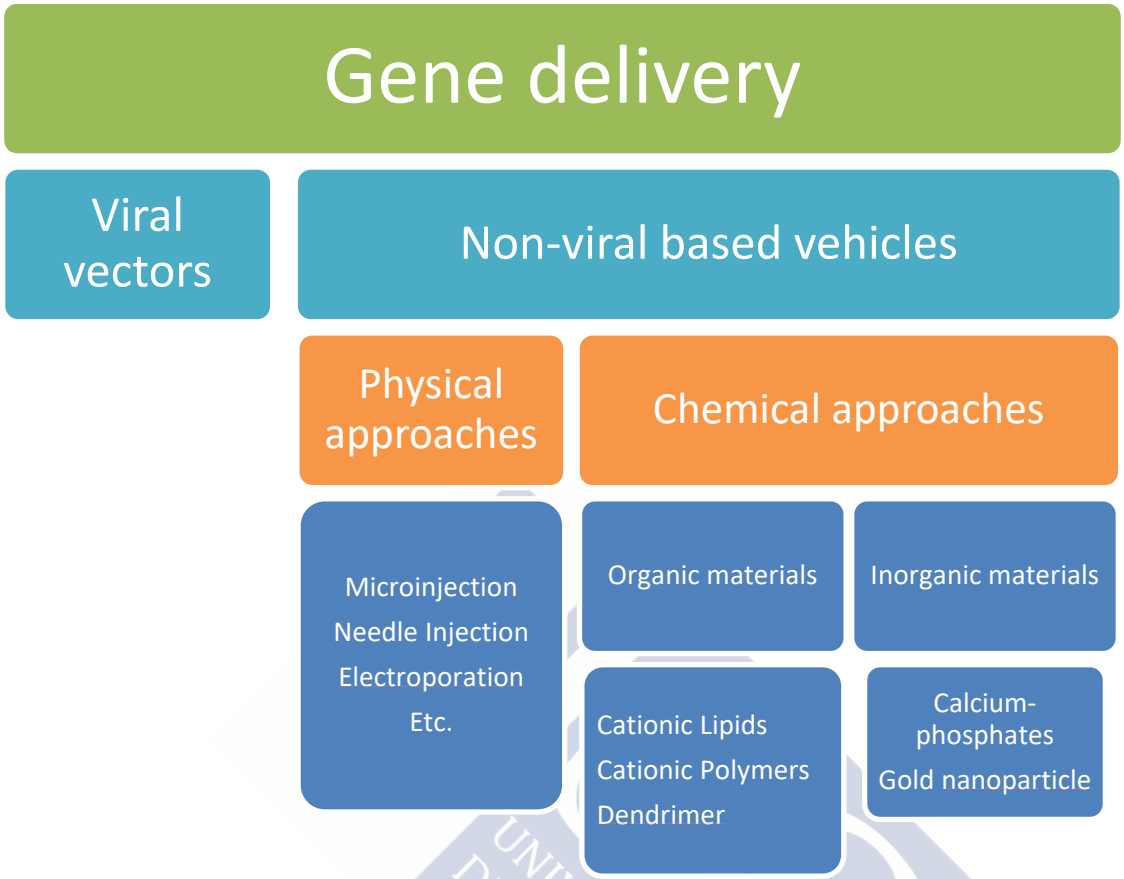

Figure 1-2. General summary of gene delivery vehicles and categorized by synthesis methods and internalisation approaches[10].

1.2 Nanoparticle-based gene delivery

In terms of chemical gene delivery methods, nanoparticle-based gene delivery systems are defined as nanoscale (1-200 nm) vehicles loaded nucleic acids. Nanoparticles of this type exhibit large surface area-to-volume ratios, and with appropriate surface chemistries can display prolonged half-life, and increasing bioavailability[11]. In the last decade, many formulations or agents have been developed for gene delivery, including organic materials (lipid-based and polymer-based vehicles, dendrimers, etc.) and inorganic carriers (calcium phosphate precipitation, gold/silver particles, etc.). Herein, we focus on introduction of lipid-based and polymer-based carriers, which have had promising results in clinical studies in the recent years [9].

Lipid-based nanoparticles (LNP) contain cationic lipids, and form micelle-like or liposome-like structures, for example the cationic lipid DOTMA (1,2-di-O-octadecenyl-3-trimethylammonium propane) is used in Lipofectin™ and DOSPA (2,3-Dioleyloxy-N-[2(sperminecarboxamido)ethyl]-*N*,*N*-dimethyl-l-propanaminium trifluoroacetate) is one of components in LipofectAMINE™, as shown in **Scheme 1-1**. By virtue of these cationic lipids, the positively charged LNP can condense various nucleic acids plasmid DNA (pDNA), small interfering RNA (siRNA), microRNA (miRNA), antisense oligonucleotides (ODNs), etc., and protect their gene cargos from degradation by nucleases, forming a nanoscale carrier (≥ 200 nm in diameter). Within commercial reagents for in vitro transfection, LipofectAMINE™ series are the most commonly used LNP as transfection reagents. In clinical trials, LNP formulations have shown advances, for example Patisiran (ALN-TTR02) which recently completed a

clinical study in phase III for patients with Transthyretin (TTR)-Mediated Amyloidosis, and commenced Expanded Access Protocol Study

As shown in **Table 1-1**, polymer-based gene delivery is a term referring to polymer mediated targeting gene in host cells, using synthetic polymers, such as polyethylenimine (PEI), polyethylene glycol (PEG), poly-L-lysine (PLL)[12], poly(β-amino ester) (PBAE)[13], poly[(2-dimethylamino) ethyl methacrylate] (pDMAEMA) [14], polyamidoamine (PAMAM) dendrimers [15], or natural macromolecules, like protamine, chitosan[16], etc. (**Scheme 1-1**).[8] The general principle is that cationic polymers condense negatively charged nucleic acids via ionic attraction, forming nanoparticle-like carriers. Among the first cationic polymer employed for condensing DNA for gene delivery was PLL, which is a biodegradable polypeptide and readily available polypeptide [17]. However, relatively low transfection efficiencies of some PLL/pDNA vehicles were found, attributable to trapping of PLL/pDNA in endosomes and lysosomes[18]. One of the reasons is that PLL polymers lack amine groups with appropriate buffering capacity for the endosomal range (pH7.4 - 5.5), as shown in **Figure 1-3**.

Polyethylenimine (PEI) is recognized as one of the most widely-used cationic polymers. Although the repeating units are simple, PEI as commercially available contains primary, secondary, and tertiary amines, providing different buffering capacities across different pH environments, which included those of endosomal compartments (**Figure 1-3**). In light of the simple repeating structure of PEI and desired outcomes of endosomal escape, PEI has become one of gold standard agents for in vitro transfection. However, PEI/gene complexes also have their limitations: firstly, the lower

stability of PEI-gene vehicles compared to PLL-complexes may limit protection of nucleic acids from nuclease degradation during delivery. It is especially important when PEI complexes carry siRNA, in comparison with pDNA[19-21]. Secondly, PEI is a non-degradable polymer, with potential side effects resulting from intracellular accumulation. Thirdly, a stoichiometric excess of PEI polymer is usually necessary in gene transfection for facilitating internalisation and endosomal escape, but this excess causes unwanted toxicity [22]. Despite those drawbacks, poly(ethylenimine) derivatives have inspired many studies, such as conjugation of repeating units of ethylenimine on biodegradable polymers for facilitating endosomal escape. For examples, Prof. Kataoka and his co-workers found conjugation of even numbers of ethylenimine units (two or four repeat units) on biodegradable polyaspartamides can improve gene-transferring efficiency due to endosomolytic effects [23]. Crosslinking of PEI polymer chains via disulfide bonds can stabilize the complexes in physiological ionic strength solution [24] and reduce PEI-caused toxicity[25]. Moreover, glucose has also been conjugated with four ethylenimine repeating units for significantly reducing cytotoxicity and those structures of glucose-linked ethylenimines are identical to the commercial reagent (Glycofect^{TM}) [26].

Although there are many doubts regarding non-degradable PEI, PEI-based gene carriers still account for most clinical trials of polymeric gene delivery (**Table 1-1**). PEI-related reagents for in vitro transfection or in vivo experiments are also commercially available, such as linear PEI commercial reagent (Jet-PEI) or saccharide-conjugated repeating ethylenimines (Glycofect^{TM}). In preclinical studies, intratumoral injection of PEI/DNA complexes showed promising luciferase gene transferring efficiency [27]. In human studies (**Table 1-1**), PEI/DNA complexes (BC-819

from BioCancell) are in phase II trials for bladder cancer via local administration. The preliminary results showed both safety and efficacy: BC-819/PEI complexes were well-tolerated and showed ability to regress tumours in 72% patients. Furthermore, EGEN-001 (an IL-12 plasmid) delivered by PEG–PEI–cholesterol lipo-polymer treated patients with platinum-resistant recurrent ovarian cancer and combined chemotherapeutic drugs for colorectal-cancer patients following cytoreductive surgery and hyperthermic intraperitoneal chemotherapy therapy (HIPEC).

Taken together, there are potentially promising clinical trials of lipid-based and polymer-based gene delivery ongoing. In comparison with viral gene delivery, nanoparticle-based vehicles can reduce unwanted severe acute toxicity and unexpected long-term side effects, but still lack efficient delivery and transfection potency to desire levels in clinical trials.

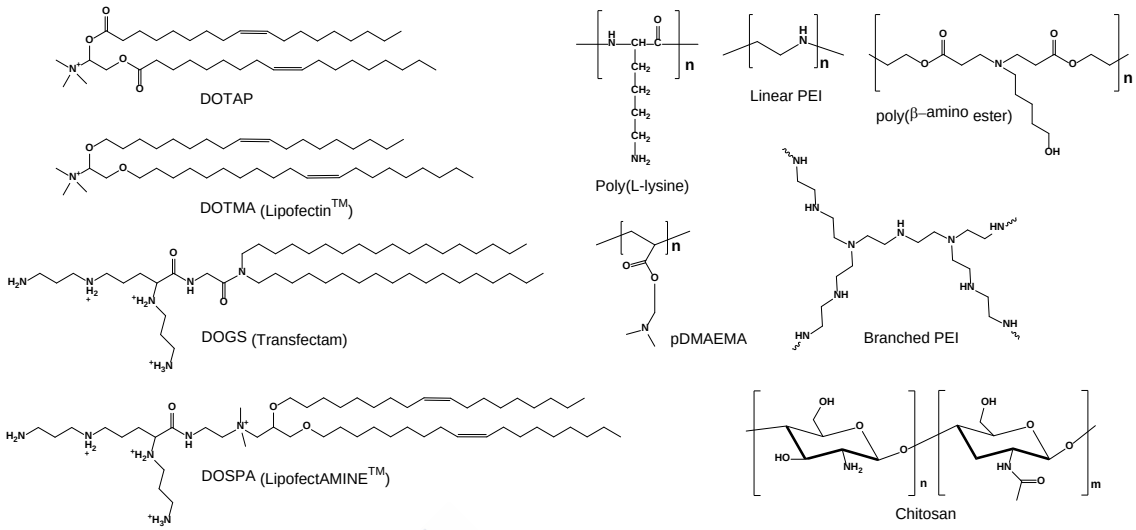

Scheme 1-1 Common-used materials in lipid-based and polymer-based gene carriers

Abbreviation: DOTAP (1,2-dioleoyl-3-trimethylammonium-propane); DOTMA (1,2-di-O-octadecenyl-3-trimethylammonium propane); DOGS (Di-octadecyl-amido-glycyl-spermine); DOSPA (2,3-Dioleyloxy-N-[2(sperminecarboxamido)ethyl]-N,N-dimethyl-l-propanaminium trifluoroacetate); PEI (polyethylenimine); PLL (poly-L-lysine); PBAE (poly(β-amino ester)); pDMAEMA (poly[(2-dimethylamino) ethyl methacrylate]); chitosan.

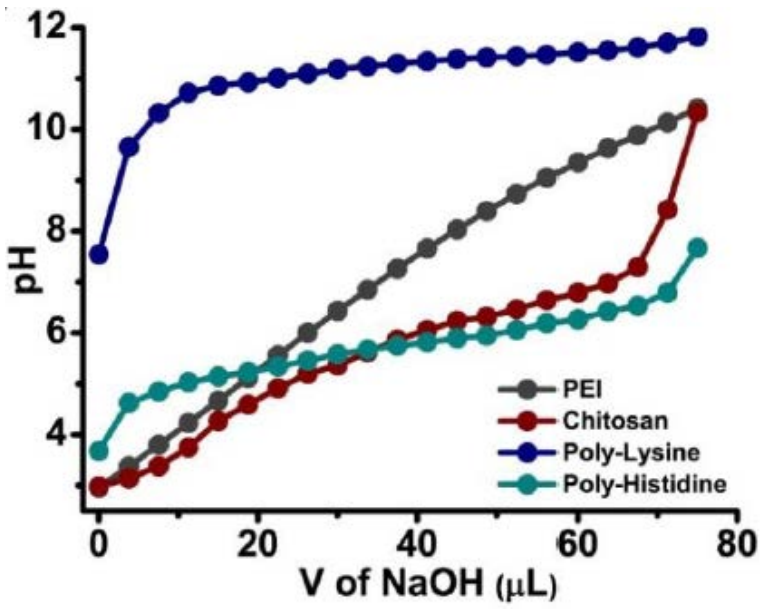

Figure 1-3. Potentiometric titration curves of various polycations. [Reproduced from Li, Y. et al. Nature communications [28], with a Creative Commons license.]

Table 1-1. Selected promising clinical trials of lipid-based and polymer-based gene therapies[2,8,9].

	Product	*Sponsor*	*Disease Route*	*cargo Target Gene*	*Status*	*ClinicalTrials gov Identifier*
Lipid-based	ALN-TTR02	Alnylam Pharmaceuticals	TTR (IV)	siRNA TTR02	Phase III Completed	NCT01960348
	ALN-VSP02	Alnylam Pharmaceuticals	Cancer (IV)	siRNA KIF11& VEGF	Phase I Completed	NCT01158079
	Atu027	Silence Therapeutics	Pancreatic cancer (IV)	siRNA PKN3	Phase I/II Completed	NCT01808638
	TKM-080301	Arbutus Biopharma	Adrenocortical, Neuroendocrine tumours (IV)	siRNA PLK1	Phase II Phase I Completed	NCT01262235
	DOTAP:Chol-fus1	MD.Anderson Cancer Center	Lung cancer (IV)	pDNA TUSC2	Phase I Completed	NCT00059605
Polymer-based	BC-819 PEI	BioCancell	Bladder cancer (Local)	pDNA BC-819	Phase II Recruitment	NCT00595088
	DTA-H19 PEI	BioCancell	Pancreatic neoplasms (Intratumoral injection)	pDNA	Phase I/II completed	NCT00711997
	ASP0113 Poloxamer	Astellas Pharma Inc.	CMV vaccine	DNA vaccine	Phase III active	NCT01877655
	DermaVir/LC002 PEI–mannose–dextrose	Genetic Immunity	HIV vaccine	DNA vaccine	Phase I/II Completed	NCT00270205
	EGEN-001 PEG-PEI-cholesterol	Gynecologic Oncology Group	Carcinoma (IP)	pDNA IL-12	Phase II Completed	NCT01118052

Note: TTR: transthyretin.; IP: intraperitoneal injection.

1.3 Difficulties in polymeric gene delivery

Although most clinical trials in gene therapies are based on viral vectors, the desire for scalable low-cost manufacturing for effective and safe gene therapies has led to the development of synthetic vehicles to deliver nucleic acids to target cells [29-31]. However, there still remain a number of challenges on the delivery routes for practical applications[32-35]. In **Figure 1-4,** administrations through circulation system (e.g. intravenous administration, IV) to whole body, eligible gene vehicles should be able to protect nucleic acid cargos from degradation by serum endonucleases and immune detection before arriving at targeting tissues. In the circulation, avoidance of clearance by the hepatic mononuclear phagocyte system (MPS) and renal excretion are major barriers limiting effectiveness of vectors following intravenous administrations. For minimizing the non-specific interactions (e.g. with opsonin protein) and to avoid the clearance in short term, polyethylene glycol (PEG) is commonly used as a nanoparticle coating polymer and enables nanoscale carriers to have "stealth properties". However, PEGylation of gene carriers also significantly reduces the interaction with target cells, causing a dilemma in terms of formulation design[36]. There is substantial literature data regarding innate excretion systems, in which macromolecules and gene delivery nanoparticles have chances to passively enter tumours or inflammation tissues via the enhanced permeability and retention (EPR) effect[37]. However, despite many successes for exploiting EPR-medicated nanoparticle gene delivery in murine models, a number of tumour types lack significant EPR effects in clinical cases, and the extent of EPR effects are considerably dependent to individual patients [38]. It is also important to note that even after the vehicles have entered tumour tissues via EPR effects, they still face other obstructions prior to successful delivery of gene cargos[39]. For example, while

malignant tumour cells are proliferating and spreading, abnormal structures of vasculatures in the tumour cause interstitial areas to form dense and complicated crosslinked matrices, containing cancer-associated fibroblasts, and interlinked hyaluronan and collagen biopolymers, etc[39]. These tumour interstitial matrixes can efficiently impede diffusion of "nanoscale" particles and separate therapeutic vehicles from tumour cells[39,40]. As a result, an effective penetration over normal organs and throughout tumour tissues is one of the most necessary requirements in gene delivery, especially in GBM cancers, which are usually infiltrative to neighbouring tissues [41].

In addition, from the perspectives of the various active pharmaceutical ingredients (API) in nanocarriers for anticancer administrations, for example chemo-, gene-, or radioisotope- therapeutic agents, the nucleic acid cargos are the most challenging one because of several additional criteria. In comparison with these three delivery systems, small chemotherapeutic drugs can still diffuse into cells even if their carriers are retained in the interstitial matrix of tumour tissues. For radionuclide cargos, therapeutic isotopes with high-penetration radiation (e.g. β-particle emitting radionuclides ^{188}Re, ^{131}I, ^{90}Y) are only required to be close to tumours, or stayed in tumour tissues and capable to offer therapeutic effects, even without release from their carriers or without internalization of tumour cells.[42,43] However, for nucleic acid delivery, gene cargos have to be delivered into cells, released from the carriers themselves, and activated by certain enzymes. Nevertheless, while gene delivery has its own difficulties, it is still likely to be the best option especially for chemotherapeutic drug-resistant, radiotherapy-resistant patients, or gene-disorder diseases.

Even across through tumoral and vessel interstitial matrixes, gene vehicles usually internalize target cells via endocytosis pathways[44,45]. Endocytosis mechanisms are the most common approaches for mammalian cells to access nutrients and manage signalling regulators, including macro-scale phagocytosis (cell eating) and pinocytosis (cell drinking), and micro-scale endocytic processes (clathrin- and caveolae/lipid raft-dependent endocytosis, etc.)[46]. For most cancer cells, nanoscale particles are usually internalised via micro-scale endocytic processes, which involve clathrin-dependent and clathrin-independent endocytosis (**Figure 1-5**), but there is no unambiguous evidence to prove which mechanisms are the main pathways for internalisation of nanovehicles, because of strong cell-type dependence and insufficiently specific agents used for inhibiting endocytic pathways[44,47]. However, except for phagocytosis, which is a common pathway for macrophages, nanocarriers entered through cell membranes via the other endocytic mechanisms have to pass through multiple endosomal compartments and then arrive the final destination at lysosomes for degradation and hydrolysis. Importantly, the degradation of nucleic acid cargos in lysosomes is one of the main obstacles to efficient non-viral gene delivery. A previous study employed lipid-based vehicles carrying siRNA-linked gold-nanoparticles (siRNA-AuNP) as cargos to offer direct evidence in quantification assay. Through in vitro and in vivo studies, only 1-2% of siRNA-AuNP in lipid-based carriers can escape from multiple endosomal compartments into the cytosol, even though the lipid/siRNA vehicles still have high efficient down-regulation of GFP expression[48]. Taken together, gene vehicles escaping from endosomal stage before lysosomal stage have become an important research topic in non-viral gene delivery.

After escape from endosomal/lysosomal compartments, the gene cargos should unload from vehicles and further arrive at destinations or be activated with specific proteins or enzymes[8]. For instance, plasmid DNA (pDNA) should be further transported to nucleus and then follow transcription and translation processes for gene expressions. siRNA and miRNA should integrate with the RNA-induced silencing complex (RISC) to activate RNA interference (RNAi) pathway. However, dissociation of gene cargos from the carrier vehicles is also one of the most difficult steps in polymeric gene delivery. For example, polycation-delivered plasmid (via PEI) can be efficiently transported to nuclei but nearly ten-times less gene-transferring expression than lipid-mediated transfection (via Lipofetamine) at the same dose. This is likely caused by difficultly complete separation between the plasmid and PEI[49]. For lipid-delivered pDNA (Lipofectamine/pDNA), high levels of reporter gene expression have found in transfected cells under active dividing period (late S/G2 phase), while polycation-delivered pDNA (PEI/pDNA) are not clearly statistic association with cell circle periods[50]. The PEI-mediated pDNA has a tendency to locate at nucleus membrane, likely driven by positive surface charge of the polycation/pDNA complex. This high tendency to target on nucleus may provide high efficacy on gene transfection, but poor dissociation of polycation and pDNA discount the amount of pDNA entering nucleus. In this thesis, we not only attempt to design a polymeric carrier for endosomal escape (slight acidic environment) but also try to address the issue for release of gene cargo in cytoplasm (physiological pH).

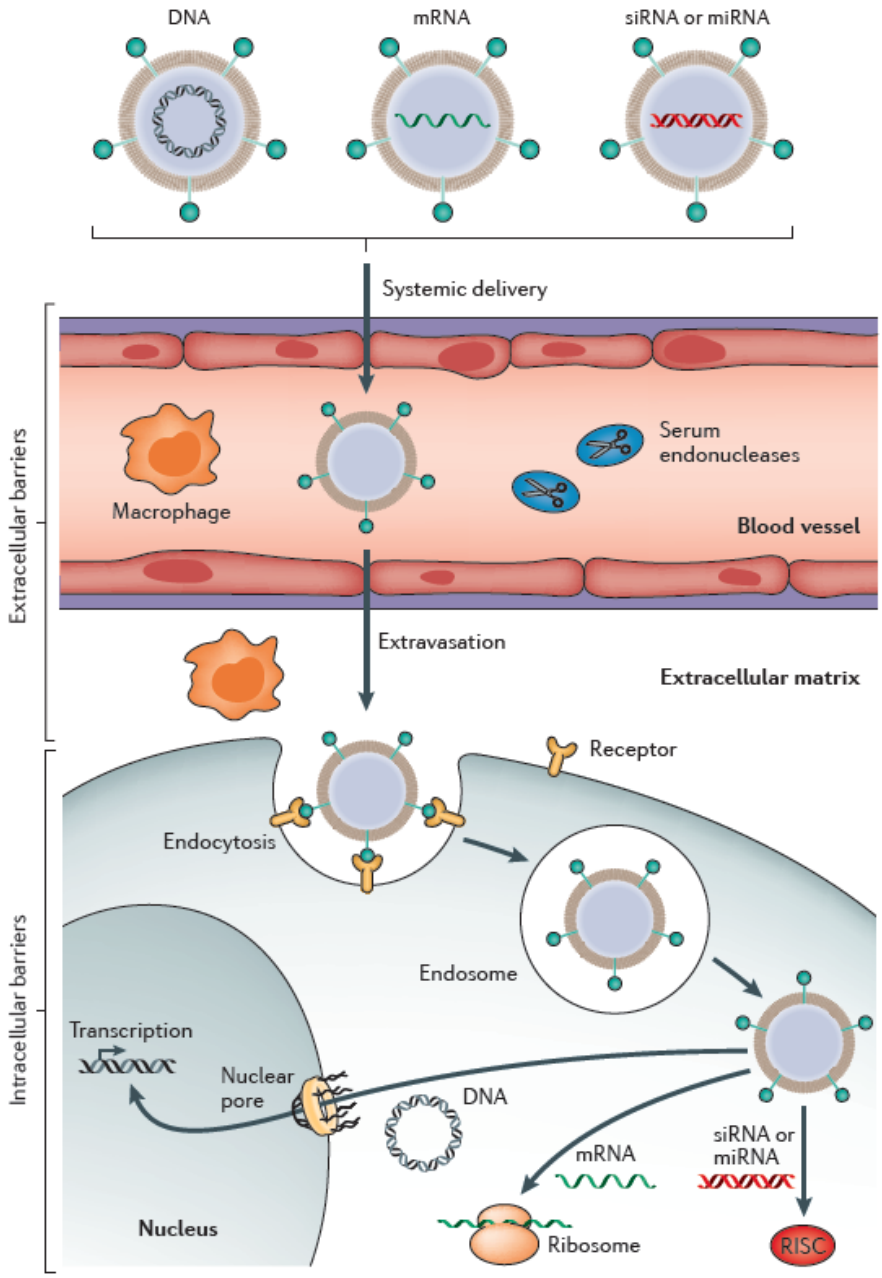

Figure 1-4. Diagram for nanoparticle-based gene delivery from IV administration to their own destinations. [Reproduced from Yin, H., et al. (2014). Nature reviews. Genetics[8] with permission]

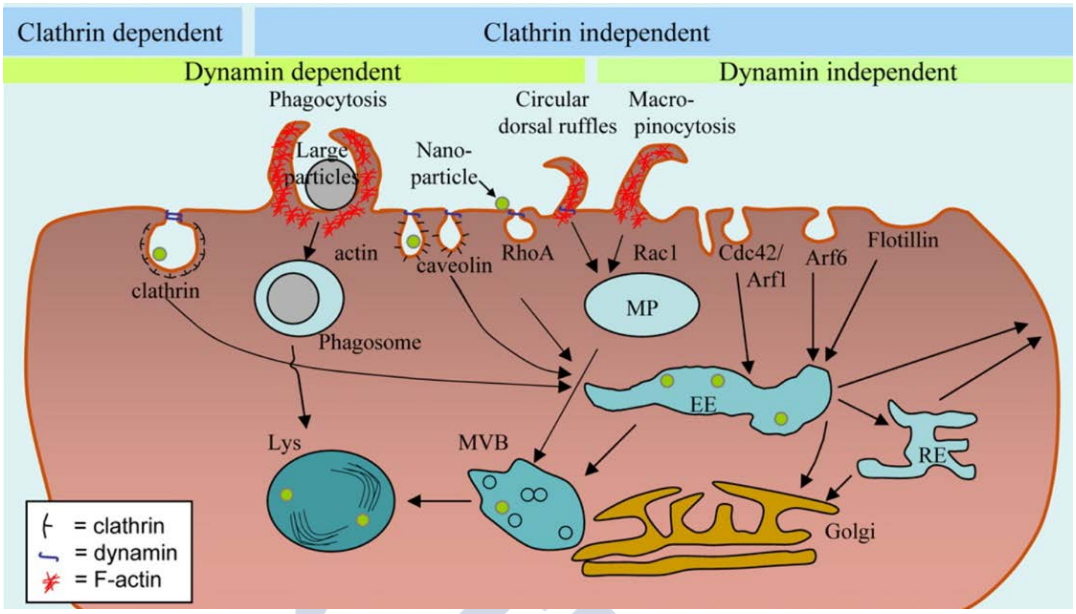

Figure 1-5. Mechanisms of endocytosis and general intracellular transport. Nanocarriers (green dots) are taken by cells via endocytosis. Macropinosomes (MP), early endosomes (EE), multivesicular bodies/ late endosomes (MVB), lysosomes (Lys), recycling endosomes (RE) [Reproduced from Iversen, T.-G., et al. (2011). Nano Today[44] with permission].

Chapter I / Capítulo I

1.4 References

1. Kotterman, M.A., Chalberg, T.W. & Schaffer, D.V. Viral vectors for gene therapy: translational and clinical outlook. *Annual review of biomedical engineering* **17**, 63-89 (2015).
2. Chen, J., Guo, Z., Tian, H. & Chen, X. Production and clinical development of nanoparticles for gene delivery. *Molecular therapy. Methods & clinical development* **3**, 16023 (2016).
3. Goff, S.P. & Berg, P. Construction of hybrid viruses containing SV40 and λ phage DNA segments and their propagation in cultured monkey cells. *Cell* **9**, 695-705 (1976).
4. Ginn, S.L., Alexander, I.E., Edelstein, M.L., Abedi, M.R. & Wixon, J. Gene therapy clinical trials worldwide to 2012–an update. *The journal of gene medicine* **15**, 65-77 (2013).
5. Wilson, J.M. Lessons learned from the gene therapy trial for ornithine transcarbamylase deficiency. *Molecular genetics and metabolism* **96**, 151-157 (2009).
6. Jin, L., Zeng, X., Liu, M., Deng, Y. & He, N. Current progress in gene delivery technology based on chemical methods and nano-carriers. *Theranostics* **4**, 240 (2014).
7. Pack, D.W., Hoffman, A.S., Pun, S. & Stayton, P.S. Design and development of polymers for gene delivery. **4**, 581 (2005).
8. Yin, H., *et al.* Non-viral vectors for gene-based therapy. *Nature reviews. Genetics* **15**, 541 (2014).
9. Wong, J.K., *et al.* Will nanotechnology bring new hope for gene delivery? *Trends in biotechnology* (2017).
10. Wang, W., Li, W., Ma, N. & Steinhoff, G. Non-viral gene delivery methods. *Current pharmaceutical biotechnology* **14**, 46-60 (2013).
11. Putnam, D. Polymers for gene delivery across length scales. *Nature materials* **5**, 439-451 (2006).
12. Olins, D.E., Olins, A.L. & von Hippel, P.H. Model nucleoprotein complexes: studies on the interaction of cationic homopolypeptides with DNA. *Journal of molecular biology* **24**, 157-176 (1967).
13. Tzeng, S.Y., *et al.* Non-viral gene delivery nanoparticles based on Poly(β-amino esters) for treatment of glioblastoma. *Biomaterials* **32**, 5402-5410 (2011).

14. van de Wetering, P., Cherng, J.-Y., Talsma, H. & Hennink, W.E. Relation between transfection efficiency and cytotoxicity of poly(2-(dimethylamino)ethyl methacrylate)/plasmid complexes. *Journal of Controlled Release* **49**, 59-69 (1997).
15. Dufès, C., Uchegbu, I.F. & Schätzlein, A.G. Dendrimers in gene delivery. *Advanced drug delivery reviews* **57**, 2177-2202 (2005).
16. Csaba, N., Köping-Höggård, M. & Alonso, M.J. Ionically crosslinked chitosan/tripolyphosphate nanoparticles for oligonucleotide and plasmid DNA delivery. *International Journal of Pharmaceutics* **382**, 205-214 (2009).
17. Wu, G.Y. & Wu, C.H. Receptor-mediated in vitro gene transformation by a soluble DNA carrier system. *Journal of Biological Chemistry* **262**, 4429-4432 (1987).
18. Akinc, A. & Langer, R. Measuring the pH environment of DNA delivered using nonviral vectors: implications for lysosomal trafficking. *Biotechnology and bioengineering* **78**, 503-508 (2002).
19. Jere, D., *et al.* Akt1 silencing efficiencies in lung cancer cells by sh/si/ssiRNA transfection using a reductable polyspermine carrier. *Biomaterials* **30**, 1635-1647 (2009).
20. Bolcato-Bellemin, A.-L., Bonnet, M.-E., Creusat, G., Erbacher, P. & Behr, J.-P. Sticky overhangs enhance siRNA-mediated gene silencing. *Proceedings of the National Academy of Sciences* **104**, 16050-16055 (2007).
21. Lee, S.-Y., *et al.* Stability and cellular uptake of polymerized siRNA (poly-siRNA)/polyethylenimine (PEI) complexes for efficient gene silencing. *Journal of Controlled Release* **141**, 339-346 (2010).
22. Yue, Y., *et al.* Revisit complexation between DNA and polyethylenimine—effect of uncomplexed chains free in the solution mixture on gene transfection. *Journal of Controlled Release* **155**, 67-76 (2011).
23. Uchida, H., *et al.* Modulated protonation of side chain aminoethylene repeats in N-substituted polyaspartamides promotes mRNA transfection. *Journal of the American Chemical Society* **136**, 12396-12405 (2014).
24. Peng, Q., Zhong, Z. & Zhuo, R. Disulfide cross-linked polyethylenimines (PEI) prepared via thiolation of low molecular weight PEI as highly efficient gene vectors. *Bioconjugate chemistry* **19**, 499-506 (2008).
25. Breunig, M., Lungwitz, U., Liebl, R. & Goepferich, A. Breaking up the correlation between efficacy and toxicity for nonviral gene delivery. *Proceedings of the National Academy of Sciences* **104**, 14454-14459 (2007).
26. Fichter, K.M., Ingle, N.P., McLendon, P.M. & Reineke, T.M. Polymeric nucleic

acid vehicles exploit active interorganelle trafficking mechanisms. *ACS nano* **7**, 347-364 (2012).

27. Coll, J.-L., *et al.* In vivo delivery to tumors of DNA complexed with linear polyethylenimine. *Human gene therapy* **10**, 1659-1666 (1999).
28. Li, Y., *et al.* Molecular basis of cooperativity in pH-triggered supramolecular self-assembly. *Nature communications* **7**, 13214 (2016).
29. Zelikin, A.N., Ehrhardt, C. & Healy, A.M. Materials and methods for delivery of biological drugs. *Nat Chem* **8**, 997-1007 (2016).
30. Kanasty, R., Dorkin, J.R., Vegas, A. & Anderson, D. Delivery materials for siRNA therapeutics. *Nat Mater* **12**, 967-977 (2013).
31. Yin, H., *et al.* Non-viral vectors for gene-based therapy. *Nature Reviews Genetics* **15**, 541-555 (2014).
32. Scholz, C. & Wagner, E. Therapeutic plasmid DNA versus siRNA delivery: Common and different tasks for synthetic carriers. *Journal of Controlled Release* (2012).
33. Krivitsky, A., *et al.* Structure–Function Correlation of Aminated Poly(α)glutamate as siRNA Nanocarriers. *Biomacromolecules* **17**, 2787-2800 (2016).
34. Moghimi, S.M. & Wagner, E. Nanoparticle Technology: Having Impact, but Needing Further Optimization. *Molecular Therapy* **25**, 1461-1463 (2017).
35. Lachelt, U. & Wagner, E. Nucleic Acid Therapeutics Using Polyplexes: A Journey of 50 Years (and Beyond). *Chemical Reviews* **115**, 11043-11078 (2015).
36. Verhoef, J.J. & Anchordoquy, T.J. Questioning the use of PEGylation for drug delivery. *Drug delivery and translational research* **3**, 499-503 (2013).
37. Maeda, H., Wu, J., Sawa, T., Matsumura, Y. & Hori, K. Tumor vascular permeability and the EPR effect in macromolecular therapeutics: a review. *Journal of controlled release* **65**, 271-284 (2000).
38. Prabhakar, U., *et al.* Challenges and key considerations of the enhanced permeability and retention effect for nanomedicine drug delivery in oncology. (AACR, 2013).
39. Jain, R.K. & Stylianopoulos, T. Delivering nanomedicine to solid tumors. *Nat Rev Clin Oncol* **7**, 653-664 (2010).
40. Pluen, A., *et al.* Role of tumor–host interactions in interstitial diffusion of macromolecules: Cranial vs. subcutaneous tumors. *Proceedings of the National Academy of Sciences* **98**, 4628-4633 (2001).
41. Mangraviti, A., *et al.* Polymeric nanoparticles for nonviral gene therapy extend

brain tumor survival in vivo. *ACS nano* **9**, 1236-1249 (2015).

42. O'Donoghue, J.A., Bardies, M. & Wheldon, T.E. Relationships between tumor size and curability for uniformly targeted therapy with beta-emitting radionuclides. *Journal of nuclear medicine : official publication, Society of Nuclear Medicine* **36**, 1902-1909 (1995).
43. Hsu, W.-H., *et al.* The PEGylated liposomal doxorubicin improves the delivery and therapeutic efficiency of 188Re-Liposome by modulating phagocytosis in C26 murine colon carcinoma tumor model. *Nuclear Medicine and Biology* (2014).
44. Iversen, T.-G., Skotland, T. & Sandvig, K. Endocytosis and intracellular transport of nanoparticles: present knowledge and need for future studies. *Nano Today* **6**, 176-185 (2011).
45. Von Gersdorff, K., *et al.* The internalization route resulting in successful gene expression depends on both cell line and polyethylenimine polyplex type. *Molecular Therapy* **14**, 745-753 (2006).
46. Kumari, S., Swetha, M. & Mayor, S. Endocytosis unplugged: multiple ways to enter the cell. *Cell research* **20**, 256-275 (2010).
47. Doherty, G.J. & McMahon, H.T. Mechanisms of endocytosis. *Annual review of biochemistry* **78**, 857-902 (2009).
48. Gilleron, J., *et al.* Image-based analysis of lipid nanoparticle-mediated siRNA delivery, intracellular trafficking and endosomal escape. *Nat Biotech* **31**, 638-646 (2013).
49. Cohen, R.N., van der Aa, M.A., Macaraeg, N., Lee, A.P. & Szoka, F.C. Quantification of plasmid DNA copies in the nucleus after lipoplex and polyplex transfection. *Journal of Controlled Release* **135**, 166-174 (2009).
50. Brunner, S., Fürtbauer, E., Sauer, T., Kursa, M. & Wagner, E. Overcoming the nuclear barrier: cell cycle independent nonviral gene transfer with linear polyethylenimine or electroporation. *Molecular Therapy* **5**, 80-86 (2002).

Chapter II / Capítulo II

Characterisation and Optimisation of Polyphosphazene-based Gene carriers via Thiol-ene Click chemistry

Chapter II / Capítulo II

Abstract

Considering their possibilities including biodegradability and versatility, polyphosphazenes were selected as the polymeric backbone for gene delivery. However, there is a limitation on the classical side-chain substitution of polyphosphazene, which cannot react with compounds having more than one nucleophilic terminal group without protection/deprotection procedures. A breakthrough to overcome that limitation would be a simple, selective and efficient method to add directly side chains to the backbone. Herein, we employed a thiol-ene addition reaction to synthesize cationic and anionic side-chain polyphosphazenes. Concretely, we reacted a polyphosphazene precursor with α, ω-aminoalkanethiols and α, ω–carboxylatoalkanethiols to yield amine side-group polyphosphazenes, as polycations, and carboxylate side-chain polyphosphazenes, as polyanions. After that, we designed complexes composed of cationic and pH-sensitive anionic polyphosphazenes. Based on physicochemical characterisation and transfection screening with a pDNA encoding GFP/Luciferase, polyphosphazene with primary amines derived from cysteamine were chosen the most efficient cationic materials, while polyphosphazenes with alkylcarboxylic acids derived from 6-mercaptohexanoic acid were the most efficient anionic materials. Through the optimization of binary polyionic gene complex on the 2D monolayer model in vitro in this chapter, we can further investigate gene-release mechanisms and evaluate effects of the selected "mixed complexes" on the 3D-culture and in vivo situations in the following chapters.

Chapter II / Capítulo II

2.1 Introduction

2.1.1 Basic chemical properties of polyphosphazene

Polyphosphazene is a general term for polymers having a backbone made of repeating units of phosphazene, phosphorus-nitrogen alternative arrangement, which can be configured as circle or linear species. In general, the linear polyphosphazenes were $N{=}PR_1R_2$, and as shown in **Figure 2-1a**, the structure of polyphosphazenes is built by phosphorus covalently linked to nitrogen via σ-σ bond and σ-π bond alternatively, but differing with the familiar bonds in carbon-based compounds. Each phosphorus atom offers five electrons and each nitrogen provides another five electrons, forming alternatively saturated and unsaturated bonds on the backbones. Among of them, two electrons of phosphorus are used for side chain conjugation, and two electrons of nitrogen remained of a lone-pair (**Figure 2-1 b**). Although the linear backbone contained unsaturated bonds, the $d\pi$(P)−$p\pi$(N) bond is expected flexible rotation, because several *3d* orbitals of phosphorus provide more chances to hybrid with the p_z orbital of nitrogen once the π bond undergoes torsions (**Figure 2-1 c**)[1]. As the calculation suggested, the bond energy of inherent torsional barrier in the phosphazene backbone is as low as only 100 cal per bond.[2,3] Moreover, such hybridisation brings delocalization-stabilization effects similar to aromatic compounds p_π(C)−p_π(C).

In the molecular conformation, linear polyphosphazenes are significantly influenced by their side groups (i.e. Cl, OCH_2CF_3, etc.). In general, the phosphazene skeleton is easily distorted by its side groups, occupying a trans-trans planar or cis-trans planar conformation[4]. Theoretically, most of polyphosphazenes are favour to be as

cis-trans planar form, in view that the side chains can keep maximum distance to each other, minimizing the internal repulsions (**Figure 2-1 d**)[1,5]. Taken the poly(dichlorophosphazene) as an example, the Cl···N attractions and Cl···Cl repulsions force such cis-trans form and confirmed by X-ray measurement[4].

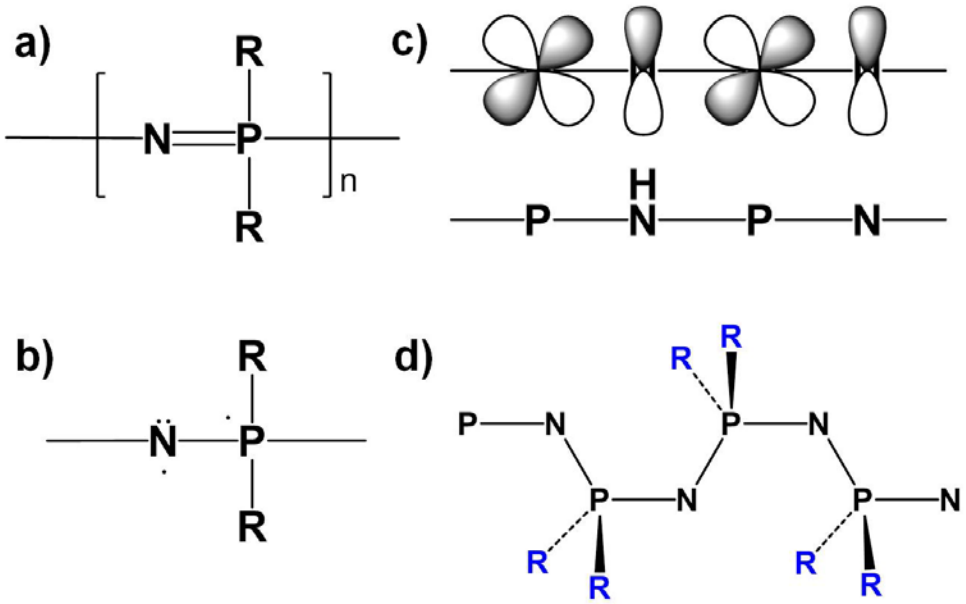

Figure 2-1. General structures of polyphosphazene (a), electron arrangement in the phosphazene bond (b) and its orbital hybridisation in (c), in which phosphorus provides d_{xz} to hybrid with p_z of nitrogen. (d) cis-trans planar conformation of repeating phosphazene backbone.

2.1.2 Synthesis of polyphosphazene and nucleophilic substitution

Although the inaugural synthesis of polyphosphazene had been reported by Stokes at 1897, the product was polymerised at high-temperature and long time for formation of insoluble elastomers known as inorganic rubber. The first stable synthesis of

polyphosphazene and its use for biomedical application were reported by Prof. Allcock group[6], starting several broad interest from the research community and from industry. In the most general procedure for non-crosslinked polyphosphazene synthesis, the precursor poly(dichlorophosphazene) (PDCP) is prepared in a first step, and then the final polymer is formed by nucleophilic substitution of desired side chains. Based on the raw monomers, synthetic methods of PDCP can be classified in those starting from cyclic trimers (i.e. hexachlorocyclotriphosphazene) and those starting from non-cyclic monomers (i.e. dichlorophosphinoyl-iminotrichloro phosphorene, $Cl_3P=N\text{-}P(O)Cl_2$, or trichloro(trimethylsilyl)phosphoranimine, $Cl_3P=NSiMe_3$).[7] In the former method, the polymerisation is typically thermo-initiated and ring-opening reaction propagates towards linear PDCP (**Figure 2-2 a**). Many advanced technologies for PDCP synthesis by this general method have been published recently including catalysed polymerisation[8,9] and solvent-mediated stabilization[10]. Although the mechanism of this ring-opening polymerisation is still open to debate, the most broadly accepted mechanism is that one phosphorus-chloride bond of the cyclic trimer would be cleaved by heating above 250-260 ºC, inducing the opening of next cyclo-triphosphorazene and starting the chain propagation reaction (**Figure 2-2 a**). In the terminal step, the reactive head of the polyphosphazene chain ($\sim N=PCl_2^+$) can recapture the chloride anion as the reaction temperature decreases. However, the reaction is extremely sensitive to contamination of water or other nucleophiles, which cause unwanted cross-linking, precipitation of an insoluble material (i.e. Stokes' "inorganic rubber") and lack of reproducibility between batches regarding physical properties. For avoiding water contamination and simplifying the synthesis process, a solvent-free polymerisation (melt polymerisation reaction) would be more suitable than a polymerisation in solvent[9]. In addition, for achieving high-yield polymerisation of PDCP, which can omit further

purification in the first polymerisation and directly conjugate with side chains via nucleophilic substitution, proper catalysts were reported as a necessary compartment in this reaction[8,9]. Boron trichloride (BCl_3) and aluminium chloride ($AlCl_3$) are strong Lewis acids that facilitate the extraction of the chloride on the trimers and act as catalysts for cyclic trimer activation **(Figure 2-3)**[8]. Boron trichloride may have the additional advantage of reducing the possibility of crosslinking by eliminating trace amounts of water in the polymerisation by forming $B(OH)_3$. Sohn et al. also reported that aluminium chloride can be used as a catalyst in polyphosphazene polymerisation to yield PDCP with a Mw range between 10K and 100K Da, which could be suitable in many biomedical applications, especially drug delivery[9]. The combination of solvent-free polymerisation with the efficient catalyst make PDCP a more easy-accessible polymer material, even laboratories only with basic facilities for organic chemical synthesis.

Another method to synthesize PDCP was via living-cationic polymerisation using phosphorus pentachloride (PCl_5) as the initiator **(Figure 2-2 b)**[11]. In this approach, the polymer products would have narrow polydispersity (Mw/Mn), and the reaction can be carried out at room temperature. Other advantages of this reaction are its control over the molecular weight. The monomer $Cl_3P{=}N\text{-}Si(CH_3)_3$, however is not available in standard commercial vendors and the catalyst, PCl_5, is a dangerous compound classified as third level health hazard.

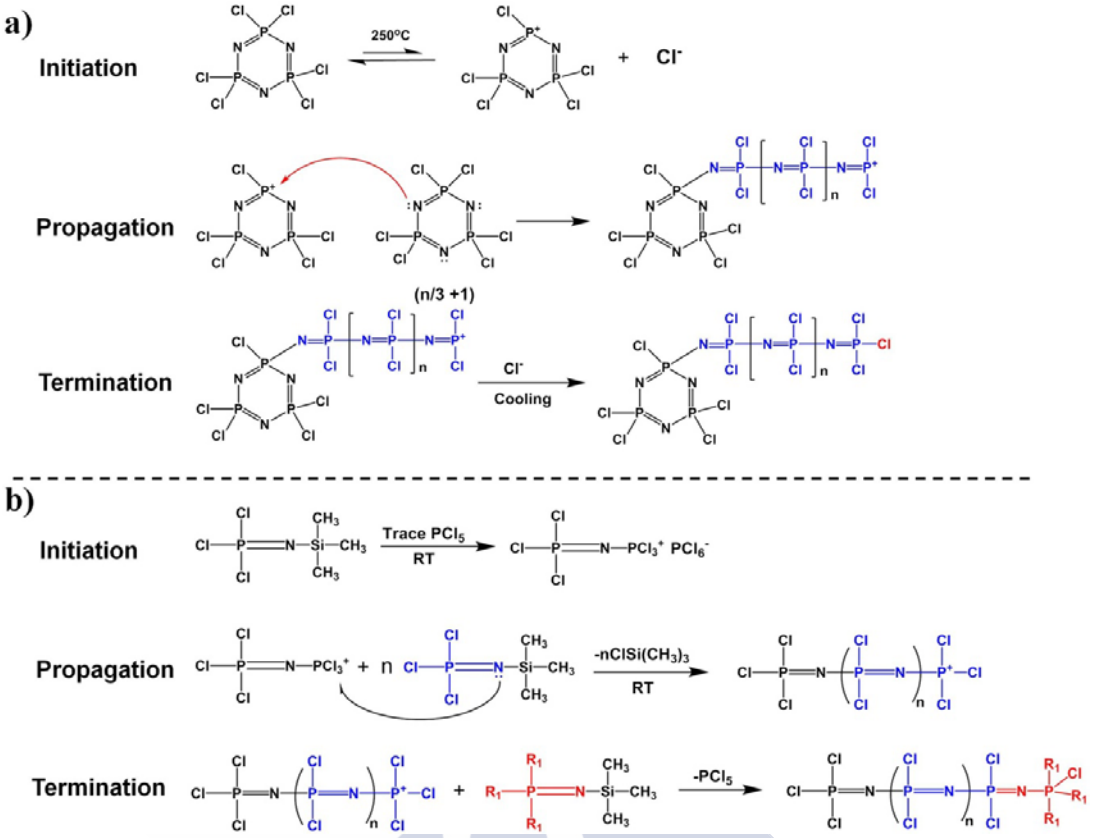

Figure 2-2. Synthesis mechanisms for polyphosphazene polymerisation. (a) Ring-opening polymerisation of cyclo-triphosphorazene and (b) living-cationic polymerisation of trichloro(trimethylsilyl)phosphoranimine to yield linear poly(dichlorophosphazene) (PDCP).

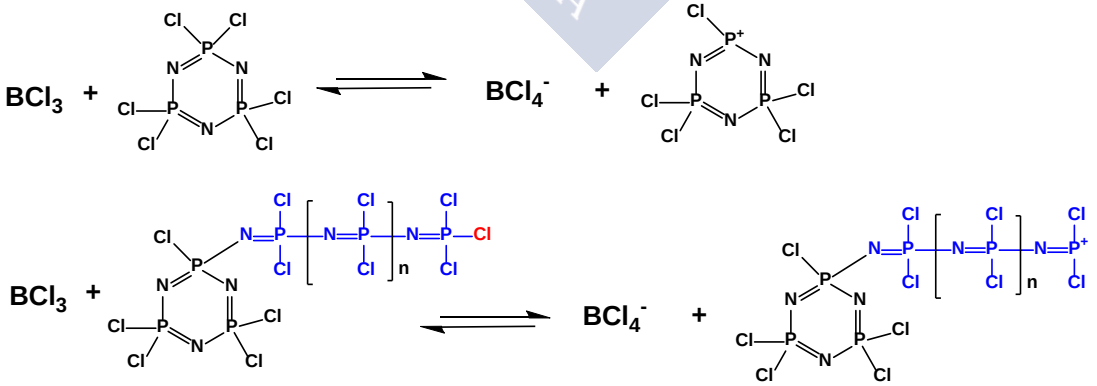

Figure 2-3. Lewis acid, Boron trichloride (BCl_3) as a catalyst for ring-opening polymerisation of linear PDCP.

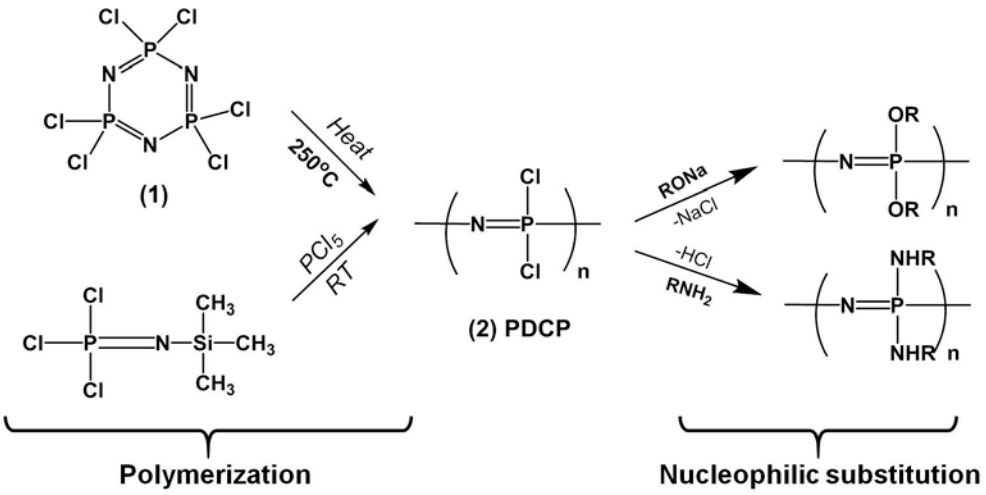

Figure 2-4. Two dominant classes of nucleophile to substitute chlorides by functional side chains, including amines or alkoxides.

2.1.3 Nucleophilic substitution and click-chemistry addition extension

Following polymerisation of PDCP, this polymer can be recognized as a precursor, which can derive different polyphosphazenes via nucleophilic substitution reactions.[6,12,13] PDCP provides an easy-coupling platform for conjugation with potential side-chain candidates, in which nucleophile terminals can substituted chlorine of PDCP to attach on the polyphosphazene backbone. There are two main classes of nucleophile terminal groups to substitute the chloride to desired side chains, generally either amines or alkoxides (**Figure 2-4**). However, side-chain candidates with more than one hydrophilic or nucleophilic terminal group cannot be added directly on the backbone. In other words, the candidates having over two functional groups (amines, imines, thiols, acids, or polar amino acids etc.) need to go through protection/deprotection procedures

for the nucleophilic substitution step. Otherwise, the excess nucleophilic terminal group would cause crosslinking due to double substitutions on intra-macromolecules or between macromolecules. Fortunately, a library of polyphosphazenes have extensively developed[14,15], including several nucleophilic substitutions of alkene, alkyne, or vinyl series on the polyphosphazene backbone, such as allylamine[14,15], 2-Aminoethyl methacrylate[16], allyl glycinate[17], methacrylic acid[18,19], and propargylamine[20] (**Figure 2-5**). In the previous studies, most double-bond introductions on PPZ backbone were usually utilised for radical photo-polymerisation to form hydrogel or to improve the mechanical strengthens.[16,17,19,21] Only few studies from Prof. Qian, Y. C. and Huang, X.J. groups reported thiol-ene and azide/alkyne click reactions for conjugating biomolecules (i.e. glucose) on polyphosphazenes[15,22]. These modifications bring additional versatility to these polymers and allow the introduction of side chains with several nucleophiles[15].

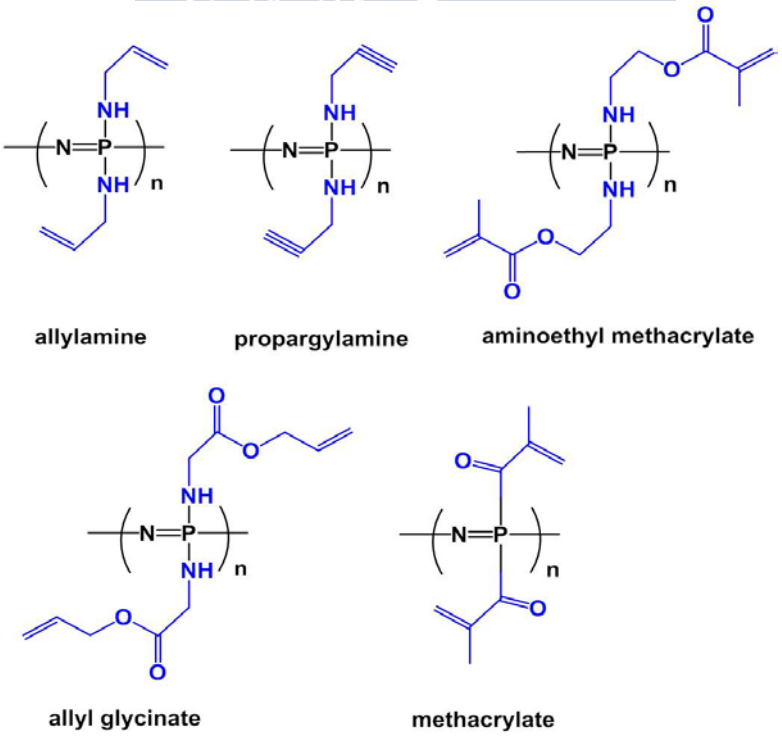

Figure 2-5 Potential "side-chain" added polyphosphazenes for thiol-ene, thiol-yne, and azide/alkyne click addition reactions.

2.1.4 Biodegradable of poly(organophosphazenes)

Poly(organophosphazene)s are a class of polymers derived from a backbone of repeated phosphazenes and having organic functional side groups. The main advantages of poly(organophosphazenes) are derived from its structural flexibility derived from the different side chains that can be linked, and interestingly tunable biodegradability of the backbones. Regarding this, the mechanism for hydrolysis of polyphosphazene is also controversial but three hypothetic mechanisms have been put forward **(Figure 2-6)**[23-25]. In the same mechanisms, the side groups might react with the phosphazene backbone and accelerate polymer hydrolysis while in other cases the side chains of polyphosphazenes may be eliminated from their backbone first, and finally the backbone would be hydrolysed to phosphates and ammonia[12]. What is clear is that unlike other biodegradable polymers, the degradation rate of polyphosphazenes is extremely dependent on the substituting side groups and their ratio if there is more than one type[26]. For example, among amino-acid ester polyphosphazenes in solid-state hydrolysis tests, the degradation of different amino acids attached polyphosphazenes is governed by hydrophobicity and steric hindrance of the side chains. For examples, the degradation rate of side-chain PPZ: ethyl glycinate (degradation half time, $T_{1/2}$ ~3 months) < alanine ($T_{1/2}$ ~6 months) < valine ($T_{1/2}$ ~ 1 year) ≦ phenylalanine ethyl ester ($T_{1/2}$ ~1 year).[12,27,28] When analysing two water-soluble polyphosphazenes with the same terminal functional side group, a tertiary amine, but linked to the polyphosphazene backbone by an different nucleophile group, the authors found that alkoxide-substituted

poly(2-dimethylamino-ethoxy)phosphazene ($T_{1/2}$ ~7days) was degraded faster than the amine-substituted poly(2-dimethylaminoethylamino)phosphazene ($T_{1/2}$ ~ 24 days)[29].

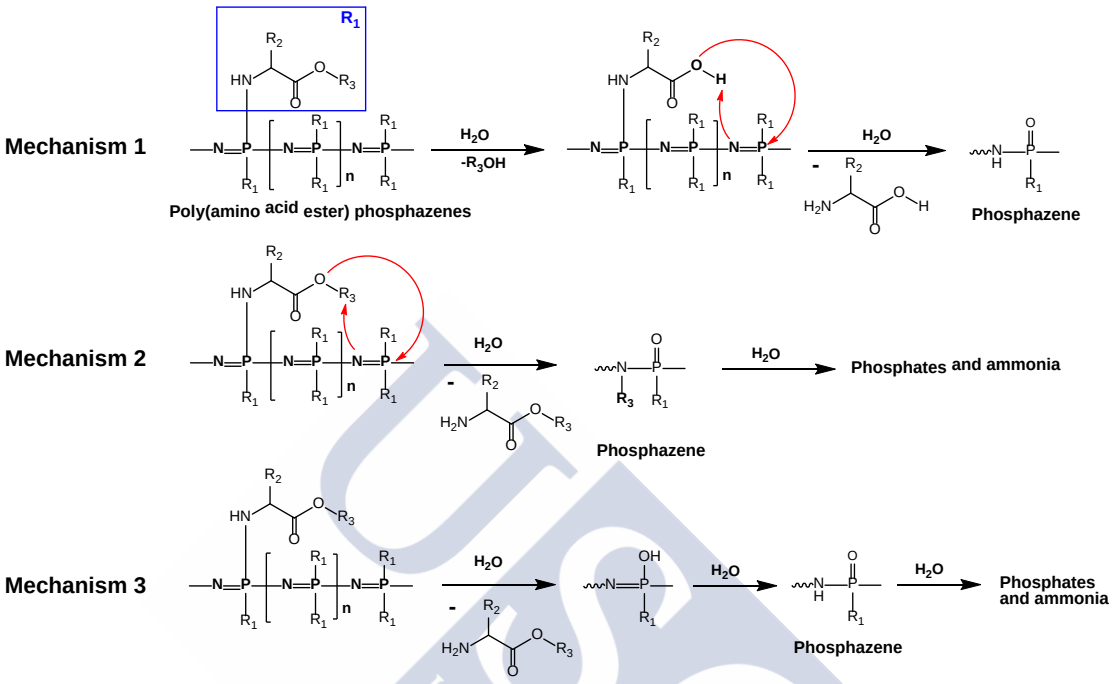

Figure 2-6. The three common hypotheses of poly(amino acid ester)phosphazenes for degradation mechanisms. [Adapted from Allcock, H. R. et al. [30], Polymer Chemistry 2012, with permission]

2.1.5 Applications of polyphosphazene

In views of plentiful candidates of side chain attaching to repeating phosphazene units, there are more than 700 different polyphosphazenes derived from this backbone, providing wide ranges of applications (**Table 2-1**)[27]. As an inorganic-organic polymer, polyphosphazene has some advantages over organic polymers, such as higher ultraviolet or gamma-radiation stability as well as better thermal stability. Broadly potential

candidates as side groups generated different physical and chemical properties in this material family, for examples from elastomeric to glass states (T_g from -105 to >180ºC), from water-soluble to super hydrophobic properties, from bio-inert to bio-active modifications[3].

As mentioned in chemical properties (**Section 2.1.1**), the phosphazene-composed backbone is flexible due to the orbital hybridisation of $d\pi$(P)−$p\pi$(N), giving rise to potential in elastomeric characters[3]. The first polyphosphazene used in commercial elastomer is a mixture of at least two side-chains attached on the backbone, which are including CF_3CH_2ONa and $CHF_2(CF_2)_xCH_2ONa$[31]. Through these fluoroalkoxy side groups, they offer highly random distribution in the structure, reducing the chances of inter-chain alignment and crystallinity, creating more “free volume” inside elastomers for polymer movement and dislocation once the materials received distortional deformation[32]. From industrial needs, polyphosphazenes have been used in fire-resistant or heat-, electrical-, and sound-insulation materials. Poly(aryloxyphosphazene) was employed as heat- and sound-insulation rubber tube and fire-resistant composite materials are utilized in circuit boards[3]. Poly[*bis*(trifluoroethoxy)phosphazene] was made as super-hydrophobic materials for water-proofing surface coating. Poly[bis(methoxyethoxyethoxy)phosphazene), MEEP, was used as solid solvents for lithium salts in battery industry. The side chains of MEEP are oligo(ethylene oxide), whose oxygen atoms can help separate ion-pair, and cations and anions can early migrate to negative and positive electrode under applied electric current, respectively[33]. Poly(ethylene oxide) is also potential in ionic conduction but the reason why MEEP is superior to poly(ethylene oxide) is that the non-/low-crystalline MEEP do not form microcrystalization to interrupt ionic conductor, yielding a high ionic conductivity.

In biomedical application, polyphosphazenes have attracted particular interests due to versatile side chains, tunable bio-erodible and bio-stable properties, including drug/gene/protein delivery, tissue engineering, vaccine delivery, and bio-inert elastomers for dental treatments[30,34]. Nowadays hundreds of derivatives have been synthesized and formulated to various products in biomedical applications. For example, amino acid ester polyphosphazenes have been widely studied[30] and applied to prepare fibres or scaffolds by electrospinning for bone tissue engineering[35]; amphiphilic polyphosphazenes have been used for the preparation of nanoscale polymeric carriers in controlled drug delivery[36,37]. For vaccine delivery the most advanced prototypes are based on polyphosphazenes with carboxylic acids side chains, being the most poly[di(carboxylatophenoxy)-phosphazene]. This materials has been used as a vaccine adjuvant, showing effective immune-stimulating activity in a variety of in vitro and in vivo models[27,38]. Moreover, recent studies have shown that polyphosphazenes can effectively deliver small drugs, proteins and nucleic acids in a number of therapeutic settings[39-45]. The versatility of polyphosphazene chemistry is also important from scale-up and manufacture perspectives[15,43,46]. For many industrial applications, it is desirable to have 'platform' materials that can be manufactured in bulk and adapted or modified for specific purposes. For pharmaceutical applications, a single precursor polymer that can be tailored for different therapies would be highly advantageous.

In this chapter, we have optimised a polyphosphazene platform, which have substituted by allylamines for preparation of a series of cationic and anionic derivatives via thiol-ene grafting chemistries using α, ω-aminoalkanethiols (**4** & **5**) and α, ω–carboxylatoalkanethiols (**7** to **10**) in **Figure 2-7**). The resulting cationic

polyphosphazenes were of appropriate charge to bind nucleic acids into polyelectrolyte complexes suitable for gene delivery, while the carboxylic acid functionalized polyphosphazene derivatives displayed varying degrees of anion content dependent on environmental pH. By combining these materials in the presence of nucleic acids, we aimed to generate mixed polyelectrolyte complexes with sufficient positive charge to retain stability in extracellular environments, but with induced changes in charge and hydrophobicity once inside acidic intracellular compartments.

Industrial elastomer/resin	Polyelectrolyte in battery	Biomedical applications
• Thermoplastic or sound insulation. • Fire-resistant circuit boards	• Li-polymer battery • Dye-based solar cells • Membrane fuel cells	• Sustained-release hydrogel • Nanofibers for regeneration • Controlled delivery of medicines or vaccines

Table 2-1. Applications of polyphosphazene in various industries.

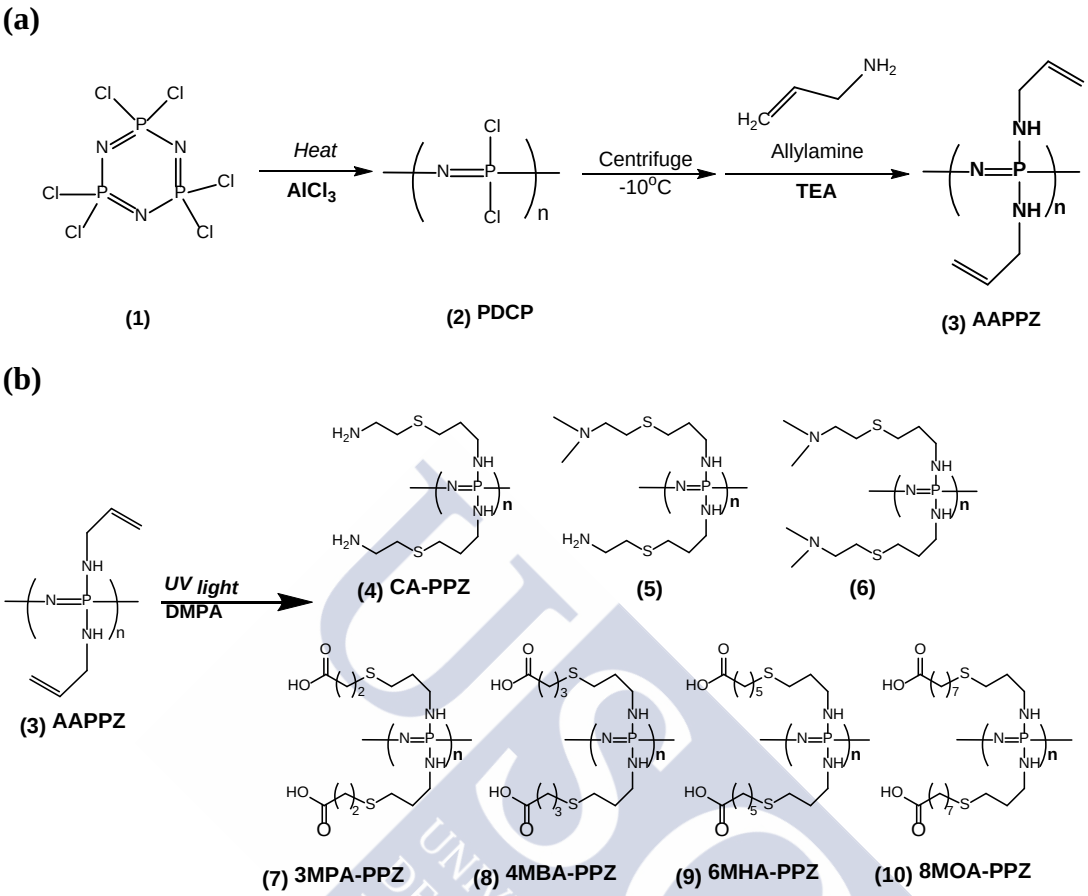

Figure 2-7. A small library of ionic polyphosphazene. (**a**) Ring-opening polymerisation of polyphosphazene and (**b**) functionalization by thiol-ene click addition for controlled gene delivery.

2.2 **Materials and methods**

2.2.1 Materials

Hexachlorocyclotriphosphazene (99%), Aluminium chloride (99.99%), triethylamine (TEA), cysteamine, 2-(dimethylamino)ethanethiol hydrochloride (DMAES), 2,2-dimethoxy-2-phenylacetophenone (DMPA), branched poly(ethyleneimine) 25K (PEI), 3-mercaptopropionic acid (3MPA), 4-mercaptobutyric acid (4MBA), 6-mercaptohexanoic acid (6MHA), 8-mercaptooctanoic acid (8MOA), heparin sodium salt (from porcine intestinal mucosa), anhydrous tetrahydrofuran (THF), 2,2,2-trifluoroethanol (TFE), anhydrous diethylene glycol dimethyl ether (Diglyme), Ethidium bromide (EtBr), Poly-L-lysine (Mw 30K-70K) were all purchased from Sigma-Aldrich and used as received.

2.2.2 Synthesis of the precursor poly(allylamino-phosphazene)

Poly(dichlorophosphazene) (PDCP) was prepared as previously described.[9] A pre-dried flask was loaded with 5.0 g (14.4 mmol) of hexachlorocyclotriphosphazene and aluminium chloride as a catalyst. The reactor was filled with high-purity nitrogen and heated to an initial temperature of 240-250 $^{\circ}$C. After the polymerization for 3 hours, the reactor was cooled to 120 $^{\circ}$C, and 8mL of diglyme was injected into the reactor to solubilize the crude product and to minimize crosslinking[10]. The aluminium chloride was removed by centrifugation (7000 g at -10 $^{\circ}$C. The product identity was confirmed by ^{31}P-NMR in a co-solvent of diglyme/deuterated chloroform (1:3). Subsequent nucleophilic substitution at the chlorine phosphorus centres[18] was performed by

transferring the product supernatant into a pre-dried flask containing 50 mL of anhydrous THF, where TEA (3 eq to chlorine) and allylamine (3 eq to chlorine) were added. The reaction was carried out in ice for 24 hours and then for an additional 24 hours at room temperature. For purification, the mixture of raw products was filtered to remove the trimethylamine hydrochloride and the desired polymer in THF was precipitated in double-volume water (THF:water 1:2), then in pure water. The precipitated polymer, poly(allylamino-phosphazene) (AAPPZ), was collected and dried *in vacuo*. (Yield~4.61 g, 68 %).

2.2.3 Synthesis of cationic and anionic polyphosphazenes by thiol-ene reactions

After synthesis of the precursor AAPPZ, we introduced two different amine side-chains (cysteamine and DMAES) with different composition ratios, to provide cationic functionality, via thiol-ene addition reaction of the thiol termini of both compounds with the alkenyl side chains of the allyl repeat units. Analogous reaction to install various carboxylic acid groups were carried out using 3-mercaptopropionic acid (3MPA), 4-mercaptobutyric acid (4MBA), 6-mercaptohexanoic acid (6MHA) and 8-mercaptooctanoic acid (8MOA). Firstly, AAPPZ (100 mg, 0.637 mmol) in trifluoroethanol (TFE, 8 mL) was mixed with the designated mercaptoalkyl amine or mercaptoalkyl carboxylic acid (3 eq. to allyl group) and flushed with nitrogen gas before adding 2,2-dimethoxy-2-phenylacetophenone (0.05 eq. to allyl groups). The thiol-ene reaction was initiated under UV irradiation (λ=365 nm) for 3 hours, and then the crude product was directly dialysed against an aqueous solution (molar mass cut-off 7 kDa) until the resulting solution became completely clear. The products were recovered by freeze-drying from aqueous solution as powdery solids. The polymers

were analysed by ^{1}H and ^{31}P NMR spectra, and purity and molecular weight were measured by ^{1}H-DOSY.

2.2.4 Formation of polyphosphazene-based complexes

A plasmid DNA (pDNA) is a bi-functional coding for enhanced green fluorescent protein (EGFP) and luciferase from firefly photinus pyralis was used throughout this thesis, except for confocal imaging because of minimum background fluorescence. In this pDNA, wild-type EGFP was modified to enhance the fluorescence excitation and emission at 488 nm and 507 nm, respectively. *Photinus pyralis* luciferase was chosen as it emits yellow-green light with maximum at 560 nm during across the pH range of 7.5-8.5. Cationic polyphosphazenes with the varying side-chain ratios of cysteamine and DMAES were dissolved in 10 mM HEPES pH 5.0. The anionic side-chain polyphosphazenes were dissolved in 10 mM HEPES pH 8.2 and the pDNA was in pure water. Complexation was performed under intense vortex mixing for 30 second at various ratios of positively-charged amine moieties on the polymer to negatively-charged phosphates on the pDNA (N/P ratio). In the case of the mixed cationic and anionic polyphosphazenes, the polycationic PPZ condensed both the anionic polymers and the pDNA in one step. These polymeric complexes were characterized by their stoichiometric composition ratio, in terms of positive amines (N), negative carboxylates (C) and negative DNA phosphates (P), i.e. N/C/P ratio.

2.2.5 Characterization

2.2.5.1 Nuclear Magnetic Resonance Spectroscopy (NMR)

^{1}H and ^{31}P NMR spectra were recorded on a Bruker 400 and DRX-500 spectrometers. ^{1}H Diffusion-ordered spectroscopy (^{1}H-DOSY) was recorded on Varian Inova 750 (750MHz). Solvents used were $CDCl_3$, D_2O, MeOD or Acetone-d_6. All chemical shifts are reported in parts per million (ppm) relative to tetramethylsilane (TMS) or known solvent peak positions.

2.2.5.2 Gel Permeation Chromatography (GPC)

Molar masses of polymers were determined via gel permeation chromatography using a Shimadzu Prominence UPLC system fitted with a DGU-20A5 degasser, LC-20AD, CBM-20A LITE system controller, SIL-20A autosampler, CTO-20A oven and RID-10A refractive index detector. Separations were performed on a series of Aquagel 30-40-50 (300 x 7.8 mm, 5 mm bead size, Agilent UK) columns fitted with a matching guard column (50 x 7.8 mm). The mobile phase was acidic buffer solution (1M acetic acid and 0.3 M NaH_2PO_4) at 1 mL/min flow rate and separations were performed at 37 $^{\circ}$C. Column calibration was achieved using Poly(2-vinylpyridine) Easi Vials (2 mL) standards (668 Da–211k Da, Polymer Standards Service, USA).

2.2.5.3 Dynamic light scattering (DLS) and Zeta Potential Measurements

Dynamic light-scattering and zeta potential measurements were performed using a Nanosizer ZS instrument (Malvern, UK) at 25 $^{\circ}$C, equipped with a He-Ne laser (λ=633 nm) with a backscatter angle of 173º. For zeta potential, measurements were performed in 1 mM KCl. Hydrodynamic radii distributions were calculated with Malvern software. From standard auto correlation functions, diffusion coefficients were related to particle hydrodynamic radius via the Stokes Equation:

$R_H = \kappa_B T/6\pi\,\eta\,D$ (**Eq. 2-1**)

Where R_H is the hydrodynamic radius, κ_B is the Boltzmann constant, T is the temperature, and η is the viscosity of the solvent. In addition, it was assumed that particles were spherical and non-interacting.

2.2.5.4 Electron Microscopy

The morphologies of the polymeric complexes were probed by transmission electron microscopy (JEOL JEM-2010) in negative staining mode using phosphotungstic acid (PTA, 2 % w/v). The complex suspensions (10 μL of solutions at a plasmid concentration of 62.5 μg/mL) were dropped onto a TEM grid (Carbon Film CF400, Electron Microscopy Sciences) and left for 5 min for attaching on the grid, and then residual solution was blotted away by capillary force. Afterwards, the PTA solution was added to the grid for 1 min and then the grids were washed with pure water and dried under low-pressure prior to TEM imaging.

2.2.6 Potentiometric titration, gel electrophoresis

The buffering capacities of cationic and anionic polyphosphazenes were determined by initial dissolution of the polymer in MilliQ water to give a concentration of 50 mM of side-chain units. The anionic polymer solutions (0.5 mL) were adjusted to pH 11 with 1 N NaOH and then titrated with 1 N HCl. In between each addition, the polymers were agitated under vortex for 30 second and allowed to stabilize for another 30 second prior to pH measurement. For cationic polymers, solutions of the same

concentration were adjusted to pH 2 with 1 N HCl then titrated with 1 N NaOH using the same method as for the anionic polymers. pKa calculation was performed by Henderson-Hasselbalch equation (**Eq 2-2**) based on the data of potentiometric titration curves. The titration curve data were re-plotted to scatter diagrams by pH against Log ($[A^-]/[HA]$), and pKa was obtained by a linear fitting between pH 8 and pH 5. Protonation degree (α) vs. pH was calculated from the potentiometric titration curves. Herein Alpha (α) represented the percentage of protonated carboxylic acid groups or amine groups in the whole anionic/cationic polyphosphazene, and the calculation of α was shown below[35,37,38]:

$$pH = pKa + Log(\frac{[A^-]}{[HA]}) \qquad \textbf{(Eq 2-2)}$$

$$\alpha = \frac{C_p}{C_A} = \sum_{i=0}^{n}(C_{HCl} - C_{[H^+]}) - C_{[OH^-]} \Big/ C_A \qquad \textbf{(Eq 2-3)}$$

Here, taking anionic polymers as an example, C_A denotes total concentration of alkyl-carboxylic side groups in the polyanionic solution; C_p denotes the concentration of protonated alkyl-carboxylic acid groups; C_{HCl} denotes each addition of HCl concentration; $C_{[H+]}$ is the concentrations of free $[H^+]$, which can be measured by pH meter, and $C_{[OH^-]}$ is the concentration of initial $[OH^-]$ in the test solution, adjusted by NaOH in the beginning for ensuring all carboxylic acids in the de-protonation state; i=0 is the initial point, where we defined 0 % as the protonated alkyl-carboxylic acid groups around pH 11; n is the number of HCl additions. There is an assumption that the total volume keeps a constant during the titration (the volume percentage of each addition of HCl is 0.004 of total volume).

For estimating the binding efficiency of pDNA complexation, gel electrophoresis was performed using 1 % agarose containing (0.5 μg/mL) ethidium bromide (EtBr) at 110 V for 50 min. Each sample was prepared to a 30 μL volume containing 1 μg plasmid. In heparin displacement tests, each polymer/DNA complex sample was challenged with different mass ratios of heparin to plasmid, using samples at a fixed volume (30 μL) and incubated for 1 hour at 37 °C.

2.2.7 Preparation of Cy3-CA-PPZ and Cy5-pDNA for FRET

For tracking and investigating polymer and pDNA in vitro and in vivo, we labelled cyanine 3 (Cy3) and cyanine 5 (Cy5) on the polycation CA-PPZ and blank pDNA, respectively. Firstly, for labelled CA-PPZ, 0.5 mg of Cy3-NHS (from GE) was dissolved in DMSO and 8.2 mg of CA-PPZ was suspended in 0.5 mL HEPES pH 8.2 and diluted to 3.5 mL with DMSO. The Cy3-NHS solution and CA-PPZ solution are mixed in an amber vial and stirring for reaction overnight under light protection. The purification is via dialysis against pure water for 72 hours with renewing water frequently. After that, the Cy3-labelled CA-PPZ was dried by lyophilisation and stocked in -20 °C.

For Cy5-labelled pDNA preparation, we used the Cy5 Label IT® kit (Mirus), following with the manufacturers' instructions. Briefly, pDNA was added to Label IT® reagent at the ratio of 0.25 μL to 1 μg pDNA. The reaction was performed under shaking at 37 °C for 1 hour. Afterwards, 0.1 volumes of 5 M sodium chloride and 2 volumes of cold 100% ethanol were added into the reaction and the mixture was left for at least 30 min at -20 °C. The Cy5-labelled pDNA was isolated by centrifugation

into a pellet. For removing possible impurities, the pellet was washed with 70% ethanol and re-suspended in pure water. The complexation of Cy3-CA-PPZ and Cy5-pDNA was described above and loaded in 96-well plates. The fluorescent intensity was measured by Fluorimetry (Synery H1, Biotek) with excitation / emission wavelengths set at 500 nm / 565 nm for Cy3 and at 645 nm / 676 nm for Cy5. The FRET efficiency is calculated by the equation: FRET efficiency = $I_{(Ex500\text{-}Em676)}$ / $I_{(Ex500\text{-}Em565)}$.

2.2.8 Transfection and cytotoxicity

For 2D transfection and cytotoxicity studies, U87MG or GBM1 cells were cultured in Dulbecco's Modified Eagle Medium (DMEM, Sigma) containing 10 % fetal bovine serum, 2 mM Glutamine and 100 mg/L penicillin-streptomycin and maintained at 37 $^{\circ}$C under a 5 % CO_2 atmosphere. For 2D cultures, the cells were seeded at a density of 25000 cells/cm^2 in 24-well plates and incubated 24 h prior to transfection. Then, polymer:pDNA complexes were added at various pDNA concentrations in Opti-MEM for 4 h. After this time, the formulations and cells were incubated with fresh growth medium for additional 48 h. The transfected cells in 24-well plates were evaluated via fluorescence microscopy and quantified by Luciferase assay kits (from Promega). Cytotoxicity was evaluated by MTT assays (Promega). Briefly, the transfected cells were treated with 10 µL 12 mM MTT/PBS solution and incubated with 100 µL phenol-red free media in each well for 4 h. After the supernatant was removed, 50 µL DMSO aliquots were added to the wells of MTT-labelled cells, and then mixed and incubated for 10 min before being analysed in a plate reader with absorbance wavelength at 540 nm.

Chapter II / Capítulo II

2.3 Results and discussion

2.3.1 Synthesis of the precursor Allylamino-attached polyphosphazene

The strategy for syntheses of various substituted polyphosphazenes was via conventional thermal ring-open polymerisation of cyclic monomer hexachlorophosphazene (**1**) and reaction of the resultant poly(dichlorophosphazene) with allylamine under basic conditions to afford vinylic side-chains[15]. Firstly, the ring-opening polymerisation was initialised by high temperature (~240 ºC) with catalyst Aluminium chloride ($AlCl_3$) and without any solvents. In traditional solvent-free polymerisation for polyphosphazene, the product easily crosslinked by traces of water, forming a rubber-like solid. In the present time, the catalyst ($AlCl_3$) would help in minimizing crosslinking because of its high affinity to water and reacts forming hexahydrate $[Al(H_2O)_6]Cl_3$. In addition, it significantly speeded up the reaction time to 3 hours, because the catalyst effectively takes chloride away from the trimer at the beginning of the reaction, facilitating the initiation of the polymerisation and contributing to a decline in the molecular weight distribution (PI) and molecular weight of poly(dichlorophosphazene) (**2, PDCP**)[9]. For subsequent thiol-ene click chemistry, we chose the simplest allyl-terminal group as side chain, which is allylamine (**Figure 2-8**). In view of minimum water pollution, we designed a simple and effective purification procedure after the melt polymerisation. Once the polymerisation is completed, the reactor would be cooled to approximately 120 °C and anhydrous diethylene glycol dimethyl ether (diglyme) was injected into the reactor. The solvent is known to minimise crosslinking of PDCP and to stabilise the crowd product PDCP as well as for stabilising the crude product[10]. However, if the temperature of the reactor dropped below 100 °C,

the crude polymer started solidifying and precipitating even addition of diglyme. After suspension in diglyme, the crude product will be chilled to -10 °C in an ice bed (ice plus salt). The low temperature minimised crosslinking but also significantly reduced the solubility of aluminium chloride, which could be precipitated efficiently by centrifuge. Therefore, the main advantages to this synthesis protocol are that they allow purification from the catalyst and other impurities in a streamlined way while optimising polymer stability. After ring-opening polymerisation, the crude products were transferred to a super-dry reactor with THF as solvent for nucleophilic substitution of allylamine. Following that, the product was purified via filtration to remove TEA-Cl, and then, precipitated in water. In this study, we attempted to simplify chemical synthesis and minimise the use of organic solvents, but diglyme and THF are still used. Future research might try to replace THF with water or alcohol to move this chemistry towards a greener approach.

The final product AAPPZ should not be completely dried by lyophilisation likely because of its crystallization that renders a product that can be re-dissolved in only few solvents (i.e. TFE and 5-10 % phosphoric acid solution). For the polymer characterisation, the polymer samples were dried at low pressure overnight. PDCP was characterized by ^{31}P-NMR and nucleophilic substitution at the P-Cl bonds with allylamine to generate the key precursor polymer. As shown in **Figure 2-8**, the major single peak shifted from 21.2 ppm to -16.0 ppm in the ^{31}P-NMR spectra, confirming that hexachlorocyclotriphosphazene has been polymerised to PDCP. Also, the single peak of PDCP shifts to 3.6 ppm after the allylamine substitution reaction, confirming that allylamine has substituted chlorine and its nitrogen atom has bound to the phosphoric atom on the backbone. In the ^{1}H-NMR spectra, there are two peaks at 5.80 ppm and 5.09

ppm corresponding to protons of the allyl group, which provided a second confirmation of the successful introduction of allyl groups in the polyphosphazene. Furthermore, an NMR-DOSY experiment confirmed that allylamino-polyphosphazene (AAPPZ) diffused as a macromolecular entity. The overall reaction yield is 32.4 % (2.2 g / 6.77 g).

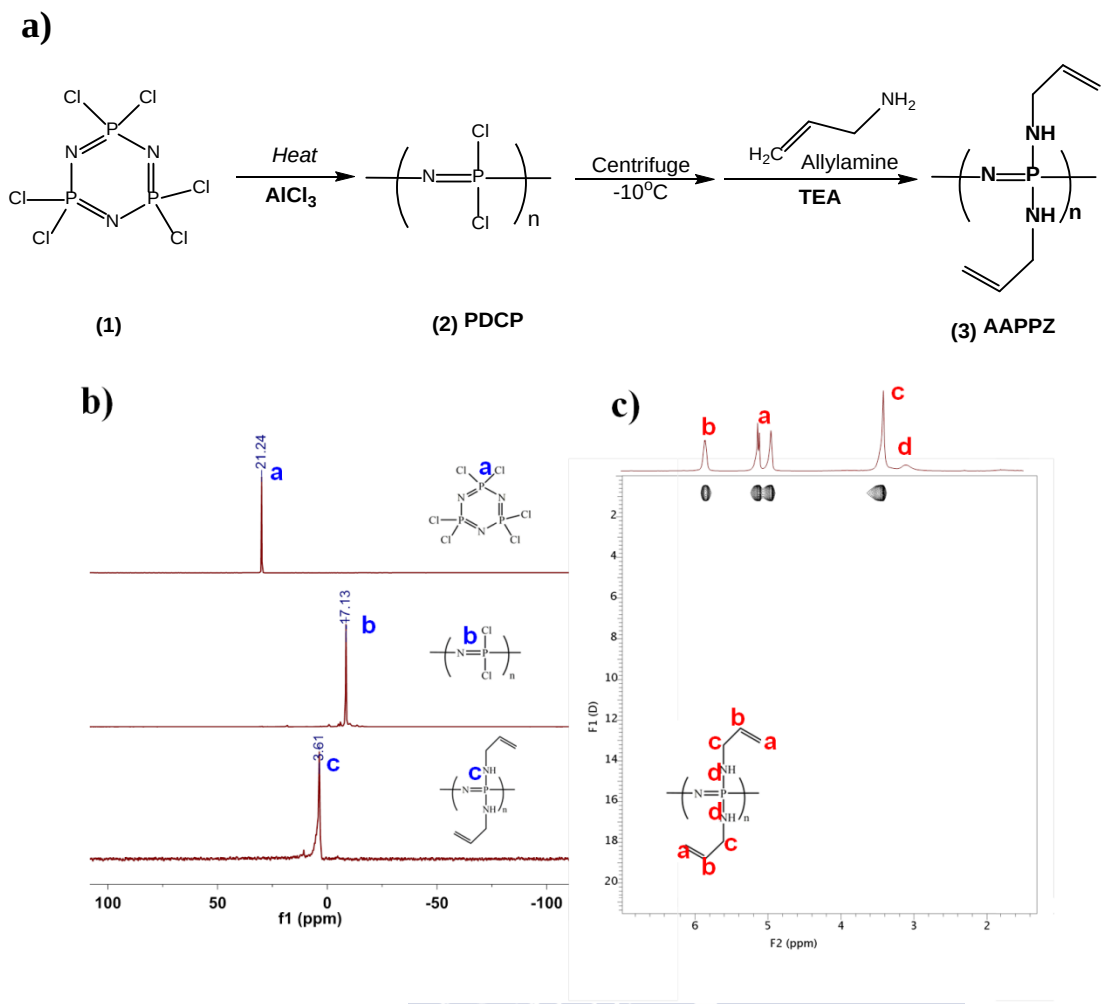

Figure 2-8. Synthesis and characterization of the polyphosphazenes. **a**) Synthesis of ionic polyphosphazenes via thermal ring-open polymerisation, nucleophilic substitution and thiol-ene click chemistry. (**b**) ^{31}P-NMR spectra of hexachlorocyclotriphosphazene, Poly(dichlorophosphazene) (PDCP), and allylamino-polyphosphazene (AAPPZ). (**c**) ^{1}H-NMR-DOSY of AAPPZ.

2.3.2 Synthesis of ionic polyphosphazene via thiol-ene click addition

The advantages of this precursor AAPPZ is that it is amenable to thiol-ene derivatisation, and here we applied this reaction to yield a series of polycations (**4-6**) and polyanions (**7-10**) (**Figure 2-7**). Firstly, we introduced the different cationic side chains on the backbone via thiol-ene click chemistry **(4-6)**. For cysteamine-introduced polyphosphazene **(4)**, high conversion rate (cationic moiety/allyl group) ≧90% and the high reaction yields (≧71%) were achieved by one direct thiol-ene reaction in TFE. However, the conversion efficiency of when introducing both cysteamine and DMAES or only DMAES in the solvent as TFE was lower 60-70%. We hypothesized that this reduction in the efficiency was caused by charge-repulsion of the tertiary amine of DMAES. To address this issue, we prepared a home-made buffer, sodium phosphite 10 mM and sodium sulfate 50 mM pH 8.2 as reaction media where we expected the sulfate ions to shield the ionic repulsion of the tertiary amine[47]. Using this customized aqueous buffering solution as reaction medium, the conversion rate from allyl group to cationic groups was improved to ≧96% (**Figure 2-9a**). In the ^{1}H-NMR spectra, the peaks of the allyl group almost disappeared after the thiol-ene reaction, whereas the two peaks at 1.83 ppm and 1.29 ppm attributed to the protons from −S−CH_2−C**H_2**−CH_2− (peak **b'**) and −S−CH(C**H_3**)− (peak **b''**) confirmed the successful addition of thiol groups on the precursor. Furthermore, the ratio of protonation of the amine groups would be affected by the chemical shifts of neighbouring protons, especially for tertiary amines. For cationic polyphosphazene, we adjusted pH of deuterium oxide to around pH 9-10, inducing the peak (**g**) of −S−CH_2−CH_2−N(**CH_3**)**$_2$** shifting to around 2.35 ppm, for accurate calculation of the primary to tertiary amine ratio. The intensity of the peak at 2.35 ppm (**g**) increased with increasing ratio of DMAES introduced on the backbone, which indicates the increasing ratio of tertiary amines introduced to the backbone.

A range of different anionic (**7-10**) side-chains polymers were also generated from AAPPZ via thiol-ene click chemistry. Reactions proceeded to a high degree (≧99% substitution of the allyl groups by the cationic side-chains) and good overall yield (≧71%). Product identities were confirmed by ^{1}H-NMR (**Figure 2-9b**).

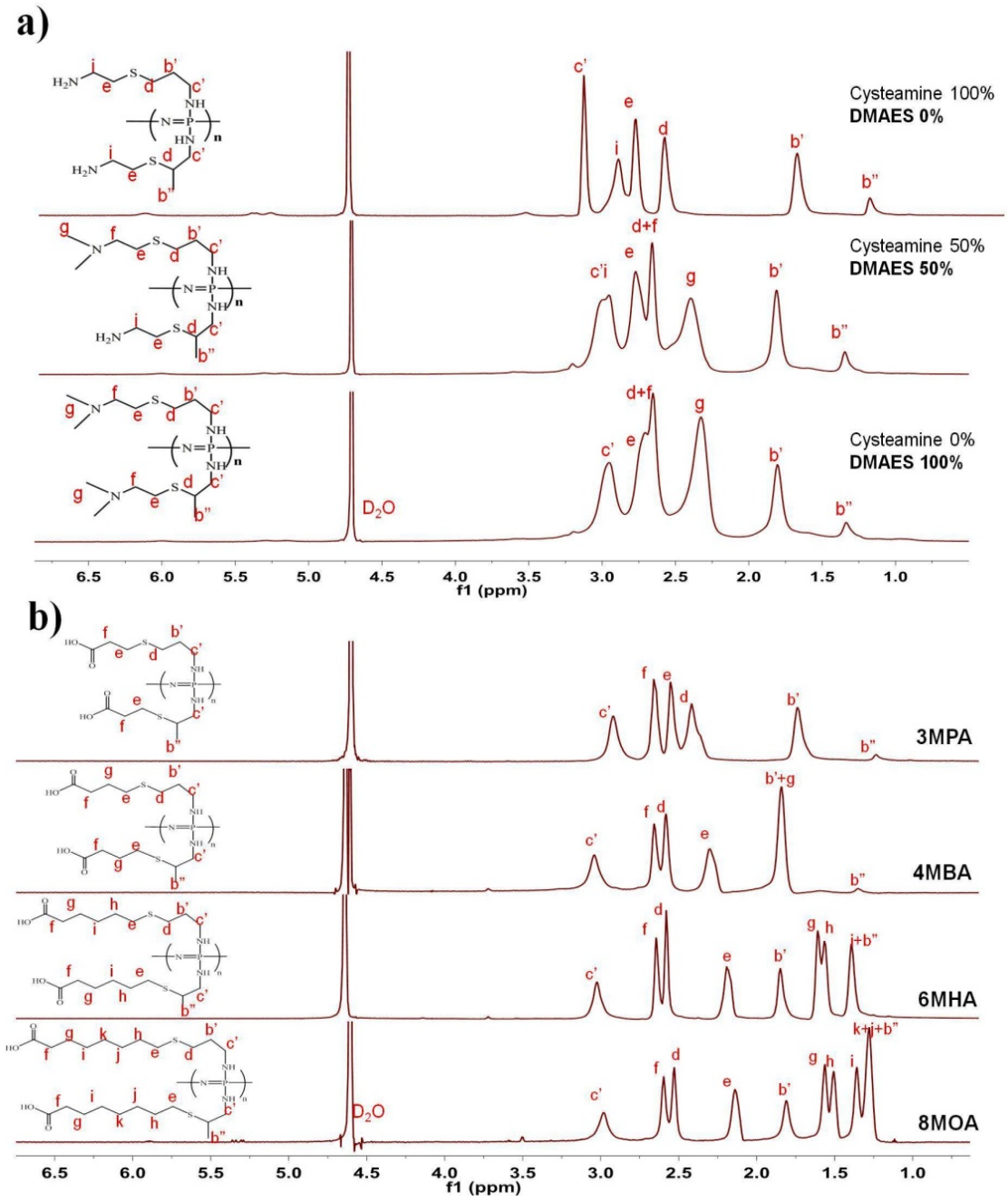

Figure 2-9. Proton-NMR of ionic polyphosphazenes. (**a**) Proton-NMR of cationic

functionalized polyphosphazenes with cysteamine and/or 2-(dimethylamino)ethanethiol (DMAES) at the ratios of 100:0, 50:50, and 0:100, prepared via thiol-ene addition. The polymers were dissolved in D_2O, pH 9-10. (**b**) Proton-NMR of anionic functionalized polyphosphazenes with aliphatic chains of diverse lengths, prepared via thiol-ene addition.

For further confirming the structure of cationic polyphosphazene, correlation spectroscopy (COSY) and Heteronuclear Single-Quantum Correlation spectroscopy (HSQC) were performed (**Figure 2-10**). COSY is a two-dimensional NMR spectrum for a homonuclear correlation, here for ^1H to ^1H correlation. The cross peaks on diagonal line represent the correlation of the protons with themselves and generate the same peaks as the regular proton spectrum. The other cross peaks are symmetric against the diagonal and correspond to two nuclei coupling. When we analysed the cationic polymers by COSY, we could easily identify a spin group of the peak **b'** with its neighbouring peaks **c'** and **d**, and another one with peaks **i** and **e**. More interestingly, there is a small cross peak derived from a coupling pair of peaks c' and d, indicating that the **c'** (–P−NH−C**H$_2$**−) is located at higher chemical shift than the peak **i** (H_2N−C**H$_2$**−CH_2−) around pH 7, even though their chemical shifts are very close. Since most of these groups are formed by the thiol-ene addition of the allyl group, these provided further proof of the final structure of the compounds.

On the other hand, HSQC presents heteronuclear correlations that separate between one single bond. In HSQC, we can separate low chemical shifted carbons corresponding to those having C−S and C−C bonds and high chemical shifted carbons (i.e. C−N bonds) (**Figure 2-10b**). These spectra allowed us to confirm that peaks (**i**)

and (**c'**) are associated to C−N protons, further supporting our molecular assignment. It also should be carefully considered the effect of pH on the proton NMR chemical shifts of ionic polymers causing a satellite peak near to peak (**c'**).

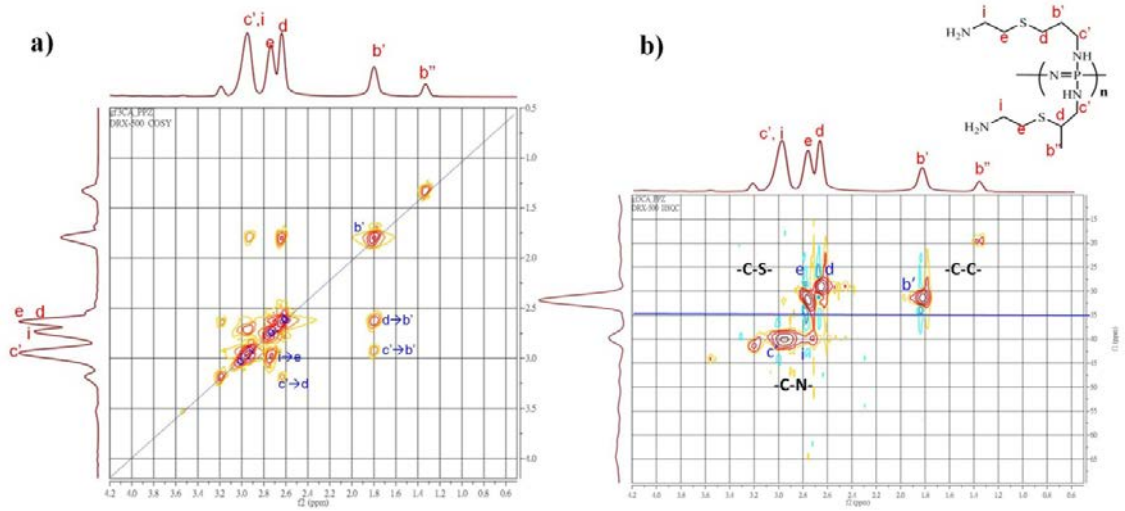

Figure 2-10. 2D spectra of high-Mw CA-PPZ. (a) ^{1}H-^{1}H COSY spectra and (b) ^{1}H-^{13}C HSQC spectra.

Although the literatures indicate that the molecular weight of PDCP can be adjusted by the feeding ratio of catalyst ($AlCl_3$), the reported Mn range of polyphosphazene was from 10K to 100K, hardly of any significance when coupled with large polydispersity. Herein, we measured the molecular weight of cationic polyphosphazenes instead of AAPPZ, because the crystallization of completely dried AAPPZ caused issues of solubility, while cationic polyphosphazenes are much easier dissolved in aqueous buffer[15]. In addition, the purification after click addition to cysteamines on the backbone is through dialysis by cut-off Mw 7K, which may influence the molecular weight of the final product. We focused our characterization on cysteamino-introduced polyphosphazene (CA-PPZ) which is the most important

cationic material in this study (**Table 2-2** and **Figure 2-11**). We observed that by changing catalyst addition rate (5 wt% and 10 wt% to monomer) we could prepare CA-PPZ with low MW (~26KDa) and high (~36KDa). In both cases, the polydispersity was narrow, likely due to the effective purification after the ring-opening polymerisation by the centrifuge method and filtration after thiol-ene click reaction, which both had removed highly crosslinked fractions from the raw products.

Table 2-2. Molecular weight and distribution measured by GPC (n=3)

Cationic PPZ	Mw	Mn	PI
HMw CA-PPZ	35921 ± 3936	24515 ±6622	1.54 ±0.36
LMw CA-PPZ	25954 ± 2387	16693 ±1864	1.56 ±0.05

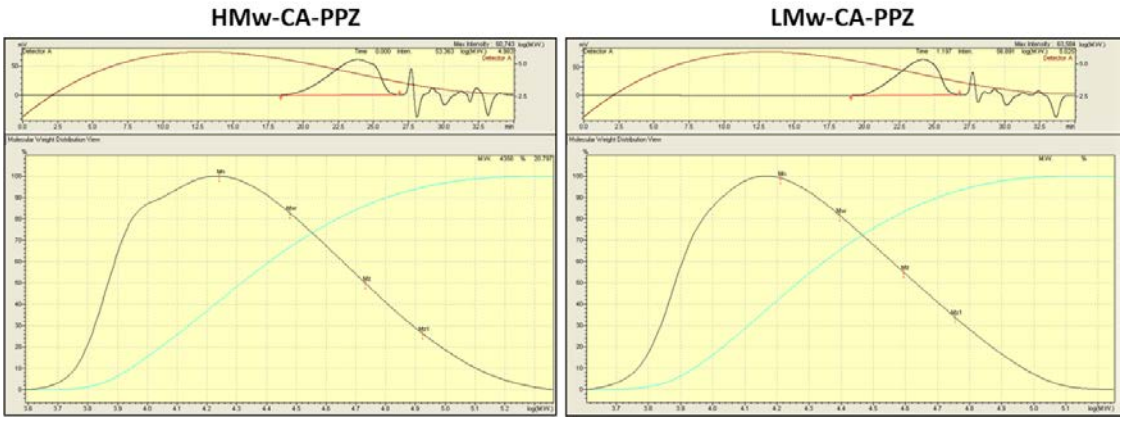

Figure 2-11. The molecular weight distribution of high and low molecular weight CA-PPZ. The molecular weight distribution was measured by GPC and column calibration was achieved using Poly(2-vinylpyridine) standards.

2.3.3 Acid-base buffering capacity of ionic polyphosphazenes

The polymers were intended as nucleic acid carriers, for which their abilities to act as 'proton-sponges' and/or membrane disruptors[48] would be highly dependent on their ability to accept protons and to change their hydrophilic / lipophilic balance across intracellular pH ranges. The protonation profiles of the polycations were thus determined by potentiometric titrations (**Figure 2-12 a,d**). As expected, the amine side-chain polymers remained protonated across cytosolic and endolysosomal pH ranges and their buffering ranges were higher than pH 8. However, the various aliphatic acid side-chain polymers, derived from 3-mercaptopropanoic acid (3MPA), 4-mercaptobutanoic acid (4MBA), 6-mercaptohexanoic acid (6MHA), and 8-mercaptooctanoic acid (8MOA) exhibited buffering regions across the range of pH 8 to pH 5 (**Figure 2-12 f**). For these anionic polymers, the titration was performed from high to low pH, and in this process, the polymers became hydrophobic due to protonation of alkylcarboxylic acid and precipitated at certain point. Because of this precipitation, we only can obtain "apparent pKa" for these pH-sensitive polyanions. The pKa values were calculated by Henderson-Hasselbalch equation, by which the titration data was re-plotted to scatter diagrams and then fitted with linear regression. As shown in (**Figure 2-12 b,e**), the apparent pKa of alkylcarboxylate side-chain PPZ increased while the alkane section of side chains extended. This is likely that longer alkane chain on the alkylcarboxylate-PPZ presents more hydrophobic features once their carboxylate groups are protonated. In light of this, we screened different alkylcarboxylates as side chains on the PPZ backbone based on the process and clearly shows that those polyanions possess high pH-sensitivity and the capacity to change their aggregation behaviour around endosomal pH.

For further understanding of their buffering capacity, these titration curves were converted to line charts plotting protonation degree (α) against pH (**Figure 2-12 c,f**). The largest shift in the proportion of ionized side chains over the critical physiological pH to early endosomal pH (pH 7.4 to 6.0) was exhibited by 6MHA-PPZ, with an overall change in protonation of 61.9±3.6%. This was significantly higher than the other anionic polymers (**Table 2-3**).

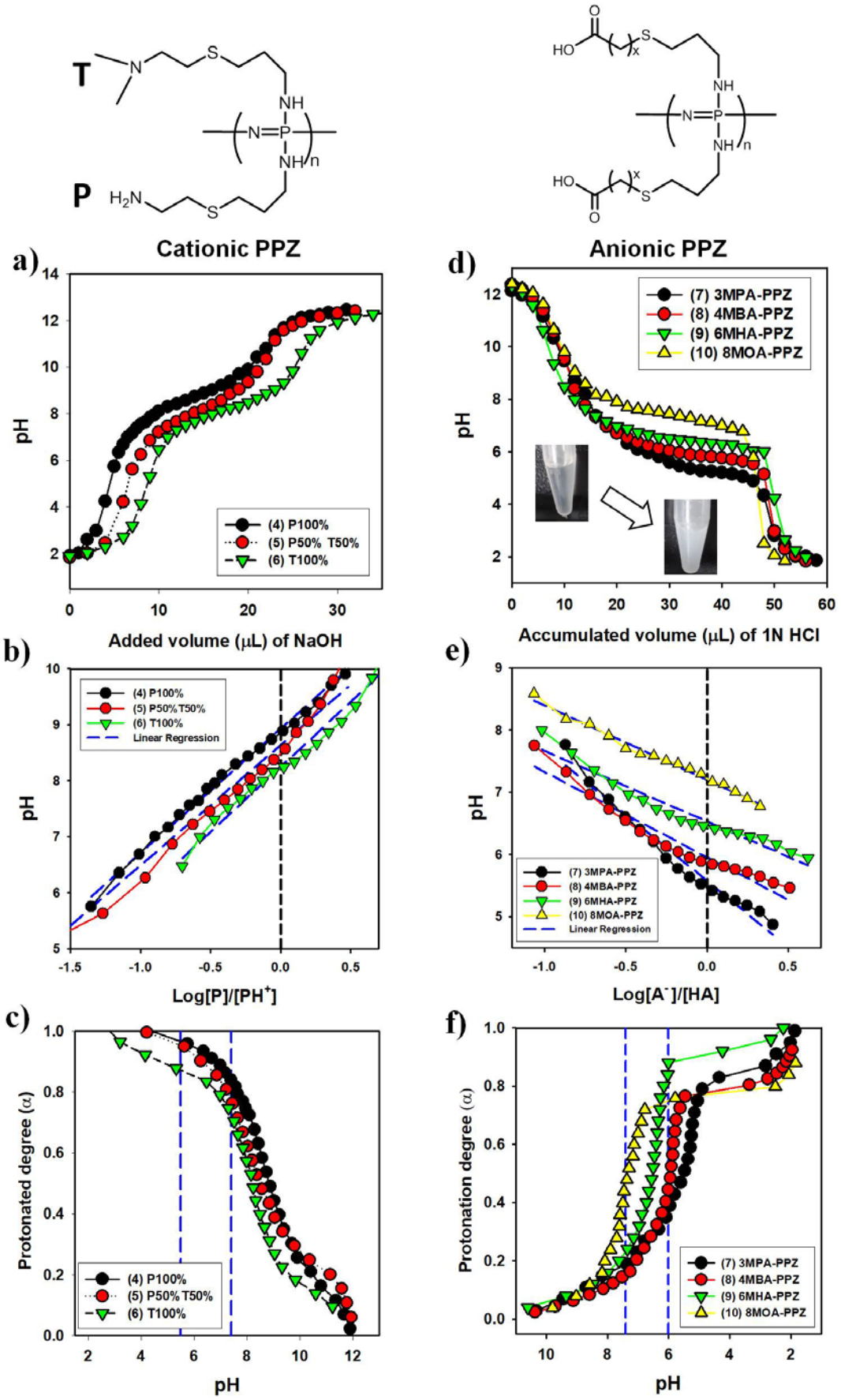
T
P
Cationic PPZ
Anionic PPZ
a)
d)
pH
(4) P100%
(5) P50% T50%
(6) T100%
(7) 3MPA-PPZ
(8) 4MBA-PPZ
(9) 6MHA-PPZ
(10) 8MOA-PPZ
b)
e)
Added volume (μL) of NaOH
Accumulated volume (μL) of 1N HCl
Linear Regression
Log[P]/[PH+]
Log[A-]/[HA]
c)
f)
Protonated degree (α)
Protonation degree (α)

Figure 2-12. Protonation profiles of ionic polyphosphazenes analysed by potentiometric titration curves. (**a**) Potentiometric titration curves of cationic polyphosphazenes, only primary amines attached (P100%) (CA-PPZ), half primary and half tertiary amines attached (P50% T50%) CA-/DMAES-PPZ, and only tertiary amine attached (T100%) (DMAES-PPZ). (**b**) pKa calculation of polycations by a scatter diagram of Log [P/PH^+] against pH. [P] represents the concentration of amine side-groups on the PPZ and [PH^+] is the concentration of protonated amine-side groups. (**c**) Protonation degree (α) of different cationic polymers against pH. (**d**) Potentiometric titration curves of anionic polyphosphazenes with different lengths of alkylcarboxylic acid. (**e**) pKa calculation of polyanions by a scatter diagram of Log [A^-/HA] against pH. [A^-] represents the concentration of carboxylate side-groups on the PPZ and [HA] is the concentration of protonated carboxylic acid side groups. (**f**) The protonation degree of different anionic polyphosphazenes against pH.

Table 2-3. Apparent pKa and percentage of protonation between pH 7.4 and 6.0 of anionic polyphosphazenes. Data derived from potentiometric titrations ($n \geqq 3$).

Polyanion	3MPA	4MBA	6MHA	8MOA
Apparent pKa	5.56±0.09	5.89±0.07	6.55±0.08	7.14±0.10
△α (pH 7.4 – 6.0)	19.7%±3.2%	29.1%±4.0%	61.9%±3.6%	29.7%±2.6%

2.3.4 Particle characterization of polyionic gene complexes

For the characterization of ionic polyphosphazene complexes, we screened how several factors affected the physicochemical properties of the complexes. The factors analysed were N/P ratio of polycation/pDNA complex, addition of anionic polyphosphazenes, and the ratio between cationic and anionic polyphosphazenes. In the whole screening, every complex was loaded with same amount of pDNA. Here, we abbreviated the composition ratio of polymeric complexes between polycationic amines (N), polyanionic carboxylates (C), and negative DNA phosphates (P) to N/C/P.

Firstly, the cationic polymers (CA-PPZ) were screened for polyelectrolyte complex formation with plasmid DNA (pDNA) at varying N/P ratios (**Figure 2-13a**). From N/P ratio 1:1 to 2:1, the surface charge of the complexes undergoes inversion from -15 mV to net positive values, showing that at N/P ratio 1:1 the plasmid is not completely covered by the cationic polyphosphazene. At N/P = 8, the diameters of the complexes were all close to 80 nm and the zeta potentials close to +40 mV, and these characteristics did not increase with further additions of polycation.

When CA-PPZ complexes were formed in the presence of the various PPZ polyanions (at the 8:4 ratio of amines to carboxylic acids in the mixture), the diameters increased to ~100 nm and the zeta potential decreased to approximately +30 mV (**Figure 2-13b**), indicating further neutralization of the CA-PPZ. The characteristics of the complexes, however, did not change by introducing alkylcarboxylate-PPZ with different aliphatic chains. In addition, the size of the complexes did not significantly increase with the addition of higher amounts of the polyanion 6MHA-PPZ, but the total derived count rate in the light scattering experiments increased over one order of

magnitude compared to the same complexes without the anionic PPZ. This indicated that tighter particulate complexes were formed in the presence of polyanionic PPZs (**Figure 2-13c**).

For further investigation on our binary polyionic complexes, we employed Nanoparticle Tracking Analysis (NTA, from Malvern) to measure particle size distribution and concentration. In **Figure 2-14**, the three-axis scatter charts showed that the scattered light intensity increased with increasing 6MHA-PPZ mixing ratio. This change is particularly visible when comparing intensity distributions between 8:0:1 and 8:1:1 complexes, but the change was maintained at compositions with higher amounts of 6MHA-PPZ. Despite of that, NTA experiments determined that all polymer complexes, independent on the introduction of higher amounts of 6MHA-PPZ, had similar amounts of particle numbers (**Figure 2-14**). Trying to reconcile these results with the intensity plots and the DLS, we suggest that the introduction of 6MHA-PPZ in the complexes only increased particle density, making more compact complexes, instead of generating a higher amount of particles.

Another tool for nanocomplex characterization is Transmission Electron Microscopy (TEM) imaging, which could help us understand the morphology of the different polymer complexes (**Figure 2-15**). Both CA-PPZ:pDNA and CA-/6MHA-PPZ:pDNA complexes are spherical. Compared to CA-PPZ:pDNA, 6MHA-PPZ mixing in CA-PPZ complexes show more defined boundaries when imaged by TEM. This might be a further indication of a more compact structure in complexes having 6MHA-PPZ, and would support the hypothesis on PPZ complex structure put forward by DLS and NTA data.

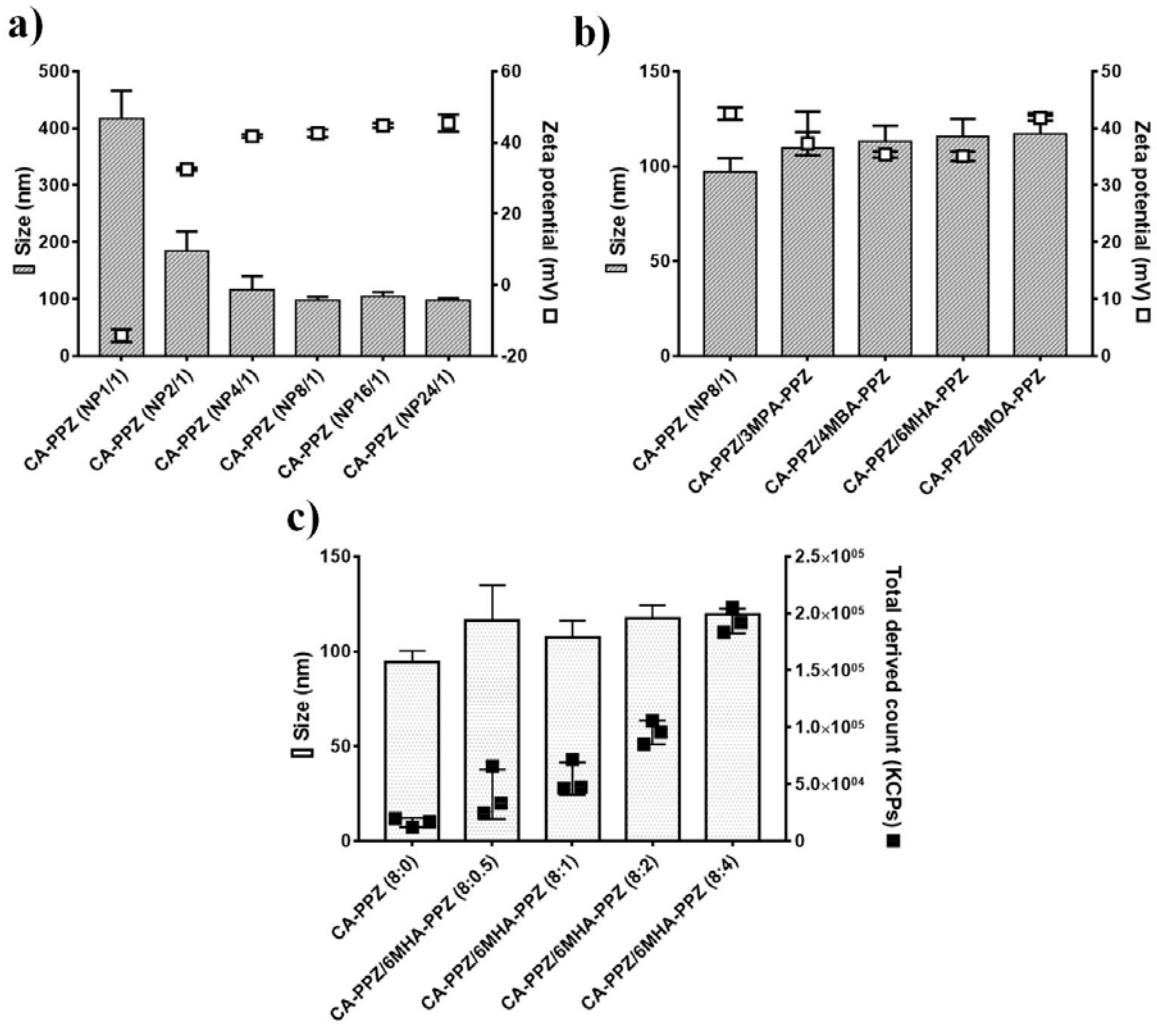

Figure 2-13. Characterisation of ionic PPZ gene complexes. Hydrodynamic size and zeta potential of CA-PPZ:pDNA with different N/P ratios in **a)** and of CA-PPZ:pDNA complexes mixed with different polyanions in b) and at a ratio of CA-PPZ amines, anionic PPZ carboxylates and pDNA phosphorous (N/C/P) of 8:4:1 was used. c) The particle sizes and total derived counts (KCPs) of CA-PPZ:pDNA complexes (8:1 N/P ratio) mixed with increasing amounts of 6MHA-PPZ (from 8:0 to 8:4 N/C ratio).

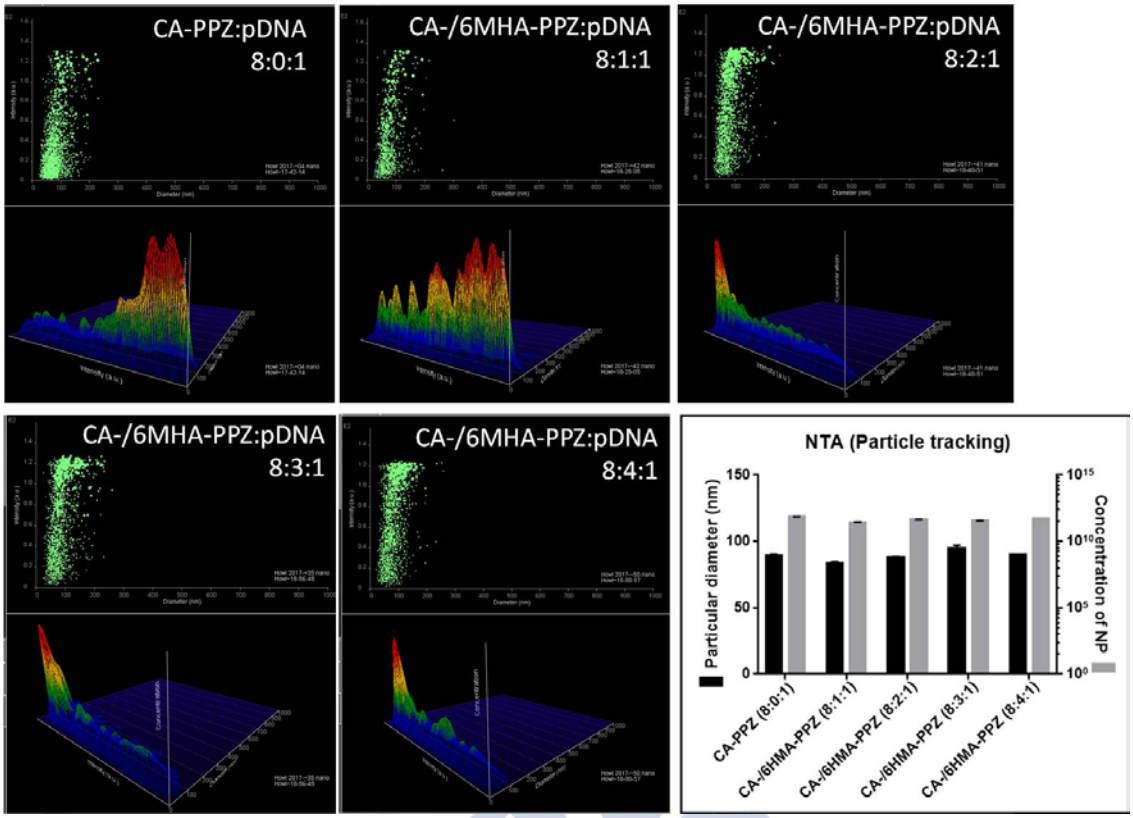

Figure 2-14. Nanoparticle Tracking Analysis of polyionic complexes. A fixed ratio of polycation CA-PPZ condensed various ratios of polyanion 6MHA-PPZ and the same amount of pDNA. In the green scatter graph (up) showed the relationship between particle size (X-axis) and light scattering intensity (Y-axis). For the 3D graphs (down), the three-axes represented particle size (X-axis), light scattering intensity (Y-axis) and concentration (particle number/mL in Z-axis). The quantification of particle size and concentration above were shown in the bar chart graph.

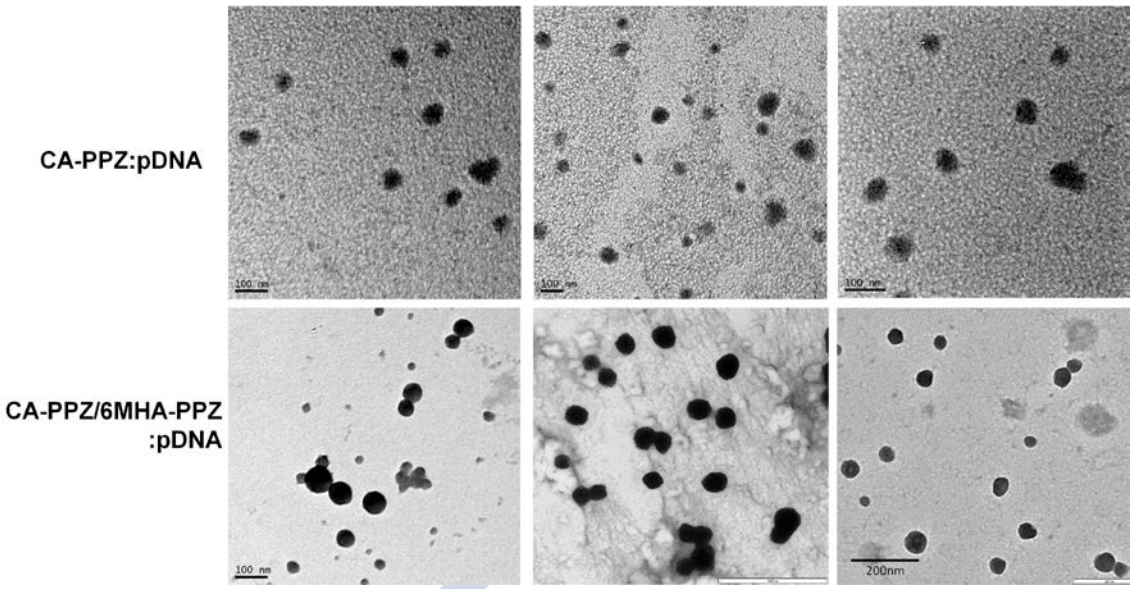

Figure 2-15 TEM images of CA-PPZ:pDNA and CA-/6MHA-PPZ:pDNA complexes in three independent experiments.

2.3.5 Binding efficiency of polyionic gene complexes

Following the physicochemical particle characterisation, we investigated the pDNA-binding efficiency of polymeric complexes and pDNA release in the presence of a competitor. Agarose gel electrophoresis experiments were performed in the absence and presence of the competing strong polyelectrolyte heparin to test the ability of the different polyplexes for retaining pDNA. The data indicated that tertiary-amine PPZ complexes, particularly 100% tertiary amine groups quickly released their pDNA cargo by incubation with heparin, as shown by pDNA bands migrating from the loading location (**Figure 2-16a**). Indeed, these experiments indicate that complexes loose efficiency in pDNA-binding as primary amines are substituted by tertiary-amines. This conclusion is supported by other references from the literature.[49,50] Complexes of

CA-PPZ:pDNA and CA-/6MHA-PPZ:pDNA were also analysed by agarose gel electrophoresis and then challenged with heparin under simulated endosomal (pH 5) and standard physiological (pH 7.4) conditions (**Figure 2-16 b)**. There was less pDNA release from both CA-PPZ:pDNA and CA-/6MHA-PPZ:pDNA complexes at pH 5 than at pH 7, reasonably due to increased protonation of polyions in the more acidic environments. When competing with heparin at pH 5, increasingly-protonated CA-PPZ:pDNA complex showed stronger binding of pDNA, and even a 4-fold mass ratio excess of heparin is not enough to release the pDNA escape. In comparison, the loading bands of CA-/6MHA-PPZ:pDNA complexes at pH 5 were apparent from 2-fold heparin excess, indicating that the structure is loose enough to allow ethidium bromide (EtBr) intercalation, but clear release was evident starting from 4-fold heparin excess. At pH 5, both complexes would be protonated and induced more positively charged amines to bind with pDNA, but this loose structure of CA-/6MHA-PPZ:pDNA complexes might be related to the hydrophobicity of protonated 6MHA-PPZ at pH5, and the reduction of the its interaction between the cationic polymers and nucleic acids.

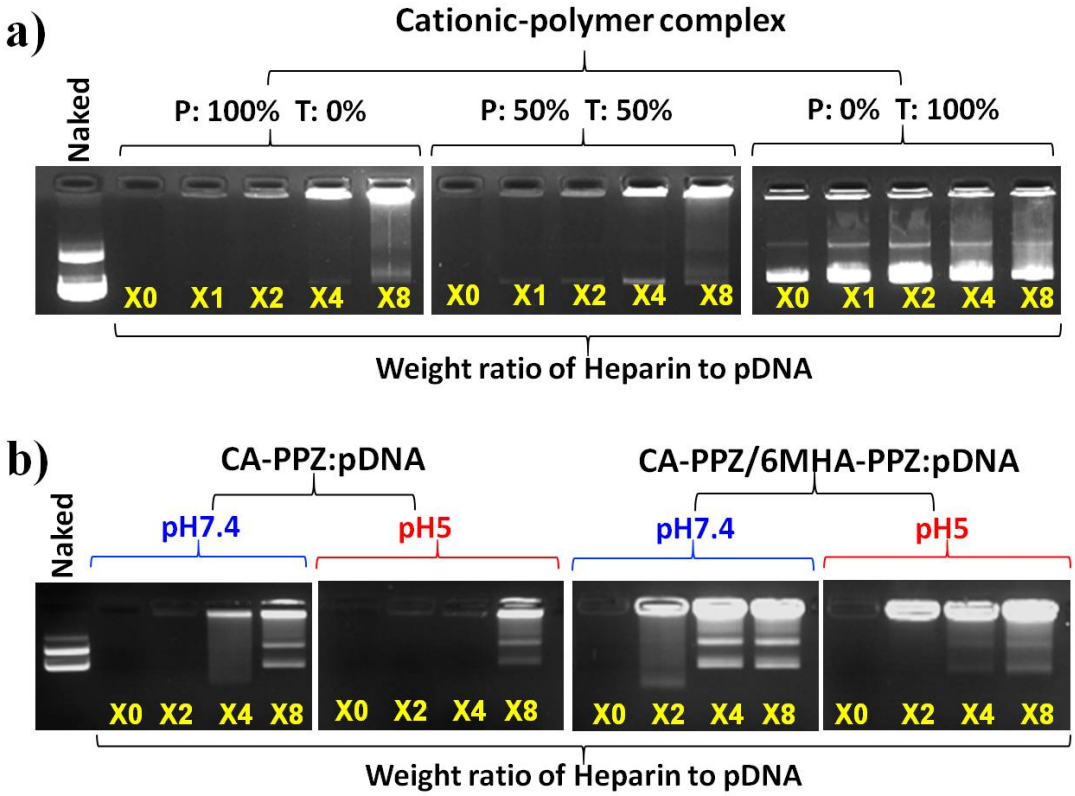

Figure 2-16. Binding efficiency test. (**a**) Gel retardation and heparin-displacement tests of complexes prepared with PPZs having 100% primary amines (P100%), P50% or P0% (8:1 N/P ratio). The remaining substitutes of each polymer corresponded to tertiary amines: T0%, T50% and T100%, respectively. (**b**) Gel electrophoresis and heparin-displacement tests of CA-PPZ:pDNA complexes and CA-/6MHA-PPZ:pDNA (8:4:1 N/C/P ratio) complexes at pH 7.4 and pH 5.

To obtain further information on the molecular interactions between CA-PPZ, 6MHA-PPZ, nucleic acids, and the competitive binding with strong anionic polyelectrolyte (e.g. Heparin sulfate or Dextran sulfate)[51]. Hetero-Förster resonance energy transfer (FRET) techniques were utilized for understanding of this complexation. To perform these experiments, two pH-independent fluorescent dyes that were a well-known fluorescent pair for FRET were selected: cyanine 3 (Cy3) and

cyanine 5 (Cy5)[51,52]. FRET has been employed to measure dynamic association or dissociation between donor fluorophore (Cy3) and accepter fluorophore (Cy5) at the nanometre scale. When the donor and acceptor are very close, the emission spectra of donor partly overlap with the excitation spectra of acceptor; thus, the emission of donor would transfer partial energy to the acceptor, and the transferring efficiency would be inversely proportional to the distance between the donor and acceptor. In this study, CA-PPZ was conjugated with Cy3 as donor and pDNA was labelled by Cy5 as acceptor, and then formed a binary fluorescently labelled nanocomplex. By the way, through this fluorescent probe (Cy5) labelled on pDNA, we can further evaluated how much pDNA can be loaded in the polymer complexes, using a high-speed centrifuge to separate unbound Cy5-pDNA from polymeric Cy5-pDNA nanocomplex[53]. The association efficiency of Cy5-pDNA loaded in PEI, CA-PPZ, and CA-/6MHA-PPZ complexes were 82±1.4%, 85±8%, and 97±2%, respectively, based on the fluorescent intensity measurement.

In **Figure 2-17a**, the Cy5 maximum emission spectra at around 676 nm showed an increase in intensity with higher amounts of 6MHA-PPZ in the system. Indeed, compared to CA-PPZ:pDNA (CA-plex), mixing of complexes CA-PPZ, 6MHA-PPZ, and the same amount of pDNA (Mix-plex) revealed increasing Cy5 intensity until N/C 8:3 ratio, and a saturation of the effect between N/C ratios of 8:3 and 8:4. This data clearly indicated that 6MHA-PPZ compacts CA-PPZ:pDNA complexes. On the other hand, low FRET efficiency of CA-PPZ:pDNA complexes indicate some distance between these components inside the nanoparticles. Although CA-PPZ complex showed higher capacity to counteract the presence of an electrostatic competitor for pDNA (i.e. heparin sulfate or dextran sulfate) than CA-/6MHA-PPZ complexes

(**Figure 2-16b**), this capacity does not seem related to a more compact structure but rather to the capacity of the "positively charged" CA-PPZ to also condense heparin until full neutralisation is achieved. In **Figure 2-17b**, CA-PPZ complexes showed increasing intensities of the Cy5 emission peak as they are incubated with more dextran sulfate up to a mass ratio of 0.4 with respect to pDNA, indicating further nanocomplex reticulation. As this threshold ratio was surpassed with higher amounts of dextran, CA-PPZ complex showed a significant decrease in FRET efficiency as it was observed with CA-/6MHA-PPZ complex. This process can be attributed to the dissociation and displacement of the CA-PPZ:pDNA interaction, causing an increase in the distance between acceptor (Cy5-pDNA) and donor (Cy3-CA-PPZ). The advantage of FRET is to measure the proximity between donor and acceptor at small nanometric scale (i.e. 1 nm to ~10 nm). However, this technique does not inform reliably about distances above this range and therefore, it does not constitute a definitive conformation of pDNA release from the cationic complexes, yet presenting the interaction of polycation and pDNA in the early stage when strong polyanion displaced pDNA from the complexes. For further understanding of the release mechanism, we analysed intercellular distributions of polycation and pDNA using confocal microscopic images (in **Chapter 3.3.2**).

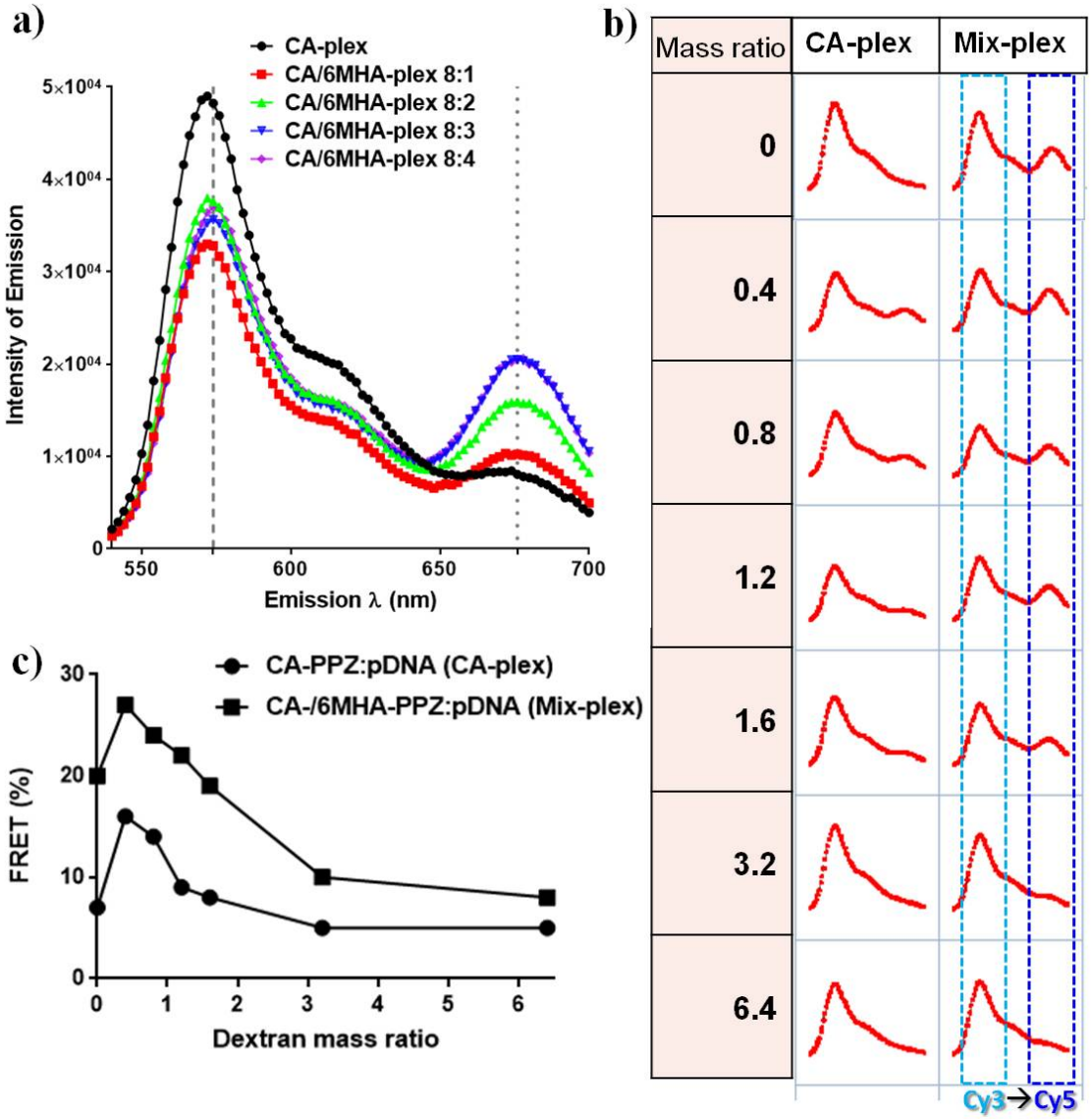

Figure 2-17. FRET evaluation of molecular interaction between Cy3-labelled CA-PPZ and Cy5-labelled pDNA. (**a**) Scanning emission spectra of Cy3-CA-PPZ complexed with Cy5-pDNA (CA-plex) or Cy3-CA-plex mixing polyanion 6MHA-PPZ (Mix-plex) at different mole ratios of amines on the CA-PPZ to carboxylic acids on 6MHA-PPZ. (**b**) Spectra and (**c**) FRET efficiency (%) of either CA-plex or Mix-plex incubating with various mass ratios of dextran sulfate.

2.3.6 Optimisation of polyionic complexes by in vitro transfection

Complexes based on cationic PPZs were initially assessed for their ability to transfect U87MG glioblastoma cells when cultured as adherent monolayers. Here PPZ-based complexes were loaded with pDNA encoding GFP and luciferase sequences. GFP was used for qualitative observation of transfection, while luciferase was used to quantify this process. To select the optimal formulations, the transfection efficiency and the toxicity of different formulations were measured. In the first screening (**Figure 2-18 a, b**), the most favourable compromise between transfection efficiency and cell viability occurred at N/P ratio (8:1) of primary amine-PPZ:pDNA with high molecular weight (36k Da). Albeit of the highest gene-transferring expression at N/P16, the toxicity at this ratio was deemed too severe. For low molecular weight of CA-PPZ, the best condition for transfection was at N/P 24, but the high amount of cationic polymer induced cell death. Considering the effectiveness and cytotoxicity, the high molecular weight of CA-PPZ at N/P 8 was chosen in the following studies.

In the screening of PPZ with different cationic side chains, polymers substituted with cysteamines (primary amine) were more effective for inducing gene expression than DMAES (tertiary amine). This results was similar to that of previous study[54] where random poly(methacrylate) copolymers with different ratios of tertiary to primary amines were analysed for gene transfection. In this work, the most efficient polymer was also the one with only primary amines. The main reason may be that the primary amine group can offer tightly binding with the plasmid, whereas the two methyl groups of DMAES could generate steric hindrance, reducing binding efficiency with pDNA (**Figure 2-16 a**). Another reason might be that polymers with tertiary

amines such as poly(2-(dimethylamino)ethyl methacrylate) (pDMAEMA) seem to require higher molecular weight to achieve their highest efficiency of gene-transfer[55]. The minimum Mw of pDMAEMA to have the optimal transfection with pDNA in the COS-7 and OVCAR-3 cell-line is 300 KDa; in contrast, low Mw pDMAEMA (Mw ≦63 kDa) had 5 times less transfection efficiency than the optimal condition. The importance of high Mw in pDMAEMA was explained by more effective condensation of pDNA and by a capacity to avoid nanocomplex collapsed prior to internalisation. However, we had selected PPZ platform with only Mw 10K-100K in views of the transfection data obtained previously, and of their easier degradation and minimum polymer-induced toxicity. In light of this, the low binding capability of tertiary amines may not be a suitable gene delivery based on this low-Mw PPZ platform.

In order to provide for an endosomal escape mechanism and release of nucleic acid cargos, we prepared CA-PPZ:pDNA complexes integrating carboxylate side-chain PPZs (3MPA-, 4MBA-, 6MHA-, or 8MOA-PPZ), with buffering capacities at different pH range (**Figure 2-12**). Luciferase expression assay were run in U87MG monolayers using these complexes as gene carriers and PEI:pDNA complexes at the same N/P ratios as positive control (**Figure 2-19**). The mixing CA-/6HMA-PPZ:pDNA complex showed the highest level of transgene expression and a neat reduction in cytotoxicity compared to the parent CA-PPZ:pDNA complex. Similar enhancements in transfection were not observed in the mixed complexes with the other polyanionic PPZs, in view of the unique effect that we attributed to the significant change in protonation of 6MHA-PPZ at endosomal pH as described earlier. Besides this effect, all polyanionic PPZs reduced the cytotoxicity of the complexes, which can be attributed to partial shielding of the cationic charges of CA-PPZ. The transfection enhancing effect of

6MHA-PPZ is also effective with other cationic polymers with similar structure such as poly-L-lysine (PLL), and translates to other clinically relevant glioblastoma models such as the primary cell model GBM1 with remarkable efficacy[56] (**Figure 2-20**). It is interesting to note that 6MHA-PPZ seems also capable of improving cell transfection in combination with another common-used polycation (PLL), which are also low endosomal escape properties. Although 6MHA-PPZ mixing in CA-PPZ complexes seem to be particularly efficient (**Figure 2-20**), which likely attributed to our above optimization of this cationic PPZ platform.

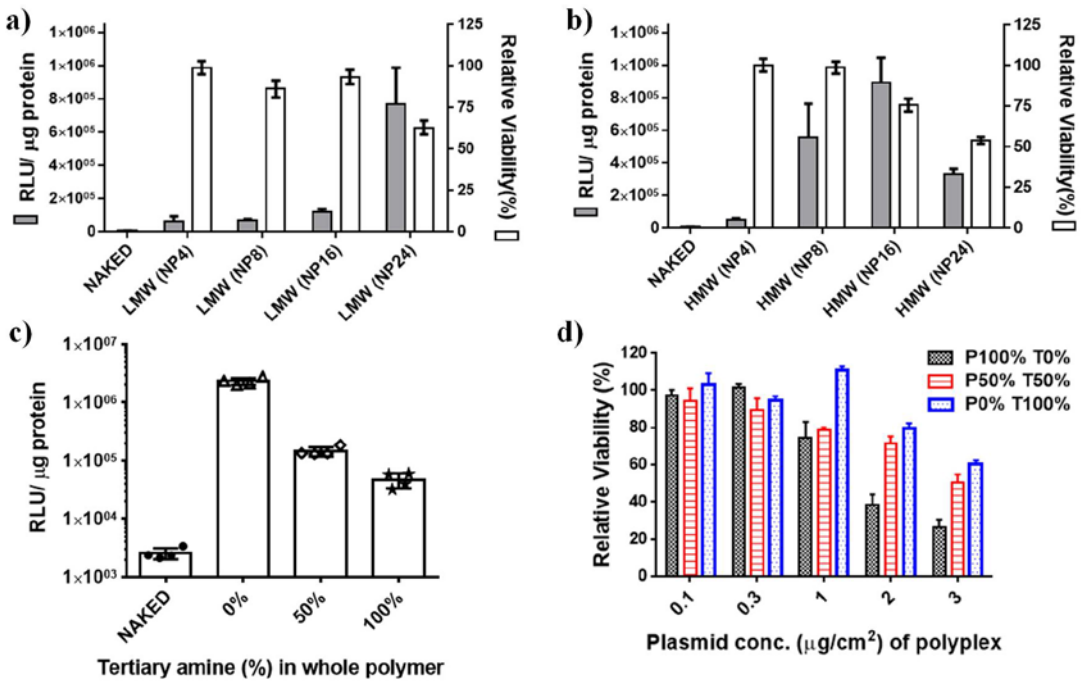

Figure 2-18. (**a, b**) Optimisation of polycationic complexes via luciferase expression and cell viability of CA-PPZ/pDNA complexes with low molecular weight (LMw 26K) and high molecular weight (HMw 36K) at different N/P ratios. (**c**) Luciferase expression upon transfection with complexes of different polycationic PPZs (T0%, T50%, T100%) and pDNA (1 µg/cm^2 pDNA dose and 8:1 N/P ratios). (**d**) Cell viability after 48h transfection via MTT assays.

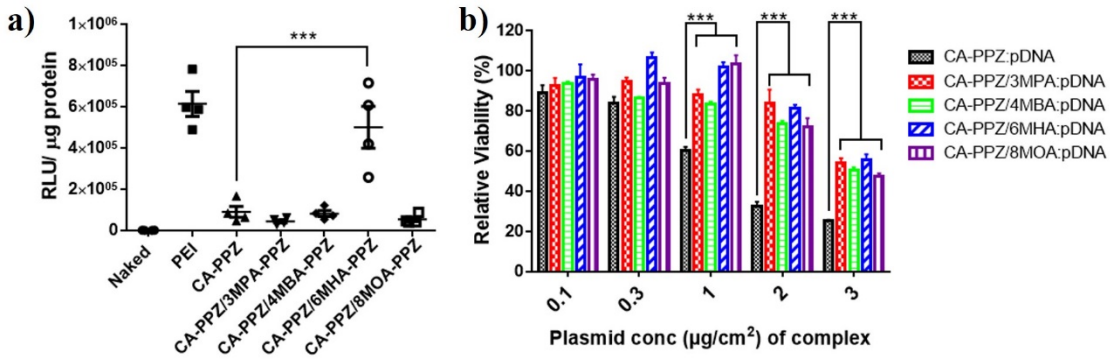

Figure 2-19. Optimisation of CA-PPZ complexed with various anionic polymers. (**a**) Luciferase expression by quantification of relative luminescence unit (RLU)/µg protein obtained upon transfection of U87MG cells with CA-PPZ:pDNA complexes (8:1 N/P ratio) and different CA-PPZ/polyanionic PPZ:pDNA complexes (N/C/P ratio of 8:4:1, pDNA dose 1 µg/cm^2). Transfection with PEI:pDNA is shown as an internal control. (**b**) Cell metabolic activity at 48h post-treatment with different concentrations of the same complexes.

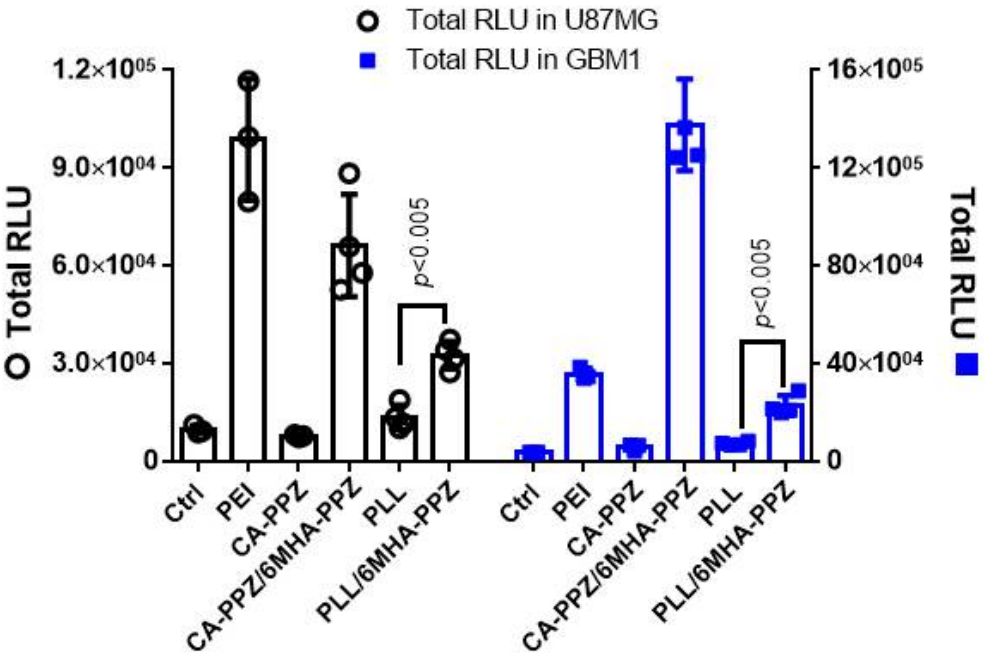

Figure 2-20. Investigation of optimized polyanion boosting luciferase expression upon cell transfection with various polycations (CA-PPZ or poly-L-lysine). A comparison was performed between at alone (8:1 N/P ratios) and after mixing with 6MHA-PPZ (8:4:1 N/C/P ratio). Data obtained in U87MG and in the primary cell line GBM1.

2.4 Conclusion

A versatile polymeric gene delivery system platform was established based on polyphosphazenes modified by thiol-ene addition reactions. Based on these materials, a small library of cationic or anionic gene-delivery polymers was screened for optimized physicochemical properties, gene-binding efficiency, low cytotoxicity, and high gene transfection. The optimal system was generated with polyphosphazene modified with primary amines (CA-PPZ) and mixed with another polyphosphazene with the anionic polymer (6MHA-PPZ) and pDNA. This system showed transfection efficiency/toxicity ratios above one order of magnitude higher than the parent polycation:pDNA system. This improved transfection can be explained by the high buffering capacity and the pH-induced hydrophobicity of 6MHA-PPZ in the endosomal environment. Besides, DLS, NTA, FRET and TEM indicated that the addition of 6MHA-PPZ generates more compact complexes that efficiently release their gene cargo once in the presence of another strong anionic polyelectrolyte. The nanocomplexes based on the CA-/6MHA-PPZ:pDNA mixture were considered of sufficient interest for further studies in more advanced disease models.

2.5 References

1. Allcock, H. *Phosphorus-nitrogen compounds: cyclic, linear, and high polymeric systems*, (Elsevier, 2012).
2. Dewar, M., Lucken, E. & Whitehead, M. 490. The structure of the phosphonitrilic halides. *Journal of the Chemical Society (Resumed)*, 2423-2429 (1960).
3. Mark, J.E., Allcock, H.R. & West, R. *Inorganic polymers*, (Oxford University Press, 2005).
4. Allcock, H.R. & Arcus, R.A. Crystalline Transitions and Related Physical Properties of Poly (dichlorophosphazene). *Macromolecules* **12**, 1130-1136 (1979).
5. Cowley, A., Dewar, M. & Jackson, W.R. Restricted rotation around phosphorus-nitrogen bonds. *Journal of the American Chemical Society* **90**, 4185-4186 (1968).
6. Allcock, H.R. Polyphosphazenes: new polymers with inorganic backbone atoms. *Science* **193**, 1214-1219 (1976).
7. De Jaeger, R. & Gleria, M. Poly (organophosphazene) s and related compounds: synthesis, properties and applications. *Progress in polymer science* **23**, 179-276 (1998).
8. Sennett, M.S., Hagnauer, G.L., Singler, R.E. & Davies, G. Kinetics and mechanism of the boron trichloride-catalyzed thermal ring-opening polymerization of hexachlorocyclotriphosphazene in 1, 2, 4-trichlorobenzene solution. *Macromolecules* **19**, 959-964 (1986).
9. Sohn, Y.S., Cho, Y.H., Baek, H. & Jung, O.-S. Synthesis and Properties of Low Molecular Weight Polyphosphazenes. *Macromolecules* **28**, 7566-7568 (1995).
10. Andrianov, A.K., Chen, J. & LeGolvan, M.P. Poly (dichlorophosphazene) as a precursor for biologically active polyphosphazenes: synthesis, characterization, and stabilization. *Macromolecules* **37**, 414-420 (2004).
11. Honeyman, C.H., Manners, I., Morrissey, C.T. & Allcock, H.R. Ambient temperature synthesis of poly (dichlorophosphazene) with molecular weight control. *Journal of the American Chemical Society* **117**, 7035-7036 (1995).
12. Allcock, H.R., Pucher, S.R. & Scopelianos, A.G. Poly [(amino acid ester) phosphazenes]: synthesis, crystallinity, and hydrolytic sensitivity in solution and the solid state. *Macromolecules* **27**, 1071-1075 (1994).

13. Allcock, H.R., Reeves, S.D., Nelson, J.M., Crane, C.A. & Manners, I. Polyphosphazene Block Copolymers via the Controlled Cationic, Ambient Temperature Polymerization of Phosphoranimines. *Macromolecules* **30**, 2213-2215 (1997).
14. Huang, X., Yin, L. & Tang, X. Synthesis and characterization of a new organic-inorganic hybrid polyphosphazene polymer. *Science in China Series B: Chemistry* **51**, 46-50 (2008).
15. Qian, Y.C., *et al.* A versatile approach to the synthesis of polyphosphazene derivatives via the thiol–ene reaction. *Journal of Polymer Science Part A: Polymer Chemistry* **50**, 5170-5176 (2012).
16. Potta, T., Chun, C. & Song, S.-C. Dual cross-linking systems of functionally photo-cross-linkable and thermoresponsive polyphosphazene hydrogels for biomedical applications. *Biomacromolecules* **11**, 1741-1753 (2010).
17. Rothemund, S., *et al.* Degradable Glycine-Based Photo-Polymerizable Polyphosphazenes for Use as Scaffolds for Tissue Regeneration. *Macromolecular bioscience* **15**, 351-363 (2015).
18. Qian, Y.-C., Chen, P.-C., He, G.-J., Huang, X.-J. & Xu, Z.-K. Preparation of polyphosphazene hydrogels for enzyme immobilization. *Molecules* **19**, 9850-9863 (2014).
19. Nykänen, V.P.S., Nykänen, A., Puska, M.A., Silva, G.G. & Ruokolainen, J. Dual-responsive and super absorbing thermally cross-linked hydrogel based on methacrylate substituted polyphosphazene. *Soft Matter* **7**, 4414-4424 (2011).
20. Ren, N., *et al.* Controllable glycosylation of polyphosphazene via radical thiol–yne click chemistry. *Journal of Polymer Science Part A: Polymer Chemistry* **50**, 3149-3157 (2012).
21. Heyde, M., *et al.* Synthesis and characterization of novel poly [(organo) phosphazenes] with cell-adhesive side groups. *Biomacromolecules* **8**, 1436-1445 (2007).
22. Huang, X., *et al.* "Click Chemistry" as a Facile Approach to the Synthesis of Polyphosphazene Glycopolymers. *Macromolecular Chemistry and Physics* **212**, 272-277 (2011).
23. Teasdale, I. & Brüggemann, O. Polyphosphazenes: multifunctional, biodegradable vehicles for drug and gene delivery. *Polymers* **5**, 161-187 (2013).
24. Lakshmi, S., Katti, D.S. & Laurencin, C.T. Biodegradable polyphosphazenes for drug delivery applications. *Advanced drug delivery reviews* **55**, 467-482 (2003).

25. Wilfert, S., *et al.* Water-soluble, biocompatible polyphosphazenes with controllable and pH-promoted degradation behavior. *Journal of Polymer Science Part A: Polymer Chemistry* **52**, 287-294 (2014).
26. Singh, A., *et al.* Effect of side group chemistry on the properties of biodegradable L-alanine cosubstituted polyphosphazenes. *Biomacromolecules* **7**, 914-918 (2006).
27. Andrianov, A.K. *Polyphosphazenes for biomedical applications*, (John Wiley & Sons, 2009).
28. Allcock, H.R., Pucher, S.R. & Scopelianos, A.G. Poly [(amino acid ester) phosphazenes] as substrates for the controlled release of small molecules. *Biomaterials* **15**, 563-569 (1994).
29. Luten, J., *et al.* Water-soluble biodegradable cationic polyphosphazenes for gene delivery. *Journal of Controlled Release* **89**, 483-497 (2003).
30. Allcock, H.R. & Morozowich, N.L. Bioerodible polyphosphazenes and their medical potential. *Polymer Chemistry* **3**, 578-590 (2012).
31. Allcock, H.R., Maher, A.E. & Ambler, C.M. Side group exchange in poly (organophosphazenes) with fluoroalkoxy substituents. *Macromolecules* **36**, 5566-5572 (2003).
32. Neilson, R.H. & Wisian-Neilson, P. Poly (alkyl/arylphosphazenes) and their precursors. *Chemical Reviews* **88**, 541-562 (1988).
33. Ratner, M.A. & Shriver, D.F. Ion transport in solvent-free polymers. *Chemical Reviews* **88**, 109-124 (1988).
34. Baillargeon, A.L. & Mequanint, K. Biodegradable polyphosphazene biomaterials for tissue engineering and delivery of therapeutics. *Biomed Res Int* **2014**, 761373 (2014).
35. Carampin, P., *et al.* Electrospun polyphosphazene nanofibers for in vitro rat endothelial cells proliferation. *Journal of Biomedical Materials Research Part A* **80**, 661-668 (2007).
36. Akram, M., *et al.* Polyphophazenes as anti-cancer drug carriers: From synthesis to application. *Progress in Polymer Science* **39**, 1987-2009 (2014).
37. Zheng, C., Qiu, L. & Zhu, K. Novel polymersomes based on amphiphilic graft polyphosphazenes and their encapsulation of water-soluble anti-cancer drug. *Polymer* **50**, 1173-1177 (2009).
38. Andrianov, A.K., *et al.* Poly [di (carboxylatophenoxy) phosphazene] is a potent adjuvant for intradermal immunization. *Proceedings of the National Academy of Sciences* **106**, 18936-18941 (2009).
39. Martinez, A.P., Qamar, B., Fuerst, T.R., Muro, S. & Andrianov, A.K.

Biodegradable "Smart" Polyphosphazenes with Intrinsic Multifunctionality as Intracellular Protein Delivery Vehicles. *Biomacromolecules* **18**, 2000-2011 (2017).

40. Peng, Y., Zhu, X.M. & Qiu, L.Y. Electroneutral composite polymersomes self-assembled by amphiphilic polyphosphazenes for effective miR-200c in vivo delivery to inhibit drug resistant lung cancer. *Biomaterials* **106**, 1-12 (2016).
41. Gao, M.H., Zhu, X.M., Wu, L.P. & Qiu, L.Y. Cationic Polyphosphazene Vesicles for Cancer Immunotherapy by Efficient in Vivo Cytokine IL-12 Plasmid Delivery. *Biomacromolecules* **17**, 2199-2209 (2016).
42. Ma, C.Y., *et al.* Water-Soluble Cationic Polyphosphazenes Grafted with Cyclic Polyamine and Imidazole as an Effective Gene Delivery Vector. *Bioconjugate Chemistry* **27**, 1005-1012 (2016).
43. Meng, L.J., *et al.* One-pot synthesis of highly cross-linked fluorescent polyphosphazene nanoparticles for cell imaging. *Polymer Chemistry* **6**, 3155-3163 (2015).
44. Teasdale, I. & Bruggemann, O. Polyphosphazenes: Multifunctional, Biodegradable Vehicles for Drug and Gene Delivery. *Polymers* **5**, 161-187 (2013).
45. Zhang, P.C., Zhang, Z.W., Yang, Y.X. & Li, Y.P. Folate-PEG modified poly(2-(2-aminoethoxy)ethoxy)phosphazene/DNA nanoparticles for gene delivery: Synthesis, preparation and in vitro transfection efficiency. *International Journal of Pharmaceutics* **392**, 241-248 (2010).
46. Hu, L., *et al.* A facile method to prepare composite and porous polyphosphazene membranes and investigation of their properties. *Rsc Advances* **4**, 35769-35776 (2014).
47. Wernersson, E., *et al.* Effect of association with sulfate on the electrophoretic mobility of polyarginine and polylysine. *J Phys Chem B* **114**, 11934-11941 (2010).
48. Martens, T.F., Remaut, K., Demeester, J., De Smedt, S.C. & Braeckmans, K. Intracellular delivery of nanomaterials: how to catch endosomal escape in the act. *Nano Today* **9**, 344-364 (2014).
49. Wolfert, M.A., *et al.* Polyelectrolyte vectors for gene delivery: influence of cationic polymer on biophysical properties of complexes formed with DNA. *Bioconjugate chemistry* **10**, 993-1004 (1999).
50. Zhu, C., *et al.* Cationic methacrylate copolymers containing primary and tertiary amino side groups: controlled synthesis via RAFT polymerization,

DNA condensation, and in vitro gene transfection. *Journal of Polymer Science Part A: Polymer Chemistry* **48**, 2869-2877 (2010).

51. Shrestha, D., Jenei, A., Nagy, P., Vereb, G. & Szöllősi, J. Understanding FRET as a research tool for cellular studies. *International journal of molecular sciences* **16**, 6718-6756 (2015).
52. Mansoor, S.E., Palczewski, K. & Farrens, D.L. Rhodopsin self-associates in asolectin liposomes. *Proceedings of the National Academy of Sciences of the United States of America* **103**, 3060-3065 (2006).
53. Csaba, N., Köping-Höggård, M. & Alonso, M.J. Ionically crosslinked chitosan/tripolyphosphate nanoparticles for oligonucleotide and plasmid DNA delivery. *International Journal of Pharmaceutics* **382**, 205-214 (2009).
54. Sprouse, D. & Reineke, T.M. Investigating the Effects of Block versus Statistical Glycopolycations Containing Primary and Tertiary Amines for Plasmid DNA Delivery. *Biomacromolecules* **15**, 2616-2628 (2014).
55. van de Wetering, P., Cherng, J.-Y., Talsma, H. & Hennink, W.E. Relation between transfection efficiency and cytotoxicity of poly(2-(dimethylamino)ethyl methacrylate)/plasmid complexes. *Journal of Controlled Release* **49**, 59-69 (1997).
56. Kroonen, J., *et al.* Human glioblastoma-initiating cells invade specifically the subventricular zones and olfactory bulbs of mice after striatal injection. *International Journal of Cancer* **129**, 574-585 (2011).

USC
UNIVERSIDADE
DE SANTIAGO
DE COMPOSTELA

Chapter III / Capítulo III

Evaluation of binary-polyions gene complexes in intracellular distribution and transfection in vitro 3D spheroid models

This work has been done in collaboration with the Medical School of the University of Nottingham

Chapter III / Capítulo III

Abstract

Following efforts on screening a small library of potential side chains for enhanced polyphosphazene formulation (CA-/6MHA-PPZ complex) by pDNA transfection in 2D culture, this chapter would cover several potential mechanisms for 6MHA-PPZ facilitated endosomal escape. For understanding intracellular distribution, Cy5-labelled pDNA was delivered by either CA-PPZ or mixing CA-PPZ with 6MHA-PPZ to the U87MG cells and then analysed for intracellular locations related to lysotracker (late-endosomal and lysosomal markers). Through ImageJ analysis, it was shown that pDNA in CA-/6MHA-PPZ complexes are better able to escape from endolysosomal compartments than the CA-PPZ-only analogue. The release of pDNA after endosomal escape was also confirmed by confocal microscopy images, further confirming that the 6MHA-PPZ helped release of pDNA as well. Through optimisation and mechanistic analysis, further transfection experiments were performed in 3D culture spheroid models, which provide bio-relevant microenvironments related to in vivo tumour models and which also preserve genetic profiles of the tumour cells. On the basis of GFP expression, CA-/6MHA-PPZ complexes showed high transfection efficiencies in U87MG spheroids of sizes up to with 250 μm diameter. Tomographic imaging also demonstrated that CA-/6MHA-PPZ complexes transferred gene cargos through the core of the spheroids and were able to transfect cells at lower doses, compared to the polycation-only complexes, CA-PPZ and PEI. Finally, the polymeric complexes were tested in xenograft models on mice. These in vivo transfection evaluations were through intra-tumoral injection of CA-/6MHA-PPZ complexes, and luciferase expression in these experiments was similar to those of PEI/nucleic acid complexes. The H&E stained images of transfected tumours indicated no significant

sign of cell death in all polymer-nucleic acid complex treatments. Taken together, the gene-transfer studies in 2D, 3D in vitro models and xenograft models in vivo, demonstrated that the addition of 6MHA-PPZ enhanced transfection efficiency of polycations-nucleic acid complexes and many be considered promising for further gene therapy experiments.

3.1 Introduction

3.1.1 Endocytosis of polymeric gene-carriers and endosomal escape

Endocytosis is a term used to describe a series of pathways by which cells obtain nutrients, control inter- and intra-cellular signalling, and regulate receptor expressions. Endocytic pathways are also primary routes for nanoscale vehicles to cross plasma membrane.[1,2] Endocytosis mechanisms include macro-scale endocytic processes (phagocytosis and macropinocytosis) and micro-scale endocytic processes (clathrin-mediated, caveolin-dependent/independent endocytosis, and dynamin-dependent/ independent endocytosis, etc.). For polymeric gene complexes, Wagner group reported that the internalisation of PEI complexes into mammal tumour cell-lines was strongly dependent on the particle sizes. Thus, small PEI complexes were internalised via caveolae/raft-dependent routes[3], and large aggregated PEI complexes (diameter <1 μm) by clathrin-independent pathways or macropinocytosis pathways.[4,5] In nearly all cases, most of the complexes were found in endosomal compartments[6] which is the normal fate for most nanocarriers following internalisation via endocytosis. Escape from endosomal compartments is one of the pivotal challenges for endocytosis-related intracellular gene delivery[7-9], because if the carriers are retained in these vesicles as the late endosomes mature to lysosomes, enzymes in the resultant acidic environment can very efficiently degrade any nucleic acid cargos. Although the mechanisms of endosomal escape are still not entirely clear now, many hypotheses have been proposed and scientific experiments designed to test the concepts[10]. However, it is generally accepted that endosomal environments are gradually acidified by ATP-driven transport during the process of endocytosis, and this acidification can be exploited by pH-responsive polymers. These materials can

destabilize endosomal membranes through the "proton-sponge effect"[11,12], endosomolysis[13], or membrane fusion[14] as shown in **Figure 3-1**. In all cases, the gradual acidification in endocytosis is one of key triggers for the gene delivery system response.

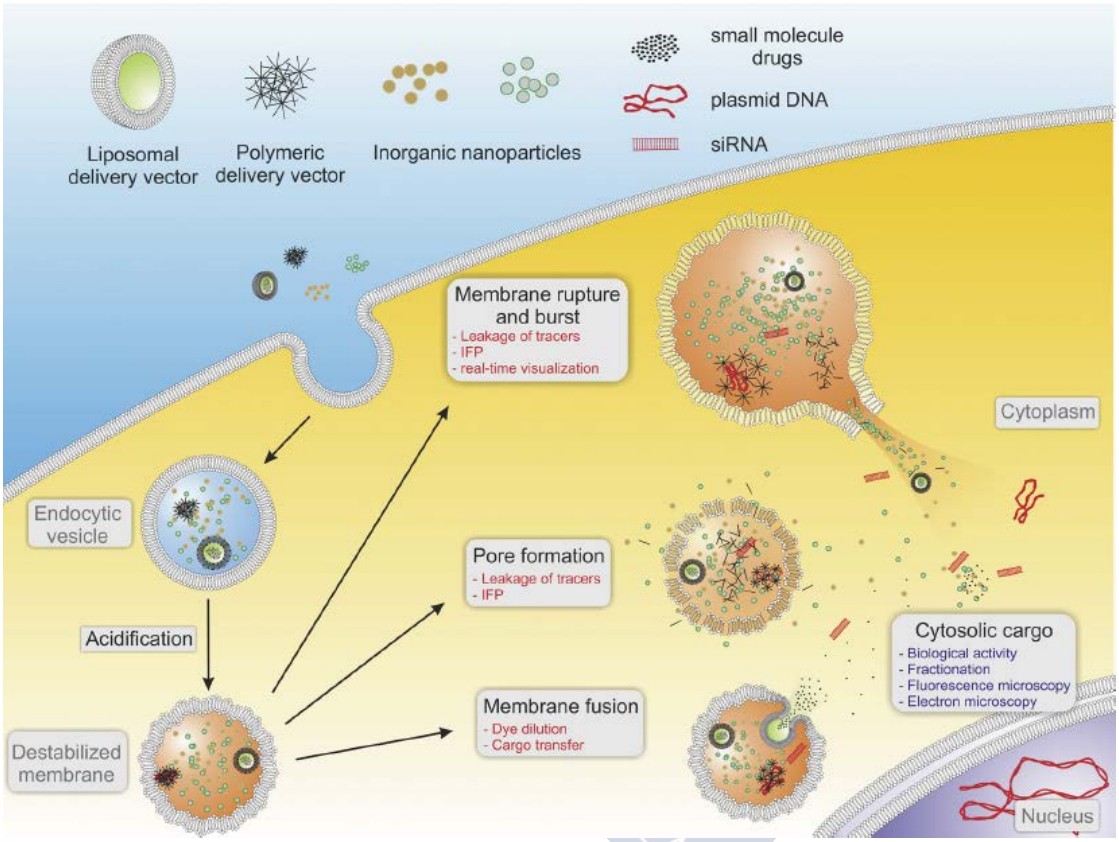

Figure 3-1. The common of hypotheses for endosomal escape for nanocarriers. [reproduced from Martens, T. F., et al. (2014). Nano Today[10] with permission]

3.1.2 Buffering capacity for endosomal escape

For the proposed mechanisms of nanocarriers escaping from endosomal compartments, the most well-known mechanism is the "proton-sponge" effect. After formation of early-endosomal vesicles, V-type proton ATPases continue to pump protons across the endosomal membrane during vesicular maturation until lysosomal compartments are formed with a pH range of 5.0 - 4.5, and during this process, counter-ions cross the transmembrane channel to balance electric potential[15]. When polymeric-based or lipid-based gene carriers, containing excess un-protonated functional groups with pKa values close to the endosomal pH range, they can be protonated and thus buffer the active-transported protons. Through absorbed excess protons and accumulation of counter-ions (e.g. Cl^- or SO_4^-) inside endosomes, the increasing osmotic gradient causes hypotonic shocks, thus inducing the influx of H_2O, which in turn causes swelling of endosomal compartments. The high osmotic pressure contributes to endosomal destabilization, triggering endosomal rupture and release of cargos inside. It should be emphasised that this is not the only pathway[2,16] and mechanisms of endosomal escape strongly depend on differences in the design of carriers. When the endosomal compartments became acidified, there are several effects on the endosomal leakage. Firstly, increasingly protonated polycations provide higher positively charged surfaces of nanoparticles, which cause the cationic carriers to repel each other and favour interactions with the negative endosomal membranes. This causes membrane damages and pore formation[17], as demonstrated by histidine-rich peptide H5WYG [18] and GALA [19] and other polymers with pKa values between 7.0 to 5.5.[20] Secondly, it is known that certain viruses escape from endosomal traps via pH-sensitive proteins, such as HA-2 subunits[21], which expose hydrophobic α-helical

domains in slightly acidic environments in order to disrupt endosomal membranes[22]. Two other well-known examples of membrane disruptors are the anionic amphiphilic peptides are INF7 and E5WYG [10,22]. Thirdly, for lipid-based vehicles or amphiphilic materials, a fusion of the introduced amphiphiles and phospholipid-based membranes can happen, especially in the case of which cationic lipids undergo association with negatively-charged membranes[10,18]. Through membrane fusions, the cargos in the nanocarriers can be introduced to the cytosol and released directly[23] (**Figure 3-1**).

3.1.3 pH-sensitive polyanions for endosomal escape

On the basis of the potential mechanisms above, many strategies have proposed buffering functional groups into cationic polymer chains, like poly- or oligo-histidine[20], aminoethylene repeats[24], diisopropylamino side groups.[25] However, those buffering side chains are located on nitrogen atoms as potential positively charged functional groups, but there are very few designs utilizing anionic side chains or polyanions for improving buffering capacity of nanocarriers. Although some studies have employed anionic polymers to mix with or to coat on cationic complexes for protein delivery[26] and gene delivery[27], most of the polycation/polyanion complexes to date have been used for nanoparticle construction. Of these, only a few of them have been designed to utilise stimuli-responsive polyanions, especially for endosomal pH responsiveness. In general, designs of pH-sensitive polyanions can be classified into four strategies, including cleavable anionic side chains[28,29], pH-sensitive zwitterionic polymers[30,31], poly(propylacrylic acid)-copolymers (PPAA)[32-35], and poly(β-malic acid) (PMLA) copolymers [36,37], as shown in **Figure 3-2**.

Firstly, the cleavable anionic side-chains are designed by intramolecular nucleophilic amides and neighbouring carboxylic acid groups. Once in slightly acidic environments, the amide groups are cleaved by acid-catalysed hydrolysis, generating free amine groups, resulting in the terminal side chains switching from negatively charged carboxylates to positively charged amines[38] (**Figure 3-2a**). However, these charge-reversal polymers have only used to date for small-molecule chemotherapeutic drugs. Secondly, for pH-sensitive zwitterionic polymers, anionic terminal groups were introduced on tertiary amines, elaborately designing the pKa of the carboxylic acid groups at outmost layer to target the slight acidic tumour microenvironment (pH 6.9－6.5)[30,31] (**Figure 3-2b**). However, this well-designed formulation was only used as a carrier for hydrophobic drugs and would be difficult to manipulate in the gene carriers because the negatively charged nucleic acids would perturb the ordering of the zwitterionic polymers, likely causing nanoparticular structures collapse.

The Hoffman and Stayton groups have utilised PPAA-copolymers for endosomolysis since 1999 [32,39]. They screened a library of substituted poly(acrylic acid)s with different hydrophobic chain sections, finding specific pH-inducing hydrophobic poly(acrylic acid)s which possessed membrane disruption ability at slightly acidic environments via haemolysis studies. Furthermore, advanced endosomolytic block-co-polymers were synthesized by controlled reversible addition fragmentation chain transfer polymerisation (RAFT) of PPAA and butyl methacylate (BMA) and cationic side-chain monomers for siRNA delivery (**Figure 3-2c**). Although these PPAA copolymers introduced polyanions in gene delivery, the non-biodegradable polymer backbone and complicated synthesis procedures may obstruct pharmaceutical applications, but the strategy indeed inspired further studies. A recent example is a

membranolytic PMLA copolymer, which is a biodegradable polyanion containing abundant carboxylic terminal groups. However, without further chemical modification, PMLAs do not have membrane disruption capacity due to low pK_a (~3.5) and high hydrophilicity. As a result, some studies have optimized the amphiphilicity of PMLA conjugated with hydrophobic peptides for pH-sensitive membrane disruption[36]. After the optimisation, only conjugation with a short peptide (triple leucine) on PMLA backbone is significantly capable to rupture liposomal membranes at pH 5. In this strategy, a biodegradable backbone PMLA conjugated with tri-leucine as side chains for successfully breaking liposomal membranes. PMLA is also widely used for covalent nanoconjugation with antibody (antiEGFR)[37,40] or chemotherapeutic drugs (e.g. temozolomide)[41]. To sum up, there are few reports that have used related polymers in nanoformulations for gene therapy applications.

As noted above, although some studies have utilized polyanions or anionic terminal groups of zwitterionic polymers to enhance endosomal escape, there are rare uses of anionic groups for co-formulation with polycations in order to minimise side effects and maximise gene-transfer efficiency to date. The reasons for this include biodegradation capabilities, as complicated synthetic polymers are of less interest for the human-use, due to a lack for prior validation in clinical trials and in PICS/GMP production. In addition, it can be troublesome using zwitterionic polymers for polymer-gene nanocomplex systems, because when zwitterionic polymers are condensed with anionic nucleic acids, it is difficult to control and maintain zwitterionic sections at the outer layer and polycation sections with complexed nucleic acids in the core. This is likely why the zwitterionic polymers are frequently used for delivery of hydrophobic drugs, in which van der Waals interaction provide the driving forces for

forming nanoscale particles[29,30].

According to the previous chapter, the optimal cysteamine-attached poly(phosphazene)s (CA-PPZ) was selected by in vitro transfection studies, while the carboxylic acid functionalized poly(phosphazene) derivatives possessed varying degrees of anion content dependent on environmental pH. By combining these materials in the presence of nucleic acids, we expected the mixed binary polyionic complexes to escape more effectively than conventional polycation/nucleic acid complexes from endolysosomes, which have been considered to be the most significant intracellular barriers to effective gene delivery.[42-45]

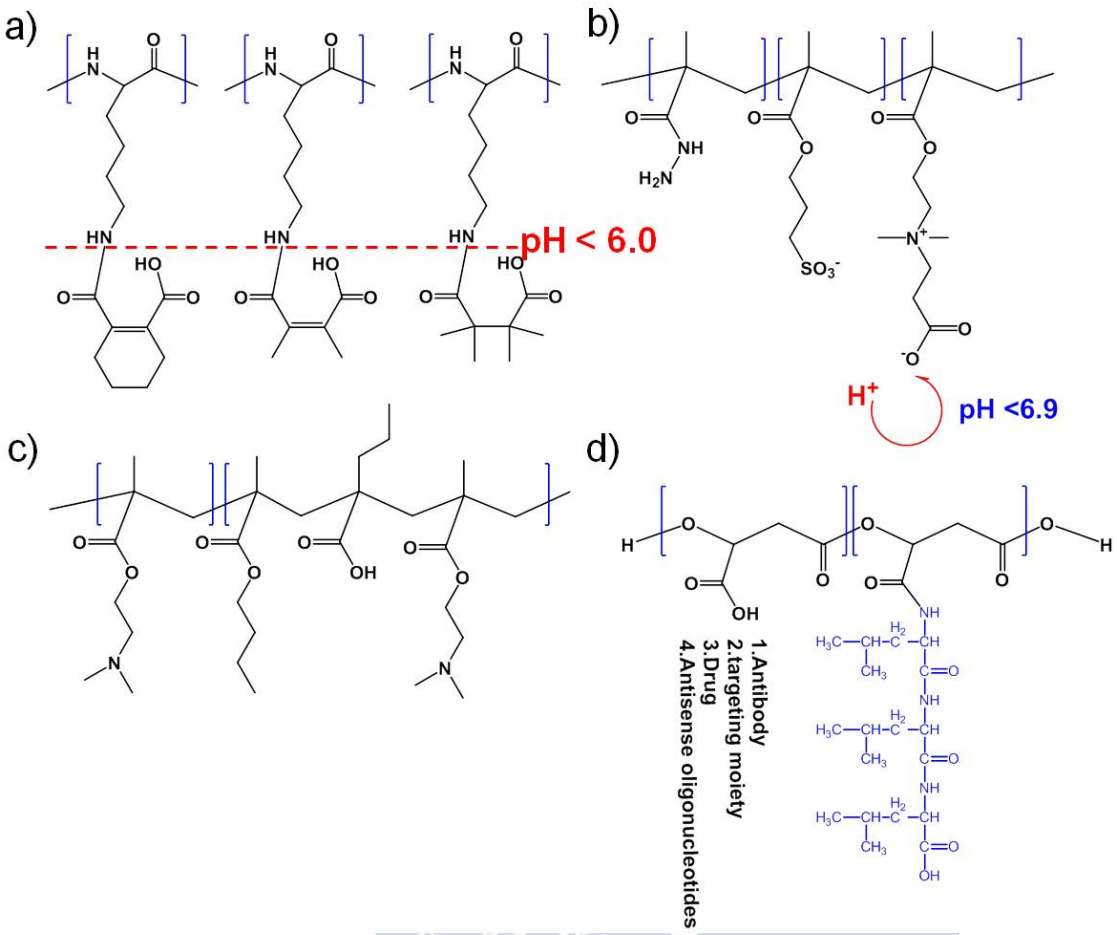

Figure 3-2. Chemical structures of pH-sensitive polyanions in the literatures. a) Cleavable anionic side chains; b) pH-sensitive zwitterionic polymers; c) poly(propylacrylic acid)-co-block polymers; d) nanoconjugate poly(β-malic acid) (PMLA) copolymers with linear trimers of leucine.

3.1.4 Three dimensional in vitro cultures

Traditional two-dimensional cell mono-layers have been used for formulation screening for several decades but also have been questioned due to lack of clinical validation and whether they are representative for physiologically relevant situations [46,47]. Three-dimensional cultures are better able to provide tissue-like architecture (e.g. extracellular matrix)[48] and fundamental tumour microenvironments, like nutrient and oxygen gradients [49], cell-cell interactions, and gene expression profiles[50]. Engineered 3D tumour models can be derived from simple mono-/multiple-cellular spheroids (cell aggregation) to complicated microfluidic scaffold systems or larger scale bioreactors. For establishing simple spheroid models, the predominant method is growing tumour cells or co-culture specific cells in a limited space to force them to gather and attach to each other, which then results in the cells forming a sphere-like aggregate. The common protocols are designed to limit cells in specific spaces, including using hydrogels, scaffolds, cell culture dishes or plates with non-adherent coatings, or suspending cells in hanging drops[51]. Dependent on the models, additions of growth factors and small molecular signals are necessary[52] and the scale of spheroid diameter is approximately from few millimetres to sub-millimetres[53]. Other 3D models utilising microfluidic devices or bioreactors can set-up large scale multi-cellular objects (~several centimetres), develop vascular lumens[54] or endothelial cell layers[55] for bio-relevant tests in pharmaceutical applications (**Figure 3-3**).

In this thesis, we employed a liquid-overlay method to produce spheroids, which used ultra-low attachment U-shape plates to maintain cells in aggregates while they formed sphere-like tumour-mimetic clumps. This model has previously been shown to

simply generate, with good reproducibility and efficient screening of large numbers of formulations[56,57]. These kinds of spheroid models have been used in screening anticancer drug or related formulations, but a few studies have utilised spheroids to evaluate nucleic-acid delivery. In addition, more importantly for this study, the 3D-culture spheroids are more capable to retain the genomic profiles of GBM cell-lines than 2D counterparts[50]. In this study, we tested transgene expression in spheroids of GBM cells before in vivo studies. Consequently, in 2D cell monolayer, we can assume that all the cells receive an equal dose of the polymeric gene complex at the same time, while in millimetre-scale spheroids, the nanocarriers were obstructed to reach in the core parts by ECM or hypoxia phenomena, etc.

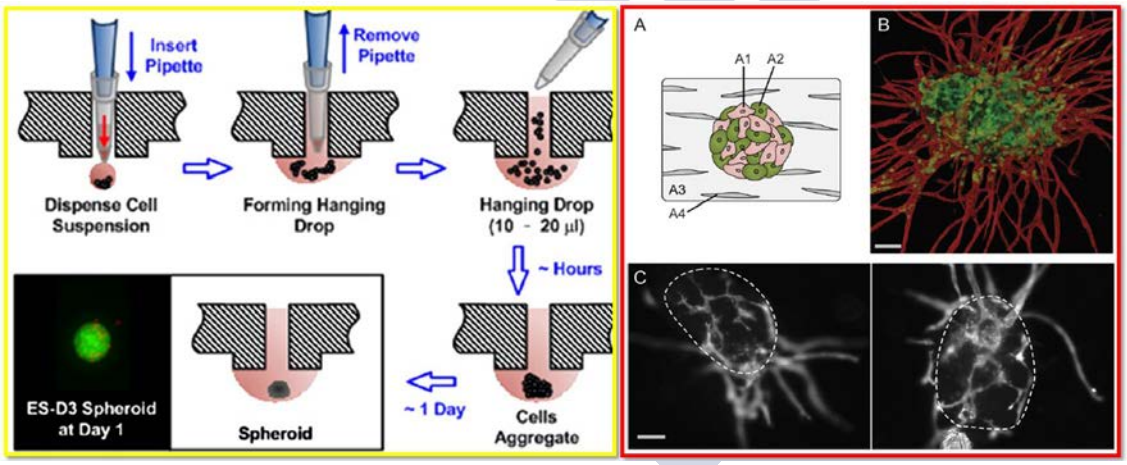

Figure 3-3. Different in vitro models in 3D cultures. The block with yellow outline (left) shows the hanging drop method to produce spheroids [Reproduced from Tung, Y.-C. et al. Analyst[53] with permission]. The block with the red outline (right) presents pre-vascularised tumour spheroids, which are made by co-culture of endothelial cells (A1) and tumour cells (A2) growing in fibroblast containing fibrin-gels (A4 and A3). The label B shows the endothelial layer (red signals) stained by anti-CD31 and GFP-transduced tumour cells (green signals) [Reproduced from Ehsan, S. M. et al.

Integrative Biology[55] with permission].

3.1.5 Three dimensional reconstructed imaging

Optical/fluorescence microscopes have been widely applied in different fields for a hundred years, but several challenges of 3D-structure imaging still restrict the progress of investigation in large biological objects (>100 μm), and in time-lapse imaging (time-course experiments), relevant for dynamic penetration studies of nanoparticle-treated spheroids. These limitations include the wide point spread function (PSF), limits in excitation light penetration, photobleaching, and speed of imaging[58]. In comparison with traditional confocal laser-scanning microscopy (CLSM), two-photon microscopy (2PM) utilizes two photons with long wavelength (near-infrared) as the excitation energy, allowing high signal to noise rate, low photobleaching, and most importantly deep penetration in biological samples. Although 2PM has high resolution and high-penetration excitation, there are some difficulties in time-lapse imaging by this technique because of low scan speed and non-linear photobleaching[58,59]. The Light-Sheet Fluorescent Microscope (LSFM) uses excitation focused on selective planes to illuminate samples and collect emission signals from the direction perpendicular to the excitation path (**Figure 3-4a**). Firstly, in view of its sheet-like scanning, the acquisition speed is much higher than point-scanning methods (CLSM and 2PM) and occurs with insignificant photobleaching or phototoxicity. Another interesting advantage is a rotation-available sample holder (**Figure 3-4b**), which enables LSFM to collect emission signals from different directions, which then overcomes limitations of penetration and allows reconstruction and multi-view imaging via appropriate software[60]. The limitations of

LSFM include lower spatial resolution and poor light collection, compared to 2PM and CLSM (**Figure 3-4d**). In addition, LSFM has the wide point-spread function (PSF), explaining why LSFM has the lower axial resolution of the various 3D imaging microscopes. Despite these deficiencies, LSFM is still a valuable tool to investigate tissue mimics, such as 3D-spheroid models and zebrafish models.

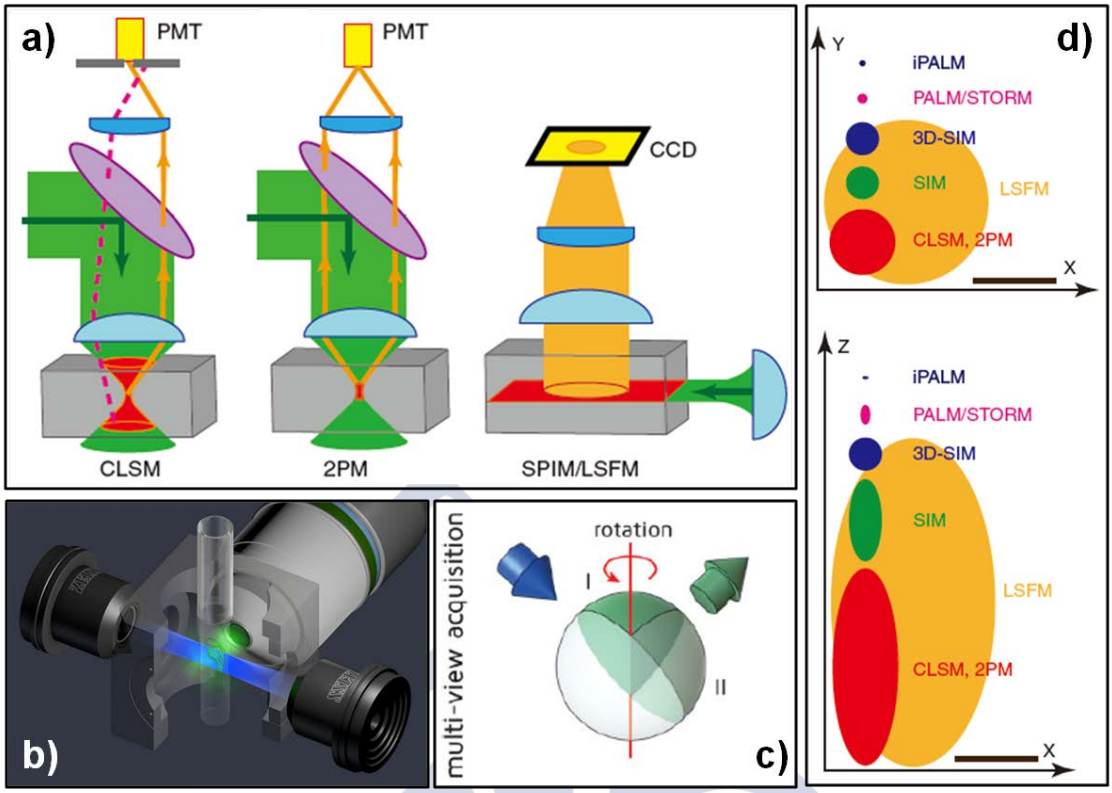

Figure 3-4. Fluorescence microscopes for 3D-reconstructed images. (**a)** Optical pathway profiles of microscopes for large biological subjects. [Adapted from Fischer, R. S. et al. Trends in cell biology[58]] (**b)** The LSFM we used in this thesis (Zeiss Z1). [Reproduced from Zeiss website, Lightsheet Z1] (**c)** Multi-view acquisition by rotated samples in LSFM [Adapted from Huisken, J. BioEssays[60]] (**d)** Comparison with effective point-spread function between different microscopes. The scale bar is 0.25 μm. [Adapted from Fischer, R. S. et al. Trends in cell biology[58], with permission]

Abbreviations used are the following: ***CLSM*** *(confocal laser-scanning microscopy);* ***iPALM*** *(interferometic photoactivated localization);* ***LSFM*** *(Light-sheet based fluorescent microscopy);* ***PALM*** *(photoactivated localization microscopy);* ***2PM*** *(two-photon microscopy);* ***SIM*** *(structured illumination microscopy).*

Chapter III / Capítulo III

3.2 Materials and Methods

3.2.1 Haemolysis tests

Rat blood samples were collected in K2E tubes containing EDTA (BD Vacutainer®) and were centrifuged at 1000 rcf for 5 min. After washing with PBS three times under the same centrifuge conditions, the red blood cells were re-suspended in PBS 7.4 and PBS 5.5 at the concentration of 3 %(wt/volume). The erythrocyte solution was allocated across 96 wells and incubated with either CA-PPZ:pDNA or CA-/6MHA-PPZ:pDNA complexes for 2 hours at 37 °C under mild shaking. Then, the plates were centrifuged and the supernatants transferred to a new plate for colorimetric analysis. The absorption of the released haemoglobin was measured in a 96-well plate reader at an excitation wavelength of 570 nm. The maximum haemolysis (positive control) was established using cells treated with 1 %(v/v) Triton X100 and the minimum value was set by treatment with PBS either at pH 7.4 or PBS at pH 5.5.

3.2.2 Confocal imaging on 2D monolayer

For maintaining cell-lines, U87MG cells were cultured in Dulbecco's Modified Eagle Medium (DMEM, Sigma) containing 10 % fetal bovine serum, 2mM Glutamine and 100 mg/L penicillin-streptomycin and maintained at 37 °C under a 5 % CO_2 atmosphere. For intracellular tracking studies, 25K of U87MG cells were attached on poly-L-lysine coating 8µ-Slides (Ibidi) in 200 µL growth media for at least 24 hours and then treated with polymeric complexes carrying Cy5-labelled pDNA (prepared by Label IT® kit from Mirus) for 4 hours. Then the media was changed to fresh growth media for further incubation over an additional 20 hours. After this period, treated cells

were incubated with 50 nM of Lysotracker-green (Invitrogen) and 5 µg/mL Hoechst 33342. Finally, confocal images (Leica SP5X) in live cells were taken.

For pDNA release study, the CA-PPZ was been labelled with Cy3-NHS as described in **Section 2.2**. The polymeric complexes of Cy3-CA-PPZ and Cy5-pDNA with 6MHA-PPZ were treated in U87MG cells in OptiMEM for 4 hours and then incubated in growth media for the desired time. Before confocal imaging, the cells were stained with 5 µg/mL Hoechst 33342. Finally, the confocal images (Leica SP5X) of live cells were taken.

3.2.3 Transfection and tomographic scanning in a 3D spheroid model

For establishing 3D spheroids of U87MG cells, ultra-low attachment 96 well round-bottom plates (Corning®) were seeded with 250 - 5000 U87MG cells per well in growth media and with six replicates for experimental conditions. The plates were centrifuged at 200 rcf for 5 min to cause cell accumulation and stimulate spheroid formation. After three days, the spheroids were adjudged ready for transfection studies. The spheroids were treated with different polymeric complexes with different concentrations for 16 hours in OptiMEM and further incubated in growth media for 80 hours. GFP expression was quantified from each spheroid at 96 h post-treatment via ImageJ (Fiji) analysis directly using built-in histogram functions (**Figure 3-10**). The volume of the spheroids was calculated from phase-contrast microscopic images (Nikon Eclipse Ti) using a ImageJ plugin (Fiji package) macro program,[61] which measured spheroid area (A) from defined regions of interest (ROI). Then, the spheroid area was used to determine the radius (R=[A/π]^(1/2)) and calculated the volume

assuming the cell aggregates formed an equivalent sphere. To quantify metabolic activity in the spheroids, a resazurin reduction assay was performed. Briefly, the spheroids were treated with resazurin (60 µM) in the growth media and incubated at 37 °C for 4 hours. Following that, the 96-well plate was measured with a FlexStation II plate reader set at an excitation wavelength of 530 nm and at an emission of 590 nm. The evaluation of membrane integrity in the cell was performed using 7AAD (5 µL per well, 50 µg/mL) and fluorescence observed in the mCherry channel (Ex 560/55 and filter 630/60) at the fluorescence microscope.

In **Figure 3-10**, the quantification of fluorescence intensity in spheroid model was selected via ROI and histogram curves of fluorescence intensity (FI) compared with the non-treated group as control (media-only). GFP-positive counts were recorded when FI were higher than the maximum FI of non-treated groups, whose intensities were decided as thresholds (also as negative control) (**Eq. 3-1**). For GFP-gene transferred expression, there is no optimal positive control. For this reason, we presented herein the quantification via the percentage of GFP positive pixels. There were at least four replicates in each independent experiment and displayed data were analysed by Prism software from four to nine independent experiments.

$$GFP\ Positive\ Pixels\ \% = \frac{\sum Pixels_{(\text{whose FI>threshold})}}{\sum Pixels} \qquad \textbf{(Eq 3-1)}$$

For 7AAD, the threshold is defined from the mean of fluorescent intensity (Mean FI) in the untreated group as 0% and the mean FI of 0.5 %(v/v) triton X-100 treated group as 100%. The percentage of 7AAD signals of treated spheroids are expressed as below.

$$Mean\ FI\ of\ 7AAD\ signals = \frac{\sum pixel \times FI}{\sum Pixels} \quad \textbf{(Eq 3-2)}$$

$$7AAD\ Positive\ \% = \frac{(Mean\ FI\ of\ treated\ \text{spheroids}) - (Mean\ FI\ of\ \text{non-treatment})}{(Mean\ FI\ of\ TritonX\ treatment) - (\ Mean\ FI\ of\ \text{non-treatment})} \quad \textbf{(Eq 3-3)}$$

For 3D imaging, spheroid samples were fixed with 4% paraformaldehyde (PFA) first and their nucleus stained with DAPI. The fixed spheroids were loaded in appropriate glass capillaries with 1% low-melt agarose. The imaging was performed by light sheet fluorescent microscopy LSFM (Light-sheet Z.1, Zeiss) and presented in the same fluorescence intensity scale using ImageJ software.

3.2.4 GFP/Luciferase transfection in xenografted model

All in vivo experiments had been approved by the Research Ethics and Animal Welfare Committee at the Instituto de Salud Carlos III, Madrid, (PROEX 224/14) in agreement with the European Union and national directives. A subcutaneous xenograft model of GBM was established as previously described[62]. Briefly, athymic nude Foxn1nu mice were subcutaneously injected with 1 million fresh U87MG cells (in 80 µL cultured media and 20 µL Matrigel (BD)) on both flanks. When tumour sizes reached around 100-150 mm^3, polymer complexes with the GFP/Luciferase plasmid were injected inside the tumour directly. One week later, before the mice were sacrificed, they were treated with Luciferin 50 mg/kg by IP injection. The transfected tumours were excised and imaged by In Vivo Imaging System (IVIS®).

3.3 Results and discussion

3.3.1 Membrane disruption of binary-polyions complexes

Many literature reports have emphasized the importance of endosomal escape in the process of gene/drug delivery, for which two proposed mechanisms are the "proton sponge" effect and membrane disruption due to the acidified endosomal environment[10]. The effects of biomaterials related to membrane disruption are usually assessed in assays prior to practical bio-applications by two common methods, i.e. haemolysis of red blood cells (RBC) from mammals[32,39] and rupture teats of artificial liposomes[37]. Herein, we chose the erythrocyte membrane as a model because the RBC model can not only evaluate the endosomolytic effects but also can indicate the potential of other cell-material interactions in the body.

The polymer-only and polymeric complex formulations were added to murine RBC, as shown in **Figure 3-6a** and **b**, respectively. Firstly, either only cationic CA-PPZ or only anionic 6MHA-PPZ were incubated with RBC. As expected, CA-PPZ polymers caused severe haemoglobin release due to strongly positive charges, similar to other cationic polymers, like poly-L-Lysine (PLL)[63,64]. In comparison to CA-PPZ, the anionic polyphosphazene (6MHA-PPZ) presented high compatibility with RBC at physiological pH, even when incubated with high concentrations of 6MHA-PPZ and at pH 5.5, but the haemolytic capacity of 6HMA-PPZ were still insignificant. For nanocomplex formulations, CA-PPZ:pDNA complex caused higher haemolytic effects than CA-/6MHA-PPZ:pDNA, triggering pH-independent membrane disruption. On the contrary, the CA-/6MHA-PPZ:pDNA showed low haemolysis percentage at physiological pH but caused higher haemoglobin release at the endosomal pH (**Figure**

3-6c). There may be several reasons that caused this low pH-induced erythrocytic membrane rupture. Firstly, protonated 6MHA-PPZ reduced neutralisation of CA-PPZ at the acidic situation, making positively charged CA-PPZ more capable to interfere with the cell membranes in a similar manner to the highly-haemolytic CA-PPZ:pDNA complexes. Another reason may be that the protonated 6MHA-PPZ presented hydrophobic regions able to insert into the phospholipid bilayers of RBC, resulting in membrane disruption. In comparison to 6MHA-PPZ only, this system did not cause strong haemolysis, but its complex formulation did have haemolytic effects on the erythrocytes at pH 5.5. This is likely caused by aggregation of 6MHA-PPZ polymers due to protonation, resulting in insignificant interaction with RBC. On the other hand, for the 6MHA-PPZ polymers mixed in CA-PPZ complexes, partial protonation and surface presentation of the new-hydrophobic side-chains out from the 'coronae' of the complexes and as 'suspending status' may have raised the haemolytic capability of the complexes.

In general, the percentages of haemolysis in the assays were calculated from the scale between negative control (PBS only) and positive control (Triton-X 100), but this scale is directly affected by the initial number of RBC. As a result, a proper ratio of formulation to RBC should be considered but it is difficult to ensure consistency in complicated practical situations. Normally, the blood cell concentration of nude mice (body weight 20-25 g) is around 7×10^9 to 13×10^9 RBC/mL,[65] and herein we treated the same concentration of polymeric complexes with two initial concentrations of RBC; one located around the murine blood concentration, and another was 25 % of the physiological RBC number. The figures confirmed the CA-/6MHA-PPZ:pDNA can stimulate haemoglobin release under slightly acidic conditions (pH 5.5) in both

concentrations of RBC, but the percentages of haemolysis were amplified in the assays with the lower initial number of RBC.

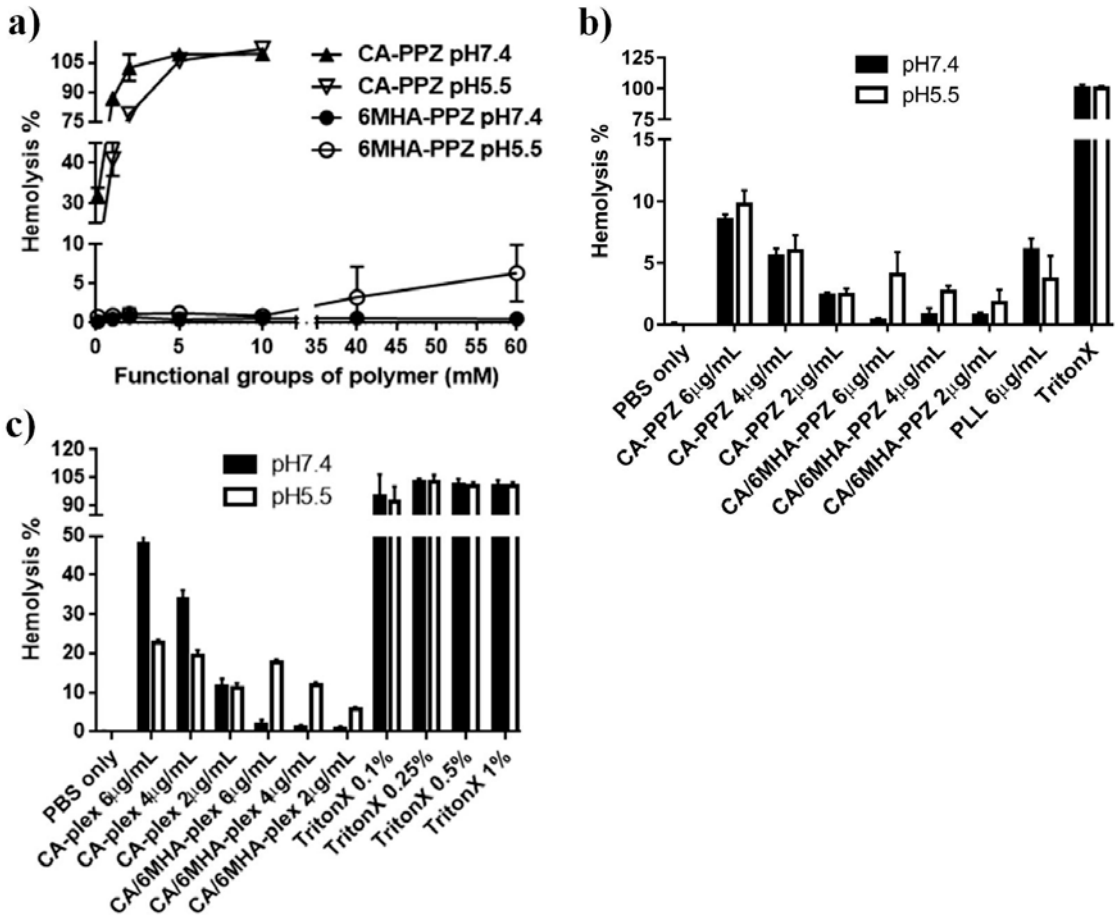

Figure 3-6. Haemolysis evaluation of PPZ-based polyions or nanocomplexes. **a**) haemolysis percentages of either CA-PPZ or 6MHA-PPZ in different concentration ranges. **b**) haemolysis percentages of CA-PPZ complex (CA-PPZ:pDNA, N/P 8:1), CA-/6MHA-PPZ:pDNA complex (N/C/P 8:4:1) with different doses incubated with murine red blood cells for 2 h for 37 ^{o}C. The initial amount of RBC is 1×10^{10} per mL and the 100% haemolysis is defined by the absorption value via treatment of 1% Triton X100. **c**) Haemolysis assay in the initial number RBC at 2.5×10^{9} per mL.

3.3.2 Intracellular distribution of binary-polyions complexes

For deeper understanding of the interaction of CA-PPZ and CA-/6MHA-PPZ complexes with tumour cells, internalisation and intracellular trafficking assays of the complexes were evaluated by flow cytometry and confocal microscopy, respectively. CA-PPZ and CA-/6MHA-PPZ were complexed with Cy5-labelled pDNA and incubated with U87MG cells under the same treatment conditions described previously for the transfections in 2D monolayers. Confocal micrographs (**Figure 3-7a**) and flow cytometry (**Figure 3-7c, d**) indicated similar levels of cellular uptake for both prototypes. However, there were significant differences in the intracellular distribution of Cy5-labeled pDNA for both prototypes in relation to a late endosome / lysosome marker (Lysotracker, Invitrogen). At 24h post-treatment, the Cy5-labelled pDNA carried by CA-/6MHA-PPZ complexes was more broadly distributed in the cytosol, and distal to the green-stained lysosomes. CA-PPZ:pDNA complexes remained inside lysosomes, resulting in yellow signals in the confocal merged image (**Figure 3-7a, bottom**). The analysis of fluorescence intensities in the confocal images at 24h post-treatment indicated that the co-localization ratios (Manders' overlap coefficient, **Figure 3-7c**) of Cy5-pDNA to lysosomal markers were different for both prototypes and confirmed that the addition of 6MHA-PPZ facilitates escape of the complexes from the endosomal compartments. One of the suggested reasons is that 6MHA-PPZ has high buffering capacity particularly in the early endosomal pH range (pH 7.4 – 6.0). Furthermore, we hypothesized that these results might be related to a capacity of 6MHA-PPZ to destabilize biological membranes at endosomal pH. At pH 5.5 CA-/6MHA-PPZ:pDNA complexes showed a clear haemolytic effect similar to those

observed for PLL complexes, while CA-/6MHA-PPZ:pDNA complexes showed minor haemolysis at physiological pH (**Figure 3-6**).

After escape from endosomal components, another limitation for polycation-mediated delivery is the difficulty to release nucleic acids from complexation with the polycation, in order to pDNA to be further delivered to nuclei[66,67]. Herein we tracked the distribution of pDNA and polycations simultaneously in the cells, via labelling of polycation CA-PPZ and pDNA with Cy3 and Cy5, respectively. In general, the time-course images revealed the high co-localisation between pDNA and CA-PPZ in both formulations (**Figure 3-8**). However, CA-/6MHA-PPZ complexes were better able to release pDNA from CA-PPZ complexation, especially at 48h post-treatment while compared to CA-PPZ:pDNA. At 24 h post-treatment, there were some red-orange signals (tiny CA-PPZ co-localized with pDNA) in the cells treated with CA-/6MHA-PPZ, probably showing some polycations retained with pDNA. Following that, the images of cells treated with CA-/6MHA-PPZ complexes clearly showed more released pDNA at 48 h. At 72 h post-treatment, the signals of Cy3 and Cy5 were weakened due to proliferation of the cells resulting in dilution of total fluorescent intensity. In contrast, the high amount of yellow signals in CA-PPZ:pDNA treated cells showed highly correlated co-localisation between pDNA and CA-PPZ. This intracellular release evaluation was followed by endo/lysosomal localisation studies, in which CA-/6MHA-PPZ complexes were shown to be distal to endolysosomal compartments (**Figure 3-7b**). From both confocal-imaging evaluations, it can be concluded that most of the pDNA was still condensed in the PPZ complexes, even after endosomal escape and diffusion in the cytosol, but the mixing of 6MHA-PPZ with CA-PPZ complexes acted as a

pH-controlled trigger for proton-buffering endosomal escape and as a facilitator for dissociation of CA-PPZ and pDNA.

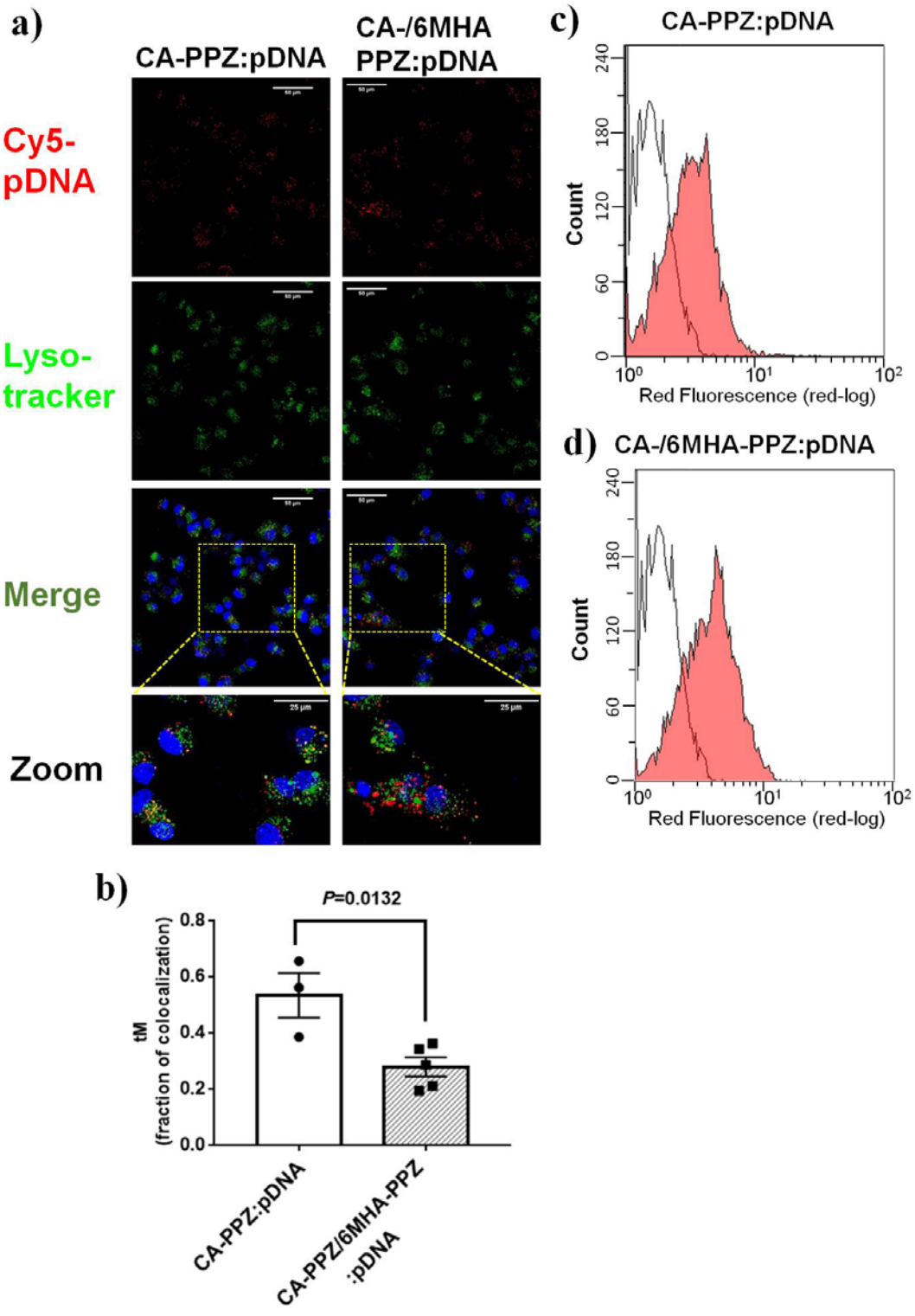

Figure 3-7. Comparison of the intracellular trafficking of two selected PPZ prototypes. **(a**) Intracellular distribution after 24h of Cy5-labeled pDNA (red) and a late-endosome/ lysosome compartment marker (Lysotracker, in green) upon delivery of CA-PPZ:pDNA or CA-/6MHA-PPZ:pDNA complexes. (**b**) Internalisation of both complexes carrying Cy5-labeled pDNA after 4h incubation with U87MG cells measured by Fluorescence Activated Cell Sorting. (**c**) Co-localization of pDNA with the late-endosome/ lysosome compartment calculated by image analysis (ImageJ, Coloc2 plugin).

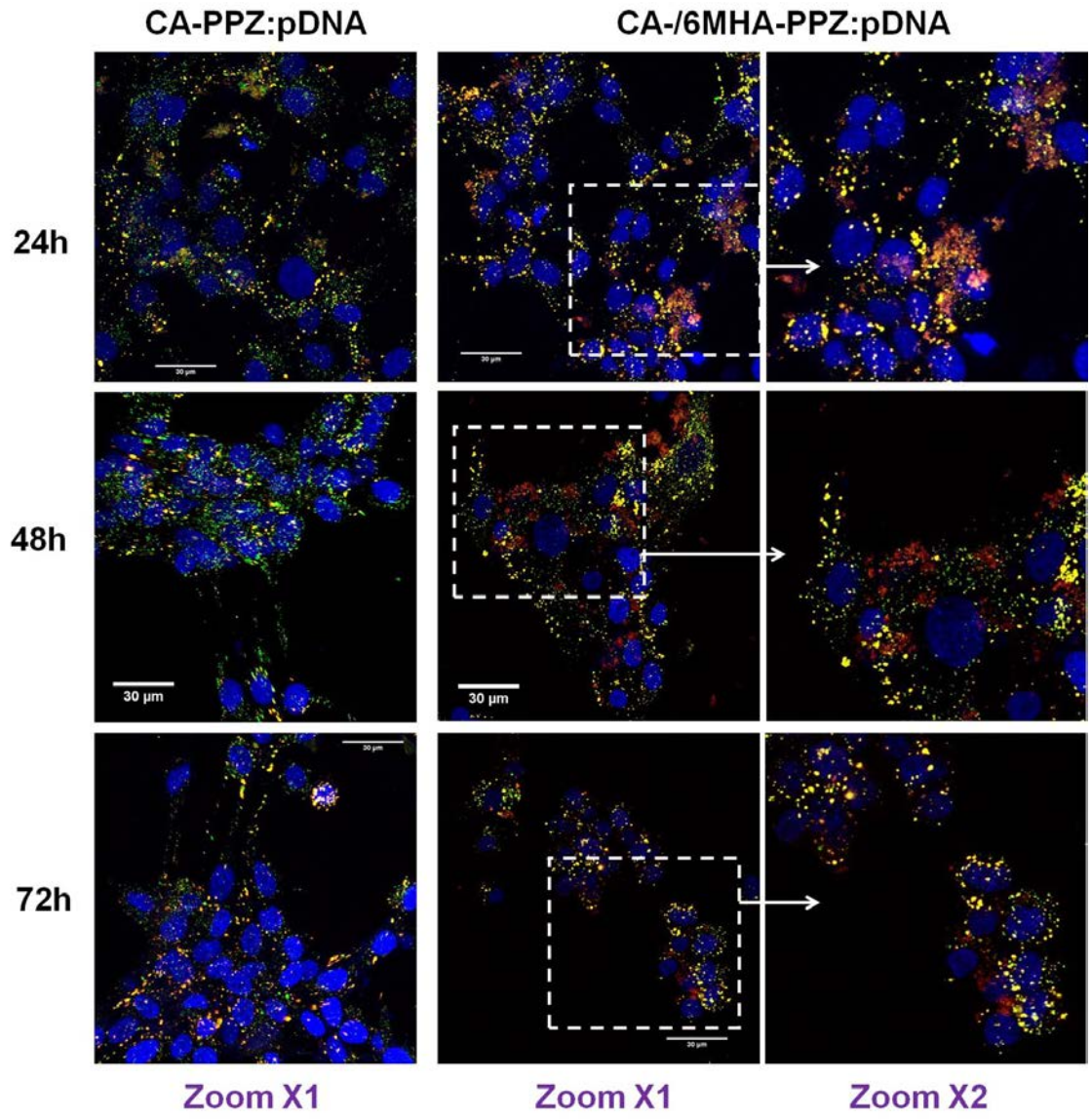

Figure 3-8. Confocal images of Cy3-CA-PPZ (green) complexes with Cy5-pDNA (red) for intracellular dynamic distribution after 24, 48, and 72 h treatments in U87MG cell monolayer.

3.3.3 Transfection of binary polyionic complex on 3D spheroid model

Following demonstration of transgene expression in 2D monolayers, we established three-dimensional spheroids of U87MG cells as simple mimics of residual tumour regions around glioblastoma-margin areas after surgery or radiotherapy.[68] The cells grew as spheroids (diameter ~250 μm) following a three-day incubation period and Light-Sheet Fluorescent Microscopy (LSFM) was used for tomographic scanning in this tumour model. PPZ:pDNA complexes were assayed on the spheroids to evaluate any inherent toxicity by measuring spheroid size and metabolism through analysis of phase-contrast images and resazurin reduction assays (Alamar Blue), respectively, following the previously published methods by our group[57,61] (**Figure 3-9**). Spheroids treated only with pDNA reduced slightly in volume after 16 hours in OptiMEM media, most likely due to some nutrient depletion over this period. Incubation of the spheroids with the CA-PPZ:pDNA complexes at 4 μg/mL caused a significant decline in volume to 87.4±3.2% of the initial value ($P < 0.004$), whereas CA-/6MHA-PPZ:pDNA complexes did not cause a statistical shrinkage ($P = 0.132$) at the same dose. In resazurin reduction assays, the metabolic activities of CA-/6MHA-PPZ:pDNA treated spheroids were slightly higher than the untreated spheroids, whereas CA-PPZ:pDNA treated spheroids at both DNA doses (2 μg/mL and 4 μg/mL) showed no significant difference in metabolic activity compared to non-treated spheroids. These experiments indicated no marked toxicity for the mixed cationic/anionic PPZ complexes.

Further tolerability assays were performed monitoring cell membrane damage with 7-Aminoactinomycin D (7AAD) on the previously used spheroid model. These experiments were performed in parallel with transgene expression levels of Green

Fluorescent Protein (GFP) upon pDNA delivery with different polymer complexes (**Figure 3-11**). CA-/6MHA-PPZ successfully delivered the GFP encoding pDNA as demonstrated by the percentage of GFP-positive pixels at the regions of interest (ROIs) of spheroid images (56.2 ± 7.9% and 88.9 ± 4.1% for pDNA doses of 2 and 4 μg/mL, respectively). **Figure 3-10** shows examples of ROI selection and histogram analysis. These GFP levels were significantly higher than those obtained with CA-PPZ:pDNA and PEI:pDNA. Regarding 7AAD staining, there were no statistic differences between polymeric complexes at the same dose, resulting from the strong positive values of the spheroids incubated with Triton X-100. In summary, the spheroid model experiments indicated that CA-/6MHA-PPZ:pDNA complexes achieved better transfection / toxicity ratios than CA-PPZ:pDNA and the laboratory standard PEI:pDNA system.

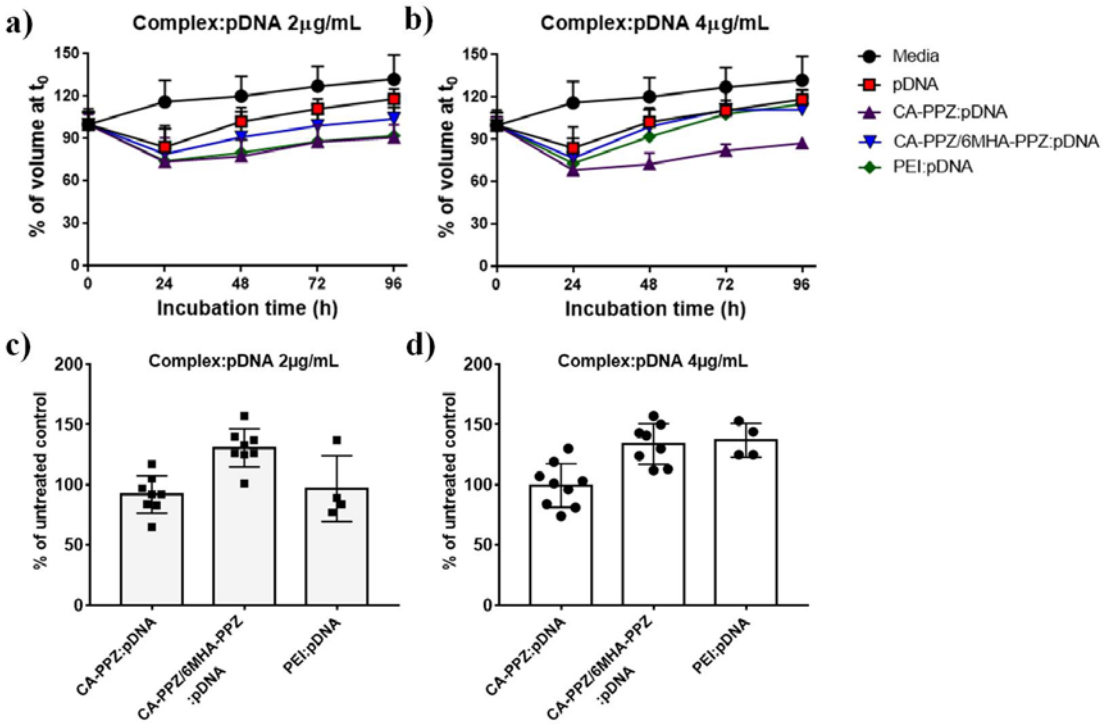

Figure 3-9. Polyphosphazene complex cytotoxicity as measured by spheroid volume and metabolic activity in U87MG spheroids. Initial spheroid diameter was ~ 250 µm at time 0 (t_0) and was measured over time after treatment with polymer complexes with pDNA 2 µg/mL in **a**) and 4 µg/mL in **b**). Metabolic activity of U87MG spheroids treated with different polymer complexes in (**c, d**). Data is normalized to spheroids cultured in media-only group.

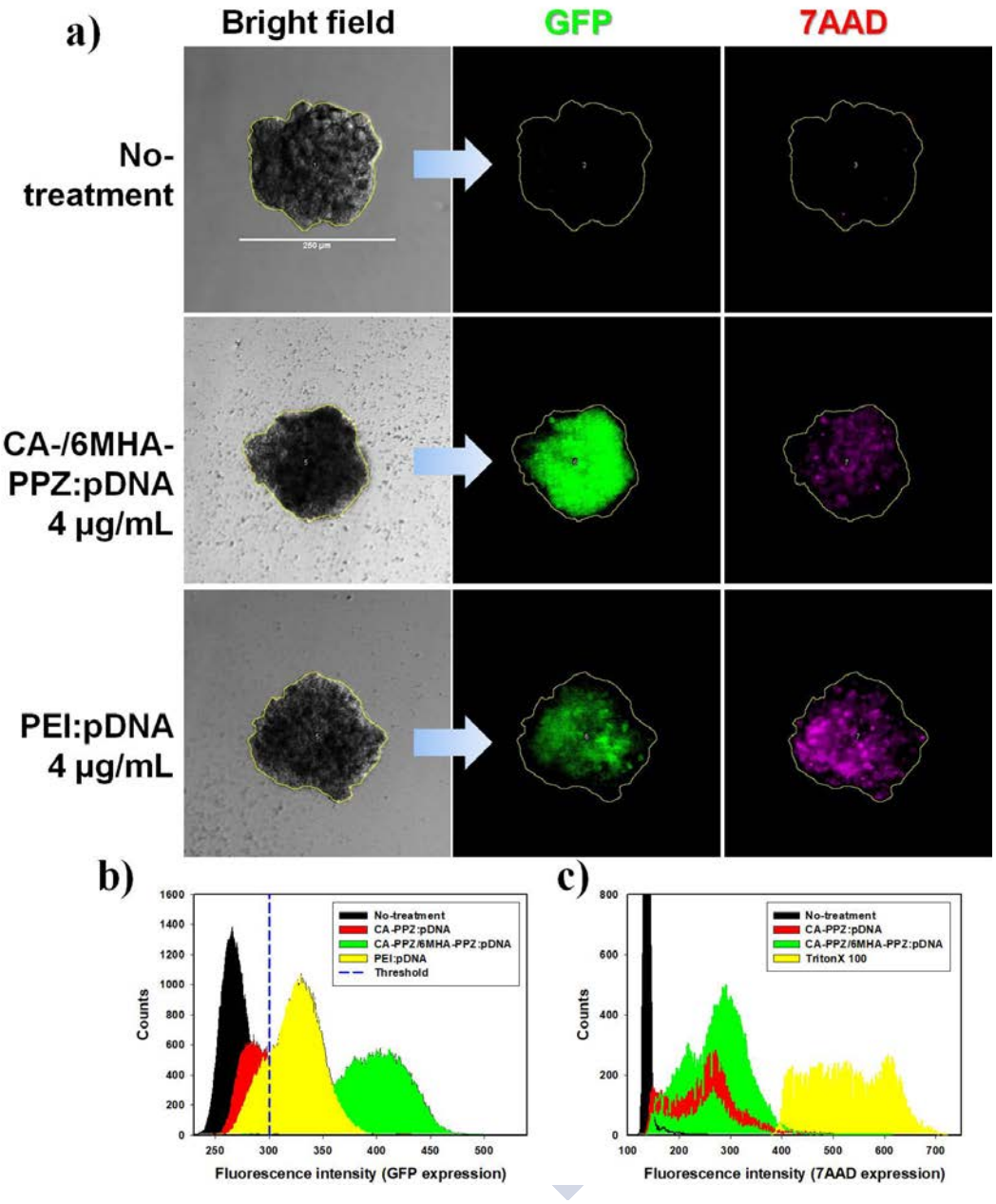

Figure 3-10. Diagrams showing the region-of-interest (ROI) selection in spheroid areas (**a**) and corresponding analysis via GFP (**b**) and 7AAD (**c**) fluorescent intensity histograms of spheroids treated with polymeric complexes with pDNA 4 µg/mL.

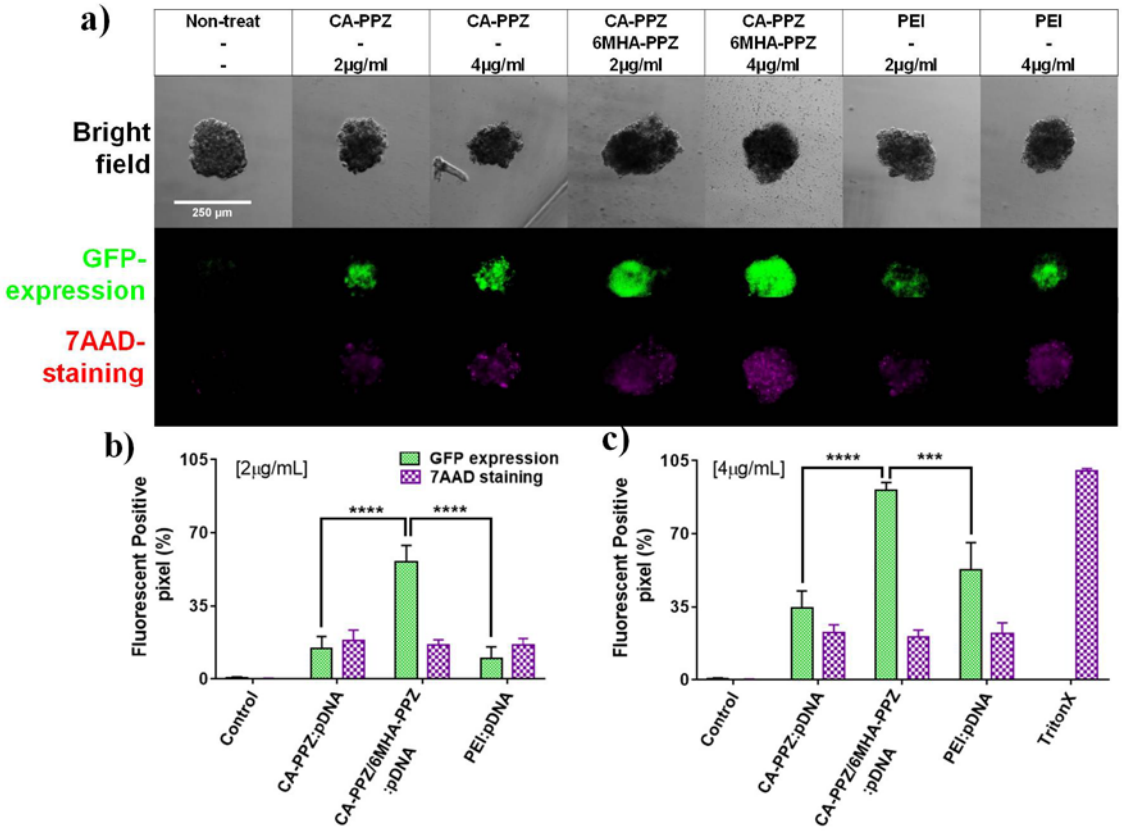

Figure 3-11. Transfection efficacy and viability of U87MG spheroids treated with polymeric complexes at two pDNA doses. (**a**) Overlay microscopy images showing GFP-expression and 7AAD-staining of U87MG-spheroids after treatments by CA-PPZ:pDNA (N/P 8:1) and CA-PPZ/6MHA-PPZ:pDNA (N/C/P 8:4:1) at the pDNA doses of 2 and 4 µg/mL. (**b, c**) Quantification of GFP-fluorescence and 7AAD signals from the ROIs of spheroids in four independent experiments; spheroids treated with 2 µg/mL pDNA are analyzed in (**b**), those treated with 4 µg/mL in (**c**) (**** represents $P <$ 0.001 and *** is $P < 0.005$, analyzed by a one-way ANOVA with a Dunnett's multiple comparison test with a single pooled variance).

3.3.4 Tomographic scanning in transfected spheroid in 3D

To gain further insight on the delivery system penetration and gene transfer throughout the spheroids, fluorescence tomographic scanning was performed by light-sheet fluorescent microscopy (LSFM) (**Figure 3-12**), and tomographic-scanning videos of those transfected spheroids will show in supplemental files [or in the thesis presentation]. When the spheroids were treated with complexes at the higher pDNA dose (4 μg/mL), homogeneous GFP transfection was apparent even in the core of the spheroids treated with CA-PPZ:pDNA and CA-/6MHA-PPZ:pDNA, although GFP fluorescence was most intense in the latter system. At the lower pDNA dose (2 μg/mL) CA-/6MHA-PPZ:pDNA complexes still provided consistent transfection in most of the spheroids, whereas transfection for CA-PPZ:pDNA and PEI:pDNA was clearly weaker with low GFP expression (**Figure 3-12a**). This effect suggests a more efficient gene delivery for CA-/6MHA-PPZ:pDNA than CA-PPZ:pDNA and PEI:pDNA systems in this 3D model.

These data also indicated that this mixed polycations-DNA-polyanion system had a surprising capacity to move through a 3D tumour structure of 250μm-diameter spheroids. Maximum intensity projections (**Figure 3-12b**) indicated strong fluorescence throughout the spheroids transfected with the CA-/6MHA-PPZ:pDNA complexes and supported our previous observations. The results showed that mixing of 6MHA-PPZ in CA-PPZ complexes enhanced penetration into this size of spheroids and facilitated gene-transfection expression, even in the core of spheroids. Regarding to penetration in spheroids, many key factors are involved, including particle size and surface charges, type of cell models, treatment concentration, etc. In LSFM images, the

higher dose (4 μg/mL) of polymeric complexes demonstrated deeper penetration efficacy and higher gene-transferring efficiency than the low dose of treatments (2 μg/mL). As shown in **Figure 3-12**, the PEI-complexes and CA-PPZ complexes at pDNA dose 2 μg/mL generated only faint green signals through the whole spheroids. For this polycation-only pDNA complexes (N/P 8), the minimum pDNA dose for transfection in this model has to be 4 μg/mL. In contrast, significant GFP expression was found in treatment by the low dose of CA-/6MHA-PPZ complexes. As the dose increasing to 4 μg/mL of CA-/6MHA-PPZ complex, significant GFP expression was shown throughout the spheroids. The results showed strong dose-dependent penetration in spheroid models.

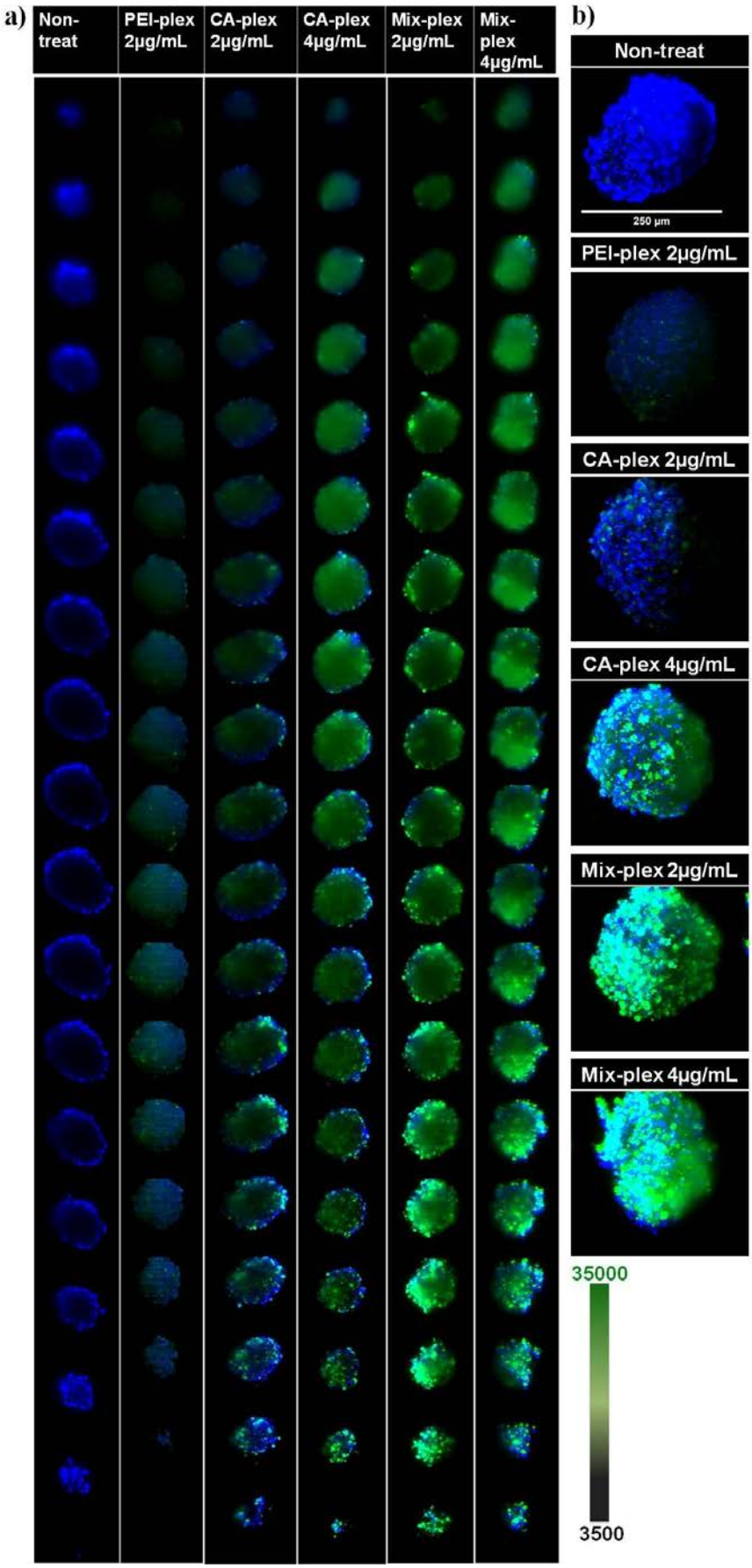
a)
Non-treat
PEI-plex 2µg/mL
CA-plex 2µg/mL
CA-plex 4µg/mL
Mix-plex 2µg/mL
Mix-plex 4µg/mL
b)
Non-treat
250 µm
PEI-plex 2µg/mL
CA-plex 2µg/mL
CA-plex 4µg/mL
Mix-plex 2µg/mL
Mix-plex 4µg/mL
35000
3500

Figure 3-12. 3D tomographic images of GFP-transfected spheroids taken by LSFM. **a**) 3D section images of CA-PPZ:pDNA complexes (CA-plex) and CA-/6MHA-PPZ:pDNA complexes (Mix-plex) treated spheroids (diameter ~250 μm) at two pDNA doses of 2 μg/mL and 4 μg/mL. **b**) Maximum intensity projections along Z-axis (XY projection) images of spheroids treated with different polymer:pDNA complexes at two doses. The images were taken by LSFM. Blue corresponds to DAPI staining; green to GFP fluorescence. The all fluorescence images were analysed by ImageJ and processed under the same scale of fluorescence intensity.

In addition, gene transfection was also dependent on size of spheroids. For instance, although the small size of spheroids (~250 μm diameter) was chosen for suitable screening by LSFM, we also evaluated gene expression in larger (≥ 400 μm diameter) spheroids (**Figure 3-13**) where we found limitation in transport to the spheroid cores as compared to those tested previously. This could be explained in two ways. First, the nanocarriers were unable to transport to the tumour core due to extended distance. Secondly, the tumour cells in the inner core of these large tumour spheroids may have been necrotic due to low oxygen tension and lack of nutrients, thereby unable to transfect GFP gene and expression, even if CA-/6MHA-PPZ complexes clearly diffused to the centre of the spheroids.

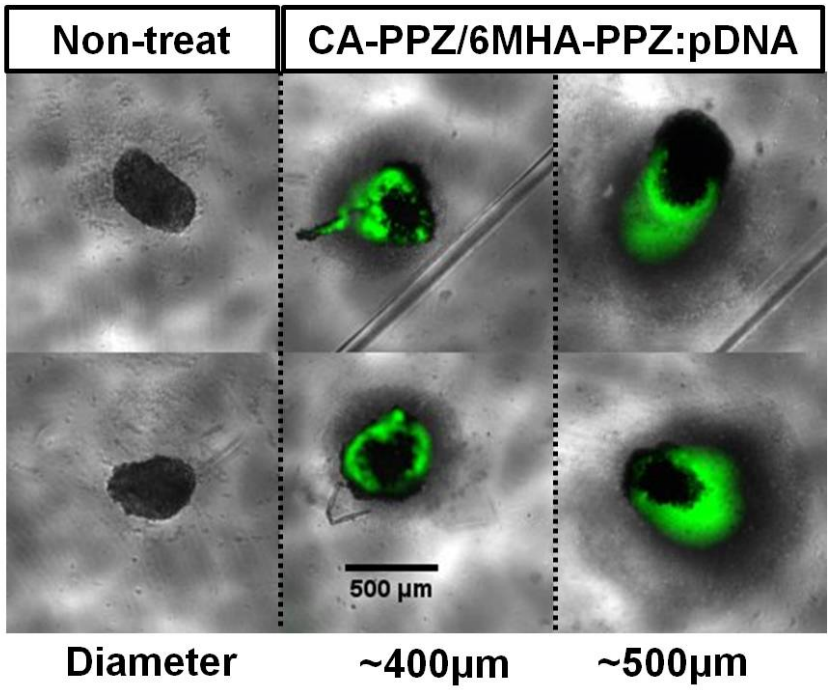

Figure 3-13. Transfection by CA-/6MHA-PPZ complexes carrying GFP-encoding plasmid in large spheroids (Diameter ≧400μm).

3.3.5 GFP/Luciferase transfection in xenograft model

We next evaluated gene-transfer efficiency of the binary ionic PPZ:nucleic acid complexes in centimetre-scale xenograft tumours *in vivo*. Nude mice were subcutaneously implanted with U87MG cells on the flanks, and when the tumours attained a size of 100 – 150 mm^3, polymeric complexes with the bi-functional plasmid (encoding GFP and Luciferase) were injected intra-tumorally (16 µg pDNA for each tumour). At the end of the experiment, tumours were excised, sectioned and observed by IVIS (**Figure 3-14 a, b**) and hematoxylin and eosin (H&E) stains (**Figure 3-15**). The data indicated that the tumours were transfected by all the polymeric complexes compared with non-treated tumours. ROI quantification of luciferase expression (**Figure 3-14b)** showed that the CA-/6MHA-PPZ:pDNA complexes were similar in transfection efficacy to the PEI-DNA complexes and achieved around 1.5-fold higher transgene expression than CA-PPZ:pDNA. In GFP-expression images, the semi-quantification of polymeric complexes indicated similar results with those of luciferase expression. However, either GFP fluorophores (λ_{em} = 507 nm) or luciferase-reported luminescence (λ_{em} = 560 nm) may not the best options for evaluation of in vivo gene transfection due to low penetration of light with yellow-green wavelength in living tissues[69]. This may be caused by the large error bars in statistical analysis due to technical difficulties, including the depth of tumour to inject the complexes, tumour shapes, tumour microenvironments, natural green autofluorescence. Here we recommend to choose plasmid encoded mCherry or mPlum proteins[70] for in vivo gene transfection studies, because their emission wavelengths are located in the range of red or near far red, which have better penetration through the tissues. The transfected tumours were then sliced and stained by H&E for evaluation of

transfection-induced toxicity (**Figure 3-15**). The H&E stained images showed there was no significant toxicity after those in vivo transfection. Compared with transfection in 2D monolayer, lower side-effects in gene expression were found in PPZ-complex treated 3D spheroids and xenograft tumours of glioblastoma U87MG. Regarding this, 3D cultures and xenograft tumours can provide a relevant micro-environment limiting accessibility of the polymeric carriers, such as ECM impeding drug/carrier diffusion[61,71,72], and also better able to preserve the properties of tumour stem cells[73]. In the literatures, 3D spheroid models have been employed for investigation of chemo-sensitivity in several cancers[72,74,75], in which GBM spheroids and their primary cell-lines are better able to resist chemotherapeutic alkylating agents (e.g. TMZ) than 2D traditional cell models[47]. The data indicated that a lead formulation, CA-/6MHA-PPZ carrier improved effectiveness of gene delivery in two bio-relevant models, underscoring their potential in RNA interference therapy in glioma stem cell-like properties.

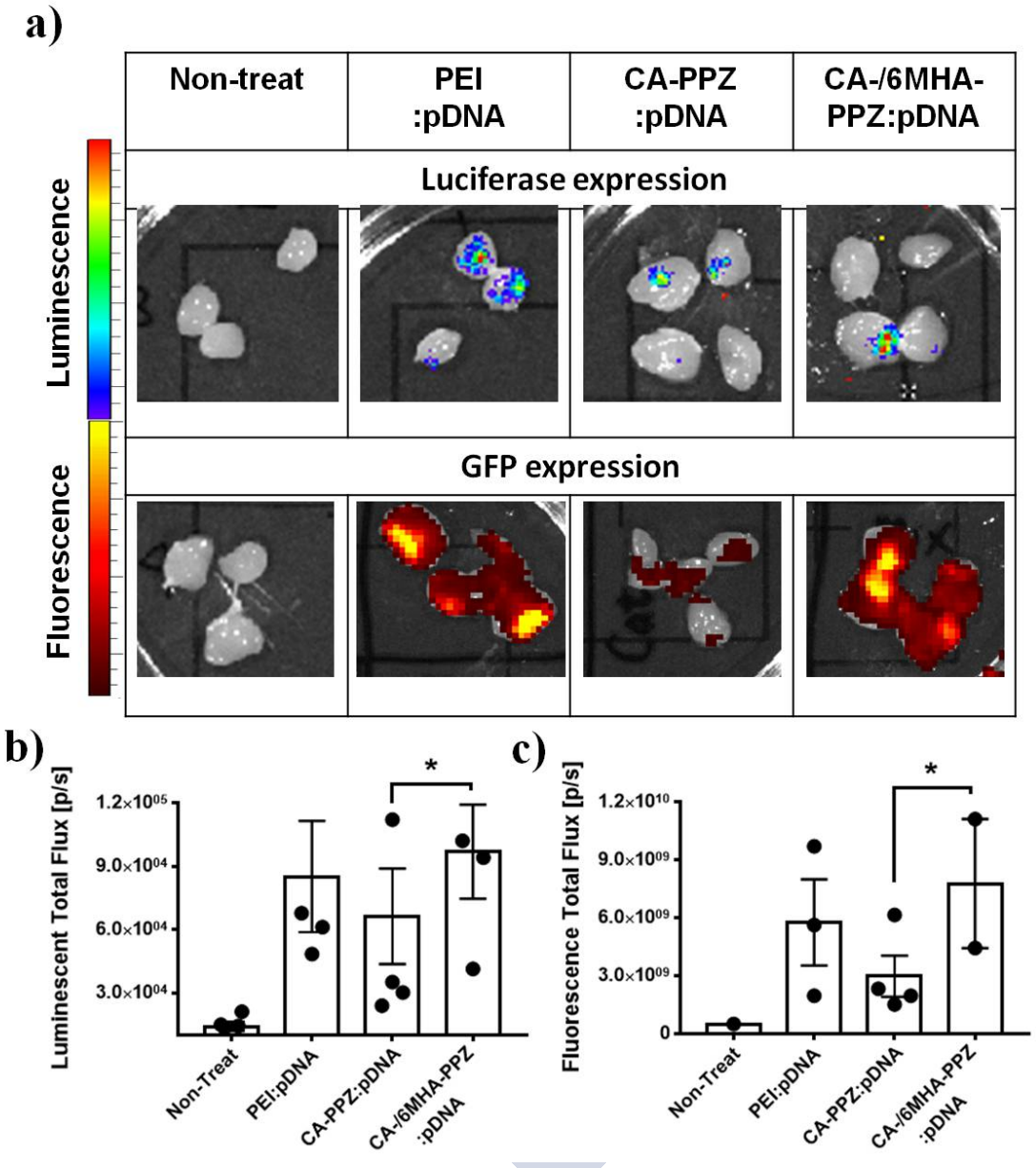

Figure 3-14. Transfection of polymeric complexes on xenograft tumours of U87MG cell-line. **a**) IVIS images of luciferase/GFP transfected U87MG tumours in nude mice. Quantitative analysis in the tumour regions for the luminescence of luciferase expression in **b**) and fluorescence of GFP expression in **c**). (* $P < 0.5$, analysed by a one-way ANOVA with a Dunnett's multiple comparison test with a single pooled variance) N≧3 expect for GFP expression of CA-/6MHA-PPZ complex.

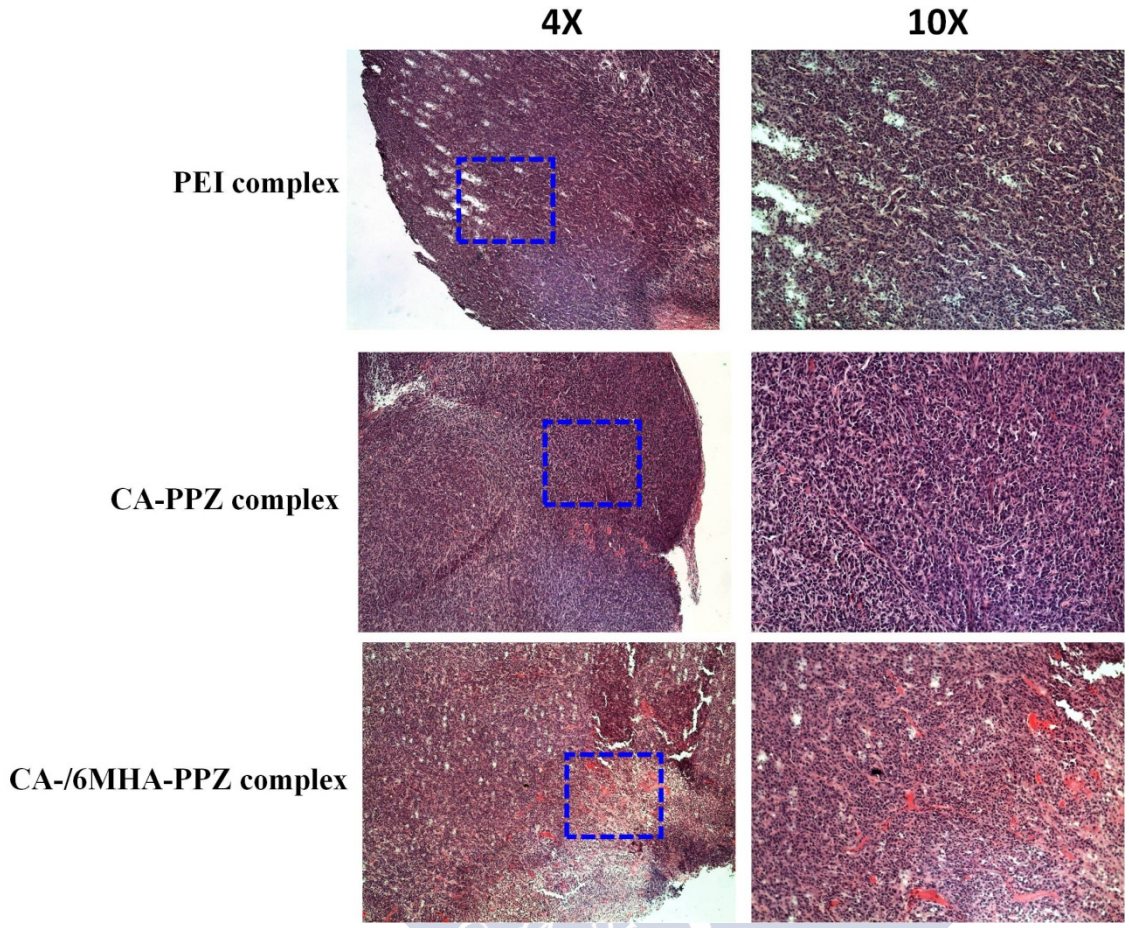

Figure 3-15. Hematoxylin and eosin (H&E) stains in histology. The H&E stained sections of PEI:pDNA complex treated, CA-PPZ complex treated, and CA-/6MHA-PPZ complex treated U87MG-xenograft tumours after IVIS imaging.

3.4 Conclusion

In this chapter, we designed several proof-of-concept experiments for 6MHA-addition in order to facilitate endosomal escape of polymer-gene complexes as well as controlled release of nucleic acids from their complexes. In the confocal images, the CA-/6MHA-PPZ complex was demonstrated to be better able to separate from the lysosome marker and release in the cytosol regions. Through labelling of Cy3 in polycations and Cy5 in pDNA, the intracellular distribution analysis provided clear evidence for pDNA release, which is one of the major obstacles especially for polycation-mediated delivery. However, 6MHA-PPZ mixing with CA-PPZ complexes significantly boosted the release of pDNA after 48h treatment. Following the optimisation in 2D monolayer, 6MHA-PPZ mixing in CA-PPZ complexes also showed higher transfection efficiency in a bio-relevant 3D spheroid model compared to CA-PPZ-only complexes. Tomographic scanning images confirmed the transfection profile inside the 3D spheroids, indicating penetration and transfection efficiencies are dependent on the treatment doses and 6MHA-PPZ addition. Finally, preliminary evaluations of in vivo transfection confirmed CA-/6MHA-PPZ complexes can transfer gene cargoes and express transgene via local administration in a U87MG xenograft model. In the next chapter, we chose this optimal formulation for RNAi therapeutic application.

Chapter III / Capítulo III

3.5 References

1. Kumari, S., Swetha, M. & Mayor, S. Endocytosis unplugged: multiple ways to enter the cell. *Cell research* **20**, 256-275 (2010).
2. Iversen, T.-G., Skotland, T. & Sandvig, K. Endocytosis and intracellular transport of nanoparticles: present knowledge and need for future studies. *Nano Today* **6**, 176-185 (2011).
3. Von Gersdorff, K., *et al.* The internalization route resulting in successful gene expression depends on both cell line and polyethylenimine polyplex type. *Molecular Therapy* **14**, 745-753 (2006).
4. Xiang, S., *et al.* Uptake mechanisms of non-viral gene delivery. *Journal of Controlled Release* **158**, 371-378 (2012).
5. Hufnagel, H., Hakim, P., Lima, A. & Hollfelder, F. Fluid Phase Endocytosis Contributes to Transfection of DNA by PEI-25. *Molecular Therapy: the Journal of the American Society of Gene Therapy* **17**, 1411-1417 (2009).
6. Wieffer, M., Maritzen, T. & Haucke, V. SnapShot: endocytic trafficking. *Cell* **137**, 382. e381-382. e383 (2009).
7. Lu, Y., *et al.* Enhanced endosomal escape by light-fueled liquid-metal transformer. *Nano Letters* **17**, 2138-2145 (2017).
8. Gilleron, J., *et al.* Image-based analysis of lipid nanoparticle-mediated siRNA delivery, intracellular trafficking and endosomal escape. *Nat Biotech* **31**, 638-646 (2013).
9. Lechardeur, D., Verkman, A. & Lukacs, G.L. Intracellular routing of plasmid DNA during non-viral gene transfer. *Advanced drug delivery reviews* **57**, 755-767 (2005).
10. Martens, T.F., Remaut, K., Demeester, J., De Smedt, S.C. & Braeckmans, K. Intracellular delivery of nanomaterials: how to catch endosomal escape in the act. *Nano Today* **9**, 344-364 (2014).
11. Akinc, A., Thomas, M., Klibanov, A.M. & Langer, R. Exploring polyethylenimine-mediated DNA transfection and the proton sponge hypothesis. *The journal of gene medicine* **7**, 657-663 (2005).
12. Behr, J.-P. The proton sponge: a trick to enter cells the viruses did not exploit. *CHIMIA International Journal for Chemistry* **51**, 34-36 (1997).
13. Uchida, H., *et al.* Odd–even effect of repeating aminoethylene units in the side chain of N-substituted polyaspartamides on gene transfection profiles. *Journal of the American Chemical Society* **133**, 15524-15532 (2011).
14. Xu, Y. & Szoka, F.C. Mechanism of DNA release from cationic liposome/DNA

complexes used in cell transfection. *Biochemistry* **35**, 5616-5623 (1996).

15. Mindell, J.A. Lysosomal acidification mechanisms. *Annual review of physiology* **74**, 69-86 (2012).
16. Selby, L.I., Cortez-Jugo, C.M., Such, G.K. & Johnston, A.P. Nanoescapology: Progress toward understanding the endosomal escape of polymeric nanoparticles. *Wiley Interdisciplinary Reviews: Nanomedicine and Nanobiotechnology* (2017).
17. Leroueil, P.R., *et al.* Wide varieties of cationic nanoparticles induce defects in supported lipid bilayers. *Nano Letters* **8**, 420-424 (2008).
18. Yuba, E., *et al.* pH-Sensitive fusogenic polymer-modified liposomes as a carrier of antigenic proteins for activation of cellular immunity. *Biomaterials* **31**, 943-951 (2010).
19. McCarthy, H.O., *et al.* Development and characterization of self-assembling nanoparticles using a bio-inspired amphipathic peptide for gene delivery. *Journal of Controlled Release* **189**, 141-149 (2014).
20. Benns, J.M., Choi, J.-S., Mahato, R.I., Park, J.-S. & Kim, S.W. pH-sensitive cationic polymer gene delivery vehicle: N-Ac-poly (L-histidine)-graft-poly (L-lysine) comb shaped polymer. *Bioconjugate chemistry* **11**, 637-645 (2000).
21. Cho, Y.W., Kim, J.D. & Park, K. Polycation gene delivery systems: escape from endosomes to cytosol. *Journal of pharmacy and pharmacology* **55**, 721-734 (2003).
22. Moore, N.M., Sheppard, C.L., Barbour, T.R. & Sakiyama-Elbert, S.E. The effect of endosomal escape peptides on in vitro gene delivery of polyethylene glycol-based vehicles. *The journal of gene medicine* **10**, 1134-1149 (2008).
23. Zelphati, O. & Szoka, F.C. Mechanism of oligonucleotide release from cationic liposomes. *Proceedings of the National Academy of Sciences* **93**, 11493-11498 (1996).
24. Uchida, H., *et al.* Modulated protonation of side chain aminoethylene repeats in N-substituted polyaspartamides promotes mRNA transfection. *Journal of the American Chemical Society* **136**, 12396-12405 (2014).
25. Qiu, L., Zheng, C. & Zhao, Q. Mechanisms of drug resistance reversal in Dox-resistant MCF-7 cells by pH-responsive amphiphilic polyphosphazene containing diisopropylamino side groups. *Molecular pharmaceutics* **9**, 1109-1117 (2012).
26. Reguera-Nuñez, E., *et al.* Implantable controlled release devices for BMP-7 delivery and suppression of glioblastoma initiating cells. *Biomaterials* **35**, 2859-2867 (2014).

27. Smith, T.T., *et al.* In situ programming of leukaemia-specific T cells using synthetic DNA nanocarriers. *Nature Nanotechnology* (2017).
28. Zhou, Z., *et al.* Charge-reversal drug conjugate for targeted cancer cell nuclear drug delivery. *Advanced Functional Materials* **19**, 3580-3589 (2009).
29. Yuan, Y.Y., *et al.* Surface charge switchable nanoparticles based on zwitterionic polymer for enhanced drug delivery to tumor. *Advanced materials* **24**, 5476-5480 (2012).
30. Wang, Z., *et al.* Surface protonation/deprotonation controlled instant affinity switch of nano drug vehicle (NDV) for pH triggered tumor cell targeting. *Biomaterials* **62**, 116-127 (2015).
31. Zhang, Y., *et al.* Synthesis and biological properties of water-soluble polyphenylthiophene brushes with poly (ethylene glycol)/polyzwitterion side chains. *Polymer Chemistry* **8**, 1672-1679 (2017).
32. Murthy, N., Robichaud, J.R., Tirrell, D.A., Stayton, P.S. & Hoffman, A.S. The design and synthesis of polymers for eukaryotic membrane disruption. *Journal of Controlled Release* **61**, 137-143 (1999).
33. Kyriakides, T.R., *et al.* pH-sensitive polymers that enhance intracellular drug delivery in vivo. *Journal of Controlled Release* **78**, 295-303 (2002).
34. Convertine, A.J., Benoit, D.S., Duvall, C.L., Hoffman, A.S. & Stayton, P.S. Development of a novel endosomolytic diblock copolymer for siRNA delivery. *Journal of Controlled Release* **133**, 221-229 (2009).
35. Convertine, A., *et al.* pH-responsive polymeric micelle carriers for siRNA drugs. *Biomacromolecules* **11**, 2904-2911 (2010).
36. Ding, H., *et al.* The optimization of polymalic acid peptide copolymers for endosomolytic drug delivery. *Biomaterials* **32**, 5269-5278 (2011).
37. Ding, H., *et al.* Inhibition of brain tumor growth by intravenous poly (β-L-malic acid) nanobioconjugate with pH-dependent drug release. *Proceedings of the National Academy of Sciences* **107**, 18143-18148 (2010).
38. Xu, P., *et al.* Targeted Charge-Reversal Nanoparticles for Nuclear Drug Delivery. *Angewandte Chemie International Edition* **46**, 4999-5002 (2007).
39. Murthy, N., Chang, I., Stayton, P. & Hoffman, A. pH-sensitive hemolysis by random copolymers of alkyl acrylates and acrylic acid. in *Macromolecular Symposia*, Vol. 172 49-56 (Wiley Online Library, 2001).
40. Fujita, M., *et al.* Brain tumor tandem targeting using a combination of monoclonal antibodies attached to biopoly (β-L-malic acid). *Journal of Controlled Release* **122**, 356-363 (2007).
41. Patil, R., *et al.* Temozolomide delivery to tumor cells by a multifunctional nano

vehicle based on poly (β-L-malic acid). *Pharmaceutical Research* **27**, 2317-2329 (2010).

42. Krivitsky, A., *et al.* Structure–Function Correlation of Aminated Poly(α)glutamate as siRNA Nanocarriers. *Biomacromolecules* **17**, 2787-2800 (2016).
43. Varkouhi, A.K., Scholte, M., Storm, G. & Haisma, H.J. Endosomal escape pathways for delivery of biologicals. *Journal of Controlled Release* **151**, 220-228 (2011).
44. Endoh, T. & Ohtsuki, T. Cellular siRNA delivery using cell-penetrating peptides modified for endosomal escape. *Advanced drug delivery reviews* **61**, 704-709 (2009).
45. Kang, H.C. & Bae, Y.H. pH-tunable endosomolytic oligomers for enhanced nucleic acid delivery. *Advanced Functional Materials* **17**, 1263-1272 (2007).
46. Cox, M.C., Reese, L.M., Bickford, L.R. & Verbridge, S.S. Toward the broad adoption of 3D tumor models in the cancer drug pipeline. *ACS Biomaterials Science & Engineering* **1**, 877-894 (2015).
47. Stock, K., *et al.* Capturing tumor complexity in vitro: Comparative analysis of 2D and 3D tumor models for drug discovery. *Scientific Reports* **6**, 28951 (2016).
48. Enam, S.A. & Klaus, E. Role of extracellular matrix in tumor invasion: migration of glioma cells along fibronectin-positive mesenchymal cell processes. *Neurosurgery* **42**, 599-608 (1998).
49. Sutherland, R.M., *et al.* Oxygenation and Differentiation in Multicellular Spheroids of Human Colon Carcinoma. *Cancer Research* **46**, 5320-5329 (1986).
50. Hamer, P.D.W., *et al.* The genomic profile of human malignant glioma is altered early in primary cell culture and preserved in spheroids. *Oncogene* **27**, 2091 (2008).
51. Mehta, G., Hsiao, A.Y., Ingram, M., Luker, G.D. & Takayama, S. Opportunities and challenges for use of tumor spheroids as models to test drug delivery and efficacy. *Journal of Controlled Release* **164**, 192-204 (2012).
52. Griffith, L.G. & Swartz, M.A. Capturing complex 3D tissue physiology in vitro. *Nature reviews Molecular cell biology* **7**, 211-224 (2006).
53. Tung, Y.-C., *et al.* High-throughput 3D spheroid culture and drug testing using a 384 hanging drop array. *Analyst* **136**, 473-478 (2011).
54. Miller, J.S., *et al.* Rapid casting of patterned vascular networks for perfusable engineered three-dimensional tissues. *Nature materials* **11**, 768-774 (2012).

55. Ehsan, S.M., Welch-Reardon, K.M., Waterman, M.L., Hughes, C.C. & George, S.C. A three-dimensional in vitro model of tumor cell intravasation. *Integrative Biology* **6**, 603-610 (2014).
56. Vinci, M., *et al.* Advances in establishment and analysis of three-dimensional tumor spheroid-based functional assays for target validation and drug evaluation. *BMC biology* **10**, 29 (2012).
57. Ivanov, D.P. & Grabowska, A.M. Spheroid arrays for high-throughput single-cell analysis of spatial patterns and biomarker expression in 3D. *Scientific Reports* **7**, 41160 (2017).
58. Fischer, R.S., Wu, Y., Kanchanawong, P., Shroff, H. & Waterman, C.M. Microscopy in 3D: a biologist's toolbox. *Trends in cell biology* **21**, 682-691 (2011).
59. Drobizhev, M., Makarov, N.S., Tillo, S.E., Hughes, T.E. & Rebane, A. Two-photon absorption properties of fluorescent proteins. *Nature methods* **8**, 393 (2011).
60. Huisken, J. Slicing embryos gently with laser light sheets. *BioEssays* **34**, 406-411 (2012).
61. Ivanov, D.P., *et al.* Multiplexing spheroid volume, resazurin and acid phosphatase viability assays for high-throughput screening of tumour spheroids and stem cell neurospheres. *PLoS One* **9**, e103817 (2014).
62. Zahonero, C., *et al.* Preclinical test of dacomitinib, an irreversible EGFR inhibitor, confirms its effectiveness for glioblastoma. *Molecular cancer therapeutics* **14**, 1548-1558 (2015).
63. Richardson, S.W., Kolbe, H.J. & Duncan, R. Potential of low molecular mass chitosan as a DNA delivery system: biocompatibility, body distribution and ability to complex and protect DNA. *International Journal of Pharmaceutics* **178**, 231-243 (1999).
64. Fischer, D., Li, Y., Ahlemeyer, B., Krieglstein, J. & Kissel, T. In vitro cytotoxicity testing of polycations: influence of polymer structure on cell viability and hemolysis. *Biomaterials* **24**, 1121-1131 (2003).
65. McGarry, M., Protheroe, C. & Lee, J. Cell differential assessments of peripheral blood films. *Mouse Hematology: A Laboratory Manual, Cold Spring Harbor Laboratory Press, New York*, 39-42 (2010).
66. Cohen, R.N., van der Aa, M.A., Macaraeg, N., Lee, A.P. & Szoka, F.C. Quantification of plasmid DNA copies in the nucleus after lipoplex and polyplex transfection. *Journal of Controlled Release* **135**, 166-174 (2009).
67. Han, L., Tang, C. & Yin, C. Effect of binding affinity for siRNA on the in vivo

antitumor efficacy of polyplexes. *Biomaterials* **34**, 5317-5327 (2013).

68. Kelly, P.J. Gliomas: survival, origin and early detection. *Surgical neurology international* **1**(2010).
69. Mahmood, U. & Weissleder, R. Near-infrared optical imaging of proteases in cancer. *Molecular cancer therapeutics* **2**, 489-496 (2003).
70. Day, R.N. & Davidson, M.W. The fluorescent protein palette: tools for cellular imaging. *Chemical Society Reviews* **38**, 2887-2921 (2009).
71. Ong, S.-M., *et al.* Engineering a scaffold-free 3D tumor model for in vitro drug penetration studies. *Biomaterials* **31**, 1180-1190 (2010).
72. Loessner, D., *et al.* Bioengineered 3D platform to explore cell–ECM interactions and drug resistance of epithelial ovarian cancer cells. *Biomaterials* **31**, 8494-8506 (2010).
73. Hirschhaeuser, F., *et al.* Multicellular tumor spheroids: an underestimated tool is catching up again. *Journal of biotechnology* **148**, 3-15 (2010).
74. Lv, D., *et al.* A three-dimensional collagen scaffold cell culture system for screening anti-glioma therapeutics. *Oncotarget* **7**, 56904 (2016).
75. Lv, D., Hu, Z., Lu, L., Lu, H. & Xu, X. Three-dimensional cell culture: A powerful tool in tumor research and drug discovery. *Oncology letters* **14**, 6999-7010 (2017).

Chapter IV / Capítulo IV

Mixed cationic and anionic polyphosphazene carrying therapeutic siRNA against DYRK1A: in vitro and in vivo evaluation in glioblastoma cancer

This work has been done in collaboration with Instituto de Salud Carlos III (UFIEC), Madrid, Spain

Chapter IV / Capítulo IV

Abstract

RNAi therapy has gained increasing attention in several genetic disorder diseases. In terms of glioblastoma cancers, glioblastoma initial cells (GICs) can be induced from originally normal brain cells (neural stem cells or astrocytes) via genetic alterations. Abundant genetic amplifications and mutations have been linked to GBM recurrence after the standard treatment comprising surgery and chemo-/radiotherapies. Highly-resistant GICs survive chemo-/radiotherapy and reproduce themselves to form relapsed tumours, causing the poor prognosis of this disease, a 5-year survival rate in clinical treatments. DYRK1A is dual-specificity tyrosine phosphorylation–regulated kinase, contributing to EGFR stability in GIC, imparting them with renewal capability. Albeit of their promising cellular activity, EGFR and DYRK1A inhibitors presented small benefits in clinical trials. siRNA therapy could achieve a more potent and selective down-regulation of this pathway, increasing the therapeutic potential of this approach. Herein, we adapted our high-effective polymeric gene nanocarriers, previously used with pDNA, for the delivery siRNA against DYRK1A. A first evaluation was performed in U87MG neurospheres and consisted on testing the capacity of siRNA-loaded nanocarriers to down-regulate DYRK1A and tumour self-renewal capacity. Then, the siRNA-complexes were injected intratumorally to xenograft mice bearing U87MG cells and co-administration with a low dose of temozolomide (5 mg/kg). The mice group treated with an active siRNA and temozolomide reduced the tumour size 50% as compared to the group treated with temozolomide and scrambled siRNA nanocomplexes. This effect was observed for most of the duration and it was significant against the control between the day 7 to the day 17 after treatment. Herein we conclude that siRNA delivered by optimized

polymeric complexes successfully knocked down endogenous DYRK1A expression and delayed xenograft tumour growth rates, indicating an efficient delivery of siRNA in glioblastoma and potential new therapeutic option for treating this disease.

4.1 Introduction

4.1.1 Glioblastoma and clinical treatments

The therapeutic goal for the study was to deliver nucleic acids as potential means to treat Glioblastoma Multiforme (GBM), a highly aggressive and malignant cancer classified as grade IV by the World Health Organization (WHO) in view of its short median survival time (14 months) after diagnosis[1]. Fortunately, some therapies have improved overall survival time for GBM patients, specifically radiotherapy. Integrated multiple techniques are able to focus precisely the radiation beams on the irregular contours of brain tumours, minimizing the side effects on normal brain tissues[2]. For resection of intracranial tumours, the upgraded image-guide and microsurgery techniques facilitate neurosurgeons precisely judging tumour boundaries, being fluorescence-guided surgery (FGS) with 5-aminolevulinic acid as an example[3]. However, many GBMs are widely infiltrative through neighbour tissues and sometimes to distant locations, making impossible to completely remove surgically all GBM cells[4]. As a result, combination therapies are typically applied after surgery for extending median survival time. The current first line treatment will typically comprise temozolomide (TMZ), an anti-tumour drug that crosses the blood brain barrier and presents therapeutic benefits, especially combination treatment with radiotherapy.[5,6] Previously, other chemotherapeutical options have been tested; for instance, carmustine-loaded wafers for controlled release of this compound after implantation at the resection site was a promising strategy. Although this implantation did not fulfil the expected clinical outcomes in terms of median survival time improvements, this practical example proposed a sustained release platform for local administration in the

future medicine[5].

Despite the therapeutic options and new technologies in clinical trials, GBM is still characterized by a high recurrence rate that reflects the resistance of leftover tumour clumps containing subpopulations of glioblastoma initiating cells (GICs)[7]. Literatures reported those subpopulations of GICs are more capable to recover and proliferate after treatment of chemotherapeutic drugs, as compared with another type of lung cancer stem cells[8]. According to The Cancer Genome Atlas (TCGA), EGFR genetic amplification/overexpression and TP53 mutation are the most common genetic alterations in GBM[1]. These genetic mutations enable GICs for resisting chemotherapy and endow them with amplified growth rates and modified signalling pathways, ultimately leading to tumour survival and relapse. Accordingly, there is dire demand for new treatment strategies for GBM, and the delivery of suicide genes or gene knockdown by siRNA are two very promising therapeutic options.

4.1.2 Suppression of EGFR in GBM therapy via inhibition of DYRK1A

As mentioned previously, TCGA initiated a project for large-scale analysis of human cancers in different dimensions, including the grade-IV glioblastoma. The key genetic alterations identified for GBM have been: (1) amplification of receptor tyrosine kinase genes, for an well-known example overexpression of epidermal growth factor receptor (EGFR); (2) activation of pathway of phosphatidylinositol-3-OH kinase; (3) dysfunction of tumour suppressor pathway, such as p53 mutation.[9] In the aberrations of amplified expression in GBM, EGFR families accounted for the most highest frequency in the surveyed samples of GBM patients (91/206 cases)[9], indicating EGFR signalling

pathways play a pivotal role in GBM pathogenesis, relating to wide ranges from the early development of tumour and proliferation, to aggressive infiltration, to therapeutic resistance[10]. However, EGFR kinase inhibitors (e.g. bevacizumab, gefitinib and erlotinib) did not fulfil the clinical expectations[11-14].

Previous studies have shown that inhibition of dual-specificity tyrosine phosphorylation–regulated kinase (DYRK1A), which can prevent endocytosis-mediated degradation of EGFR by the phosphorylation-required modulator Sprouty-2[15], causing a loss of self-renewal capacity in several primary GBM tumour initial cells (**Figure 4-1**).[16] One of main functions of DYRK1A is to catalyse autophosphorylation on serine/ threonine residues of substrates via formation of a transitory intermediate product in an activation loop of the catalytic domains that containing tyrosine residue (Tyr321)[17,18]. Not only phosphorylating Sprouty-2, but also DYRK1A mediated stabilization of platelet-derived growth factor receptor (PDGFR), which is another common overexpression receptor and associating with tumour cell proliferation. In this chapter, we used the commercial available siRNA against DYRK1A to down-regulate GBM cells and further suspend renewal capability.

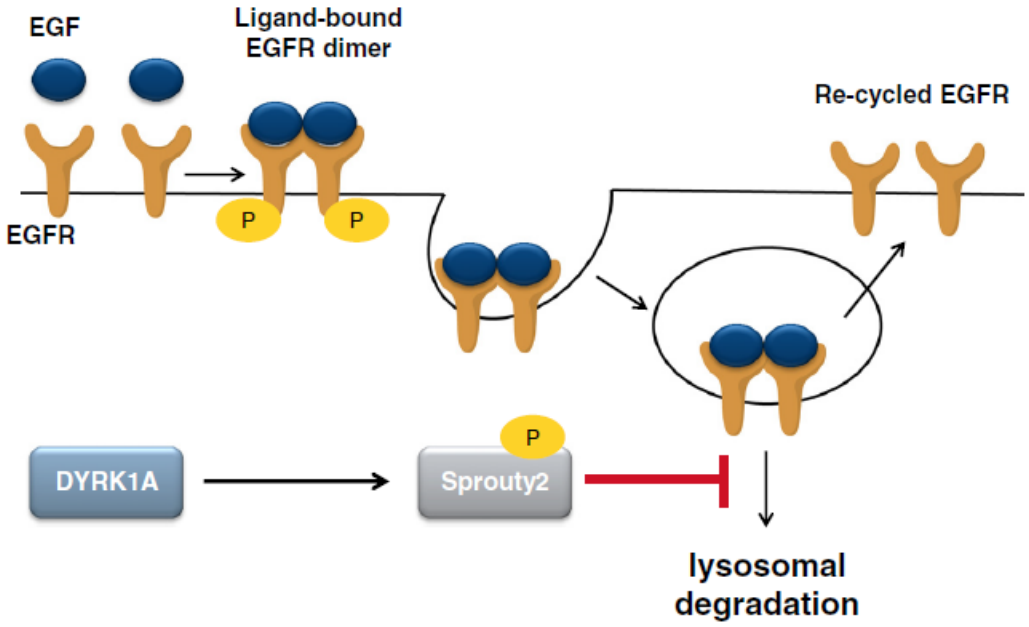

Figure 4-1. The relation pathways between DYRK1A and EGFR stabilisation. [Reproduced from Abbassi, R. et al, Pharmacology & therapeutics[19] with permission]

4.1.3. RNA interference therapy

RNA interference (RNAi) therapies are based on the introduction of foreign short RNA sequences to the cytosols where inhibit mRNA translation, down-regulating targeting gene expression. RNAi was identified by Andrew Fire and Craig C. Mello in 1998.[20] Physiologically, endogenously short double-stranded RNA molecules are cleaved and adapted by the enzyme Dicer, forming two single-stranded RNAs: the passenger and the guide-strand RNA. The guide-strand RNA will be incorporated into RNA-induced silencing complex (RISC), which is a catalytic enzyme that binds to mRNA sequences complementary to this guide stand, degrading them, and thus repressing translation [20,21]. There are several RNA molecules used in RNAi applications, including microRNA (miRNA), short interfering RNA (siRNA), short hairpin RNA

(shRNA), and Dicer substrate RNA (dsiRNA). The shRNA delivery is frequently used, delivered from shRNA-encoding plasmids, transcribed to shRNA in nucleus, and cleaved by Dicer where it incorporates in the described RNAi pathway[22]. dsiRNAs are small RNA duplexes with sequences optimized for Dicer incorporation that show increased potency. siRNA and miRNA are already processed and can integrate directly in RISC for gene silencing (**Figure 4-2**). In comparison to miRNA, siRNA is usually 100% complementary to the targeted sequence, inducing mRNA degradation. The RISC complex is then free to interact with new mRNA molecules. On the other hand, miRNA typically shows small loops and non-complementary regions and ultimately leads to inhibition of mRNA. The inhibitory effect of miRNA, therefore, is less potent, but the possibility of acting with non-perfect complementarity means that each sequence can act on gene clusters[23].

From pharmaceutical perspectives, the key task of RNAi to deliver safely siRNA to the cytosol of the targeted cells. Although some nanocarrier-siRNA formulations showed promise in clinical trials, such as ALN-TTR02 (Alnylam company), many studies still showed a clear demand for efficient delivery systems for siRNA, especially for non-targeting organs different from the liver. The critical challenges to address for improved RNA delivery are: (i) their very low bioavailability non-parenteral administration, (ii) their poor stability in physiological media, (iii) their difficulty to arrive at the targeted cells and (iv) their inefficient intracellular delivery[24]. Herein, we designed the mixed polyphosphazene derivative polymeric complexes to deliver siRNA against DYRK1A to GBM cells and reported here their therapeutic efficacy both in vitro and in vivo.

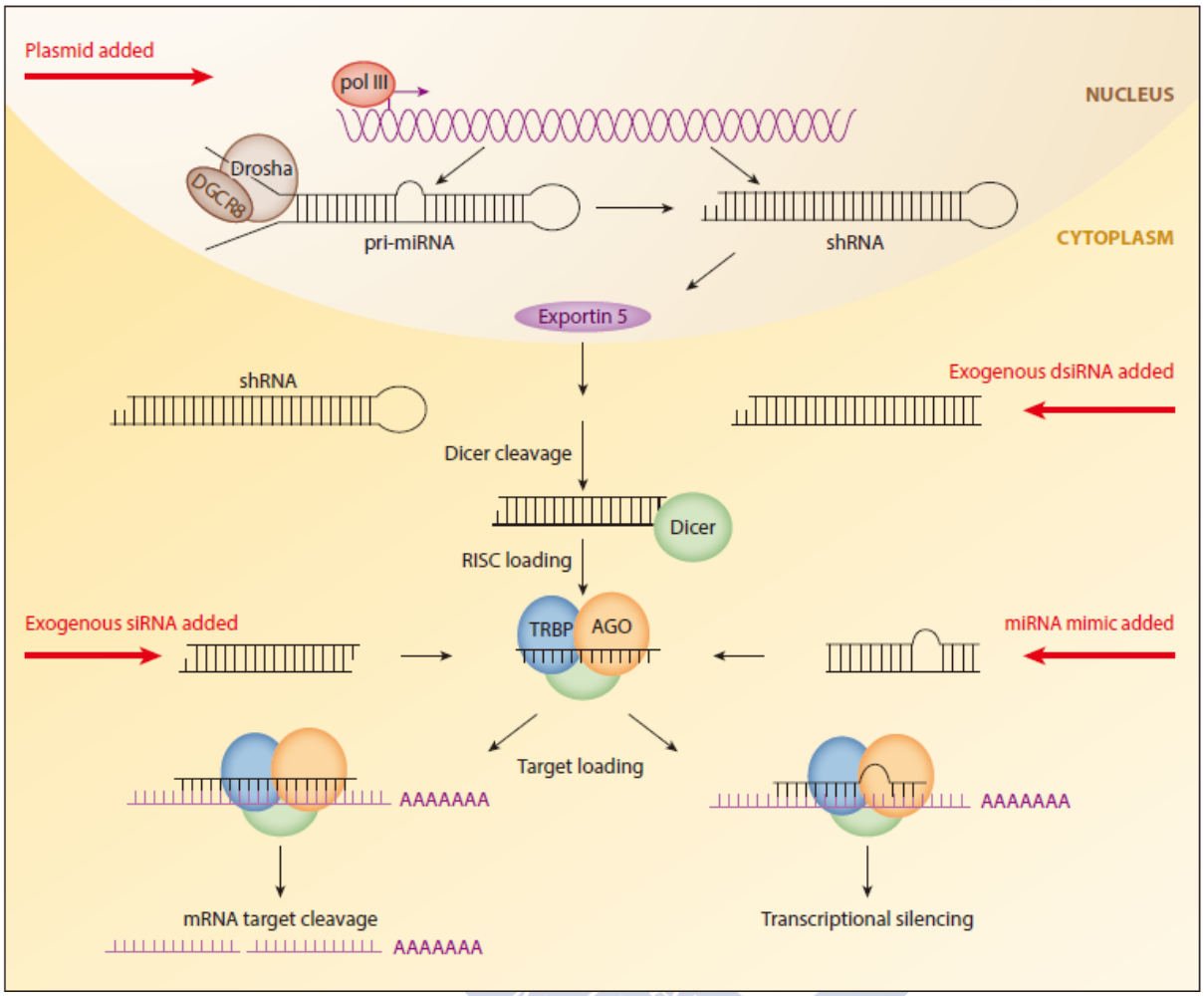

Figure 4-2. RNAi pathways. The red arrows indicated import of RNA molecules.

[Reproduced from Bobbin, M. L. et al. Annual review of pharmacology and toxicology [21] with permission]

4.2 Methods

4.2.1 Down-regulation efficiency and clonogenic assays

Complexes of polymers with siRNA for DYRK1A (ON-TARGETplus Human DYRK1A, Dharmacon) were prepared using the same ratios previously studied for polymeric complexes loaded with pDNA and added to U87MG (75K cells per well) in 12-well plates. The polymeric complex suspension was incubated with the cells for 4 hours, and then replaced by standard cell medium and maintained in culture for 24 hours. The DYRK1A silencing efficiency following siRNA delivery was then measured by qRT-PCR. Cells treated with siRNA against DYRK1A (siDYR) or a scramble sequence (siCtrl) were collected for mRNA extraction by a High-pure RNA isolation kit (from Roche) and mRNAs were trapped by on a glass fibre fleece in filter tubes. After elution of mRNA, the reverse transcription of 200 ng mRNA was performed by PrimeScript™ RT kit (from TaKaRa). The transcribed cDNA was mixed with Sybr-green and either primers of DYRK1A (Forward 5'-3': GCAATTTCCTGCTCCTCTTG; Reverse 5'-3': TTACCCAAGGCTTGTTGTCC) or primers of HPRT (Forward 5'-3': TGACACTGGCAAAACAATGCA; Reverse 5'-3': GGTCCTTTTCACCAGCAAGCT), used as a reference (housekeeping gene). Gene expression was quantified by RT-PCR (Lightcycler-480 II, Roche).

For self-renewal assays, the silenced cells were de-attached and left in a serum-free media, Neurobasal (Fisher-Scientific) supplemented with B27 (1:50), EGF (40 ng/ml) and FGF (20 ng/ml) (Peprotech) for three days to form spheroids. Then, the spheroids were dissociated by Accumax (Millipore) and the serum-starved cells were seeded on 96-well plates (250 cells/ well) for 7-10 days in the same serum-free media.

The numbers of secondary spheroids formed were counted, considering a spheroid any group with more than 4 cells clumped together.

4.2.2 Intracranial-implanted model of siDYRK1A-treated GBM cells

All in vivo therapeutic studies had been approved by the Research Ethics and Animal Welfare Committee at the Instituto de Salud Carlos III, Madrid, (PROEX 224/14) in agreement with the European Union and national directives. An intracranial-implanted model of GBM was established as previously described.[16] To investigate in vivo renewal ability of glioblastoma cells in orthotopic xenograft models, we implanted intracranially the silenced U87MG cells in cerebrum of athymic Foxn1 nude mice (Harlan Iberica)[16]. Firstly, U87MG cells were treated with the nanocomplexes at a dose of 1 µg siRNA per 100K cells for 4 h. The cells were then left in growth media for 24 hours. The treated cells in 2 µL cultured media (75K cells/mouse) were collected and injected intracranially in the nude mice using Hamilton syringe via a stereotactically guided injection system. The location of the implantation was coordinated at A-P, –0.5 mm; M-L, +2 mm; D-V, –3 mm; related to Bregma), and the animals were sacrificed at the onset of symptoms.

4.2.3 Combination of siDYR and TMZ in xenograft model in vivo

To investigate the therapeutic effectiveness of DYRK1A-silenced gene delivery in vivo, a subcutaneous xenograft model was established as the method in **chapter 3.2.4**. When tumour sizes reached around 100-150 mm^3, the polymeric complexes were injected intratumorally with 4 µg siDYR or the same amount of the scrambled

sequence (siCtrl) for each tumour/day and treated over four consecutive days (total 16 µg siRNA for each tumour). On those same days, the mice were also administered 5 mg/kg temozolomide (TMZ) by intraperitoneal injection (total dose 20 mg/kg each mice). The tumour sizes were measured by a calliper and calculated by Volume= W×W×L/2, in which W represents width and L is length (here, W < L).

4.3 Results and discussion

4.3.1 Characterisation of polymer siRNA complexes

As a therapeutic transgene, we chose a small-interfering RNA to silence DYRK1A (siDYR), a gene implicated in the stability of EGFR presentation and in tumour renewal[16,19]. The polymers/siRNA complex formulations were made using the same composition ratio (N/C/P 8:4:1) used for the polymer/pDNA complexes in previous two chapters. Particle characterization showed that substitution of pDNA by siRNA did not induce a large modification in nanocarrier size and surface charges (**Figure 4-3a**). However, there are still some slight differences between siRNA-complexes and pDNA-complexes in polydispersity index (PDI) and total derived counts (KCPs) from DLS measurement. CA-PPZ is capable to condense siRNA to form nanocomplexes yet they had lower KCPs than CA-PPZ:pDNA analogue. The KCPs value is related to the intensity of light scattered, which is related to several conditions, including particle concentration, particle density, etc. From nanoparticle tracking analysis (NTA) measurement, we observed that the concentration of CA-PPZ:siRNA ($7.17\times10^{10} \pm 6.66\times10^{9}$ /mL) is one order of magnitude lower than CA-PPZ:pDNA ($6.99\times10^{11} \pm 6.66\times10^{10}$ /mL). The tendency was reproduced in other formulation where particle concentration for CA-/6MHA-PPZ:siRNA and CA-/6MHA-PPZ:pDNA were $9.78\times10^{10} \pm 6.62\times10^{9}$ /mL and $4.81\times10^{11} \pm 5.24\times10^{9}$ /mL, respectively. The reason is likely that the short and low molecular weight of siRNA makes this molecule less efficient for condensation than pDNA[25,26]. This difficulty also caused a slightly higher polydispersity index in the particular distribution in CA-PPZ complex groups, but not found in CA-/6MHA-PPZ complexes

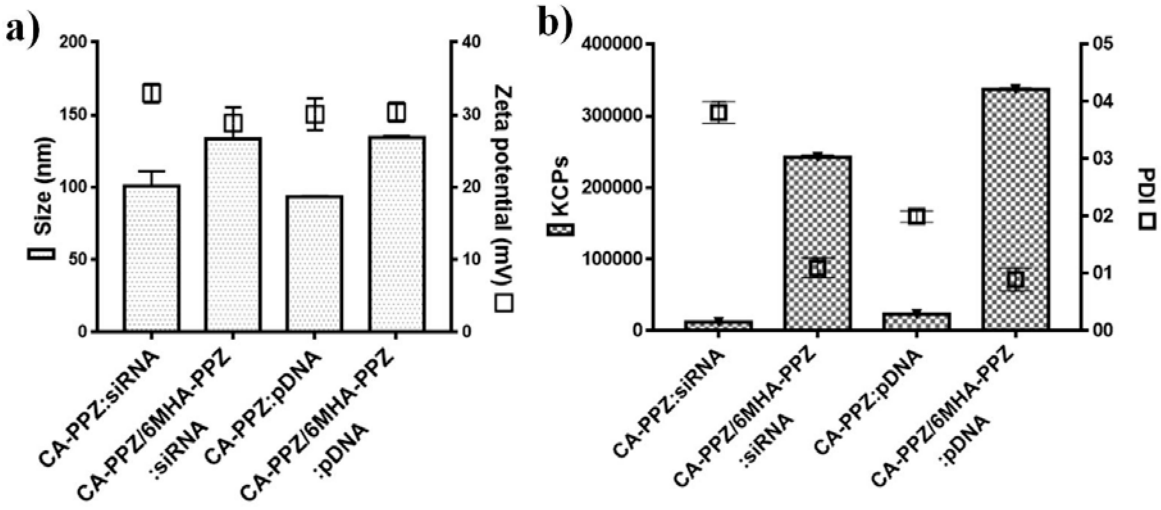

Figure 4-3. Comparisons of particle characterization data for CA-PPZ complexes and CA-/6MHA-PPZ complexes carrying either pDNA or siRNA. Particle size and surface charges are shown in **a**); total derived counts (KCPs) and polydispersity index (PDI) in **b**).

4.3.2 Down-regulation efficiency and clonogenic assays

The DYRK1A silencing efficiency was measured by qRT-PCR of DYRK1A mRNA in U87MG cells in 2D cultures (**Figure 4-4a**). CA-/6MHA-PPZ:siDYR complexes were able to silence DYRK1A expression by 70%, while the same prototype carrying a scrambled siRNA sequence (siCtrl) did not change DYRK1A expression compared to non-treated cells. In addition, CA-/6MHA-PPZ:siDYR efficacy was higher than the positive control PEI:siDYR complexes. On the other hand, CA-PPZ:siDYR complexes did not show a therapeutic effect. As a therapeutic effect of this DYRK1A reduction, tumorigenic capability was examined by a self-renewal test, which was calculated by formation of secondary neurospheres of the treated tumour

cells (clonogenic assays). The renewal capabilities of U87MG were diminished by the treatment with CA-/6MHA-PPZ:siDYR complexes, as evaluating the formation of secondary spheroids in **Figure 4-4b**. This effect on the ability to form secondary spheroids was also clear in microscopy images (**Figure 4-4 c, d, e**). Logically, none of the control groups showed any biological effect, not did the other formulation, CA-PPZ:siDYR complexes.

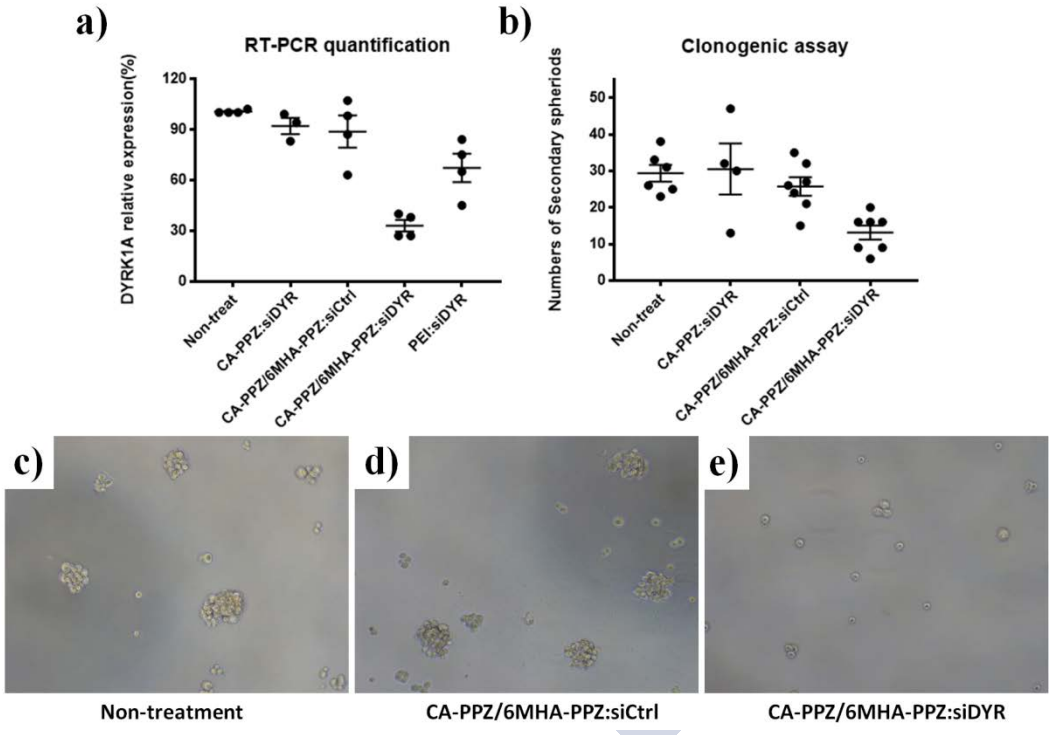

Figure 4-4. *In vitro* silencing efficacy of polymer:siDYR complexes. **a)** DYRK1A silencing effect of different polymer:siRNA complexes in 2D monolayer of U87MG cells measured by qRT-PCR. **b)** Clonogenic ability (formation of secondary spheroids) of U87MG cells after treatment with different polymer:siRNA complexes. Micrographs in (**c, d, e**) show images of secondary spheroids after treatment with CA-PPZ/6MHA-PPZ complexing either a therapeutic (siDYR) or a scrambled siRNA (siCtrl) or media only group (non-treatment).

4.3.3 Intracranial-implanted model of siDYRK1A-treated GBM cells

After the evaluation of the self-renewal capacities, we further implanted those siRNA-treated cells into the striatum of nude mice for the evaluation of silencing-efficiency in an orthotopically xenograft model. However, the data showed there is no statistical difference in the Kaplan-Meier curves between survival ratios of mice explanted CA-/6MHA-PPZ:siDYR-treated and CA-/6MHA-PPZ:siCtrl-treated cells in cerebrum (**Figure 4-5**). As shown in the figure, siDYR-treatment did not delay tumour formation and growth in this aggressive U87MG orthotopic model. However, this result might attribute to an inadequate study design. Indeed, the orthotopically explanted mice in both treatments survived for longer than 20 days after explanation. In the literature, the maximum effective silencing periods for siRNA inside tumour cells is only approximately 72 hours [27,28]. In light of this, the silencing effects of the gene therapy might have been lost during initial lag phase of tumour growth, making unfeasible that the gene medicines can benefit survival rates in this therapeutic setting. In comparison, Pilar Sánchez group has shown that GBM cells with constitutive gene silencing of DYRK1A was significantly delayed in tumour growth in the same orthotopic xenotransplantation model[16], but this constitutive gene silencing was achieved by shRNA-loaded lentiviral vectors. The advantage of shRNA delivered via viral vectors over siRNA/polymer vehicles is the gene-silencing effective time, but the viral vectors may be not an appropriate feature for the clinical applications. Taken together, albeit we obtained negative results, this study provided two important suggestions for the following studies. Firstly, it illustrated that it is necessary to provide multiple siRNA treatments in cancer therapy. Another is that siRNA only can

down-regulate expression of tumour cells, causing them to be more sensitive to chemo-/radiotherapy.[29,30] This could be used to combine siRNA treatments with other anticancer agents (e.g. Temozolomide, TMZ) during gene silencing time window.

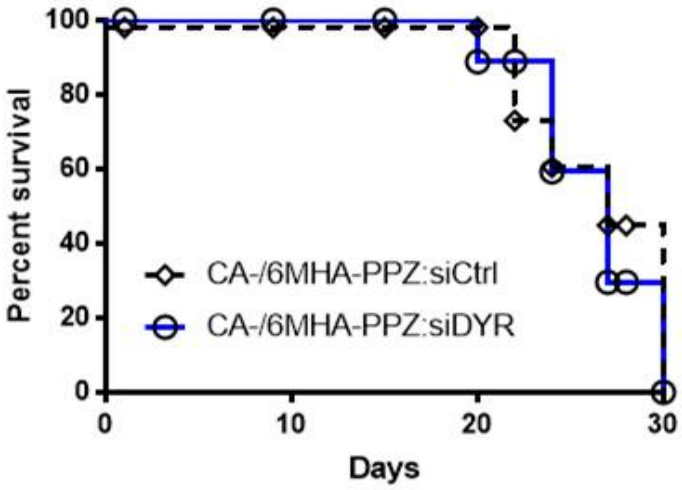

Figure 4-5. The Kaplan-Meier curve of orthotopic xenograft mice models. Polymeric siRNA complex-treated U87MG cells were intracranially injected into the cerebrum of nude mice with careful surgery and care. The survival rates presented as Kaplan-Meier curve.

4.3.4 Combination of siDYRK1A and TMZ in xenograft models

After the functional experiments *in vitro and in vivo*, a heterotopical xenograft model was prepared for multiple injections of siRNA formulation combined with the first-line chemotherapeutic agent for GBM (e.g. TMZ). The same U87MG-xenograft tumour model implanted on both flanks used in previous chapter (**Chapter 3.3.5**) was treated here with an intratumoral injection of CA-/6MHA-PPZ:siRNA (4µg) together

with an intraperitoneal injection of TMZ (5 mg/kg) once per day for 4 consecutive days (**Figure 4-6a**, red arrows). Two siRNA treatment groups were tested, including the therapeutic sequence (siDYR) and the scrambled sequence (siCtrl), both in combination with TMZ. Tumour growth started to be significantly delayed by CA-/6MHA-PPZ:siDYR complexes from day 10 to day 17 as compared to the CA-/6MHA-PPZ:siCtrl group (**Figure 4-6 a, b**). This reduction in tumour growth rate can be better appreciated by comparing the size of the treated tumours and those of the controls on the same day (**Figure 4-6 b**); tumours treated with CA-/6MHA-PPZ:siDYR were around 50% smaller than those of the control. This data underscores the therapeutic superiority when combining the first line treatment TMZ with CA-/6MHA-PPZ:siDYR complexes in relation to TMZ with the placebo (siCtrl).

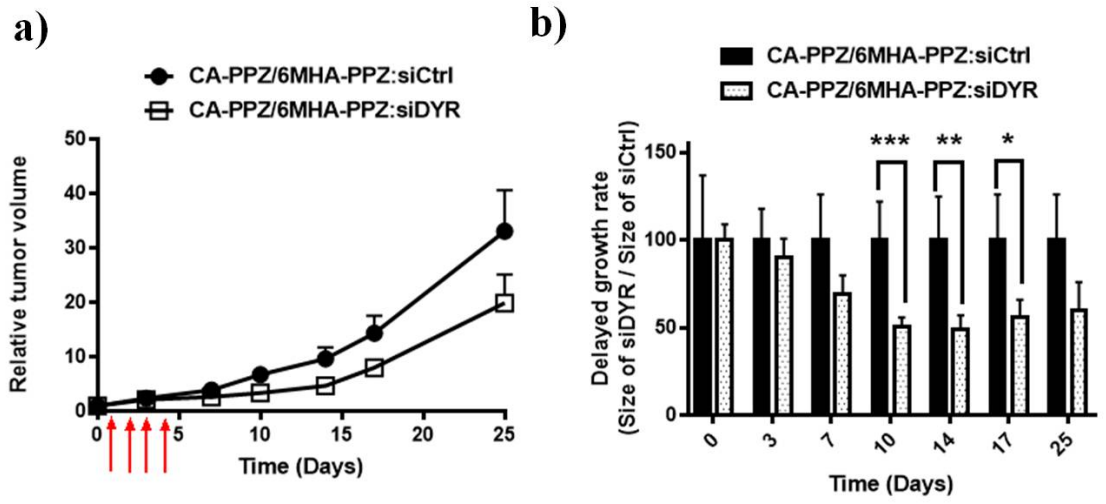

Figure 4-6 a) Relative tumour volume in a U87MG xenograft tumour model treated with CA-PPZ/6MHA-PPZ complexing either a therapeutic (siDYR) or a scrambled (siCtrl) siRNA (4 µg per tumour) and co-therapy with an intraperitoneal injection of TMZ 5 mg/kg. This treatment was repeated for 4 consecutive days (red arrows). **b)** Delayed tumour growth rate (size of siDYR treated tumours divided by the size of siCtrl

treated tumours) at different time points in the same *in vivo* experiment (n=4). *** represents $P < 0.05$, ** for $P < 0.1$ and * for $P < 0.5$, analysed by Student's t-test.

4.4 Conclusion

In this chapter, we introduced siRNA in the optimal binary polyionic (CA-PPZ/6MHA-PPZ) complex for silencing DYRK1A expression, which targets the EGF pathway and GBM reinitiation. We prepared complexes using the same composition ratios (N/C/P 8:4:1) used previously with pDNA and confirmed that this substitution causes only marginal differences in physicochemical properties. CA-/6MHA-PPZ:siDYR was able to efficiently silence the expression of DYRK1A in cell culture, and though this effect inhibit tumour reproducible capacity and formation, indicating a promising therapeutic effect. In a in vivo xenograft model, the administration of multiple injections of CA-/6MHA-PPZ:siRNA resulted in a 50% reduction in tumour growth rate for one week as compared to the same treatment loaded with a scrambled siRNA sequence. Overall, it has been shown that CA-/6MHA-PPZ can successfully deliver siDYR to U87MG cells in vitro and in vivo, as well as generating a therapeutic effect. However, the largest therapeutic benefits were only achieved with multiple injections of siRNA and in combined with a chemotherapeutic agent.

Chapter IV / Capítulo IV

4.5 References

1. Van Meir, E.G., *et al.* Exciting new advances in neuro-oncology: the avenue to a cure for malignant glioma. *CA Cancer J Clin* **60**, 166-193 (2010).
2. Pouratian, N., Crowley, R.W., Sherman, J.H., Jagannathan, J. & Sheehan, J.P. Gamma Knife radiosurgery after radiation therapy as an adjunctive treatment for glioblastoma. *Journal of Neuro-Oncology* **94**, 409 (2009).
3. Hadjipanayis, C.G., Widhalm, G. & Stummer, W. What is the Surgical Benefit of Utilizing 5-ALA for Fluorescence-Guided Surgery of Malignant Gliomas? *Neurosurgery* **77**, 663-673 (2015).
4. Ji, M., *et al.* Detection of human brain tumor infiltration with quantitative stimulated Raman scattering microscopy. *Science translational medicine* **7**, 309ra163-309ra163 (2015).
5. Westphal, M., *et al.* A phase 3 trial of local chemotherapy with biodegradable carmustine (BCNU) wafers (Gliadel wafers) in patients with primary malignant glioma. *Neuro-oncology* **5**, 79-88 (2003).
6. Stupp, R., *et al.* Radiotherapy plus concomitant and adjuvant temozolomide for glioblastoma. *New England Journal of Medicine* **352**, 987-996 (2005).
7. Singh, S.K., *et al.* Identification of human brain tumour initiating cells. *Nature* **432**, 396 (2004).
8. Eramo, A., *et al.* Chemotherapy resistance of glioblastoma stem cells. *Cell death and differentiation* **13**, 1238 (2006).
9. Network, C.G.A.R. Comprehensive genomic characterization defines human glioblastoma genes and core pathways. *Nature* **455**, 1061 (2008).
10. Zhu, H., *et al.* Oncogenic EGFR signaling cooperates with loss of tumor suppressor gene functions in gliomagenesis. *Proceedings of the National Academy of Sciences* **106**, 2712-2716 (2009).
11. Noda, S.-e., *et al.* Molecular advances of brain tumors in radiation oncology. in *Seminars in radiation oncology*, Vol. 19 171-178 (Elsevier, 2009).
12. Chamberlain, M.C. Emerging clinical principles on the use of bevacizumab for the treatment of malignant gliomas. *Cancer* **116**, 3988-3999 (2010).
13. Chakravarti, A., *et al.* An update of phase II results from RTOG 0211: A phase I/II study of gefitinib with radiotherapy in newly diagnosed glioblastoma. *Journal of clinical oncology* **24**, 1527-1527 (2006).
14. Prados, M.D., *et al.* Phase 1 study of erlotinib HCl alone and combined with

temozolomide in patients with stable or recurrent malignant glioma. *Neuro-oncology* **8**, 67-78 (2006).

15. Ferron, S.R., *et al.* Regulated segregation of kinase Dyrk1A during asymmetric neural stem cell division is critical for EGFR-mediated biased signaling. *Cell stem cell* **7**, 367-379 (2010).
16. Pozo, N., *et al.* Inhibition of DYRK1A destabilizes EGFR and reduces EGFR-dependent glioblastoma growth. *The Journal of clinical investigation* **123**, 2475-2487 (2013).
17. Lochhead, P.A., Sibbet, G., Morrice, N. & Cleghon, V. Activation-loop autophosphorylation is mediated by a novel transitional intermediate form of DYRKs. *Cell* **121**, 925-936 (2005).
18. Ionescu, A., *et al.* DYRK1A kinase inhibitors with emphasis on cancer. *Mini reviews in medicinal chemistry* **12**, 1315-1329 (2012).
19. Abbassi, R., Johns, T.G., Kassiou, M. & Munoz, L. DYRK1A in neurodegeneration and cancer: molecular basis and clinical implications. *Pharmacology & therapeutics* **151**, 87-98 (2015).
20. Fire, A., *et al.* Potent and specific genetic interference by double-stranded RNA in Caenorhabditis elegans. *Nature* **391**, 806 (1998).
21. Bobbin, M.L. & Rossi, J.J. RNA interference (RNAi)-based therapeutics: delivering on the promise? *Annual review of pharmacology and toxicology* **56**, 103-122 (2016).
22. Rao, D.D., Vorhies, J.S., Senzer, N. & Nemunaitis, J. siRNA vs. shRNA: Similarities and differences. *Advanced drug delivery reviews* **61**, 746-759 (2009).
23. Pratt, A.J. & MacRae, I.J. The RNA-induced silencing complex: a versatile gene-silencing machine. *Journal of Biological Chemistry* **284**, 17897-17901 (2009).
24. Gilleron, J., *et al.* Image-based analysis of lipid nanoparticle-mediated siRNA delivery, intracellular trafficking and endosomal escape. *Nat Biotech* **31**, 638-646 (2013).
25. Ziebarth, J.D., Kennetz, D.R., Walker, N.J. & Wang, Y. Structural comparisons of PEI/DNA and PEI/siRNA complexes revealed with molecular dynamics simulations. *The Journal of Physical Chemistry B* **121**, 1941-1952 (2017).
26. Jere, D., *et al.* Akt1 silencing efficiencies in lung cancer cells by sh/si/ssiRNA transfection using a reductable polyspermine carrier. *Biomaterials* **30**, 1635-1647 (2009).
27. Miller, J.B., *et al.* Non-Viral CRISPR/Cas Gene Editing In Vitro and In Vivo

Enabled by Synthetic Nanoparticle Co-Delivery of Cas9 mRNA and sgRNA. *Angewandte Chemie International Edition* **56**, 1059-1063 (2017).

28. Greco, C.T., Muir, V.G., Epps III, T.H. & Sullivan, M.O. Efficient tuning of siRNA dose response by combining mixed polymer nanocarriers with simple kinetic modeling. *Acta biomaterialia* **50**, 407-416 (2017).
29. Gandhi, N.S., Tekade, R.K. & Chougule, M.B. Nanocarrier mediated delivery of siRNA/miRNA in combination with chemotherapeutic agents for cancer therapy: Current progress and advances. *Journal of Controlled Release* **194**, 238-256 (2014).
30. Saraswathy, M. & Gong, S. Recent developments in the co-delivery of siRNA and small molecule anticancer drugs for cancer treatment. *Materials Today* **17**, 298-306 (2014).

Chapter IV / Capítulo IV

General Discussion

Polyphosphazenes have been considered promising materials for gene delivery since they combine biodegradability and great chemical flexibility. It was envisaged that such flexibility would be ideal for generating combinatorial chemistry screens to optimize polymer structure. Still, their application for gene delivery has remained relatively scarce because the main synthetic route for polymer modification, the nucleophilic substitution of the precursor poly(dichlorophosphazene), is problematic for most derivatives of interest. The reason is that functional groups with several nucleophilic centres (i.e. amines, hydroxides, carboxylic acids, etc.) used in gene therapy will crosslink the precursor polymer. Recently the side groups of allylamine and propargylamine have reported the introduction of click handles in PPZs for thiol-ene or thiol-yne addition[1,2], inspiring more possibilities for this polymer. In this thesis, we demonstrated that introduction of a vinyl group through the formation of a secondary polymer precursor, allylamino-poly(phosphazene) (AAPPZ), enables its simple modification with functional groups of interest for gene delivery using a thiol-ene addition reaction. By this method, PPZs with primary amines can be synthesized without any protection/deprotection reaction, and a small library of other derivatives with tertiary amines or carboxylic acid pendent groups. The streamlined synthetic process has drawn interesting structure/performance relationships. For example, PPZs substituted with tertiary amines were found to be less toxic yet more inefficient for cell transfection than those substituted with primary amines.

One of the most important findings derived from this screening has been the identification of 6MHA-PPZ, to be used as gene delivery enhancer. This polymer performs five different functions in the gene nanocarriers: (i) improving interpolymer complexation in the cationic PPZ/pDNA system, (ii) promoting the release of polynucleotides in the presence of a competitor, (iii) reducing polycation-caused toxicity, (iv) benefits in intracellular gene delivery, and (v) improving intratumoral penetration of nanocomplex in 3D tissue models. The capacity of anionic PPZs to enhance interpolymer complexation has been confirmed by comparing CA-PPZ:pDNA (8: 1 N/P ratio) and CA-/6MHA-PPZ:pDNA (8:4:1 N/C/P ratio) by dynamic light scattering and TEM imaging. Dynamic light scattering showed almost one order of magnitude increase in derived count rate in systems when 6MHA-PPZ is added (**Figure 2-13**). TEM images showed that CA-/6MHA-PPZ:pDNA had more compact morphology than CA-PPZ:pDNA complexes (**Figure 2-15**). The nanoparticle tracking assay further confirmed 6MHA-PPZ added to CA-PPZ:pDNA results in denser complexes rather than in a higher number of them (**Figure 2-14**).

Many standard polymers used for gene delivery are typically used in excess with the polynucleotide. For instance, only an N/P ratio of 3 is necessary to complex pDNA with PEI, but usually larger proportions are used for improving in vitro transfection efficiency, yet resulting in weakly bound or unbound PEI.[3,4] However, there are concerns on the fate and side effect of these unbound polymers when these systems are administered in vivo. The dense network of the CA-/6MHA-PPZ:pDNA complexes suggest that all critical elements of the preparation might be delivered together to the target cells. A most remarkable observation of the function of 6MHA-PPZ in the nanocomplexes has been its capacity to increase their efficacy/toxicity ratio over one

order of magnitude, reaching efficacies similar to the gold standard PEI:pDNA in 2D monolayer of U87MG cells (**Figure 2-19a**) and above them in a clinically relevant glioblastoma primary cell line (GBM1, **Figure 2-20**). Indeed, we observed that the introduction of any of the polyanionic-PPZs developed in the complex reduced the cellular toxicity of the prototype. Therefore, this is likely a toxicity reduction driven by charge neutralization. On the other hand, most polyanionic PPZ failed to enhance nanocomplex gene delivery efficacy with the exception of 6MHA-PPZ (**Figure 2-19a**). This is likely caused by the specific capacity of 6MHA-PPZ structure in proton buffering. When analysing the mechanism behind this improved delivery, our studies have shown that presence of 6MHA-PPZ in the nanocomplex results in lower co-localisation with the endosomal compartments (**Figure 3-7**). This efficient endosomal escape is most probably linked to the capacity of 6MHA-PPZ to rupture lipid membranes in the acid environment of the endosomes as we have confirmed by haemolysis tests (**Figure 3-6**). Herein, the complexes integrating 6MHA-PPZ were the only ones that presented negligible haemolytic effect at neutral pH, but a haemolytic effect comparable to poly-L-lysine (PLL) at the acidic pH. This membrane rupturing effect could be mediated by hydrophobization of 6MHA-PPZ as this polymer loses charges by protonation. Indeed, of all the polyanionic PPZs synthesized, 6MHA-PPZ is the only one that shifts most its charge ratio between physiological and endosomal pH (**Table 2-3, Figure 2-12**); this could be the reason why this was the only derivative to show pH-sensitive enhancing endosomal escape and high transfection efficiency. It is interesting to note that 6MHA-PPZ seems also capable of improving cell transfection in combination with standard polycations with low endosomal escape properties such as PLL, although the combination with CA-PPZ seems to be particularly efficient

(**Figure 2-20**), which likely attributed to our reasonable optimization of cationic PPZ platform in chapter 2.

Another effect that could contribute to improving cell transfection in CA-/6MHA-PPZ:pDNA complexes, and in combination with endosomal escape as discussed above, is a modulation of polynucleotide binding. Complexes should bind polynucleotides tightly enough that the drug is not release prematurely, but without compromising its release in the cytosol or cell nucleus. In this sense, we have observed that CA-PPZ/6MHA-PPZ:pDNA complexes present more efficient polynucleotide release upon incubation with the competitor heparin that the reference CA-PPZ complexes (**Figure 2-16**). Moreover, intracellular tracking images of polycation and pDNA also provided evidence that CA-/6MHA-PPZ complexes dissociate better in the cytosol (**Figure 3-8**). Both results might translate in a more efficient intracellular unpacking of the polynucleotides for the CA-/6MHA-PPZ vs. the CA-PPZ system. Similar mechanisms were the presence of a polyanion helping for polynucleotide unpacking has been previously reported by Sullivan groups[5] and L. Han groups[6].

Traditional two-dimensional cell monolayer model has been widely used for optimization of formulations but also have been questioned for validity and ability to represent physiologically relevant situations. Three-dimensional cultures are better able to provide tissue-like architecture (e.g. extracellular matrix, cell interactions)[7], fundamental tumour microenvironment traits such as nutrient and oxygen gradients[8], and also gene expression profiles alike those of clinical tumours[9]. To date very few studies have investigated nucleic acid delivery in tumour spheroids despite of the fact that they are perfectly suited as preliminary studies before in vivo and that they can

provide critical information regarding nanocomplex tumour penetration, nowadays considered one of the most important barriers in cancer drug delivery[10,11]. As observed by tomographic fluorescence imaging, CA-/6MHA-PPZ:pDNA complexes provided higher transfection in GBM spheroids as compared to CA-PPZ:pDNA and the reference PEI:pDNA complexes; this was particularly remarkable at low pDNA doses (**Figure 3-12**). This improved efficacy was also accompanied by minimizing gene-transfer toxicity. These studies found that CA-/6MHA-PPZ:pDNA complexes were able to induce clear transgene expression in the core of ~250 μm spheroids, which contrasted with the poor transfection observed for the CA-PPZ:pDNA and PEI:pDNA complexes under the same dose (2 μg/mL) (**Figure 3-11**). Overall, this results showed an unexpectedly high transfection efficacy and tumour penetration capacity for the CA-/6MHA-PPZ:pDNA formulation. This observation could be related to the physicochemical properties of CA-/6MHA-PPZ:pDNA complexes, with their partially neutralized cationic charges at physiological pH, that might shield the system from indiscriminate binding to the extracellular matrix in tumour spheroids. Although the data was more complicated to interpret due to inhomogeneous transfection levels between injection and distal sites, these results were in agreement with those from the in vivo gene delivery experiment (**Figure 3-14**).

Glioblastoma initiating cells are considered to be responsible of tumour recurrence [12], and therefore, their suppression is essential for any medicine intended to provide mid- or long-term survival benefits. In the past, we have shown that controlled release implants can deliver glioblastoma initiating cell suppressing molecules and provide a therapeutic benefit in advanced in vivo models[13,14]. In this work, following the pilot in vivo study of GFP-pDNA transgene expression, we applied the same

optimized formulation to deliver a siRNA sequence with known activity against glioblastoma initiating cells (siRNA against DYRK1A, siDYR)[15]. CA-/6MHA-PPZ:siDYR complexes presented physicochemical properties similar to those of CA-/6MHA:pDNA complexes, and were able to silence its target protein (DYRK1A) in a more consistent fashion than CA-PPZ:siDYR and PEI:siDYR (**Figure 4-4**). We confirmed that this protein silencing observed for cells treated with CA-/6MHA-PPZ:siDYR resulted in a reduction in the clonogenic index in a secondary spheroid formation assay, indicating the abrogation of the "initiating cell" phenotype of the target cells. The CA-/6MHA-PPZ:siDYR formulation was evaluated in U87MG xenograft mice, in a therapeutic scheme including co-delivery of first-line treatment drug temozolamide. The experiment found a significant delay in tumour progression in the arm receiving TMZ and CA-/6MHA-PPZ:siDYR vs. the arm receiving TMZ and CA-/6MHA-PPZ complexed with a scrambled siRNA sequence (**Figure 4-6**). Therefore, our results are consistent with an additional therapeutic benefit in combining the CA-/6MHA-PPZ:siDYR gene therapy with the standard pharmacological GBM treatment. Further studies will be needed to elucidate the possible clinical impact of this co-therapy in more advanced models and performing additional phenotypic analysis in the tumours.

General Conclusion

A synthetic strategy for the simple preparation of a small library of polyphosphazenes of interest for gene delivery was developed based on the generation of a precursor polymer with click handles, and further derivation by thiol-ene additions. This strategy has allowed us to test a variety of compounds and draw structure/function relationships. Based on the screenings, a primary amine-containing polymer (CA-PPZ) and an anionic polyphosphazene analogue (6MHA-PPZ) were selected for plasmid DNA gene delivery. These binary polyion/gene complexes displayed significantly higher transfection efficiency than the parent polycation-only system in 2D monolayers, 3D spheroids of U87MG cells and in a subcutaneous xenograft model, due to improved tumour transport and intracellular trafficking characteristics. This optimized prototype also showed indications of superior performance compared to the gold standard PEI complexes, particularly in 3D tumour models. When used for RNAi therapy, CA-/6MHA-PPZ complexes efficiently delivered siRNA against DYRK1A in U87MG cells, inducing a significant reduction of their self-renewal capability in vitro and a significant anti-tumoural effect in a glioblastoma model *in vivo*. Overall, the data established a new versatile, biodegradable polymeric gene delivery based on polyphosphazenes with remarkable capacity for transfection, tumour penetration and *in vivo* performance.

USC
UNIVERSIDADE
DE SANTIAGO
DE COMPOSTELA

References

1. Qian, Y.C., *et al.* A versatile approach to the synthesis of polyphosphazene derivatives via the thiol–ene reaction. *Journal of Polymer Science Part A: Polymer Chemistry* **50**, 5170-5176 (2012).
2. Ren, N., *et al.* Controllable glycosylation of polyphosphazene via radical thiol–yne click chemistry. *Journal of Polymer Science Part A: Polymer Chemistry* **50**, 3149-3157 (2012).
3. Boeckle, S., *et al.* Purification of polyethylenimine polyplexes highlights the role of free polycations in gene transfer. *The journal of gene medicine* **6**, 1102-1111 (2004).
4. Yue, Y., *et al.* Revisit complexation between DNA and polyethylenimine—effect of uncomplexed chains free in the solution mixture on gene transfection. *Journal of Controlled Release* **155**, 67-76 (2011).
5. Greco, C.T., Andrechak, J.C., Epps III, T.H. & Sullivan, M.O. Anionic polymer and quantum dot excipients to facilitate siRNA release and self-reporting of disassembly in stimuli-responsive nanocarrier formulations. *Biomacromolecules* **18**, 1814-1824 (2017).
6. Han, L., Tang, C. & Yin, C. Effect of binding affinity for siRNA on the in vivo antitumor efficacy of polyplexes. *Biomaterials* **34**, 5317-5327 (2013).
7. Enam, S.A. & Klaus, E. Role of extracellular matrix in tumor invasion: migration of glioma cells along fibronectin-positive mesenchymal cell processes. *Neurosurgery* **42**, 599-608 (1998).
8. Sutherland, R.M., *et al.* Oxygenation and Differentiation in Multicellular Spheroids of Human Colon Carcinoma. *Cancer Research* **46**, 5320-5329 (1986).
9. Hamer, P.D.W., *et al.* The genomic profile of human malignant glioma is altered early in primary cell culture and preserved in spheroids. *Oncogene* **27**, 2091 (2008).
10. Zhou, J., *et al.* Highly penetrative, drug-loaded nanocarriers improve treatment of glioblastoma. *Proceedings of the National Academy of Sciences* **110**, 11751-11756 (2013).
11. Song, E., *et al.* Surface chemistry governs cellular tropism of nanoparticles in the brain. *Nature communications* **8**, 15322 (2017).
12. Garcia-Mazas, C., Csaba, N. & Garcia-Fuentes, M. Biomaterials to suppress cancer stem cells and disrupt their tumoral niche. *International Journal of Pharmaceutics* **523**, 490-505 (2017).

13. Reguera-Nuñez, E., *et al.* Implantable controlled release devices for BMP-7 delivery and suppression of glioblastoma initiating cells. *Biomaterials* **35**, 2859-2867 (2014).
14. González-Gómez, P., *et al.* Controlled release microspheres loaded with BMP7 suppress primary tumors from human glioblastoma. *Oncotarget* **6**, 10950-10963 (2015).
15. Pozo, N., *et al.* Inhibition of DYRK1A destabilizes EGFR and reduces EGFR-dependent glioblastoma growth. *The Journal of clinical investigation* **123**, 2475-2487 (2013).

Annex (Anexos)

Annex (Anexos)

Annex I:

A Di-Functional Responsive Biodegradable Block-Copolymer Polyethylene Glycol-co-Polydisulfide for Gene Delivery Application

Abstract

We synthesized a novel block-copolymer Polyethylene Glycol-co-Poly(α-LiPoic Acid) (PEG-PLPA) containing a PEG block, effective for protecting drugs and labile biopharmaceuticals, and a PLPA block for controlled degradation in the tumor tissue. Besides the bio-functions, this PEG-PLPA copolymer is designed to be pH- and redox-sensitive, facilitating programmed delivery of drugs or associated nanocarriers at targeting sites. In this preliminary study, PEG-PLPA was synthesized by ring-opening polymerization of lipoic acids and then characterized by NMR, DOSY, GPC, and potentiometric titration. In formulation screening for gene delivery carriers, PEG-PLPA mixing with protamine:pDNA complexes formed of nanoscale complexes. In a redox-sensitive test, once incubated with 10 mM DTT, PEG-PLPA/protamine:pDNA complexes underwent a significant increase in particle size, even aggregating and shifting towards positive surface charge. These data indicated the loss of PEG-stealth functions likely because disulfide bonds of PLPA segments have been broken. Overall, this novel bi-functional PEG-PLPA represents approach over PEGylation dilemma since it affords a stabilizing coating for drug nanocarriers that can degrade under very defined conditions.

1. Introduction and background

In non-viral gene delivery, one of the commonest fashions to facilitate gene cargo entering live cells is polymeric-mediated gene delivery[1-3]. This delivery system has been designed as complexes of positively charged polymers with negatively charged nucleic acids. However, there is a 'trade-off' between strong electrostatic associations needed to protect the nucleic acids during delivery with a loose association required for release at targeting sites. In this work, we design a novel negatively-charged di-block copolymer to provide adequate ionic interaction for complex formation as well as pH-sensitive and redox-induced dissociation for release inside targeting cells. One of the major problems in the design of gene therapies or other drug delivery modalities is what is often termed the "PEG dilemma".[4] On one hand, coating of the drug or the nanocarrier with a protective PEG layer is often essential to prevent: (i) instantaneous aggregation in physiological media, (ii) unwanted interactions with proteins and blood components, (iii) rapid clearance from the bloodstream mediated by the phagocytic system, and (iv) potential toxicity mediated by unspecific interactions with blood or non-targeted cells[5-7]. On the other hand, this same PEG coating is known to reduce the interaction of the nanocarriers with the targeted cells, and in the specific case of gene carriers, will reduce the efficacy of the transfection process. In this context, the generation of PEG-coatings that de-associate once the therapeutic cargo has reached the targeting site ("programmed delivery systems") are of high interest. In the past, several chemistries have been described that can cleave the PEG layer by either reacting to the acidic environment typical of physiological regions such as tumors, or less often, by changes in the redox potential. Here we present a new PEG-based stabilizing polymer that can perform this de-association process by reacting with both

stimuli.

2. Materials and Methods

Lipoic acid (PLPA), PEG-SH (Mw 5000), iodoacetamide, and 1,4-Dithiothreitol (DTT) were all purchased from Sigma-Aldrich and used as received. Protamine sulfate was obtained from Yuki Gosei Kogyo Co., Ltd (Tokyo, Japan).

PEG-PLPA was synthesized by ring-opening “disulfide exchange” polymerization. Briefly, 30 mg of PEG-SH (5000 Da) was added into 100 mg of lipoic acid in 0.6 mL methanol. NaOH 2N (50 μL) was added into the reactor for acceleration of disulfide exchange and incubated for 3 days. For termination of reaction, excess iodoacetamide (90 mg in 0.5 mL water) was added and incubated for another 4 hours. After that, the raw product was precipitated in cold ethyl ether and purified by dialysis against pure water. Finally, the purified products were lyophilized and stocked in freezer for future use.

For complexation of PEG-PLPA/protamine:pDNA, protamine was dissolved in HEPES pH 5.5 firstly, and complexed with polyanions (pDNA and PEG-PLPA) in HEPES pH 8.2 with different mass ratios of protamine to pDNA and with mole ratio of carboxylic acids on PLPA and phosphate on DNA. The complexation was performed by intense vortex for 30 sec and incubated for 2 hours in room temperature. For the all characterizations, the analysis methods are same with the chapter 2 in this thesis.

3. Results and discussions

In the polymer synthesis, the ring-opening polymerization was performed by the

initiator PEG-thiol to exchange to the disulfide bonds of lipoic acids, growing polymer chains. In light this, this polymerization is also called disulfide-exchange polymerization. After that, iodoacetamide can be used as terminator for suspending the polymerization[8]. The main structure of this co-polymer is shown in **Figure 1**, which composes of a PEG segment and several repeating units of lipoic acid (PLPA). The segment of PEG provides a stealth property for in-vitro and in-vivo stability. On the other hand, the segment of PLPA offers negative charges for electrostatic-driven association with drugs or other polyionic complexes. The polymer structure was identified by proton-NMR spectra for each specific functional group (**Figure 2**) and proton-DOSY confirmed high purity of the final product. The number average molecular weight (Mn) of PEG-PLPA is 15404 Da from proton-NMR, which is similar to the result (Mn: 15285 Da) from DOSY spectra with known molecular weight of PEG standards. However, the GPC measurement of the same PEG-PLPA polymer showed around 8000 Da with PI < 1.3, which is also calibrated by PEG standards. Regarding this inconsistency, this may be caused by the hydrophobicity of PLPA segments, which is easy to form “micelles”, especially at high concentration of the polymer samples and aqueous elution phase at pH close to or lower than the pKa of the polymer. In addition to structure characterization, this polymer possesses an apparent pKa around pH 6.3, expressing their potential buffering capacity in the endosomal pH range (**Figure 3**), but also the potential for coating decoupling in the acidic environment typical of the tumoral niche.

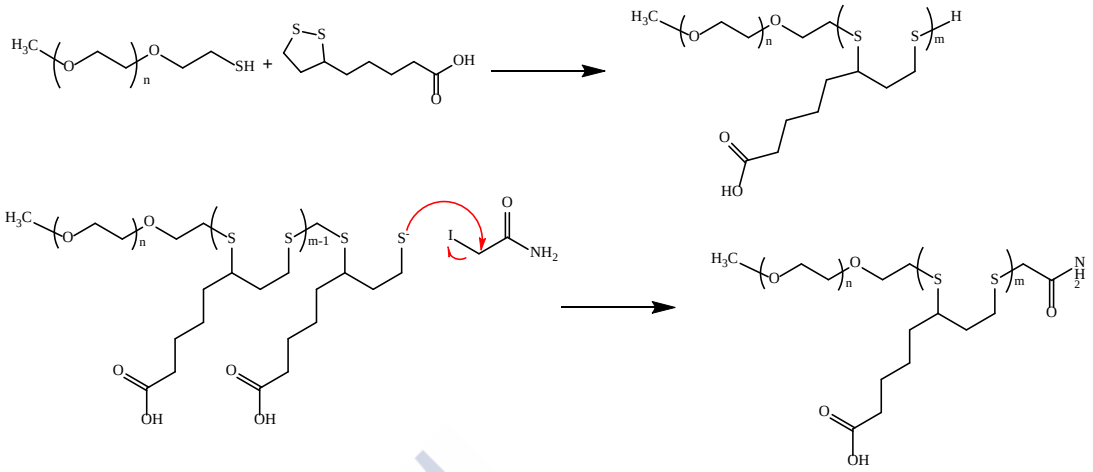

Figure 1. Ring-opening polymerization of lipoic acid and the main structure of the product PEG-PLPA.

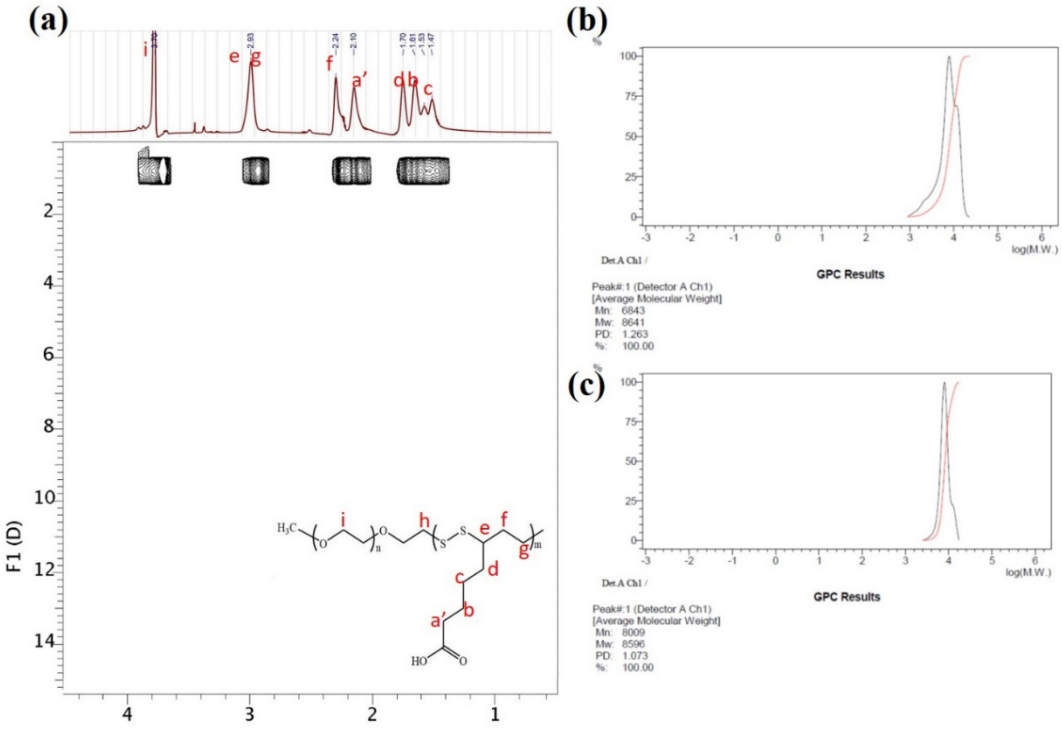

Figure 2. Polymer characterization. (**a**) Proton-NMR characterization and DOSY of PEG-PLPA. (**b**) The molecular measurement of PEG-PLPA and repeated experiments in **c**).

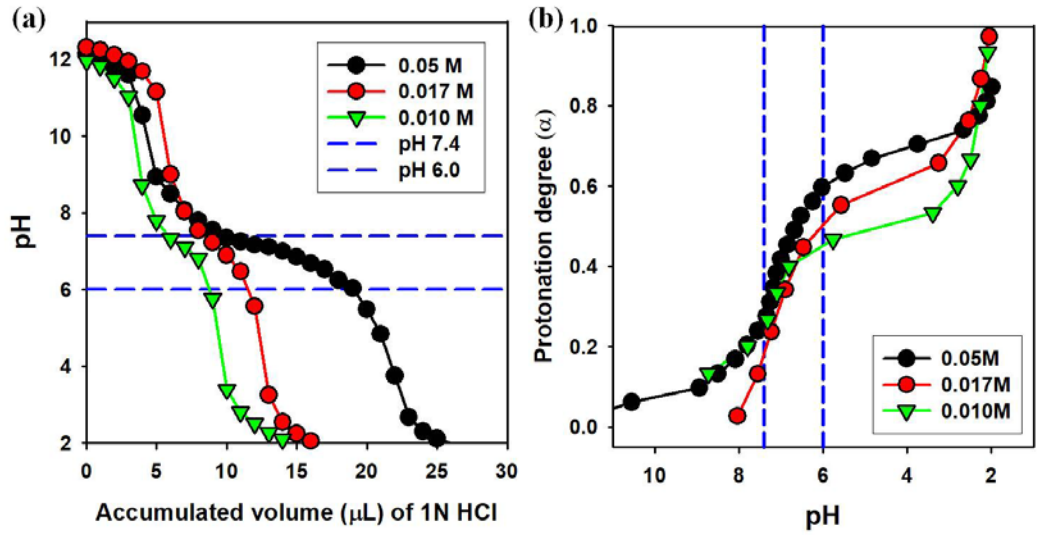

Figure 3. Potentiometric titration curves and protonation curves of PEG-PLPA in three different concentrations.

In formulation of gene delivery carriers, we chose a cationic protein, protamine sulfate as polycation and complexed pDNA to form a nanoscale gene carrier. The particle size and surface charge of protamine/pDNA complexes are shown in **Figure 4**. The diameters of complexes are around 90-100 nm and distribution in size of the nanoparticles is of low polydispersity. The surface charge of protamine:pDNA is inverted to positive values as the mass ratio of protamine to pDNA goes from 0.5 to approximately 0.66, indicating that protamine dominates the charge of polymeric complexes and excess cationic charges present on the particle surface. Here, we decided the mass ratio of protamine to pDNA 2:1 for the following studies.

After formation of polycationic complex (protamine:pDNA), PEG-PLPA is mixed into this complex. The PEG-PLPA not only facilitates ionic complex formation and improves its stability but also possesses redox-induced dissociation within the

glutathione-rich environment typical of tumor cell interior. The decoupling and polymer degradation of the polymer could also occur in the extracellular environment, induced by the proteins disulfide isomerase. In **Figure 5**, the size of PEG-PLPA mixing protamine complexes remain in the nanoscale range when stably suspended in physiological ionic strength (NaCl 150 mM). More interestingly, once the complexes incubated with 10 mM DTT (a reducing agent), the PLPA section is cleaved and the PEG segments dissociate from the nanocomplexes. As a result of the loss of the stabilizing PEG layer, the complexes are destabilized by free ions, causing aggregation (**Figure 5c**). It should be noted that the PEG-PLPA can shield positive surface charges of the nanocomplexes dependent on the ratio of polymer to DNA, but after incubation in 10mM DTT, the surface charges return from negative to positive due to the detachment of PEG and anionic polymer blocks.

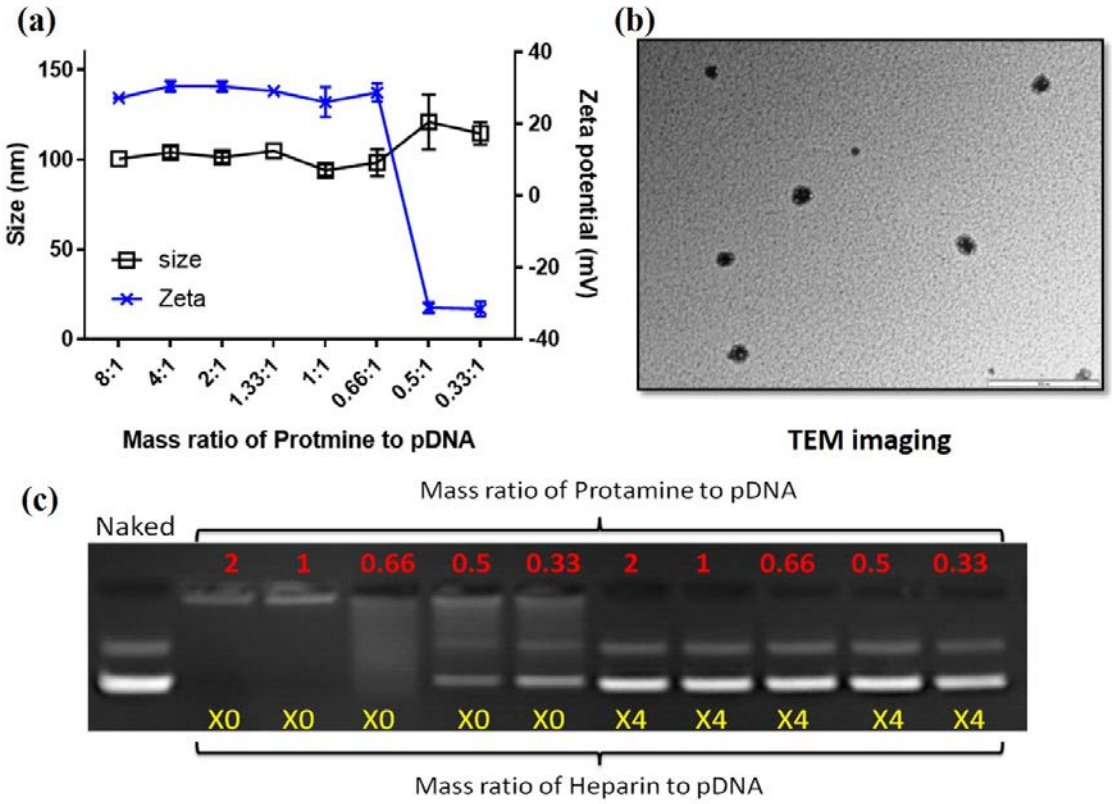

Figure 4. Particle characterization **(a)** and TEM images (**b**) of protamine:pDNA complex. (**c**) Gel retardation of protamine:pDNA complexes against different mass ratios of heparin.

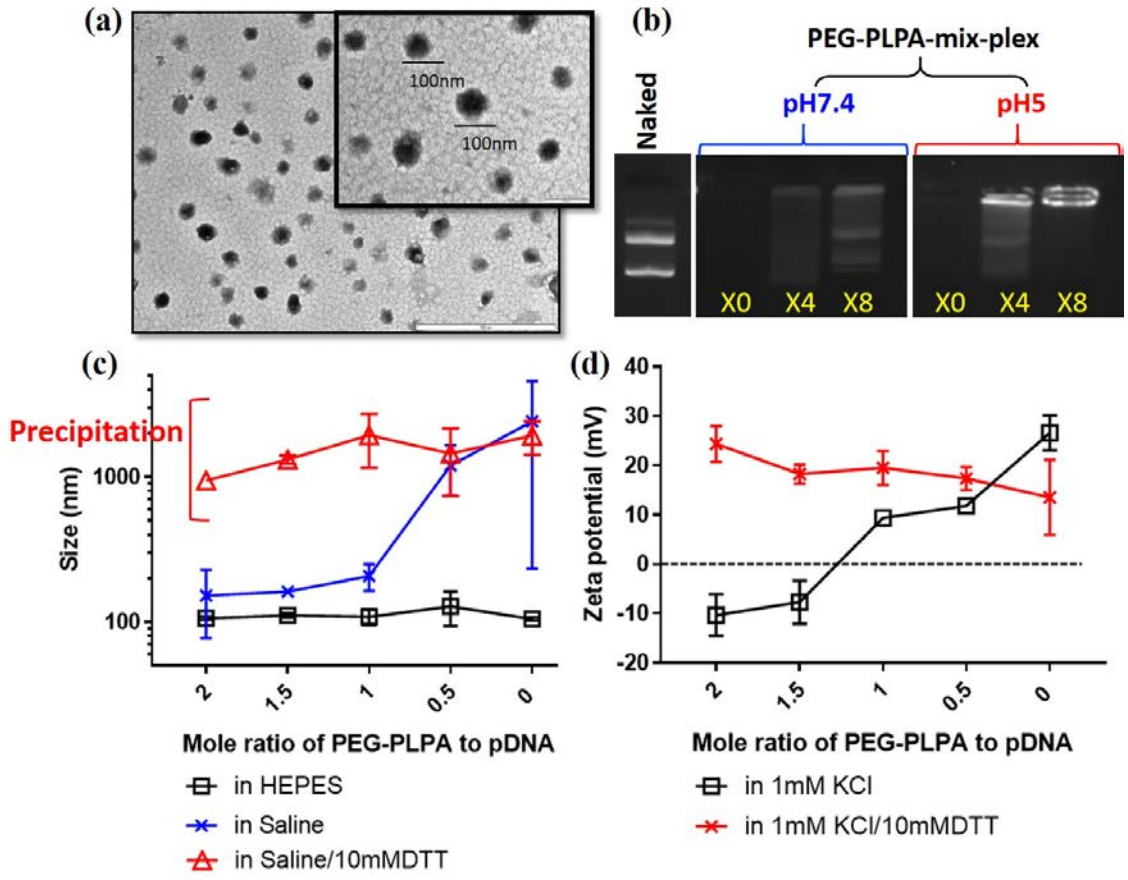

Figure 5. (**a**) TEM images of PEG-PLPA mixing in protamine/pDNA complex. (**b**) PEG-PLPA/protamine:pDNA in physiological pH 7.4 and endosomal pH 5. Particles size (**c**) and zeta potential (**d**) of PEG-PLPA/protamine:pDNA complex in different media and at different ionic strength buffer, and in the same media but in the presence of the reductive agent DTT.

4. Conclusion

The chemical composition of the polymer is simple and novel, and can be synthesized following concepts of ‘green’ chemistry. This smart polymer PEG-PLPA is sensitive by two physiological stimuli (pH and redox potential), which could be used for programmed delivery of active components or associated nanocarriers to cancer cells, for instance in polyplex tumor delivery. This copolymer acts as an excipient improving formulation stability by the well-known steric stabilization effect of PEG.

Annex (Anexos)

Annex II: Ethical permissions

I. Animal Studies:

1. Xenotrasplanted glioma cells in the flank of immunodeficient mice
2. Intracranial-implantation of siDYRK1A-treated GBM cells

All the protocols with animals were reviewed and approved by the Research Ethics and Animal Welfare Committee at our Institution (Instituto de Salud Carlos III, Madrid) (PROEX 244/14), in agreement with the European Union and national directives.

II. Primary cell-line, GBM1 cells

The primary cell line GBM1 was obtained from Dr. MD. Bernard Rogister's laboratory at the University of Liege, who obtained it from the original source Dr. Vincent Bours' laboratory. The derivation of such cell is already public knowledge and reported in the following papers. [Kroonen, J., et al. International Journal of Cancer 129, 574-585 (2011)[9] and Seidel, S., Garvalov, B.K. & Acker, T. Stem Cell Protocols 263-275 (Springer, 2015)[10]].

III. Copy right permission for this thesis

License Number	Publisher	Publication	Published year	Type of Use	Format
4336230827998	Royal Society of Chemistry	Analyst	2010	Thesis	print and electronic
Title: High-throughput 3D spheroid culture and drug testing using a 384 hanging drop array					
4335220008654	Elsevier	Nano Today	2011	Thesis	print and electronic
Title: Endocytosis and intracellular transport of nanoparticles: Present knowledge and need for future studies					
4335210880111	Elsevier	Trends in Cell Biology	2011	Thesis	print and electronic
Title: Microscopy in 3D: a biologist's toolbox					
4336221237710	Royal Society of Chemistry	Polymer Chemistry	2011	Thesis	print and electronic
Title: Bioerodible polyphosphazenes and their medical potential					
4336230673934	Royal Society of Chemistry	Integrative Biology	2014	Thesis	print and electronic
Title: A three-dimensional in vitro model of tumor cell intravasation					
4335220242821	Elsevier	Nano Today	2014	Thesis	print and electronic
Title: Intracellular delivery of nanomaterials: How to catch endosomal escape in the act					
4335221024452	Springer Nature	Nature Reviews Genetics	2014	Thesis	print and electronic
Title: Non-viral vectors for gene-based therapy					
4336240094545	Elsevier	Pharmacology & Therapeutics	2015	Thesis	print and electronic
Title: DYRK1A in neurodegeneration and cancer: Molecular basis and clinical implications					
4364600884215	ANNUAL REVIEWS	Annu Rev Pharmacol Toxicol.	2016	Thesis	print and electronic
Title: RNA Interference (RNAi)-Based Therapeutics: Delivering on the Promise?					

Pilar Sánchez Gómez, PhD
Neurooncology Unit
Chronic Disease Program
Instituto de Salud Carlos III (ISCIII)
Carretera de Majadahonda - Pozuelo, Km. 2.200.
28220 - Majadahonda (Madrid) SPAIN
Tel: +34 91 822 3265/69
e-mail. psanchezg@isciii.es

Madrid, May 18th 2018,

To whom it may concern,

This letter certifies that Wei-Hsin Hsu made stayed in the lab I direct from March to June of 2017. During that time, he performed *in vitro* and in *vivo* studies with glioma cells. These experiments were part of his PhD work, financed by the "Nanofar, Erasmus Mundus Joint Doctorate in Nanomedicine and Pharmaceutical". For the *in vivo* studies, we xenotrasplanted glioma cells in the flank of immunodeficient mice. When tumors became visible, animals were treated with intratumoral injections of polyphosphazene complexes, for effective delivery of interfering DYRK1A RNAs (twice a week) in the presence or in the absence of temozolomide (conventional chemotherapy for glioma patients). Tumor size was measured afterwards for two weeks. All these procedures were done under my supervision and all the protocols with animals were reviewed and approved by the Research Ethics and Animal Welfare Committee at our Institution (Instituto de Salud Carlos III, Madrid) (PROEX 244/14), in agreement with the European Union and national directives.

Please do not hesitate to contact me if you need any other information related to this subject.

Best regards,

Pilar Sánchez Gómez, PhD

Annex (Anexos)

Vista la solicitud presentada por PILAR SÁNCHEZ GÓMEZ, para la autorización del proyecto de memoria técnica titulada HACIA EL DESARROLLO DE TERAPIAS INDIVIDUALIZADAS PARA EL TRATAMIENTO DEL GBM DIRIGIDAS A ELIMINAR LA POBLACIÓN DE CÉLULAS INICIADORAS DEL GLIOMA:BLOQUEO DEL EJE MK/ALK, INHIBICION DE DYRK1A/EGFR, MODULACIÓN DE LA AUTOFAGIA E IDENTIFICACIÓN DE NUEVAS DIANA: a desarrollar en el centro usuario CENTRO NACIONAL DE MICROBIOLOGÍA,ISCIII con código de registro ES280800000015 y siendo el responsable del proyecto PILAR SÁNCHEZ GÓMEZ:

Visto el informe del Área de Protección Animal.

Considerando que el citado proyecto se ajusta a lo establecido en el Real Decreto 53/2013 de 1 de febrero por el que se establecen las normas básicas aplicables para la protección de los animales utilizados en experimentación y otros fines científicos, incluyendo la docencia.

Esta Dirección General ha resuelto: autorizar la realización del proyecto referenciado siempre que se mantengan las condiciones que dieron lugar a la autorización y que el personal que intervenga tenga la preparación y formación adecuada que se especifica en el citado Real Decreto.

Tal y como se indica en el informe de evaluación del proyecto presentado, éste debe ser sometido a una evaluación retrospectiva en el momento que indica dicho informe.

La presente Resolución no pone fin a la vía administrativa y contra la misma podrá interponer recurso de Alzada en el plazo de un mes a partir del día siguiente al de la recepción de esta notificación, ante el Consejero de Medio Ambiente y Ordenación del Territorio (C/ Alcalá 16, 28014 Madrid), o ante el Director General del Medio Ambiente (C/ Alcalá 16, 28014 Madrid), o en cualquiera de las formas previstas en el artículo 38.4 de la Ley 30/1992, de Régimen Jurídico de las Administraciones Públicas y del Procedimiento Administrativo Común de conformidad con lo previsto en los artículos 107, 114 y 115 de dicha Ley.

Madrid, 12 de noviembre de 2014.
EL DIRECTOR GENERAL DEL MEDIO AMBIENTE

Fdo.: Ricardo Riquelme y Sánchez de la Viña.

Ref PROEX 244/14

References

1. Yin, H., *et al.* Non-viral vectors for gene-based therapy. *Nature reviews. Genetics* **15**, 541 (2014).
2. Chen, J., Guo, Z., Tian, H. & Chen, X. Production and clinical development of nanoparticles for gene delivery. *Molecular therapy. Methods & clinical development* **3**, 16023 (2016).
3. Wong, J.K., *et al.* Will nanotechnology bring new hope for gene delivery? *Trends in biotechnology* (2017).
4. Verhoef, J.J. & Anchordoquy, T.J. Questioning the use of PEGylation for drug delivery. *Drug delivery and translational research* **3**, 499-503 (2013).
5. Duncan, R. The dawning era of polymer therapeutics. *Nat Rev Drug Discov* **2**, 347-360 (2003).
6. Pack, D.W., Hoffman, A.S., Pun, S. & Stayton, P.S. Design and development of polymers for gene delivery. **4**, 581 (2005).
7. Park, T.G., Jeong, J.H. & Kim, S.W. Current status of polymeric gene delivery systems. *Advanced drug delivery reviews* **58**, 467-486 (2006).
8. Gasparini, G., *et al.* Cellular uptake of substrate-initiated cell-penetrating poly (disulfide) s. *Journal of the American Chemical Society* **136**, 6069-6074 (2014).
9. Kroonen, J., *et al.* Human glioblastoma-initiating cells invade specifically the subventricular zones and olfactory bulbs of mice after striatal injection. *International Journal of Cancer* **129**, 574-585 (2011).
10. Seidel, S., Garvalov, B.K. & Acker, T. Isolation and culture of primary glioblastoma cells from human tumor specimens. in *Stem Cell Protocols* 263-275 (Springer, 2015).